January 1993

A Water Quality Model for Massachusetts Bay and Cape Cod Bay

Model Design and Initial Calibration

Massachusetts Water
Resources Authority

Environmental Quality Department
Technical Report No. 93-5

Massachusetts Water Resources Authority
Boston, Massachusetts

A WATER QUALITY MODEL FOR MASSACHUSETTS BAY AND CAPE COD BAY MODEL DESIGN AND INITIAL CALIBRATION

Job Number: NAIC0103

Prepared by:

HydroQual, Inc.
1 Lethbridge Plaza
Mahwah, New Jersey 07430

and

Normandeau Associates
25 Nashua Road
Bedford, New Hampshire 03102

January 1993

CONTENTS

Section Page

FIGURES

TABLES

CONCLUSIONS

A preliminary water quality model of the eutrophication and dissolved oxygen dynamics of Massachusetts and Cape Cod Bays has been formulated and an initial calibration made to observed water quality and sediment flux data. The modeling framework chosen to represent the eutrophication and sediment nutrient fluxes in the Bays was based on those developed for the U.S. Environmental Protection Agency's Chesapeake Bay and Long Island Sound Studies.

Application of the water quality model to Massachusetts and Cape Cod Bays and using October 1989 to April 1991 as the calibration period indicates:

1. Based on preliminary calibration results, the proposed water quality eutrophication and sediment submodel frameworks appear to provide a reasonable basis for modeling Massachusetts and Cape Cod Bays.

2. Based on observed data and model computations the water quality of the Bays is good relative to other coastal estuaries, such as Chesapeake Bay and Long Island Sound. In these other estuaries anthropogenic nutrient inputs have resulted in increased eutrophication and stressed habitats, in terms of hypoxia and anoxia, for living marine resources. These conditions have not been observed nor has the water quality model computed them to occur in Massachusetts Bay for the calibration period.

3. As indicated by differences between model computations and observed data, it appears as if the determination of circulation and mixing within the Bays by a time-variable fine-grid hydrodynamic model is essential to the success of modeling the fate of pollutants delivered to the Bays from the MWRA facilities and other nutrient sources.

RECOMMENDATIONS

1. Work should continue with the development of the fine-grid time-variable hydrodynamic model. Attention should be given to performing long-term computations on the order of 18 months, so as to provide circulation and mixing fields for the water quality model.

2. Consideration should be given to including the more recent Massachusetts Bays monitoring program data sets in the water quality model calibration. These data sets have more comprehensive sampling of key nutrient forms than are available for the 1989-1991 data set.

3. Consideration should also be given to expanding the spatial coverage of the sediment nutrient flux and sediment composition program. Presently nutrient flux measurements and sediment nutrient composition are available only for regions in Boston Harbor and near the proposed outfall location. It would be highly desirable to have additional sediment data in Cape Cod Bay and near the Stellwagen Bank and Stellwagen Basin.

4. Due to concerns about prohibitive computational resources required to run fine-grid water quality calculations, work should begin on hydrodynamic model grid-aggregation schemes. These grid aggregation schemes would produce an intermediate level fine-grid representation of the Massachusetts bays system. The resulting aggregated water quality model would be required to demonstrate that the transport of pollutants within the system would still be modeled accurately before calibration and production runs would be initiated.

5. The present version of the water quality model does not include a functional algal group representing toxic dinoflagellates. Therefore, a parallel track effort should be initiated, wherein

(a) the present model framework would be used to complete the analysis of the effects of moving the MWRA outfall on conventional eutrophication and dissolved oxygen dynamics, while

(b) a parallel effort be made on formulating kinetics appropriate for modeling toxic dinoflagellates.

Work on calibrating the revised toxic dinoflagellate modeling framework would begin upon completion of the conventional eutrophication modeling analysis.

SECTION 1

INTRODUCTION

1.1 INTRODUCTION

The Massachusetts Water Resources Authority (MWRA) is planning the construction of an ocean outfall, which will divert treated effluent from the Deer Island Wastewater Treatment Plant. The present Deer Island outfall is located at the entrance to Boston Harbor and will be relocated into Massachusetts Bay at a distance approximately 15 km east of Deer Island at a water depth of 32 meters. The moving of the wastewater discharge from within the confines of Boston Harbor, together with improved sewage treatment and the cessation of sludge discharge to the Harbor, is expected to result in a significant improvement in water and sediment quality within the Boston Harbor area.

Concerns have been raised about the effect of the outfall relocation will be on water quality within Massachusetts Bay. The offshore outfall discharge will bring nutrients and organic matter directly into Massachusetts Bay. Previous modeling efforts suggest that these additional nutrients and organic matter will have little effect on the environment of the Bay (U.S. EPA, 1988, Menzie-Cura, 1991). However, the previous studies used relatively simple frameworks for their analyses and, since coastal eutrophication is a complex process, these initial predictions must be constantly re-evaluated.

In order to develop a more rigorous and detailed understanding of the potential impact of the outfall relocation on the water quality of Massachusetts Bay, the MWRA has funded or partially funded a number of studies within Boston Harbor and Massachusetts Bay. Since 1989, MWRA has funded a number of hydrographic and water quality surveys of the Bay. These surveys have collected data on salinity, temperature, phytoplankton, primary productivity, nutrients and dissolved oxygen throughout Massachusetts Bay. These data represent some of the most comprehensive data available for the Bay to date. MWRA has also funded a number of benthic nutrient flux and sediment oxygen demand surveys for stations within Boston Harbor and Massachusetts Bay. Both of these programs have

been expanded within an overall water quality monitoring program the purpose of which is to provide information concerning water and sediment quality before and after the operation of the new outfall, so as to be able to evaluate its impact on the Bay and to assist in the evaluation of operational issues.

MWRA has also entered into a cooperative agreement with the U.S. Geological Survey (USGS) to develop a time-variable three-dimensional hydrodynamic model of the Bay. This model encompasses all of Massachusetts and Cape Cod Bays, and extends out, on its eastern and northern boundaries, into the Gulf of Maine. One purpose of this model is to be able to predict the transport of materials discharged from the submerged outfall within the Bay.

Since the eutrophication processes within the Bay are related to meteorological and climatic forcings, the aforementioned monitoring program would require a number of years of water quality data before statistically significant inferences concerning the impact of the outfall on Bay water quality could be drawn from the observed data. Therefore, MWRA has funded the development and calibration of a time-variable water quality model of the eutrophication processes of Massachusetts Bay. The purpose of the water quality model is to provide another tool to assist in the understanding, evaluation and prediction of water quality response in the Bay subject to changes in the treatment facility's operating parameters, particulary related to the magnitude of nutrient loadings. It is towards the latter objective that this study is oriented. In order to place this study in the proper perspective, it is appropriate to briefly review the nature of the study area itself.

1.2 PHYSICAL CHARACTERISTICS

Massachusetts Bay and Cape Cod Bay (Figure 1-1) combine to form a roughly 100x50 km semi-enclosed basin located in the south-western Gulf of Maine. For the purposes of this investigation, the geographical extent of the study area is bounded on the north-east by Cape Ann and on the south and south-east by Cape Cod and the northern tip of Cape Cod at Race Point, respectively. The depth of the Bay varies from as much as

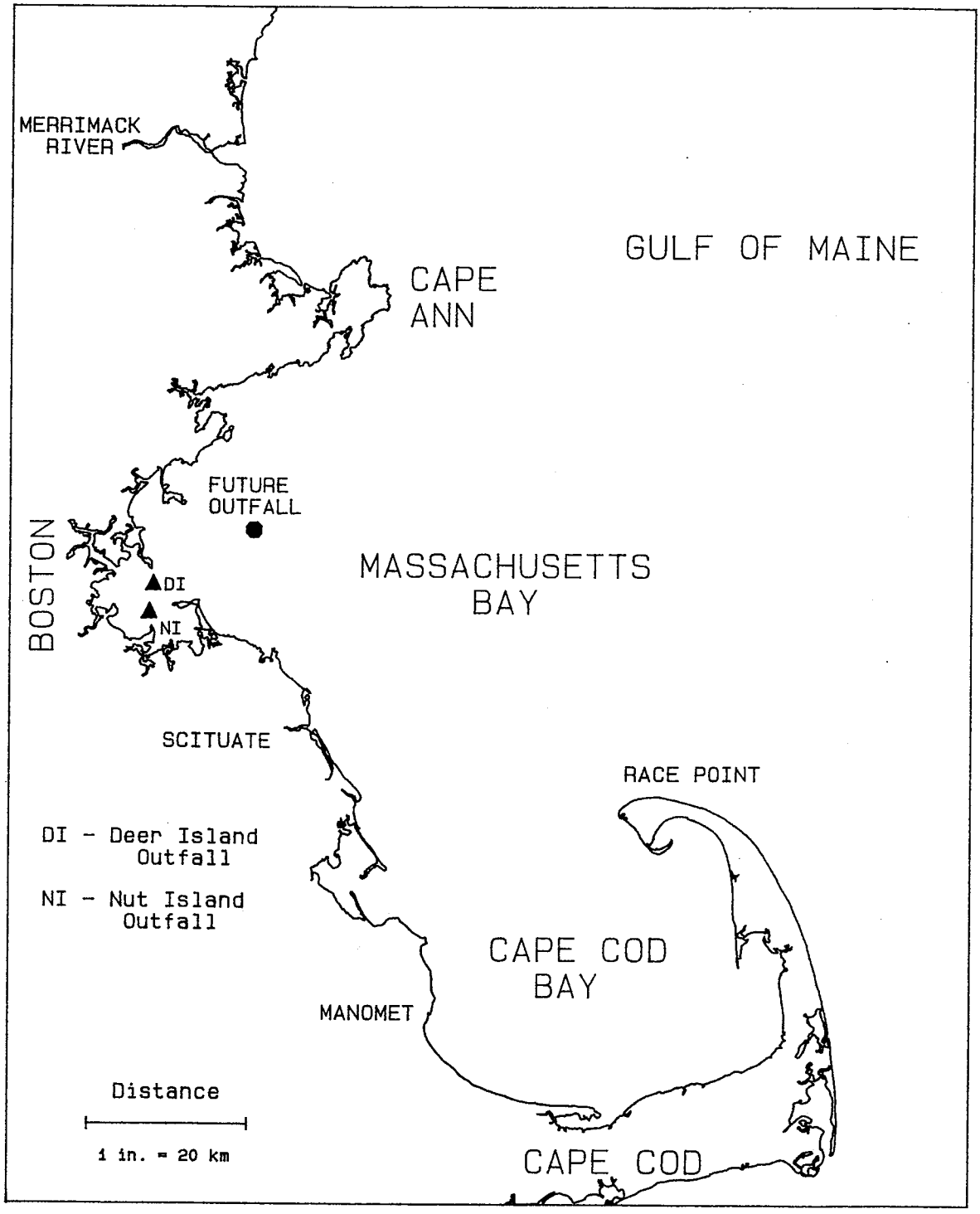

Figure 1-1

Massachusetts Bay Study Area

85 m in the deeper sections of Stellwagen Basin to tidal flats that are exposed at low tide, with an average depth of 35 m.

The major sources of freshwater to the Bay are from: municipal and industrial sewage treatment plants located in the City of Boston and other north and south shore communities; the Charles, Mystic and Neponset Rivers; groundwater inflow from along Cape Cod; and water from the Merrimack River and large rivers in Maine entrained in the Gulf of Maine coastal current.

1.3 POPULATION, LAND AND WATER USES

Over 2 million people, nearly half of the state of Massachusetts population, live in some 43 communities surrounding the City of Boston. Based on a 1991 draft report (Menzie-Cura, 1991), utilizing data from the Massachusetts Department of Environmental Protection and the National Oceanographic and Atmospheric Administration's National Coastal Pollutant Discharge file, the total drainage area (excluding the Merrimack River) of Massachusetts Bay is approximately 3700 km^2. Approximately 35 percent of the total drainage area can be categorized as urban in use (with nearly 70 percent of the urban area defined as residential, the remaining 30 percent is comprised of commercial, industrial, transportation and mixed urban land use), with the balance of 65 percent being categorized as non-urban.

The principal water uses in the Bay are shipping, transportation, sport fishing, recreational boating and recreational bathing, as well as receiving waters for wastewater discharges and a depository for dredged sediments.

1.4 WASTELOAD INPUTS

Massachusetts Bay is the recipient of domestic and industrial wastewater effluents, combined sewer overflows (CSOs), runoff from urban and non-urban areas, and from atmospheric sources (dryfall and wetfall) directly impinging on the water surface of the

Bay. Presently the major discharge to the system is from metropolitan Boston's Deer Island facility, which is currently being upgraded to provide more advanced wastewater treatment. For example, in December 1991 the discharge of sludge was ceased as an initial phase of this effort. In order to quantify the magnitude of nutrient loadings to the Bay prior to 1992 the U.S. EPA Massachusetts Bays Program funded Menzie-Cura and Associates to develop loadings estimates. This work has been completed and a draft report has been submitted to the Bays Program. (Details of nutrient loading estimates utilized in the present modeling study, drawn from the Menzie-Cura report (1991), will be provided in Section 3.)

1.5 THE EUTROPHICATION ISSUE

Of particular concern to MWRA and other regional water quality managers is how operational changes at the wastewater treatment facilities will affect the eutrophication processes within Massachusetts and Cape Cod Bays. Although phytoplankton production is an essential part of the food-chain for a given water body, excessive phytoplankton biomass resulting from high levels of nutrient enrichment can affect the overall health of the water body. This is in part due to the fact that under certain conditions excessive phytoplankton growth (eutrophication), coupled with extended periods of vertical stratification within the water column, can result in significant loss of dissolved oxygen (hypoxia) or even the total absence of dissolved oxygen (anoxia) in the bottom waters of the system. Although there have been no reported instances of anoxia or even hypoxia (defined as dissolved oxygen concentrations below 3.0 mg/L) reported for Massachusetts Bay (nor do MWRA impact studies project this to be the case), dissolved oxygen as coupled to eutrophication and anthropogenic nutrient enrichment is still of potential concern to MWRA.

Another area of interest to MWRA is how facility operations may relate to the occurrences or potential exacerbation of toxic phytoplankton blooms within Massachusetts Bay. Since 1972, blooms of the toxic dinoflagellate *Alexandrium tamarense* have caused nearly annual shellfish bed closures along the coasts of southern Maine, New Hampshire

and Massachusetts. Shellfish that ingest this dinoflagellate can accumulate its potent neurotoxins, becoming agents of paralytic shellfish poisoning (PSP). It is unclear whether these dinoflagellate blooms are introduced into Massachusetts Bay from offshore regions via wind-driven upwelling events or are transported into the Massachusetts Bay region from Maine and New Hampshire via entrainment in coastally driven Androscoggin, Kennebec and Merrimack River plumes. However, MWRA would like to understand how nutrients introduced at the outfall location may relate to this problem or change the ecological character of the phytoplankton community in the Bay.

1.6 PURPOSE AND SCOPE OF THIS STUDY

In order to better the understanding of the processes governing eutrophication in Massachusetts Bay and Cape Cod Bay, MWRA is providing funding for field, laboratory and analytical studies and an extensive outfall water quality monitoring program. In addition, funding has been provided to develop a series of computer models of Massachusetts Bay and Cape Cod Bay circulation and water quality. It is hoped that these studies and computer models will permit managers to better understand the causes of eutrophication and toxic dinoflagellate blooms and to manage nutrient inputs to assure the health of the living resources of this marine system.

This work was directed primarily towards the development of a mathematical model of the eutrophication processes of Massachusetts Bay and Cape Cod Bay. It is the first stage in the development of a coupled 3-dimensional time-variable hydrodynamic/water quality model of the Bay. The model reported herein represents a preliminary analysis of the interactions between nutrients and primary productivity within the Bay. The primary purpose of this study and its associated coarse-grid water quality model was to provide some early insight into nutrient dynamics and primary productivity relative to studies of eutrophication ongoing in other coastal systems or estuaries, such as Chesapeake Bay or Long Island Sound. This initial study is focused on the issue of conventional eutrophication as related to phytoplankton biomass, nutrients and dissolved oxygen; it does not address the issue of blooms of toxic dinoflagellates. In order to address the issue

of the impact of the MWRA outfall on toxic dinoflagellate blooms, additional refinement and development of the water quality model will be required. An additional state-variable representing toxic dinoflagellates will be required, as well as a more comprehensive understanding of their physiology and life-cycle. This analysis is expected to be performed in the second phase of this overall study of Massachusetts Bay.

This study provides a lead-in to the development of a fine-grid realization of the circulation and eutrophication dynamics of Massachusetts Bay and Cape Cod Bay. The fine-grid model will provide managers with a tool with which to make a detailed analysis of facility operations and nutrient inputs as they relate to eutrophication processes and water quality in the Bays.

1.6.1 Nature of a Mathematical Model

A mathematical model of water quality is a representation of the principal components of the environment that influence a given water quality variable. A model does not purport to represent all aspects of the actual environment; a model attempts to incorporate only those features of the problem that are most relevant. Thus, for example, a eutrophication model should incorporate such features as estuarine circulation and mixing, the input of point and nonpoint sources, the principal mechanisms of phytoplankton interactions with light, water temperature and nutrients, and the behavior of the various nutrient forms themselves. Similarly, a model of the oxygen balance of Massachusetts Bay should incorporate the same features of estuarine circulation and mixing, point and nonpoint sources, as well as the effects of atmospheric reaeration, photosynthetic oxygen production and algal respiration and sediment oxygen demand (SOD). The knitting together of the various mechanisms affecting circulation and mixing, phytoplankton behavior and dissolved oxygen is accomplished via theoretical equations (the details of which are presented in Section 2 of this report).

The spatial scope of this analysis encompasses Massachusetts Bay and Cape Cod Bay, including Boston Harbor. The eastern boundary of the model is a transect which

extends from Cape Ann on the north to Race Point (on the northern tip of Cape Cod) on the south. The model calculates spatial variations over approximately 10 to 15 km increments, as shown on Figure 1-2. Vertically, the model resolves spatial variations over a range of from 10 to 15 m, using 5 layers in the vertical plane. Temporally, the model is an 18 month computation of the annual cycle of primary productivity. Information concerning the circulation in the Bay was obtained from an aggregated version of the fine-grid hydrodynamic model. The hydrodynamic model was run to steady-state conditions for a mean winter condition. To represent the annual cycle of stratification within the Bay, the water quality model used time-varying vertical mixing coefficients, adjusted on a month to month basis so as to reproduce the observed vertical gradients in salinity and temperature in Massachusetts Bay and Cape Cod Bay. With the exception of atmospheric sources, which were varied on a monthly basis, inputs of nutrients to the model were based on an annual average. Other exogenous inputs such as incident solar radiation were input to the model on a monthly basis.

Once the geometry of the Bay is described and the inputs defined, the theoretical equations are then applied through calibration of the model to observed data. Section 4 describes this procedure.

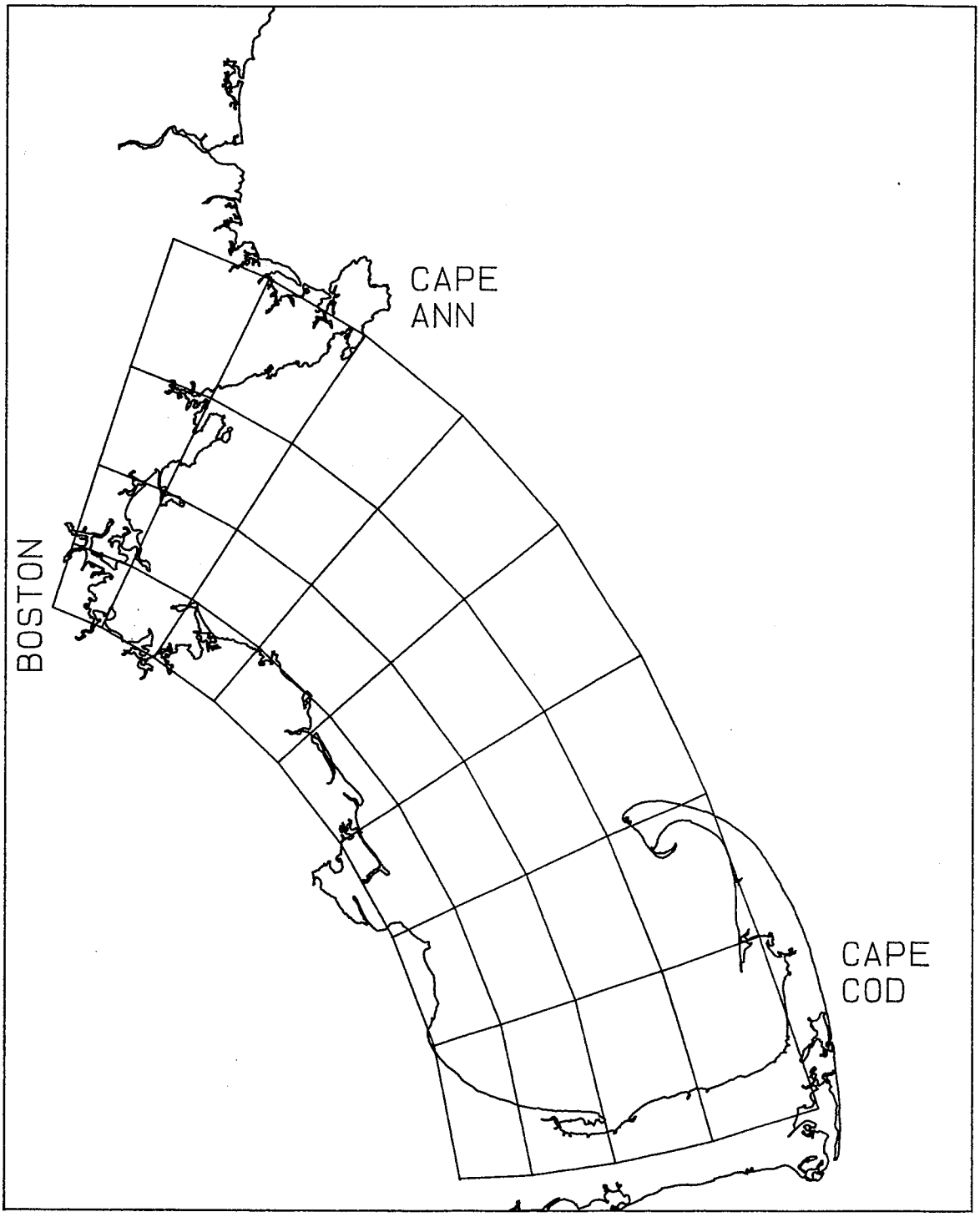

Figure 1-2

Coarse Water Quality Grid for Massachusetts Bay

SECTION 2

WATER QUALITY MODEL

2.1 INTRODUCTION

2.1.1 Conservation of Mass

The modeling framework used in this study and detailed in this report is based upon the principle of conservation of mass. The conservation of mass accounts for all of a material entering or leaving a body of water, transport of the material within the water body, and physical, chemical and biological transformations of the material. For an infinitesimal volume oriented along the axis of a three-dimensional coordinate system, a mathematical formulation of the conservation of mass may be written:

$$\frac{\partial c}{\partial t} = \underbrace{\frac{\partial}{\partial x}\left(E_x \frac{\partial c}{\partial x}\right) + \frac{\partial}{\partial y}\left(E_y \frac{\partial c}{\partial y}\right) + \frac{\partial}{\partial z}\left(E_z \frac{\partial c}{\partial z}\right)}_{\text{dispersive transport}} \underbrace{- U_x \frac{\partial c}{\partial x} - U_y \frac{\partial c}{\partial y} - U_z \frac{\partial c}{\partial z}}_{\text{advective transport}}$$

$$\underbrace{\pm S(x,y,z,t)}_{\text{sources or sinks}} + \underbrace{W(x,y,z,t)}_{\text{external inputs}} \qquad (2\text{-}1)$$

While Equation 2-1 is often taken as the "instantaneous" water quality mass balance equation, it may be interpreted as the "time-averaged over the tidal period" mass balance equation when the coefficients of the equation are chosen as follows:

c = concentration of the water quality variable [M/L^3],

t = time [T],

E = dispersion (mixing) coefficient due to tides and density and velocity gradients [L^2/T],

U = tidally-averaged net advective velocity (L/T),

S = sources and sinks of the water quality variable, representing kinetic interactions (M/L^3-T),

W = external inputs of the variable c (M/L^3-T),

x,y,z = longitudinal, lateral and vertical coordinates,

M,L,T = units of mass, length and time, respectively.

The modeling framework employed in this study is made up of three components: the transport of a water quality variable within the Bay due to density-driven currents and dispersion; the kinetic interactions between variables, and the external inputs of the water quality variable. The transport within the Bay is a complex process and is affected by freshwater inflows, temperature, wind and offshore forcings from the Gulf of Maine. The kinetics control the rates of interactions among the water quality constituents. Ideally, in a modeling effort, they should be independent of location per se, although they may be functions of exogenous variables, such as temperature and light, which may vary with location. External inputs of nutrients and oxygen-demanding material are derived from municipal and industrial discharges, combined sewer overflows (CSOs), natural surface runoff and atmospheric deposition to the water surface of Massachusetts Bay.

The purpose of this section of the report is to provide information relevant to the kinetic structure of the model; details concerning the external pollutant inputs to the model are presented in Section 3.0, while information concerning the model's calibration is presented in Section 4.0.

2.1.2 Choice of State-Variables

An important criterion for the inclusion of variables in a modeling framework is the existence of adequate field data for calibration/verification of the variable, as well as the importance of the variable in the processes being considered. As a consequence of a series of Massachusetts Bay sampling cruises conducted for MWRA and the U.S. EPA's Massachusetts Bays Program by the Bigelow Laboratory for Ocean Sciences and a joint University of Massachusetts at Boston/Woods Hole Oceanographic Institution/University of New Hampshire team, an adequate data base exists with which to begin the calibration of the water quality model. (It is expected that, during Phase 2 of this study, additional

data will become available as a result of the initiation of the MWRA's Massachusetts Bay monitoring program. These data will include measurements of more nutrients forms than are currently available and should provide a good data set to validate the model against.)

The kinetic framework employed in the Massachusetts Bay eutrophication model draws from parallel modeling efforts on the Chesapeake Bay system (HydroQual, 1989) and Long Island Sound (HydroQual, 1991) and utilizes the 25 state-variables shown in Table 2-1.

Other variables, constructed from these primary variables, are also tracked within the Bay. Phytoplankton (chl-a), total nitrogen (TN) and total phosphorus (TP) are the most important of these secondary variables.

The model framework, discussed below, incorporates these state-variables and is designed to simulate the annual cycle of phytoplankton production, its relation to the supply of nutrients and its effect on dissolved oxygen. The calculation is based on formulating the kinetics which govern the interactions of the biota and the various nutrient forms, and the application of these kinetics to Massachusetts Bay within the context of mass conservation equations.

2.2 MODEL KINETICS

The following section presents the conceptual framework for the water quality kinetics. A full set of all equations used in the model framework are presented in Appendices A - Water Column Kinetics and B - Sediment Model Kinetics.

2.2.1 General Structure

Salinity and temperature are included in the modeling framework to enable the calibration of the general transport of phytoplankton, nutrients and dissolved oxygen in Massachusetts Bay, with particular emphasis on the seasonal setup of vertical stratification

TABLE 2-1. STATE-VARIABLES UTILIZED BY THE KINETIC FRAMEWORK

1. - salinity (S)
2. - temperature (T)
3. - phytoplankton carbon - winter diatoms (P_{c1})
4. - phytoplankton carbon - summer assemblage (P_{c2})
5. - labile particulate organic carbon (LPOC)
6. - refractory particulate organic carbon (RPOC)
7. - labile dissolved organic carbon (LDOC)
8. - refractory dissolved organic carbon (RDOC)
9. - reactive dissolved organic carbon (ReDOC)
10. - algal exudate dissolved organic carbon (ExDOC)
11. - labile particulate organic phosphorus (LPOP)
12. - refractory particulate organic phosphorus (RPOP)
13. - labile dissolved organic phosphorus (LDOP)
14. - refractory dissolved organic phosphorus (RDOP)
15. - dissolved inorganic phosphorus (DIP)
16. - labile particulate organic nitrogen (LPON)
17. - refractory particulate organic nitrogen (RPON)
18. - labile dissolved organic nitrogen (LDON)
19. - refractory dissolved organic nitrogen (RDON)
20. - ammonia nitrogen (NH3)
21. - nitrite + nitrate nitrogen (NO2 + NO3)
22. - biogenic silica (BSi)
23. - available silica (Si)
24. - dissolved oxygen (DO)
25. - dissolved oxygen equivalents (O_2^*)

within the Bay. Temperature is also an important variable since the biological and chemical processes that occur within the system are temperature-mediated. In addition, temperature, together with salinity, determines the saturation value for dissolved oxygen within the water column.

For salinity and temperature there are no reaction kinetics involved, i.e. they are conservative. There are no direct sources or sinks of salinity, other than via exchange with the model boundaries or via freshwater dilution resulting from wastewater treatment facilities and from rivers (such as the Neponset, Charles, etc.) draining to the Bay. The primary source of temperature is the input of the sun's radiant energy, while the primary sink is the latent loss of heat to the atmosphere during the winter months. Rather than attempt to directly model the effects of surface thermal transfer, surface layer temperatures are assigned to the surface layer of the model according to observed data, and sub-surface layer temperatures are computed based on exchange with the surface layer.

Figure 2-1 presents the principal kinetic interactions for the nutrient cycles and dissolved oxygen. In the phosphorus system kinetics, DIP is utilized by phytoplankton for growth. Phosphorus is returned from the phytoplankton biomass pool to the various dissolved and particulate organic phosphorus pools and to DIP through endogenous respiration and predatory grazing. The various forms of organic phosphorus undergo hydrolysis and mineralization and are converted to DIP at temperature-dependent rates.

The kinetics of the nitrogen species are fundamentally the same as the kinetics of the phosphorus system. Ammonia and nitrate are used by phytoplankton for growth. Ammonia is the preferred form of inorganic nitrogen for algal growth, but phytoplankton will utilize nitrate nitrogen for growth as ammonia concentrations become depleted. Nitrogen is returned from the algal biomass and follows pathways that are similar to those of phosphorus. Organic nitrogen undergoes hydrolysis and mineralization and is converted to ammonia at a temperature-dependent rate; ammonia is then converted to nitrate

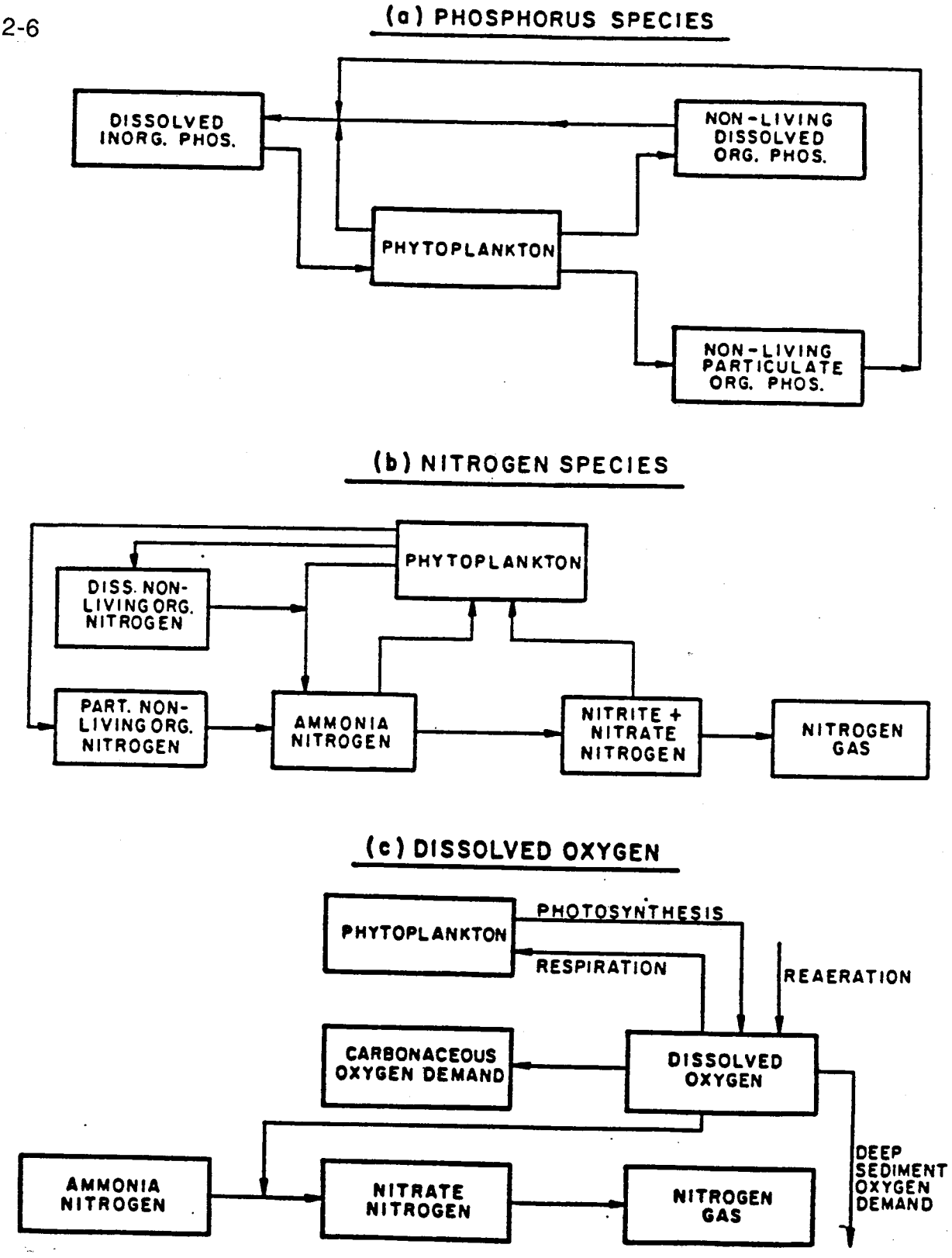

FIGURE 2-1. PRINCIPAL KINETIC INTERACTIONS FOR NUTRIENT CYCLES AND DISSOLVED OXYGEN

(nitrification) at a temperature- and oxygen-dependent rate. In the absence of oxygen, nitrate can be converted to nitrogen gas (denitrification) at a temperature-dependent rate.

Available silica is utilized by diatom phytoplankton during growth. Silica is returned to the biogenic silica pool as a consequence of algal respiration and predatory grazing and must undergo mineralization processes before becoming available for phytoplankton growth.

Dissolved oxygen is coupled to the other state-variables. The sources of oxygen included in the model are atmospheric reaeration and algal photosynthesis. The sinks of oxygen are: algal respiration; oxidation of detrital algal carbon and of organic carbon discharged from wastewater treatment plant facilities and nonpoint source discharges; nitrification; and sediment oxygen demand (SOD).

Organic carbon sources include anthropogenic inputs and the by-products of primary production and zooplankton grazing.

The water quality model also includes a coupled sediment submodel. This model was originally developed by HydroQual for the joint U.S. EPA/U.S. Army Corps of Engineers study of Chesapeake Bay. The sediment submodel can be conceived of as having three parts: the deposition of particulate organic matter (POM) to the sediment from the water column; the decay or diagenesis of the POM in the sediment; and a balance between the flux of resulting dissolved end-products back to the overlying water column and the burial of dissolved and particulate end-products via sedimentation.

2.2.2 Phytoplankton

The present version of the water quality model considers two functional phytoplankton groups: winter and summer. These distinctions are made to recognize some of the physiological differences, in terms of optimal temperature and light conditions, nutrient requirements, grazing pressures, etc., between the phytoplankton species that

dominate in each of these seasons of the year. The winter group, representing primarily diatoms, are characterized as favoring low temperature and light conditions and have a high requirement for silica, in addition to nitrogen and phosphorus, as a nutrient source for growth. The summer group represents a mixed population of phytoplankton, including greens, blue-greens, dinoflagellates and some diatoms. This group favors higher temperature and light conditions and has lower silica requirements than does the winter group.

The kinetic framework used for both functional algal groups is largely the same. Differences between the groups are expressed by the choice of model coefficients. The growth rate formulation in the present model is affected by temperature, light and available nutrients, as per Equation 2-2:

$$G_P = G_{Pmax} \bullet \underset{\text{temperature}}{G_T(T)} \bullet \underset{\text{light}}{G_I(I)} \bullet \underset{\text{nutrients}}{G_N(N)} \qquad (2\text{-}2)$$

where

$G_T(T)$ is the effect of temperature,
$G_I(I)$ is the light attenuation given by

$$G_I(I) = g(I_o, f, H, k_e) \qquad (2\text{-}3)$$

and $G_N(N)$ is the nutrient limitation given by

$$G_N(N) = g(DIP, DIN, Si) \qquad (2\text{-}4)$$

and where T is the ambient water temperature; I_o is the incident solar radiation; f is the fraction of daylight; H is the depth of the water column; k_e is the extinction coefficient or light attenuation coefficient; and DIP, DIN and Si are the available nutrient forms required for growth.

Initial estimates of G_{Pmax} were based upon previous estuarine modeling studies and were subsequently refined during the calibration process. The selected maximum growth rates are then temperature-corrected using spatially dependent, ambient water column temperature values. The temperature-corrected growth rate is computed using the following equation, which relates $G_{Pmax}(T)$, the growth rate at ambient temperature, T, to $G_{Gmax}(T_{opt})$, the growth rate at the optimal temperature, T_{opt}:

$$G_{Pmax}(T) = G_{Pmax}(T_{opt}) \bullet \theta_P^{(T-T_{opt})} \qquad T \leq T_{opt} \qquad (2\text{-}5a)$$

or

$$G_{Pmax}(T) = G_{Pmax}(T_{opt}) \bullet \theta_P^{(T_{opt}-T)} \qquad T > T_{opt} \qquad (2\text{-}5b)$$

and where θ_P is the temperature correction coefficient. The temperature-corrected growth rate is then adjusted to reflect attenuation due to ambient light and nutrient levels. A principal difference between the winter diatom group and the summer assemblage is that the winter group has a much lower T_{opt} then does the summer assemblage.

In the natural environment, the light intensity to which the phytoplankton are exposed is not uniformly at the optimum value. At the surface and near-surface of the air-water interface, photo-inhibition can occur due to high light intensities, while at depths below the euphotic zone, light is not available for photosynthesis due to background and algal related turbidity. The modeling framework used in this study extends from a light curve analysis formulated by Steele (1962). This analysis accounts for the effect of the variations of available light as a function of depth, the light intensity, I(z), at any depth, z, is related to the incident surface intensity, I_{av}, by the extinction coefficient, k_e, through

the formula $I(z) = I_{av} \exp(-k_e z)$. The reduction factor due to both the effect of non-optional light intensity and decreasing intensity as a function of depth is obtained by averaging the reduction factor over the depth H, and over time. Thus the attenuated growth rate factor, $G_I(I)$, is represented by the following integral:

$$G_I(I) = \int_o^f \frac{1}{H} \int_o^H \frac{I(z)}{I_s} e \frac{-I(z)}{I_s} + 1 \, dz \qquad (2\text{-}6)$$

where:

- $I(z) = I_{av} e^{-k_e z}$
- $e = 2.718$,
- f = the photoperiod or fraction of daylight,
- H = water column depth of segment k,
- k_e = the total extinction coefficient, computed from the sum of the base, non-algal related, light attenuation, k_{ebase}, and the self-shading attenuation due to the ambient phytoplankton population $k_c P_{chl\text{-}a}$ (m^{-1}),
- k_{ebase} = the base extinction coefficient due to background conditions created by natural turbidity or exogenous inputs and therefore can vary spatially,
- k_c = the algal related extinction coefficient per unit of chlorophyll (m^2/mg chl-a),
- $P_{chl\text{-}a}$ = the ambient phytoplankton population as chlorophyll (mg chl-a/L), where $P_{chl\text{-}a} = P_c / a_{cchl}$,
- P_c = the ambient phytoplankton population as carbon (mgC/L),
- a_{cchl} = the ratio of algal carbon to algal chlorophyll (mgC/mg chl-a),
- I_o = the total daily incident light intensity at the surface (ly/day), and
- I_s = the saturating light intensity (ly/day).

The result of this integral is:

$$G_I(I) = \frac{ef}{k_eH}\left[\exp\left(\frac{-I_o}{I_s}e^{-k_eH}\right) - \exp\left(-\frac{I_o}{I_s}\right)\right] \quad (2\text{-}7)$$

The effects of various nutrient concentrations on the growth of phytoplankton have been investigated, and the results are quite complex. As a first approximation to the effect of nutrient concentration on the growth rate, it is assumed that the phytoplankton population in question follows Monod growth kinetics with respect to the important nutrients. That is, at an adequate level of substrate concentration, the growth rate proceeds at the saturated rate for the ambient temperature and light conditions. However, at low substrate concentration, the growth rate becomes linearly proportional to substrate concentration. Thus, for a nutrient with concentration N_j in the j^{th} segment, the factor by which the saturated growth rate is reduced in the j^{th} segment is $N_j/(K_m + N_j)$. The constant, K_m, which is called the Michaelis, or half-saturation constant, is the nutrient concentration at which the growth rate is half the saturated growth rate. Since there are three nutrients, nitrogen, phosphorus and silica, considered in this framework, the Michaelis-Menten expression is evaluated for each nutrient and the minimum value is chosen to reduce the saturated growth rate,

$$G_N(N) = \text{Min}\left(\frac{DIN}{K_{mN} + DIN}, \frac{DIP}{K_{mP} + DIP}, \frac{Si}{K_{mSi} + Si}\right). \quad (2\text{-}8)$$

Three terms have been included in the modeling framework to account for the loss of phytoplankton biomass: endogenous respiration, sinking or settling from the water column and grazing. Endogenous respiration is the opposite process of photosynthesis, and as such, contributes to the death rate of the phytoplankton population. If the respiration rate of the phytoplankton as a whole is greater than the growth rate, there is a net loss of phytoplankton carbon or biomass. The endogenous respiration rate has been shown to be temperature dependent (Riley et al., 1949) and is determined via Equation 2-9,

$$k_{PR}(T) = k_{PR}(20^{o}C) \bullet \theta_{PR}^{(T-20)} \qquad (2\text{-}9)$$

where $k_{PR}(20^{o}C)$ is the endogenous respiration rate at 20°C, θ_{PR} is the temperature correction coefficient and $k_{PR}(T)$ is the temperature corrected rate. The units of k_{PR} are day^{-1}.

The sinking of phytoplankton is an important contribution to the overall mortality of the phytoplankton population. Published values of the sinking velocity of phytoplankton, mostly in quiescent laboratory conditions, range from 0.1 to 18.0 m/day. In some instances, however, the settling velocity is zero or negative. Actual settling rates in natural waters are a complex phenomenon, affected by vertical turbulence, density gradients and the physiological state of the different species of phytoplankton. An important factor shown to influence the physiological state of the algae is nutrient availability. Work by Bienfang et al. (1982) and Culver and Smith (1989) has shown that the settling rate of marine diatoms is increased primarily by low concentrations of silica, although low concentrations of nitrogen and low light availability were also found to increase diatom sinking rates. Although the net effective settling rate under nutrient stressed conditions is greatly reduced in relatively shallow, well-mixed regions of an estuary, sinking can contribute to the overall mortality of the algal population. In addition, the settling of phytoplankton can be a significant source of nutrients to the sediments and can play an important role in the generation of SOD. For these reasons, a term representing phytoplankton settling has been included in the algal mortality expression, and is determined by:

$$k_{sP} = \frac{v_{sPb}}{H} + \frac{v_{sPn}}{H} \bullet (1 - G_N(N)) \qquad (2\text{-}10)$$

where k_{sP} is the net effective algal loss rate due to settling (day^{-1}), v_{sPb} is the base settling velocity of phytoplankton (m/day), v_{sPn} is the nutrient dependent settling rate (m/day), $G_N(N)$ is defined by Equation 2-8, and H is the depth of the model segment, (m).

Zooplankton grazing may, depending upon the time of year and zooplankton biomass levels, be an important loss rate for phytoplankton. Rather than attempt to model the complex and dynamic process of zooplankton grazing and growth, a simple first order loss rate representing the effect of zooplankton grazing on algal biomass is included in the model. The loss rate due to grazing is temperature corrected as per Equation 2-11,

$$k_{grz}(T) = k_{grz}(20^oC) \bullet \theta_{grz}^{(T-20)} \qquad (2\text{-}11)$$

where $k_{grz}(T)$ is the temperature corrected loss rate due to zooplankton grazing and $k_{grz}(20^oC)$ is the loss rate at 20°C. The units of k_{grz} are day^{-1}.

The total loss rate for phytoplankton is then the sum of Equations 2-9, 2-10, and 2-11.

2.2.3 Stoichiometry and Nutrient Uptake Kinetics

A principal component in the mass balance equation for the nutrient systems in the model eutrophication framework is the nutrient uptake associated with algal growth. In order to quantify the nutrient uptake it is necessary to specify the phytoplankton stoichiometry in units of nutrient uptake per mass of phytoplankton biomass synthesized. For carbon as the unit of phytoplankton biomass, the relevant ratios are the mass of nitrogen, phosphorus, and silica per unit mass of carbon. Lacking measurements of the particulate forms of carbon, nitrogen, phosphorus and biogenic silica, this study assumed that the phytoplankton present in Massachusetts Bay are in Redfield ratios, i.e. 106C:16N:1P (atomic). For silica, it was assumed that the winter diatoms had a carbon to silica ratio of 106C:16Si (atomic) for the winter diatom functional group and a ratio of

106C:4.54Si (atomic) for the summer assemblage functional group (recognizing that only a portion of the summer assemblage is comprised of diatoms).

Once the stoichiometric ratios have been determined, the mass balance equations may be written for the nutrients in much the same way as for the phytoplankton biomass. The principal processes determining the distribution of nutrients among the various pools are: uptake of inorganic nutrients by phytoplankton for cell growth, the release of inorganic and organic nutrients algal respiration and predation processes, and the recycling of organic nutrients to inorganic forms via bacterial hydrolysis and mineralization.

Rather than attempt to model bacterial recycling of organic nutrients by including a bacterial system (for which there are little or no data with which to calibrate against), a phytoplankton-dependent saturated recycle formulation was used. The assumption is made that bacterial biomass, and hence the recycling rate, is proportional to the phytoplankton biomass. A number of field and laboratory studies (Hendry 1977, Lowe 1976, Menon et al 1972, Jewell and McCarty 1971) support this hypothesis. The saturated recycling relationship may be written

$$k(T) = k'(20^{\circ}C)\theta^{(T-20)} \frac{P_c}{K_{mPc} + P_c} \qquad (2\text{-}12)$$

where k(T) is the temperature corrected recycling rate, k'(20°C) is the saturated recycling rate at 20°C, P_c is the phytoplankton biomass, K_{mPc} is the half-saturation constant for recycling, θ is the temperture correction coefficient and C_{NPS} is the concentration of the appropriate nutrient, i.e. nitrogen, phosphorus or silica. Basically, this mechanism employs a first-order recycling that slows the recycling rate if the algal population is small, yet does not permit the recycling rate to increase in an unlimited fashion as phytoplankton biomass increases (instead the mechanism permits zero-order recycling when the phytoplankton greatly exceed the half-saturation constant). The latter assumes that at higher population

levels, other factors are limiting recycling rates or kinetics, so that it proceeds at its maximum zero-order rate.

2.2.3.1 Organic Carbon

Six organic carbon state variables are considered: reactive dissolved organic (ReDOC), labile dissolved (LDOC), refractory dissolved (RDOC), labile particulate (LPOC), refractory particulate (RPOC) and dissolved algal exudate (ExDOC). Reactive, labile and refractory distinctions are based upon the time scale of oxidation or decomposition. Reactive organic carbon decomposes on a time scale of days to a week or two, labile organic carbon decomposes on the time scale of several weeks to a month or two; refactory organic carbon decomposes on the order of months to a year. Reactive and labile organic carbon decompose primarily in the water column or else rapidly in the sediments. Refractory organic carbon decomposes much more slowly, almost entirely in the sediments.

The principal sources of organic carbon are anthropogenic inputs and natural runoff, and detrital algal carbon, which is produced as a result of predation. Zooplankton take up and redistribute algal carbon to the organic carbon pools via grazing, assimilation, respiration and excretion. Since zooplankton are not directly included in the model, the redistribution of algal carbon by zooplankton is simulated by empirical distribution coefficients.

An additional term, representing the excretion of DOC by phytoplankton during photosynthesis, is included in the model. This algal exudate is very reactive and has a time constant similar to the reactive DOC.

The decomposition of organic carbon is assumed to be temperature and bacterial biomass mediated. Since bacterial biomass is not directly included within the model framework, phytoplankton biomass is used a surrogate variable as per Equation 2-11.

2.2.3.2 Phosphorus

The Massachusetts Bay eutrophication model includes five principal phosphorus forms: labile and refractory dissolved organic (LDOP and RDOP, respectively), labile and refactory particulate organic (LPOP and RPOP, respectively), and DIP. Inorganic phosphorus is utilized by phytoplankton for growth and is returned to the various organic and inorganic forms via respiration and predation. A fraction of the phosphorus released during phytoplankton respiration and predation is in the inorganic form and readily available for uptake by other viable algal cells. The remaining fraction released is in the dissolved and particulate organic forms. The organic phosphorus must undergo a mineralization or bacterial decomposition into inorganic phosphorus before it can be used by phytoplankton.

2.2.3.3 Nitrogen

The kinetic structure for nitrogen is similar to that for the phosphorus system. During algal respiration and death, a fraction of the cellular nitrogen is returned to the inorganic pool in the form of NH_3. The remaining fraction is recycled to the dissolved and particulate organic nitrogen pools. Organic nitrogen undergoes a bacterial decomposition, the end-product of which is NH_3. Ammonia nitrogen, in the presence of nitrifying bacteria and oxygen, is converted to nitrite nitrogen and subsequently nitrate nitrogen (nitrification). Both ammonia and nitrate are available for uptake and use in cell growth by phytoplankton; however, for physiological reasons, the preferred form is NH_3.

The process of nitrification in natural waters is carried out by aerobic autotrophs, *Nitrosomonas* and *Nitrobacter*, in particular. It is a two-step process with *Nitrosomonas* bacteria responsible for the conversion of ammonia to nitrite (NO_2) and *Nitrobacter* responsible for the subsequent conversion of nitrite to nitrate (NO_3). Essential to this reaction process are aerobic conditions. In order to reduce the number of state variables required in the modeling framework, it was decided to incorporate nitrite and nitrate together as a single state variable. Therefore, the process of nitrification is assumed to

be approximated by a first-order (with respect to ammonia) reaction rate that is a function of the water column dissolved oxygen concentration and ambient temperature.

Denitrification refers to the reduction of NO_3 (or NO_2) to N_2 and other gaseous products such as N_2O and NO. This process is carried out by a large number of heterotrophic, facultative anaerobes. Under normal aerobic conditions found in the water column, these organisms utilize oxygen to oxidize organic material. However, under the anaerobic conditions found in the sediment bed or during extremely low oxygen conditions in the water column, these organisms are able to use NO_3 as the electron acceptor. The process of denitrification is included in the modeling framework simply as a sink of nitrate. This can always occur in the anaerobic sediment layer. In the water column, however, denitrification should only occur under extremely low dissolved oxygen conditions. This is accomplished computationally by modifying the linear first-order (with respect to nitrite + nitrate) denitrification rate by the expression $K_{NO3}/(K_{NO3} + DO)$. This expression is similar to the Michaelis-Menten expression; for concentrations of dissolved oxygen greater than 1 mg/L, the expression reduces denitrification to near zero, whereas for dissolved oxygen levels less than 0.1 mg/L, this expression permits denitrification to occur.

2.2.3.4 Silica

Two silica state-variables are considered: available (Si) and particulate biogenic (BSi). Available silica is dissolved and is utilized by diatoms during growth for their cell structure. Particulate biogenic silica is produced from diatom respiration and the grazing on diatoms by zooplankton. Particulate biogenic silica undergoes mineralization to available silica or settles to the sediment from the water column.

2.2.3.5 Dissolved Oxygen

A by-product of photosynthetic carbon fixation is the production of dissolved oxygen. The rate of oxygen production and nutrient uptake is proportional to the growth the of the phytoplankton, since its stoichiometry is fixed. An additional source of oxygen

from algal growth occurs when the available ammonia nutrient source is exhausted and the phytoplankton begin to utilize the available nitrate. This additional oxygen source can be seen by comparing Equations 2-13 a and 2-13 b(Morel 1983).

$$106\ CO_2 + 16\ NH_4^+ + H_2PO_4^- + 106\ H_2O \Rightarrow \text{Protoplasm} + 106\ O_2 + 15H^+ \quad (2\text{-}13a)$$

$$106\ CO_2 + 16\ NO_3^- + H_2PO_4^- + 122\ H_2O + 17\ H^+ \Rightarrow \text{Protoplasm} + 138\ O_2 \quad (2\text{-}13b)$$

The above equations present the stoichiometric description of the photosynthetic process assuming ammonium (Equation 2-13a) or nitrate (Equation 2-13b) as the nitrogen source and assuming algal biomass to have Redfield stoichiometry:

$$\text{Biomass} = C_{106}\ H_{263}\ O_{110}\ N_{16}\ P_1 \quad (2\text{-}14)$$

Oxygen-deficient or under-saturated waters are replenished via atmospheric reaeration. The reaeration coefficient is a function of the wind and temperature, and is computed using Equations 2-15 a and 2-15 b:

$$k_a\ (20^oC) = k_L/H \quad (2\text{-}15a)$$

wind

$$k_a(T) = k_a(20^oC)\theta_a^{(T-20)} \quad (2\text{-}15b)$$

temperature

where

k_L = the surface mass transfer coefficient (m/day),

H = depth (m),

and

θ_a = temperature coefficient.

Dissolved oxygen saturation is a function of both temperature and salinity and is determined via Equation 2-16 (Hyer et al., 1971):

$$DO_{sat} = 14.6244 - 0.367134 \bullet T + 0.0044972 \bullet T^2 - 0.0966 \bullet S + 0.00205 \bullet S \bullet T + 0.0002739 \bullet S^2 \quad (2\text{-}16)$$

where S is salinity in ppt.

Dissolved oxygen is diminished in the water column as a result of algal respiration, which is the reverse process of photosynthesis; as a result of nitrification; and as a result of the oxidation of carbonaceous material (including detrital phytoplankton).

2.2.4 Sediment Submodel

An important component of the water column nutrient and dissolved oxygen mass balance equations is the interaction with the sediments. In previous water quality modeling studies the SOD and nutrient fluxes were input as distributed loads. However, there was generally no effort to ensure that the SOD and nutrient fluxes bore any relationship to the delivery of organic material to the sediment. The present sediment submodel corrects that modeling deficiency and effectively closes the mass balance between the water column and the sediment.

The sediment submodel, like the water column portion of the integrated water quality model, is based on the principle of mass balance. As mentioned above the

sediment submodel accounts for the deposition of POM from the overlying water column; the diagenesis or mineralization of the POM in the sediment layer; diffusion and particle mixing transfer of the dissolved and particulate reduced species to the aerobic layer where they can react; the flux of the dissolved end-products back to the overlying water column; and the burial, via sedimentation, of particulate and dissolved species. This is illustrated on Figure 2-2. Details of the sediment mass balance and flux submodel can be found in Appendix B.

2.3 MODEL VALIDATION PROCEDURE

The overall objective of the model validation procedure is to calibrate the water quality model to the observed data, utilizing a set of model coefficients and parameters that are consistent with the observed data and field studies and are within the general ranges of values reported in the literature and accepted by the modeling community. Coincident with this objective is the goal to utilize a set of model coefficients for model validation that are consistent across spatial segments and consistent in time.

The general procedure followed is to perform a series of iterative runs of the model using estimates of the various coefficients and parameters. Comparisons are made between model output and observed data, using computer generated plots in order to make a qualitative assessment of the model's goodness of fit. This process continues through the adjustment or tuning of the model parameters until a reasonable reproduction of the observed data is attained or no further improvement is possible.

Section 4.0 provides the details of the calibration effort and presents model versus data comparisons for the final calibration run.

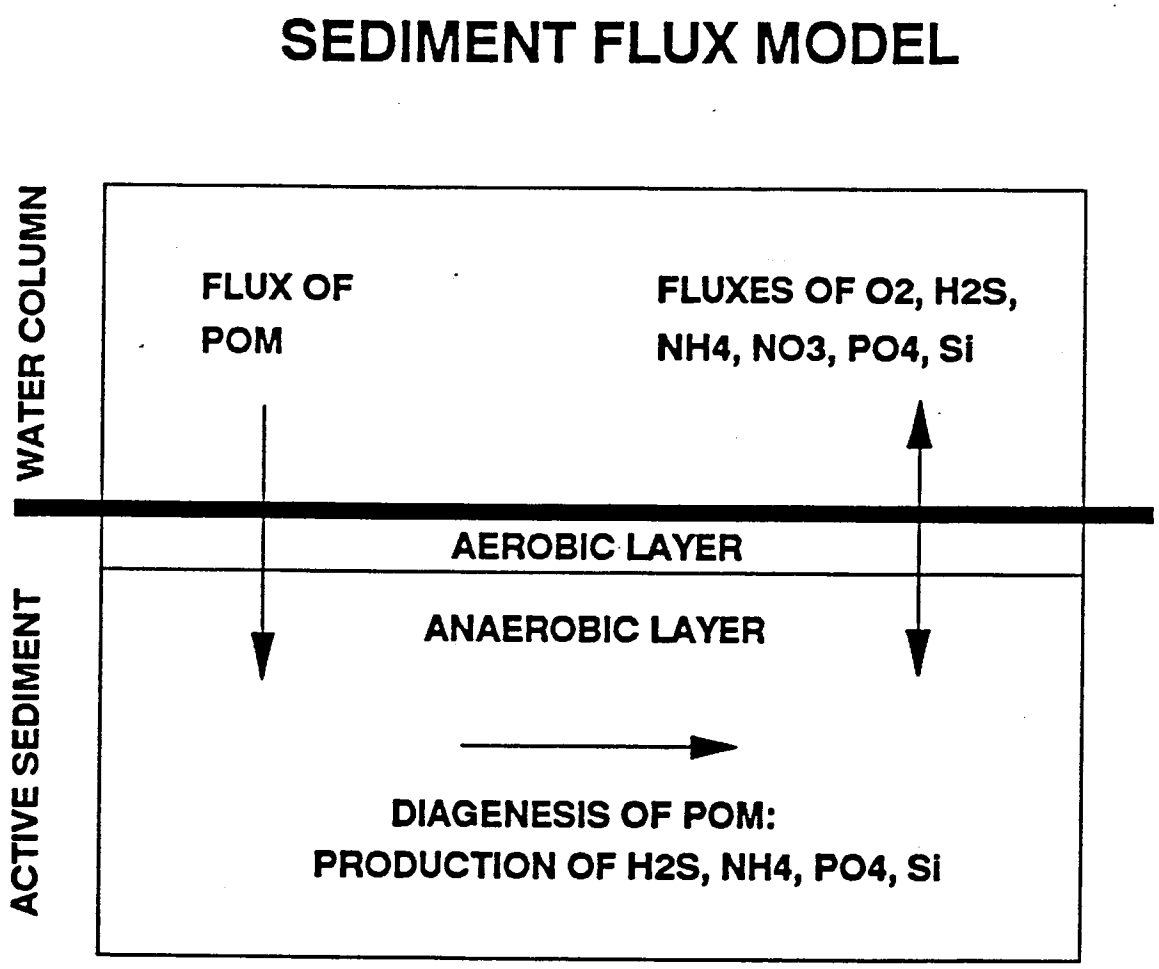

FIGURE 2-2

GENERAL STRUCTURE OF SEDIMENT FLUX MODEL

SECTION 3

POLLUTANT LOADINGS

3.1 INTRODUCTION

This section provides a review and summary of the principal inputs of nutrients and oxygen demanding material to Massachusetts Bay and Cape Cod Bay. These inputs are comprised of:

- municipal and industrial wastewater treatment plant discharges;
- combined sewer overflow loadings;
- nonpoint source loadings from study area rainfall runoff;
- river loadings;
- groundwater loadings, and
- atmospheric loadings falling directly on the water surface.

A further source of nutrients is dispersive and advective exchange from the Gulf of Maine. Without the necessary hydrodynamics this source could not be accurately modeled. No attempt to quantify this source was made. Boundary conditions and available hydrodynamics were used to represent this source of nutrients and its effect on Massachusetts and Cape Cod Bays.

The majority of the loading information used in this study was obtained from the Menzie-Cura & Associates (1991) report to the Massachusetts Bays Program. This report detailed sources and magnitudes of pollutants delivered to Massachusetts Bay and Cape Cod Bay including total nitrogen (TN), total phosphorus (TP), and biochemical oxygen demand (BOD). Model required loadings of total organic carbon (TOC) were derived using the Menzie-Cura estimates of BOD loading and an empirical TOC:BOD relationship developed by HydroQual (1991) for the Long Island Sound Study. Model required silica loadings were estimated using treatment plant flow information and estimates of silica

concentrations in wastewater effluent obtained from literature references (Coupe and Webb 1983, WEF and ASCE 1991).

Menzie-Cura developed pollutant loading estimates for the following sources: municipal and industrial treatment facilities, coastal runoff/CSOs, river discharge, groundwater, and atmospheric. The drainage area of Massachusetts Bays was divided into five basins (Merrimack River, North Shore, Boston Harbor, South Shore and Cape Cod) and annual loadings were determined for each basin.

3.2 POINT SOURCE INPUTS

Point source inputs from municipal and industrial sewage treatment facilities are the major source of nutrients and oxygen demanding material delivered to Massachusetts Bay and Cape Cod Bay. The Menzie-Cura reported provided estimates of point source nutrients in the form of TN and TP. The water quality model, however, requires information concerning the various forms of N and P; for example, organic versus inorganic, and dissolved versus particulate. For nitrogen the model requires estimates for ammonium, nitrite + nitrate, refractory particulate organic nitrogen (RPON), labile particulate organic nitrogen (LPON), refractory dissolved organic nitrogen (RDON) and labile dissolved organic nitrogen (LDON). Labile and refractory refer to the reactivity of the organic nutrient form; labile materials undergo hydrolysis and mineralizaton at a faster rate than refractory materials. Similarly, for phosphorus the model requires estimates for dissolved inorganic phosphorus (or ortho-phosphate-PO_4), refractory particulate organic phosphorus (RPOP), labile particulate organic phosphorus (LPOP), refractory dissolved organic phosphorus (RDOP) and labile dissolved organic phosphorus (LDOP). Limited information concerning the component forms of nitrogen and phosphorus was available from MWRA (monthly grab samples of treated effluent and waste sludge) and the Metcalf and Eddy pilot plant study (Metcalf and Eddy, 1990). Therefore, information from the literature (WEF and ASCE, 1991) and previous water quality modeling studies (HydroQual 1987, USA COE 1992) was used to guide the selection of the various nutrient splits.

The water quality model also requires estimates of organic carbon loadings. Since direct measurements of organic carbon were not available, it was necessary to estimate the organic carbon loadings using two methods. For wastewater treatment plants and CSOs, estimates were made using the Menzie-Cura estimates of BOD concentrations and an empirical TOC:BOD formula developed using New York City treatment plant data. For rivers and nonpoint urban runoff, loading estimates were made using ratios of TOC to BOD observed in other water quality studies. After TOC loads were computed, these loading estimates were partitioned into various carbon forms. The carbon forms included dissolved and particulate, and labile and refractory classes, similar to nitrogen and phosphorus, as well as a reactive dissolved form representing very reactive or available organic carbon associated with primary treated effluents.

Table 3-1 provides a listing of the various fractions of total nutrient apportioned to each functional form.

3.2.1 Municipal and Industrial Sewage Treatment Plants

The majority of the nutrient loads delivered to Massachusetts Bay emanate from municipal wastewater treatment plants; the contribution from industrial plants is minor. Therefore, all NPDES nutrient fractions were assigned using municipal plant splits. As can be seen in Table 3-1, the MWRA wastewater treatment facilities were assigned different nutrient splits than the other facilities. This is due to the fact that the MWRA facilities provide only primary treatment at the present time, whereas the other facilities provide secondary treatment. Secondary treatment provides a greater degree of wastewater treatment using biological means to remove pollutants from the wastewater stream. This explains why there is a smaller organic fraction in the secondary plants effluent. This also explains why nitrite and nitrate are observed in the secondary treatment plant effluent; some degree of nitrification is occurring.

As mentioned above, estimates of TOC loadings for the treatment plants were calculated by using an empirical formula based on paired measurements of BOD_5 and TOC

TABLE 3-1. NUTRIENT EFFLUENT FRACTIONS AND CONCENTRATIONS USED TO ESTIMATE POLLUTANT LOADINGS TO MASSACHUSETTS AND CAPE COD BAYS

Nitrogen

Source	NH4	NO23	LPON	RPON	LDON	RDON	Total N Load (kg/day)
Boston Harbor WTP	0.65	0.00	0.14	0.14	0.035	0.035	31,233
Other WTP	0.70	0.10	0.08	0.08	0.02	0.02	6,107
CSOs and Coastal Runoff	0.60	0.00	0.16	0.16	0.04	0.04	1,151
Riverine	0.10	0.55	0.14	0.14	0.035	0.035	2,435
Groundwater	0.00	1.00	0.00	0.00	0.00	0.00	925

Phosphorus

Source	PO4	LPOP	RPOP	LDOP	RDOP	Total P Load (kg/day)
Boston Harbor WTP	0.50	0.275	0.15	0.05	0.025	7,041
Other WTP	0.85	0.0825	0.045	0.015	0.0075	489
CSOs and Coastal Runoff	0.50	0.275	0.15	0.05	0.025	41
Riverine	0.40	0.33	0.18	0.06	0.03	48
Groundwater	No phosphorus load associated with groundwater					0

TABLE 3-1. NUTRIENT EFFLUENT FRACTIONS AND CONCENTRATIONS USED TO ESTIMATE POLLUTANT LOADINGS TO MASSACHUSETTS AND CAPE COD BAYS
(continued)

Carbon: TOC = $.7 \bullet BOD_5 + 18$

Source	ReDOC	RPOC	LPOC	RDOC	LDOC	Total TOC Load (kg/day)
Boston Harbor WTP	$0.37 \bullet BOD_5$	9mg/L	$0.33 \bullet BOD_5$	9 mg/L	-	206,634
Other WTP	$0.1 \bullet BOD_5$	9 mg/L	$0.6 \bullet BOD_5$	9 mg/L	-	72,047
CSOs	$0.6 \bullet BOD_5$	9 mg/L	$0.1 \bullet BOD_5$	9 mg/L	-	24,709
Riverine	-	$0.2 \bullet BOD_5$	$0.3 \bullet BOD_5$	$0.2 \bullet BOD_5$	$0.3 \bullet BOD_5$	13,280
Urban Runoff	-	$1.28 \bullet BOD_5$	-	$0.22 \bullet BOD_5$	-	11,692
Non-Urban Runoff	-	$0.75 \bullet BOD_5$	-	$0.75 \bullet BOD_5$	-	71
Groundwater	No carbon load associated with groundwater					0

from a number of primary and secondary treatment plants in New York City. A regression analysis using these data resulted in equation 3-1:

$$TOC = 0.7 \bullet BOD_5 + 18 \text{ (mg C/L)} \quad (3\text{-}1)$$

For the MWRA facilities the majority of the TOC was assigned to the reactive dissolved organic carbon (ReDOC) pool recognizing that this fraction is removed via secondary treatment but not primary treatment. Also for the MWRA TOC load, 40 percent of the TOC was assigned to the labile particulate organic carbon (LPOC) pool recognizing that there is a high organic carbon content associated with the high suspended solids concentrations in the effluents from primary treatment plants. The y-intercept of the TOC:BOD equation (18 mg/L) was assumed to represent the refractory portion of the organic carbon pool.

Nitrogen and phosphorus were split into their respective inorganic and particulate and dissolved organic fractions guided by WEF and ASCE (1991) and previous studies conducted on Chesapeake Bay and Long Island Sound.

Estimates of silica loadings were not available from the Menzie-Cura report. Therefore, silica loadings were estimated as the product of treatment plant flows and an assumed silica concentration of 12.5 mg/L (as guided by Coupe and Webb 1983, WEF and ASCE 1991).

3.2.2 Combined Sewer Overflows

Menzie-Cura provided estimates of the CSO loadings for the five drainage areas. Cape Cod and the South Shore have no CSO loadings. The splits for nitrogen, phosphorus and carbon are presented in Table 3-1. The fractions used to partition nutrient loads for CSOs are similar to those used for the MWRA treatment plants i.e. assumed similar to primary treated effluents.

3.3 RIVER DISCHARGE

Estimates of river discharge loadings were obtained from Menzie-Cura (1991). The fractional splits assigned for each constituent are shown in Table 3-1. No Merrimack River loading was included directly in the model as the river is outside of the coarse-grid model domain. However, the Merrimack River load can influence the model indirectly as a component of the boundary conditions at Cape Ann. The fractional splits used for nitrogen reflect the fact that nitrification is occurring in the rivers, thus converting ammonia to nitrate. Lower inorganic phosphorus fractions are attributed to algal uptake and conversion to organic phosphorus in algal cells. The distribution of carbon is split evenly between the dissolved and particulate fractions. The lack of reactive dissolved organic carbon (ReDOC) in the riverine sources is due to the assumption that all ReDOC would have undergone biological oxidation within the river by the time it flows into the Bay system.

3.4 NONPOINT SOURCES

3.4.1 Coastal Runoff

Nonpoint source inputs are associated with rainfall runoff from separate sewer systems in urban areas and from land runoff in non-urban areas which are unsewered. Estimates of these loadings were obtained from the Menzie-Cura report. These nutrient sources have a high nitrate fraction due to the nitrification occurring in the soil layer and a low phosphate fraction due to adsorption to soil particles. All of the organic carbon in the runoff has been assigned to the refractory pool assuming little or no export of labile organic carbon occurs from this source.

3.4.2 Groundwater

Groundwater loadings were estimated for only the Boston Harbor and Cape Cod drainage basins by Menzie-Cura. On a Bay-wide basis groundwater contributes only a small portion of the nitrogen. However, in the Cape Cod region, groundwater is a major contributor of nitrogen. There were no carbon or phosphorus loads included with

groundwater due to their omission in the Menzie-Cura report. All groundwater nitrogen loadings were assigned to the nitrate fraction.

3.5 ATMOSPHERIC INPUTS

Deposition of dryfall and wetfall nitrogen, phosphorus, and carbon resulting from direct impingement to the surface waters of Massachusetts Bay are included as atmospheric inputs. To estimate dryfall deposition, atmospheric concentrations of inorganic nitrogen and phosphorus and their associated dryfall deposition velocities were taken from the Menzie-Cura report. Using this information together with the surface area of the model domain, dryfall loadings were estimated. Similarly, for wetfall loading estimates, observations of inorganic phosphorus and nitrogen concentrations in precipitation were used together with average monthly rainfall for 1989 through 1991 observed at Logan Airport. To account for atmospheric sources of organic nitrogen, phosphorus and carbon, data from the Long Island Sound Study were used. No estimates of organic carbon dryfall were made. The concentrations for each pollutant used to estimate dryfall and wetfall loads can be found in Table 3-2. The observed average monthly rainfall is shown in Table 3-3.

3.6 SUMMARY

Massachusetts Bay receives pollutants from many sources around its perimeter. Boston Harbor, and in particular the MWRA facilities, dominate the loadings of nitrogen, phosphorus, and carbon to the Bay. In Figure 3-1, the relative contributions from each source of nitrogen, phosphorus and organic carbon are compared. Estimates of the Merrimack River loads were included only for reference purposes and as noted above these loadings were not included directly in the model.

Figure 3-1 shows that the Deer and Nut Island treatment plants are the major contributors of nutrients to the Bay. The other municipal discharges, however, also contribute a significant portion of the loading. Runoff, CSOs, groundwater, river discharge,

TABLE 3-2. WET FALL NUTRIENT CONCENTRATIONS AND AREAL DRY FALL RATES USED TO ESTIMATE ATMOSPHERIC LOADINGS

Constituent	Wetfall (ug/L)	Dryfall* (mg/m2-yr)
NH4	98.	49.22
NO3	242.	121.98
LDON	116.	42.80
PO4	3.88	1.34
LDOP	3.17	1.10
LDOC	1300.	-

*Menzie-Cura, 1991

TABLE 3-3. MONTHLY AVERAGE RAINFALL AT LOGAN AIRPORT FOR CALIBRATION PERIOD

Month	Rainfall (in./month)
January	2.54
February	2.55
March	3.04
April	4.80
May	3.66
June	2.13
July	3.72
August	5.92
September	4.20
October	4.74
November	4.02
December	1.67

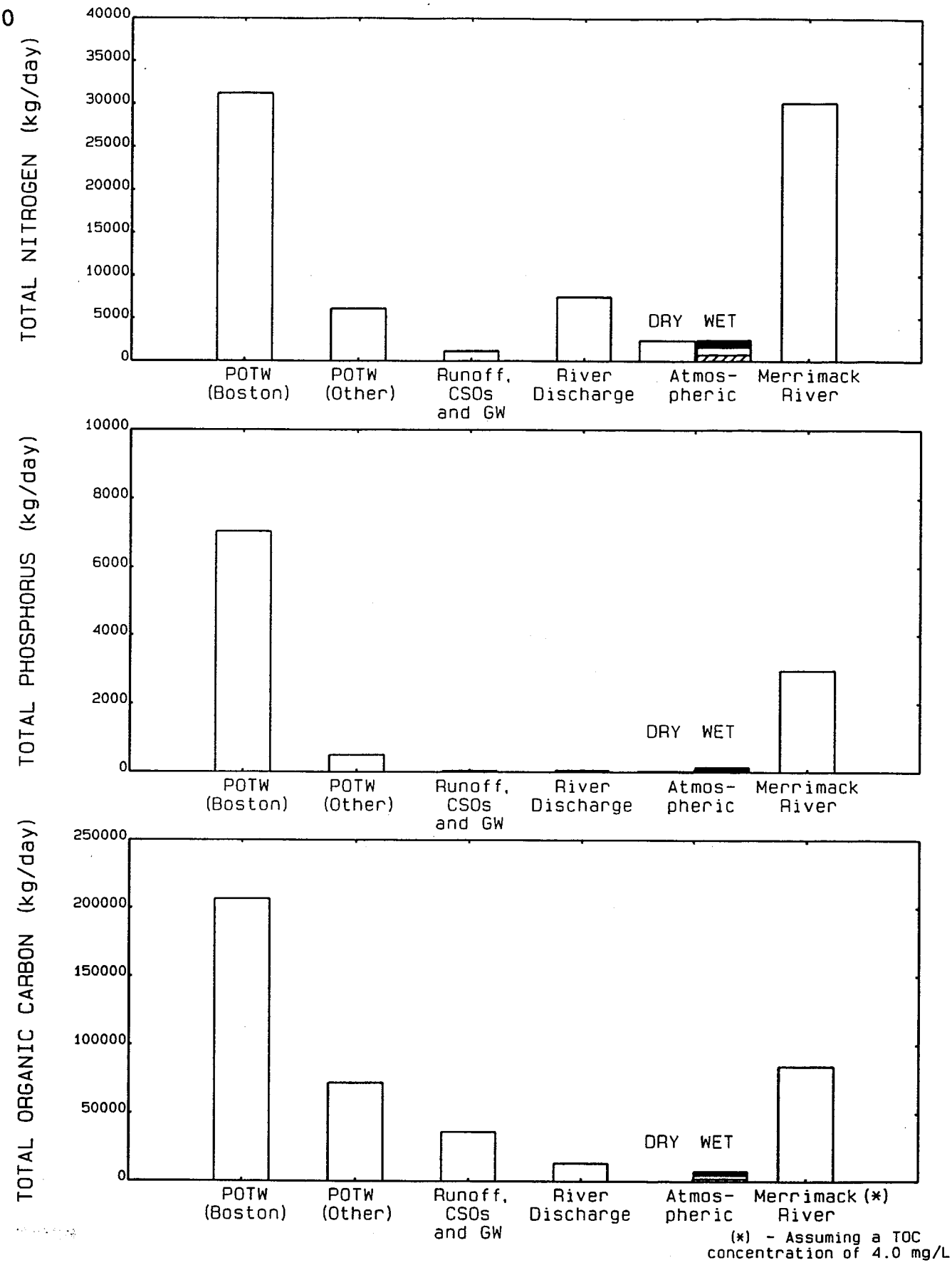

Figure 3-1

Relative Contribution of Nutrient Loadings to Massachusetts Bay and Cape Cod Bay by Source for the Calibration Period

Merrimack River included for comparison

and atmospheric deposition make up the remainder of the loading. The three shadings for the wetfall atmospheric loadings represent the maximum, mean, and minimum estimated loadings for the calibration period. Atmospheric wetfall loading is the only load that was changed on a monthly basis for the model simulation, due to available information concerning the variability of monthly rainfall.

The Massachusetts Bay water quality model requires loadings of dissolved and particulate forms of nitrogen, phosphorus, and silica as well as reactive classes of dissolved and particulate organic carbon. Loadings for the model were based on an analysis performed by Menzie-Cura for the Massachusetts Bays Program. The analysis included the Merrimack River, North Shore, Boston Harbor, South Shore, and Cape Cod drainage areas. These loadings were then assigned by HydroQual into the relevant pools for each nutrient. Loadings were assumed constant for the entire model simulation for municipal and industrial treatment plants, river discharge, CSOs, groundwater, rainfall runoff, and dry fall atmospheric deposition. Wet fall atmospheric deposition, however, was varied monthly utilizing available average monthly rainfall data.

Although all drainage areas contribute to the nitrogen, phosphorus and carbon loadings to Massachusetts Bay, the Boston Harbor drainage area contributes the majority of the loading. The Nut and Deer Island treatment plants are the major source of nutrients in the Boston Harbor drainage area.

SECTION 4

MODEL CALIBRATION

4.1 INTRODUCTION

General information concerning the Massachusetts Bay study area, kinetic structure of the water quality model, and estimated nutrient loadings has been presented in the previous sections. This section will present a summary of the application of the water quality model to Massachusetts Bay and its calibration against observed water column and sediment data. It should be noted in advance that this calibration effort was very preliminary in scope and effort. The purpose of this Phase 1 study effort was to apply a modeling framework that had been developed for the Chesapeake Bay system and Long Island Sound and determine its suitability for use in understanding the eutrophication processes in Massachusetts Bay. Coincident with this objective was the desire to identify water column processes unique to Massachusetts Bay, which would require modification of the modeling framework, and to identify data gaps or needs for model calibration, which could be filled by additional sampling or special studies as part of the overall water quality monitoring effort.

The calibration results presented below are the result of some 20 model runs, which were made to obtain a consistent set of model coefficients that are reasonable and that reproduce the observed data for all state-variables considered. With the exception of exogenous variables such as surface water temperature, solar radiation, and extinction coefficients, all biological and chemical model coefficients were constant for the 18 month calibration period. The method employed in determining the values of the model coefficients is essentially one of trial and error. The starting point was a set of model coefficients which had been developed for the Long Island Sound and Chesapeake Bay studies.

4.2 MODEL GRID

Information concerning the model geometry was obtained from a parallel modeling effort being conducted by a United States Geological Survey (USGS) study team at Woods Hole. This parallel effort is concerned with the development of a time-variable 3-D hydrodynamic model of the Massachusetts Bays system. The hydrodynamic model includes Boston Harbor, Massachusetts Bay, and Cape Cod Bay, and extends out into the Gulf of Maine. The hydrodynamic grid (presented on Figure 4-1) has a resolution which varies from 0.6 to 2 km within Massachusetts and Cape Cod Bays to approximately 6 km near the open ocean boundary, and has 10 vertical layers. This type of resolution is known as a fine-grid model. Figure 4-1 shows only the active water segments; land segments were omitted.

Use of this fine a grid resolution in water quality simulations can be computationally prohibitive, since the kinetics used in the water quality model contain so many state-variables and since a large number of simulations are required in order to calibrate the model. Therefore, for this initial calibration effort a very coarse-grid implementation of the hydrodynamic grid was utilized. The coarse-grid was created in two ways. First, a number of hydrodynamic model segments were aggregated into one water quality segment. Secondly, the outer boundary for the coarse-grid version of the water quality model was chosen to extend from Cape Ann on the north to Cape Cod on the south and therefore excluded that part of the Gulf of Maine included in the hydrodynamic model. Figure 4-2 presents the coarse-grid realization of the Massachusetts Bays study area (with the segment numbers of the surface layer segments noted on the grid).

The water quality model consists of a 4x8 horizontal grid, with a resolution of 10 to 15 km. There are 5 layers in the vertical plane, for a total of 160 model segments (as compared with almost 50,000 segments for the hydrodynamic model). In performing the water quality model grid aggregation the depth of each of the aggregated water quality model segments was the surface-area weighted average depth of the hydrodynamic model segments that comprise the aggregated water quality model segment. The advective

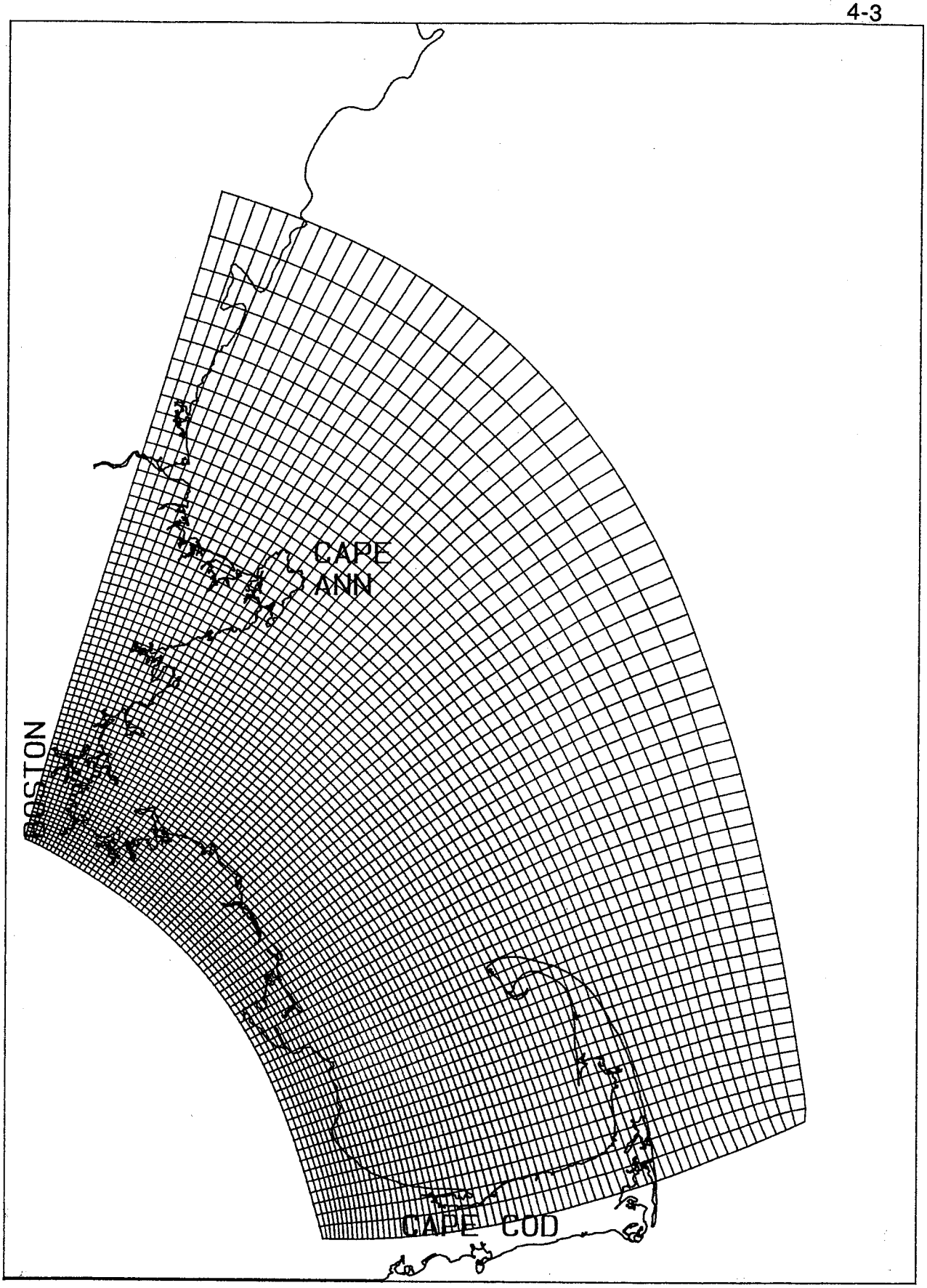

Figure 4-1

Hydrodynamic Model Grid for Massachusetts Bay

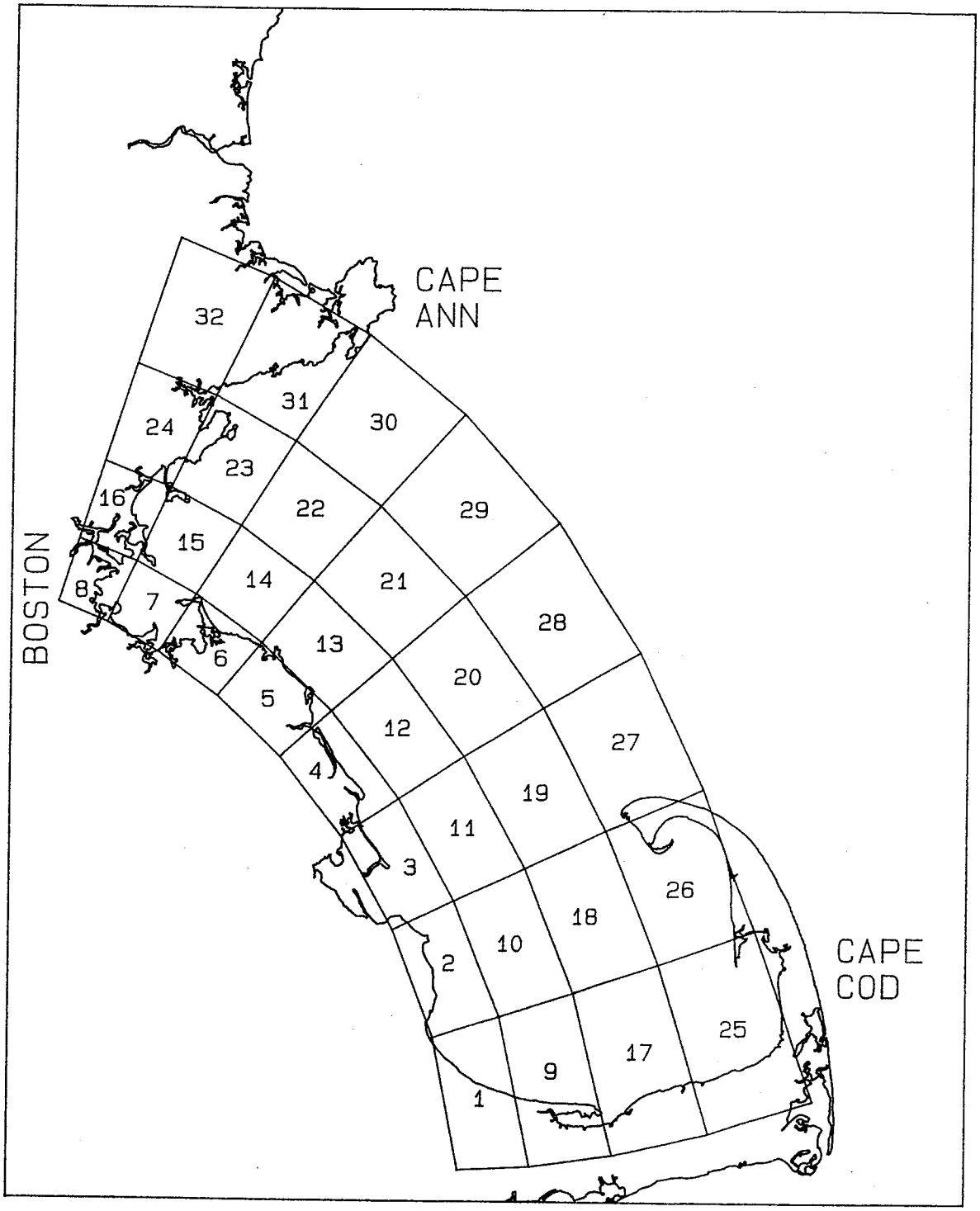

Figure 4-2

Coarse Water Quality Grid for Massachusetts Bay and Surface Layer Segment Numbers

components of the transport for the water quality model segment were determined as the sum of the flows across each of the hydrodynamic interfaces comprising the aggregated water quality model segment.

4.3 AVAILABLE DATA

As has been pointed out earlier there exists a water quality data base with which to calibrate the water quality model of Massachusetts Bay. These data were collected by the Bigelow Laboratory for Ocean Sciences and a joint University of Massachusetts at Boston/Woods Hole Oceanographic Institution/University of New Hampshire (UMB/WHOI/UNH) team. These data were obtained during a series of synoptic cruises extending from October 1989 through April 1991. Data from the Bigelow cruises are restricted to the northern portion of Massachusetts Bay, while the UMB/WHOI/UNH data cover a more extensive geographical area, including Cape Cod Bay and a portion of the Gulf of Maine. Figure 4-3 shows the locations of the Bigelow stations, while Figures 4-4 and 4-5 show the locations of the UMB/WHOI/UNH cruises. Table 4-1 presents the dates, investigators, and spatial extent of the water quality sampling cruises used for the calibration study.

Data were collected only for a limited number of water quality parameters, the principal of which were: salinity, temperature, dissolved oxygen, light extinction, ammonia nitrogen, nitrite + nitrate nitrogen, dissolved inorganic phosphorus (DIP) or ortho-phosphate, dissolved silica, particulate organic carbon (POC), phytoplankton chlorophyll-a (chl-a) and primary productivity. Vertical casts were made to measure salinity, temperature and chlorophyll fluorescence; the remaining parameters were sampled at a limited number of depths.

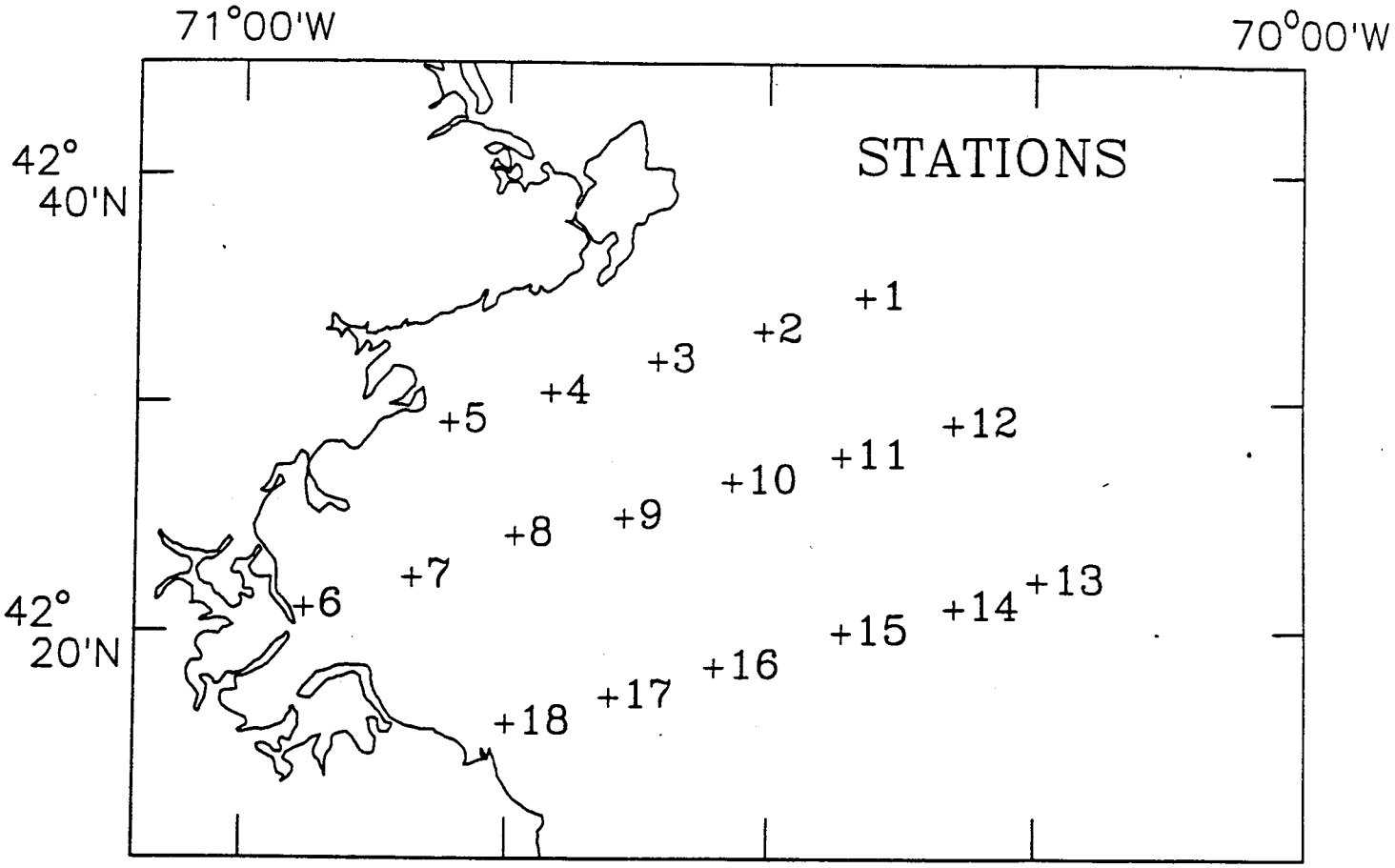

FIGURE 4-3. STATION LOCATIONS FOR BIGELOW CRUISES

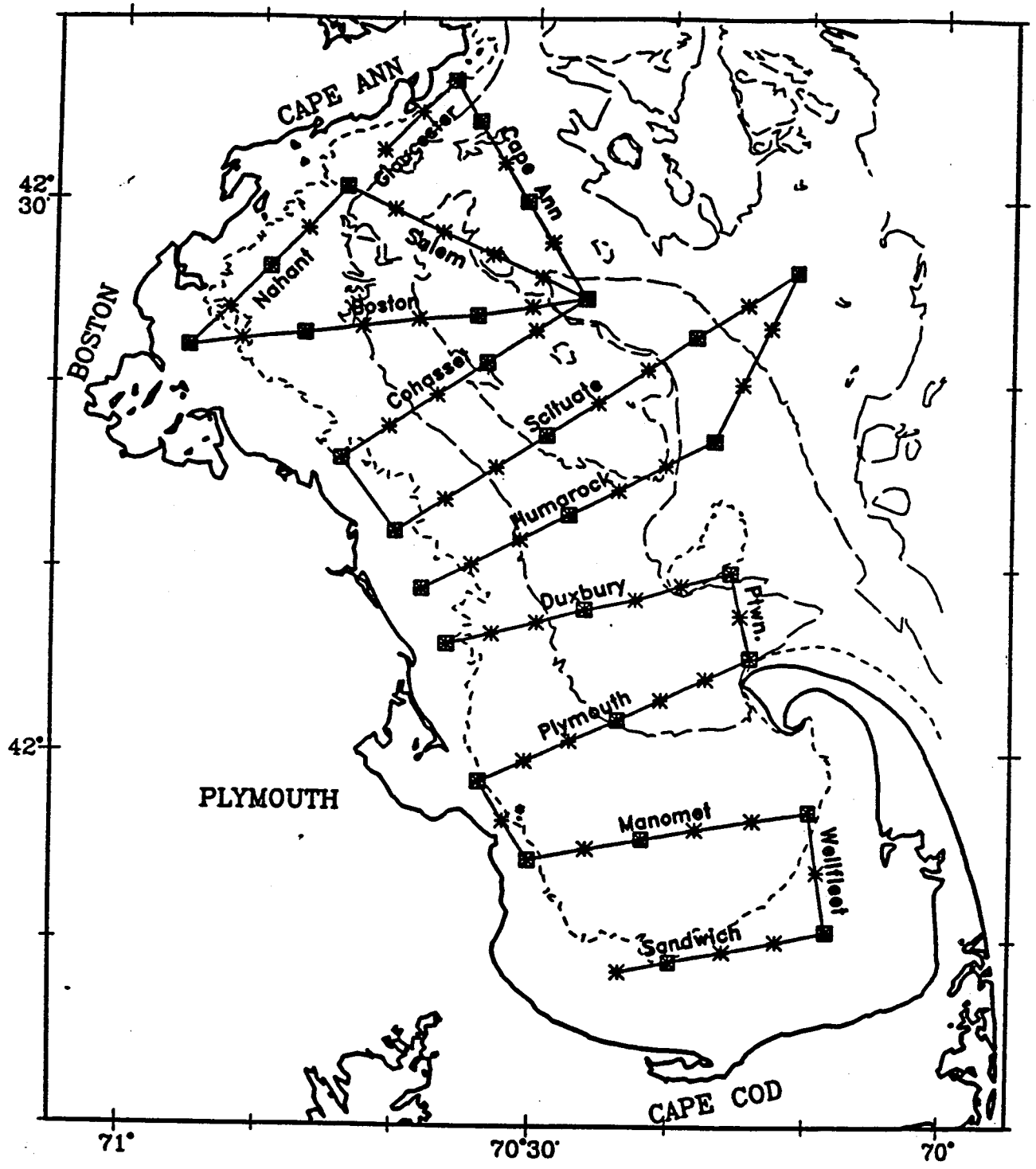

FIGURE 4-4. CRUISE TRACK FOR THE FIRST THREE SEASONAL CRUISES CONDUCTED BY WHOI/UMB

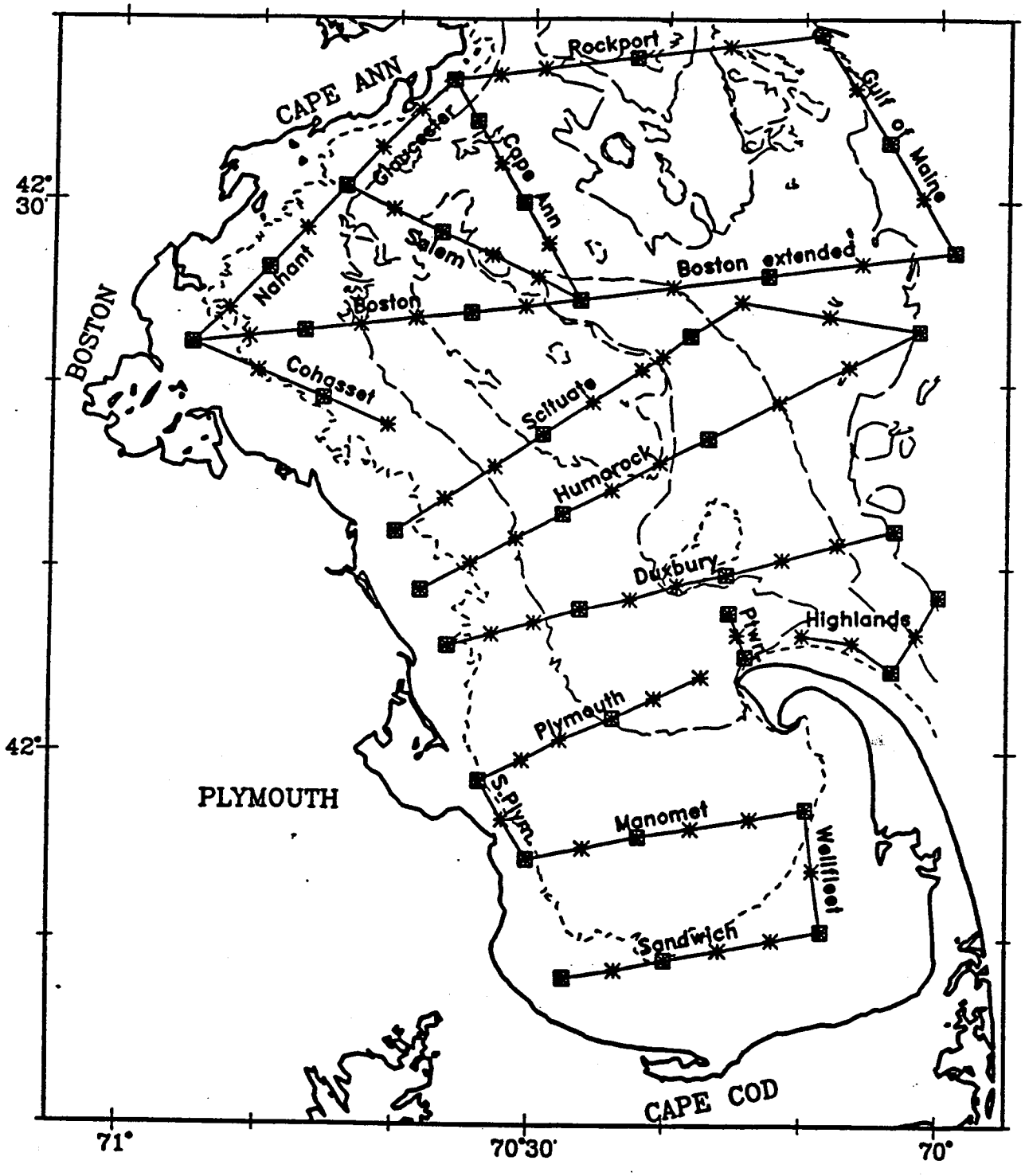

FIGURE 4-5. CRUISE TRACK FOR FINAL THREE SEASONAL CRUISES CONDUCTED BY WHOI/UMB

TABLE 4-1. MONTH FOR WHICH NUTRIENT DATA ARE AVAILABLE AND THE ORGANIZATION THAT COLLECTED THE DATA

		Station Location	
Year	Month	North Bay	South Bay
1989	October	B	
	November		
	December		
1990	January		
	February	B	
	March	B	
	April	B/U	U
	May		
	June	B	
	July	U	U
	August	B	
	September		
	October	U	
	November		
	December		
1991	January		
	February	U	U
	March	U	U
	April	U	U

B - Bigelow Laboratory for Ocean Science
U - University of Massachusetts - Boston

4.4 MODEL INPUTS

4.4.1 Boundary Conditions

The flow entering or leaving the Massachusetts Bays system from the Gulf of Maine carries with it phytoplankton, nutrients, organic carbon and dissolved oxygen. These mass fluxes may be a substantial source or sink of material to the Bays. This is an important consideration in terms of the importance of the present and expected load from metropolitan Boston. Therefore, considerable attention was made to correlate the concentrations of the various water quality state-variables to time of year. Efforts were also made to discern if there were spatial patterns to be found in the boundary data. However, lack of comprehensive spatial data precluded this determination. Therefore, the same boundary concentrations were used along the entire boundary from Cape Ann to Cape Cod. However, observed vertical gradients in water quality constituents were included in the specification of the boundary conditions.

It was not possible to discern an annual cycle in the boundary bottom water concentrations of the various water quality parameters, with the exception of salinity, temperature and dissolved oxygen. For surface waters, however, there appeared to be a seasonal cycle, with higher concentrations of phytoplankton chl-a and POC, accompanied by lowered concentrations of dissolved inorganic nitrogen (DIN), DIP and dissolved silica, in the spring, through summer and into early fall. The late fall and winter period were marked with lowered concentrations of chl-a and POC and increased concentrations of DIN, DIP and dissolved silica. Table 4-2 presents a tabulation of the concentrations used to specify the boundary conditions for the calibration period. (Note: For the phytoplankton functional groups there is some seasonal overlap, during the transitional periods between summer and winter (i.e., October/November) and winter and summer (i.e., May).

4.4.2 Extinction Coefficients

Water column transparency and, therefore, the extinction coefficient, plays an important role in primary productivity. Phytoplankton primary productivity is greater in

TABLE 4-2. OUTER BOUNDARY CONDITIONS USED FOR CALIBRATION

State-Variable	Dates	Above Pycnocline	Below Pycnocline	Units
Salinity	Oct 89 - Jan 90	32.00	33.00	ppt
	Feb 90	32.50	33.00	
	Mar 90 - Apr 90	32.00	33.00	
	May 90 - Jun 90	31.50	33.00	
	Jul 90 - Sep 90	31.50	32.50	
	Oct 90 - Feb 91	32.50	32.50	
	Mar 91	32.50	33.00	
	Apr 91	32.00	32.50	
Temperature	Oct 89	10.50	9.25	°C
	Nov 89	8.75	8.00	
	Dec 89	7.00	6.50	
	Jan 90	5.75	5.25	
	Feb 90	3.25	4.00	
	Mar 90	3.50	3.50	
	Apr 90	3.75	3.00	
	May 90	6.50	3.75	
	Jun 90	9.00	4.50	
	Jul 90	10.50	5.50	
	Aug 90	12.50	6.00	
	Sep 90	12.50	7.25	
	Oct 90	12.50	8.75	
	Nov 90	9.50	7.75	
	Dec 90	8.00	6.75	
	Jan 91	6.00	6.00	
	Feb 91 - Mar 91	4.00	4.00	
	Apr 91	5.75	4.00	
Winter Diatoms	Oct 89	0.40	0.15	µg/L chlorophyll
	Nov 89	0.75	0.30	
	Dec 89 - Apr 90	1.50	0.60	
	May 90	0.75	0.30	
	Jun 90 - Sep 90	0.00	0.00	
	Oct 90	0.40	0.15	
	Nov 90	0.75	0.30	
	Dec 90 - Apr 91	1.50	0.60	
Summer Assemblage	Oct 89	1.00	0.30	µg/L chlorophyll
	Nov 89	0.50	0.10	
	Dec 89 - Apr 90	0.00	0.00	
	May 90	1.00	0.30	
	Jun 90 - Sep 90	2.00	0.60	
	Oct 90	1.00	0.30	

TABLE 4-2. OUTER BOUNDARY CONDITIONS USED FOR CALIBRATION
(continued)

State-Variable	Dates	Above Pycnocline	Below Pycnocline	Units
	Nov 90	0.50	0.10	
	Dec 90 - Apr 91	0.00	0.00	
Carbon:				
LPOC	Oct 89	0.025	0.015	mg C/L
	Nov 89	0.022	0.014	
	Dec 89	0.019	0.013	
	Jan 90	0.016	0.012	
	Feb 90	0.015	0.010	
	Mar 90	0.010	0.025	
	Apr 90	0.050	0.040	
	May 90	0.055	0.040	
	Jun 90	0.060	0.040	
	Jul 90	0.050	0.045	
	Aug 90	0.040	0.050	
	Sep 90	0.032	0.032	
	Oct 90	0.025	0.015	
	Nov 90	0.022	0.014	
	Dec 90	0.019	0.013	
	Jan 91	0.016	0.012	
	Feb 91	0.015	0.010	
	Mar 91	0.010	0.025	
	Apr 91	0.050	0.040	
RPOC	Oct 89 - Apr 91	0.12	0.12	mg C/L
LDOC	Oct 89 - Apr 91	0.20	0.20	mg C/L
RDOC	Oct 89 - Apr 91	1.50	1.50	mg C/L
ReDOC	Oct 89 - Apr 91	0.00	0.00	mg C/L
ExDOC	Oct 89 - Apr 91	0.00	0.00	mg C/L
Phosphorus:				
LPOP	Oct 89 - Apr 91	0.0025	0.0025	mg P/L
RPOP	Oct 89 - Apr 91	0.00025	0.00025	mg P/L
LDOP	Oct 89 - Apr 91	0.01	0.01	mg P/L
RDOP	Oct 89 - Apr 91	0.001	0.001	mg P/L

TABLE 4-2. OUTER BOUNDARY CONDITIONS USED FOR CALIBRATION
(continued)

State-Variable	Dates	Above Pycnocline	Below Pycnocline	Units
DIP	Oct 89	0.024	0.030	mg P/L
	Nov 89	0.028	0.032	
	Dec 89	0.032	0.034	
	Jan 90	0.036	0.036	
	Feb 90	0.040	0.040	
	Mar 90	0.030	0.037	
	Apr 90	0.012	0.035	
	May 90	0.005	0.032	
	Jun 90	0.005	0.030	
	Jul 90 - Sep 90	0.005	0.035	
	Oct 90	0.012	0.035	
	Nov 90	0.015	0.034	
	Dec 90	0.018	0.033	
	Jan 91	0.021	0.032	
	Feb 91	0.025	0.030	
	Mar 91	0.020	0.030	
	Apr 91	0.008	0.025	
Nitrogen:				
LPON	Oct 89 - Nov 89	0.004	0.002	mg N/L
	Dec 89 - Jan 90	0.003	0.002	
	Feb 90	0.002	0.002	
	Mar 90	0.002	0.004	
	Apr 90	0.008	0.007	
	May 90	0.009	0.007	
	Jun 90	0.010	0.007	
	Jul 90	0.008	0.008	
	Aug 90	0.007	0.008	
	Sep 90	0.005	0.005	
	Oct 90 - Nov 90	0.004	0.002	
	Dec 90 - Jan 91	0.003	0.002	
	Feb 91	0.002	0.002	
	Mar 91	0.002	0.004	
	Apr 91	0.008	0.007	
RPON	Oct 89 - Apr 91	0.02	0.02	mg N/L
LDON	Oct 89 - Apr 91	0.07	0.07	mg N/L
RDON	Oct 89 - Apr 91	0.07	0.07	mg N/L

TABLE 4-2. OUTER BOUNDARY CONDITIONS USED FOR CALIBRATION
(continued)

State-Variable	Dates	Above Pycnocline	Below Pycnocline	Units
NH3	Oct 89 -Feb 90	0.010	0.010	mg N/L
	Mar 90	0.015	0.025	
	Apr 90	0.020	0.040	
	May 90	0.015	0.035	
	Jun 90	0.010	0.030	
	Jul 90	0.010	0.040	
	Aug 90 - Sep 90	0.005	0.012	
	Oct 90	0.005	0.008	
	Nov 90	0.005	0.007	
	Dec 90	0.005	0.006	
	Jan 91 - Feb 91	0.005	0.005	
	Mar 91	0.008	0.015	
	Apr 91	0.015	0.030	
NO2 + NO3	Oct 89	0.040	0.125	mg N/L
	Nov 89	0.050	0.125	
	Dec 89	0.060	0.125	
	Jan 90	0.070	0.125	
	Feb 90	0.080	0.125	
	Mar 90	0.060	0.100	
	Apr 90	0.040	0.100	
	May 90	0.027	0.100	
	Jun 90	0.015	0.100	
	Jul 90	0.015	0.125	
	Aug 90 - Oct 90	0.010	0.125	
	Nov 90	0.011	0.125	
	Dec 90	0.012	0.125	
	Jan 91	0.013	0.125	
	Feb 91	0.015	0.125	
	Mar 91 - Apr 91	0.010	0.100	
Silica:				
BSi	Oct 89 - Apr 91	0.1	0.1	mg Si/L
Si	Oct 89 - May 90	0.175	0.25	mg Si/L
	Jun 90 - Nov 90	0.065	0.25	
	Dec 90 - Apr 91	0.175	0.25	

TABLE 4-2. OUTER BOUNDARY CONDITIONS USED FOR CALIBRATION
(continued)

State-Variable	Dates	Above Pycnocline	Below Pycnocline	Units
Oxygen:				
DO	Oct 89	9.10	7.50	mg O2/L
	Nov 89	9.50	9.00	
	Dec 89	10.00	9.50	
	Jan 90	10.50	10.00	
	Feb 90 - Mar 90	10.90	10.40	
	Apr 90	10.40	9.90	
	May 90	9.90	9.40	
	Jun 90	9.30	8.80	
	Jul 90	8.90	8.40	
	Aug 90	8.20	7.70	
	Sep 90	8.00	7.50	
	Oct 90	8.20	7.70	
	Nov 90	8.40	7.90	
	Dec 90	9.40	8.90	
	Jan 91	10.20	9.70	
	Feb 91 - Mar 91	10.60	10.10	
	Apr 91	10.10	9.60	

areas of high light penetration than in light-limited areas, given the same nutrient availability. Generally, there were higher extinction coefficients in the area around Boston Harbor, due to high suspended solids loadings associated with the discharge of sludge and treated effluent from the Nut and Deer Island wastewater treatment facilities. Extinction coefficients also tended to be higher in regions of high algal biomass (as indicated by chl-a). This reflects the effect of algal self-shading. Therefore, observed extinction coefficients were corrected to base values by subtracting out the effect of self-shading using Equation 4-1.

$$k_{e_{base}} = k_{e_{obs}} - k_c \bullet \text{chl-}a_{obs} \qquad (4\text{-}1)$$

where

k_{ebase}	=	the base or background extinction coefficient related to non-algal turbidity (m^{-1}),
k_{eobs}	=	the observed water column extinction coefficient (m^{-1})
k_c	=	the extinction coefficient per unit of phytoplankton chl-a (m^2/mg chl-a)
chl-a_{obs}	=	the observed chl-a concentration (ug/L).

As noted above k_{ebase} varies spatially due to suspended solids discharges from municipal treatment facilities.

4.4.3 Reaeration Coefficients

Reaeration coefficients were determined internally in the water quality model, by providing estimates of k_L, the surface transfer coefficient for oxygen, and then using Equation 2-14a and 2-14b. A spatially and temporally constant value of 0.6 m/day was used for k_L in the calibration.

4.4.4 Water Temperature

The temperature regime of Massachusetts Bay is an important exogenous variable because it acts as a key driving force for the behavior of the Bay's phytoplankton and for temperature-mediated bacterial decomposition and recycle kinetics. Temperature is also used, together with salinity data, to calibrate the transport structure for the system. As such, considerable effort was made to define the annual cycle and vertical structure of water column temperature in the bay system.

As has been discussed in Section 2.0 only surface water temperature is treated as an exogenous variable; temperature in the sub-surface layers is computed as a water quality state-variable and is used to infer the vertical mixing coefficients for the model calibration. Details of the calibration for temperature and salinity will be presented below.

4.4.5 Solar Radiation

The second principal exogenous force determining phytoplankton growth is solar radiation. Short wave radiation from the sun is used by phytoplankton for photosynthesis. As this radiation passes through the atmosphere, it can be absorbed and scattered by gases in the air and by water vapor, clouds and dust. As a result of such processes, solar radiation reaching the earth's surface is partly in the form of diffuse radiation at the water surface. Monthly-averaged incident solar radiation were obtained from direct daily measurements made at Seabrook, New Hampshire. Table 4-3 presents the incident solar radiation as a function of time for the 18 month calibration period.

4.4.6 Fraction of Daylight

The growth rate formulation for phytoplankton used in the model, as described in Section 2.0, depends on the length or fraction of daylight, as photosynthesis takes place only in the presence of sunlight. The fraction of daylight for each day of the year may be calculated using basic trigonometry assuming that the earth is a perfect sphere.

TABLE 4-3. FRACTION OF DAYLIGHT AND SOLAR RADIATION

Year	Month	Fraction of Daylight	Total Daily Radiation (Ly/day)
1989	Oct	0.449	261
	Nov	0.398	160
	Dec	0.372	147
1990	Jan	0.386	143
	Feb	0.430	241
	Mar	0.488	343
	Apr	0.548	356
	May	0.601	416
	Jun	0.628	474
	Jul	0.615	502
	Aug	0.570	444
	Sep	0.511	356
	Oct	0.449	252
	Nov	0.398	178
	Dec	0.372	116
1991	Jan	0.386	167
	Feb	0.430	212
	Mar	0.487	275
	Apr	0.548	401

(Corrections of six to eight minutes per day, which account for atmospheric refraction of the sun's rays at sunrise and sunset, are assumed negligible.) Monthly-averaged fractions of daylight were generated using a methodology developed by Duffie and Beckman (1970), which depends on the latitude of the location of interest and the declination of the sun as a function of the time of year. Table 4-3 presents the fraction of daylight used in the model for the calibration period.

4.4.7 Particulate Organic Deposition Velocities and Sedimentation Velocities

An important parameter required by the sediment submodel is the net deposition velocity of particulate organic matter settling from the water column to the sediment. Although information concerning areas of net deposition appear to be available for Massachusetts Bay, this information had not yet been reduced for this initial calibration effort. Additionally, the nature of the coarse-grid realization of the study area used at this time did not warrant a spatially-variable deposition velocity. Instead, a spatially constant value of 0.1 m/day was used in the model. (Note: This deposition velocity of 0.1 m/day is relative to the water column.)

The sedimentation rate is the rate at which material is buried in the sediment, relative to the surface of the sediment layer, due to the deposition of fresh organic and inorganic material. Sedimentation velocities for coastal estuaries have been observed to be on the order of 0.1 to several cm/year. Sedimentation velocities of from 0.12 to 2.0 cm/year and from 0.2 to 0.6 cm/year have been estimated using Pb-210 dating for Boston Harbor and Massachusetts Bay, respectively (Fitzgerald 1980, Bothner 1987). Given the variability observed in the data and the nature of the coarse-grid of the present model as noted above, a spatially constant value of 0.25 cm/yr was used in this study. (Note: This sedimentation velocity of 0.25 cm/yr is relative to the sediment layer.)

4.5 CALIBRATION RESULTS

The ultimate goal of this project is to develop a mathematical model which describes the nutrient cycling and oxygen dynamics of Massachusetts Bay. One method for judging the adequacy of the model in describing these processes is to compare the results of model computations to observed data. Ideally, there should be little or no difference between model computation and observed data. However, there is inherent variability in the measurements of the concentrations of the water quality variables. The variability may be due to natural processes; for example, algal patchiness or the effect of local cloud cover or wind-mixing on local phytoplankton primary productivity. There is also spatial variability introduced when one compares the observed data from one or two randomly selected sampling locations to the model output of a segment. Finally, variability may also be due to measurement imprecision or measurement error, although this is probably a small component of the overall variability. Therefore, given this variability, it is unrealistic to expect a model to exactly reproduce all observed water quality. It is expected, however, that the model reproduce seasonal and spatial trends in the data, as well as the interrelationships between variables.

For example, we expect the model to reproduce the annual cycle of phytoplankton biomass and primary productivity. For the Bay this should be reflected in high algal biomass during the late spring and early summer, followed by decreasing algal biomass levels in the late summer, with highest primary productivity occurring during the summer months. The model should also be able to reproduce the super-saturated dissolved oxygen concentrations observed in the surface layer of the water column in and around the region of peak phytoplankton biomass.

Some sediment flux data were also available against which to compare model computations. The adequacy of the sediment submodel can be judged by comparing model computations against the observed sediment nutrient and oxygen fluxes. The initial sediment sampling program was more limited in scope than the water column sampling

program. Hence, the comparisons of observed and computed fluxes are more limited than the water column comparisons.

4.5.1 Water Column

Model calibration results are presented as a series of computer-generated plots which compare model computations versus observed data. These plots will be presented as a sequence of temporal plots for each station. The plots present surface and bottom computations of the concentrations of various water quality state-variables, using solid lines to represent the model output. Observed data are presented as discrete points, representing the average and the range of the data. The temporal plots present model computations at 10 day intervals.

Figure 4-2 presents the surface layer segment numbering scheme, and Figure 4-6 presents the bottom layer segment numbering scheme.

4.5.1.1 Temperature and Salinity Calibration

Before presenting the temporal calibration results for the phytoplankton, nutrients and dissolved oxygen water quality variables, a review of the calibration of the model transport will be presented.

The calibration of temperature and salinity is important for the overall transport structure of the model. During the development of the final water quality model, salinity and temperature (as well as the overall circulation and transport within the Bays) will be provided by the hydrodynamic model. As of this report, however, the hydrodynamic model was in the process of development and calibration and only an initial diagnostic run was available. It was therefore necessary to calibrate the transport structure of the Bays using salinity and temperature in the water quality model.

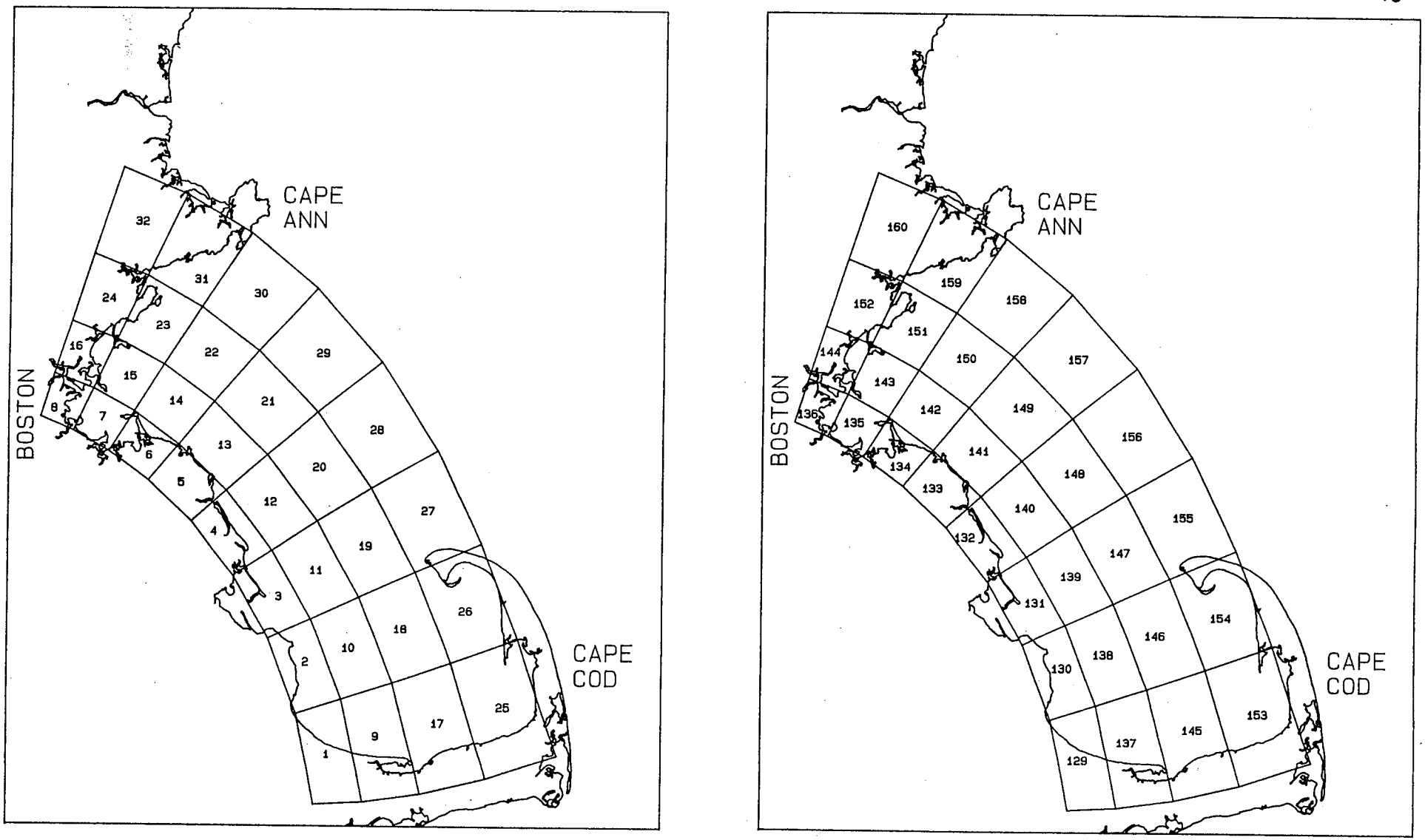

FIGURE 4-6

SURFACE AND BOTTOM SEGMENTS OF COARSE WATER QUALITY GRID

The diagnostic hydrodynamic run had no freshwater inputs in the model other than the current river discharge flow. This freshwater input was located at the future site of the outfall. This is a minor source of freshwater in such a large area and the effect was "washed out" during coarse grid aggregation. The model output was tidally averaged and therefore underestimates horizontal transport throughout the model.

The hydrodynamic model was run for average winter salinity, temperature and stratification and wind conditions with no freshwater flow except for the existing MWRA STP effluent discharge flow. Winter stratification conditions are represented by a vertically well-mixed water column. During the summer, however, the water column is vertically stratified due to surface heating, increased freshwater inflow, and reduced winds. While the net circulation patterns for these two seasons differ, the principal difference between the two seasons is in the vertical structure of stratification. This vertical structure is important because in the summertime the setup of stratification at the pycnocline prevents oxygen and nutrient transfer between the surface mixed layer and the layers below.

The modeling of the annual cycle of circulation and stratification involves the imposition of a heat flux balance within the hydrodynamic model. In order to do this, incident solar radiation, long wave radiation, sensible heat flux and latent heat flux must be included. Recognizing that ultimately a hydrodynamic model will be required to determine the circulation within the bay system, but also wishing to generate a preliminary water quality calibration, a simplified circulation was generated, in order to compute water quality, using the following approach. First, the surface temperature in the water quality model was set at a fixed value for each month based on available data. Following this, the vertical dispersion coefficients were adjusted to reproduce the seasonal pattern in observed vertical temperature and salinity. This procedure assumes that all of the incident solar heat flux is absorbed in the surface layer and that the heating in the subsurface is accomplished via diffusion and vertical mixing only.

The initial diagnostic hydrodynamic run performed for winter conditions provided the initial estimates of the vertical dispersion coefficients. In order to reproduce the

observed salinity and temperature gradients in the winter months it was necessary to assign a maximum value of 12.5cm^2/sec to the vertical mixing coefficients. For the summer period, it was determined via calibration that reducing the vertical dispersion by a factor of 50 between layer boundaries found between 10 and 15 meters would best represent the pycnocline and reproduce the sharp gradients observed in salinity and temperature at this depth for the entire Bay. In addition, vertical mixing was also reduced by a factor of five between all non-pycnocline vertical layers to represent summertime conditions. The times chosen to switch from a well-mixed period to a stratified period and vice versa were based on available data and were modified during the calibration. Table 4-4 presents the stratified and non-stratified periods, as well as the maximum vertical dispersion coefficient assigned during those periods.

In order for the calibration to be complete, the model would have to reproduce the stratification no matter what the depth of the segment. Three "columns" of model segments were chosen for the calibration, each with a different depth of water: a deeper column (Segment 20), one with medium depth (Segment 10), and a shallow segment (Segment 3). Efforts were made to best reproduce the observed data in all three groups with a consistent pycnocline depth and vertical mixing coefficients.

TABLE 4-4. VERTICAL DISPERSION COEFFICIENTS

Time Period	Stratified (S) or Well Mixed (M)	Pycnocline Interface (P) Nonpycnocline Interfaces (N)	Maximum Vertical Dispersion Coefficient (cm^2/s)
10/1/89-10/31/89	S	P	0.25
	S	N	2.50
11/1/89-3/15/90	M	P	12.50
	M	N	12.50
3/16/90-10/31/90	S	P	0.25
	S	N	2.50
11/1/91-3/31/91	M	P	12.50
	M	N	12.50
4/1/91-4/30/91	S	P	0.25
	S	N	2.50

The calibration of the vertical mixing was an iterative process and involved the simultaneous adjustment of vertical mixing coefficients, surface temperature and boundary

temperature and salinity. The surface temperature across Massachusetts Bay can vary spatially during a particular time period. For this modeling effort, a surface temperature was assigned for each segment during each month of the calibration. Surface temperature was assigned to best fit the available data. Due to limited salinity data throughout the year, the boundary conditions were open to some question. Therefore in order to produce the best fit to the data, the salinity boundary conditions were adjusted as needed. These adjustments, however, were well within the range of available data. Figures 4-7 through 4-12 present typical model output compared with temperature and salinity data. The data are shown for the April, July and October of 1990, and February, March and April of 1991 cruises. The data are plotted as mean and range at five meter depth intervals for each station. The mean is represented by a circle; the range of the data is shown by horizontal bars on either side of the mean. The model computation is presented as a solid line step function representing the valve in each vertical layer.

Calibration results for segment 20, and the segments below it, are presented on Figures 4-7 and 4-8. The model calibration for temperature during the well-mixed periods of February and March is quite favorable. During the transition periods of April, when stratification begins, and October, when the fall overturn is initiated, the model also seems to fit the data. However, the model has difficulty with some of the structure of the water column. In July, the model is predicting stratification at the proper depth, but it is not reproducing the amount of temperature stratification observed to at the mid-depths. This is identified by the sharp gradients in the temperature data. The salinity in the deepest segment fits well during non-stratified periods. The model has more difficulty during the transition periods. The model fit is not representative of the observed stratification. The model begins to show some stratification during July; however, it does not follow the 1.5 ppt range seen in the data. The data in April of 1991 shows strong stratification which the model does not reproduce. The current model has no freshwater sources, other than the MWRA outfalls, which are assumed constant. This makes the salinity stratification difficult to model. (This model inadequacy is expected to be corrected during the second phase of this study.)

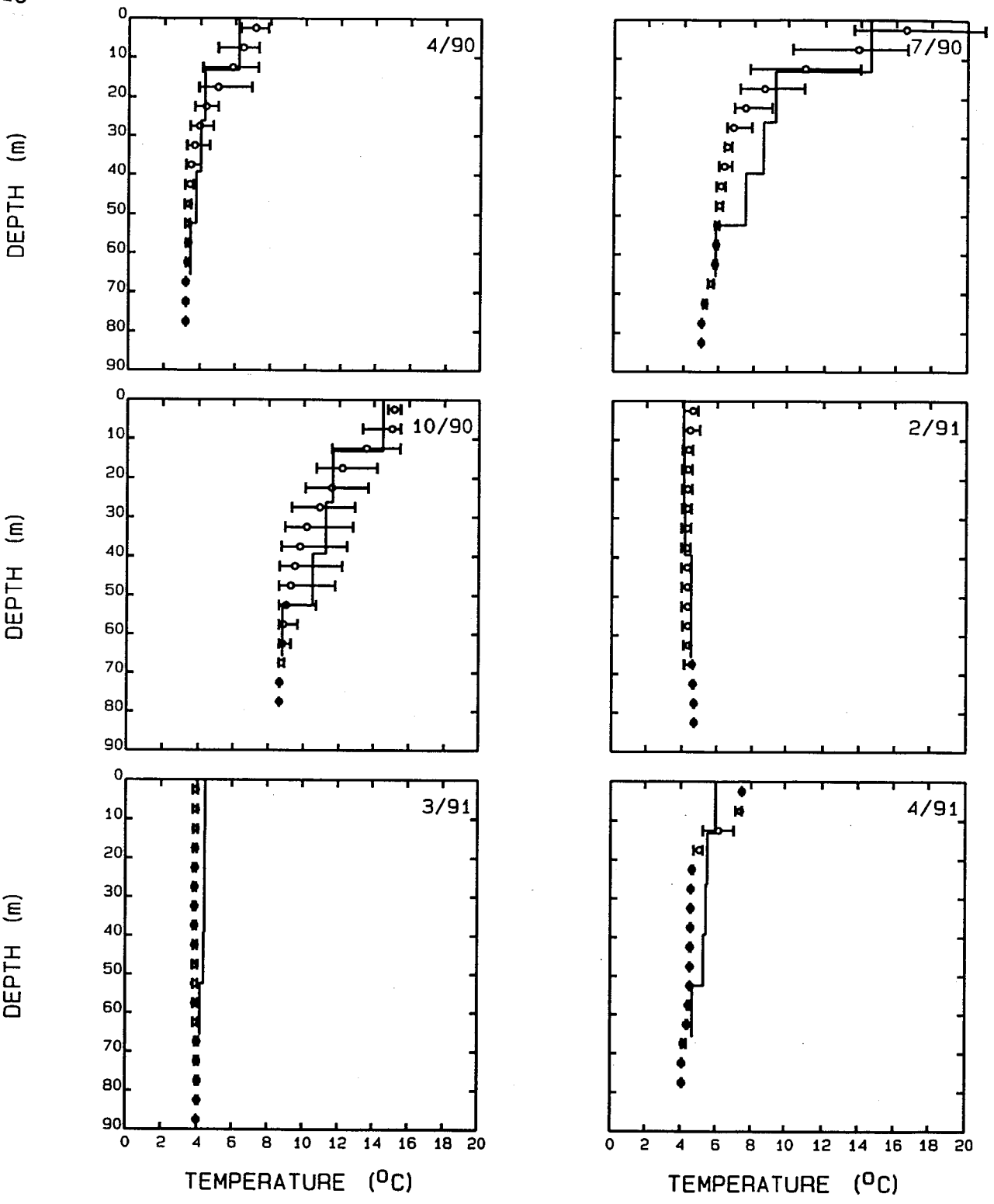

Figure 4-7

1990-1991 Temperature Calibration Results
for Segments 20, 52, 84, 116, 148
in the Center of the Study Area

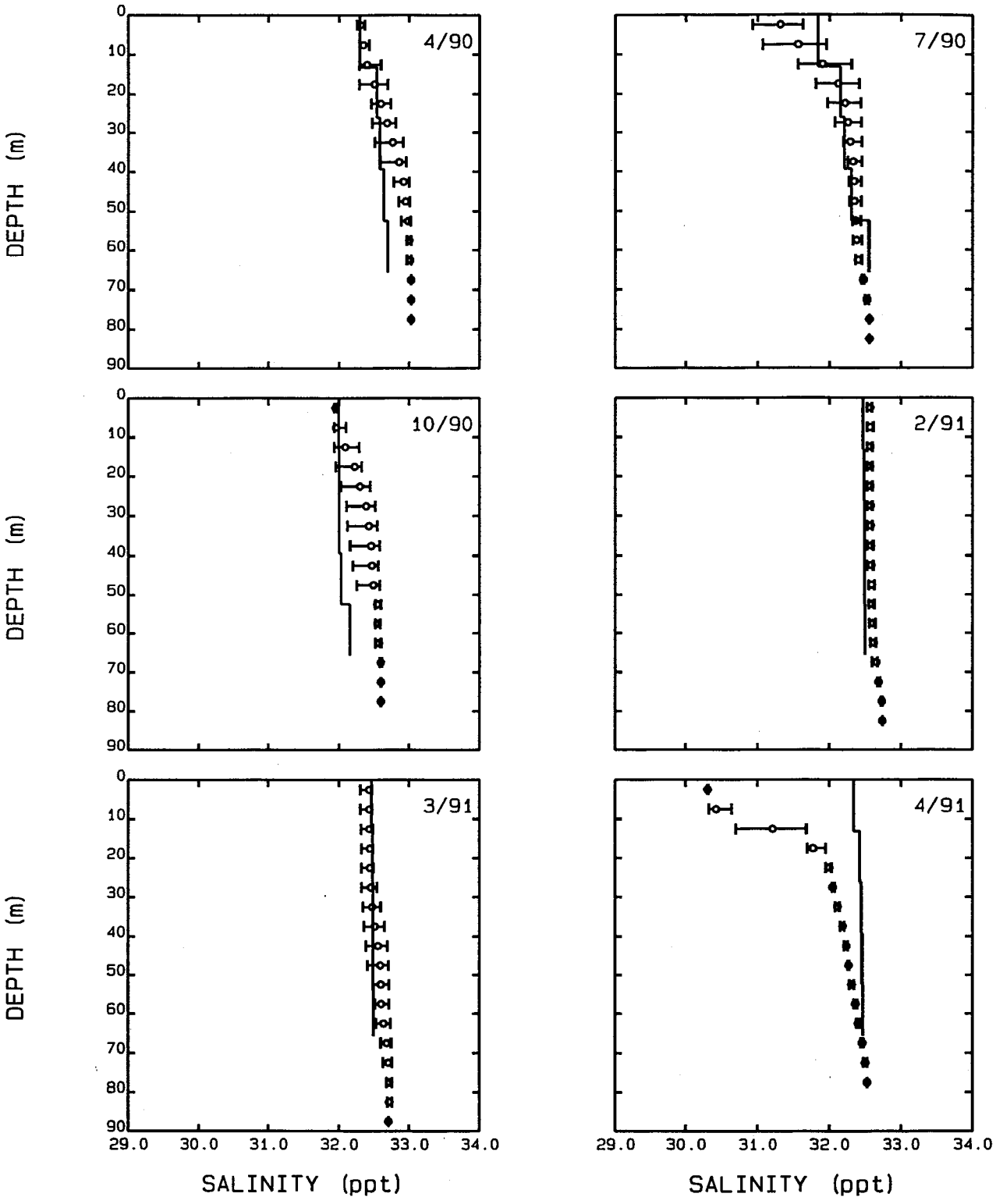

Figure 4-8

1990-1991 Salinity Calibration Results
for Segments 20, 52, 84, 116, 148
in the Center of the Study Area

Initial calibrations were based on segment 20, a deep segment in the center of the study area. Once a satisfactory model fit was obtained for this "column" of segments, model output was compared to shallower segments and vertical mixing coefficients were adjusted so that the model adequately fit the temperature and salinity data regardless of the segment depth. Figures 4-9 and 4-10 present the calibrations of temperature and salinity for segment 10, a medium depth segment in Western Cape Cod Bay. Again, the calibration for temperature during February and March is representative of the data. During the transition periods of April and October, the model does not follow the shape of the data, but generally fits the data with errors on both the high side and low side. In July, the model follows the shape of the data, but is computing temperatures higher than the data. Data were not available for April of 1991. When compared to the salinity data in Figure 4-10, the computed salinity values tend to be higher than the data.

The model fit for February and March is a fair representation of the data, displaying the well-mixed water column. Model output for the transition periods is more stratified than the data. The stratified period of July is not well represented by the model. In Figure 4-8, segment 20, the model is computing lower values than the data; however, the model predictions are high for segment 10. This may indicate that the model's inability to reproduce the salinity data is caused by inappropriate (i.e. winter) horizontal mixing and circulation, rather than inaccurate boundary conditions.

Figures 4-11 and 4-12 present the calibration for segment 3, a shallow segment off Plymouth Harbor. The temperature calibration is similar to that for segment 10. The model does not always follow the same trend as the data, however, it is generally close to the data. The salinity data calibration for segment 3 is especially poor. This illustrates the difficulty of grid aggregation. In this particular segment some of the original hydrodynamic segments, within Duxbury Bay, were omitted due to the coarse grid structure. This caused a small flow and solid imbalance, which created a loss of salinity in the model, thereby creating the extreme stratification in Figure 4-12. This imbalance is small and would not be expected to have a significant affect on the rest of the water quality model. The final model grid configuration should correct this problem.

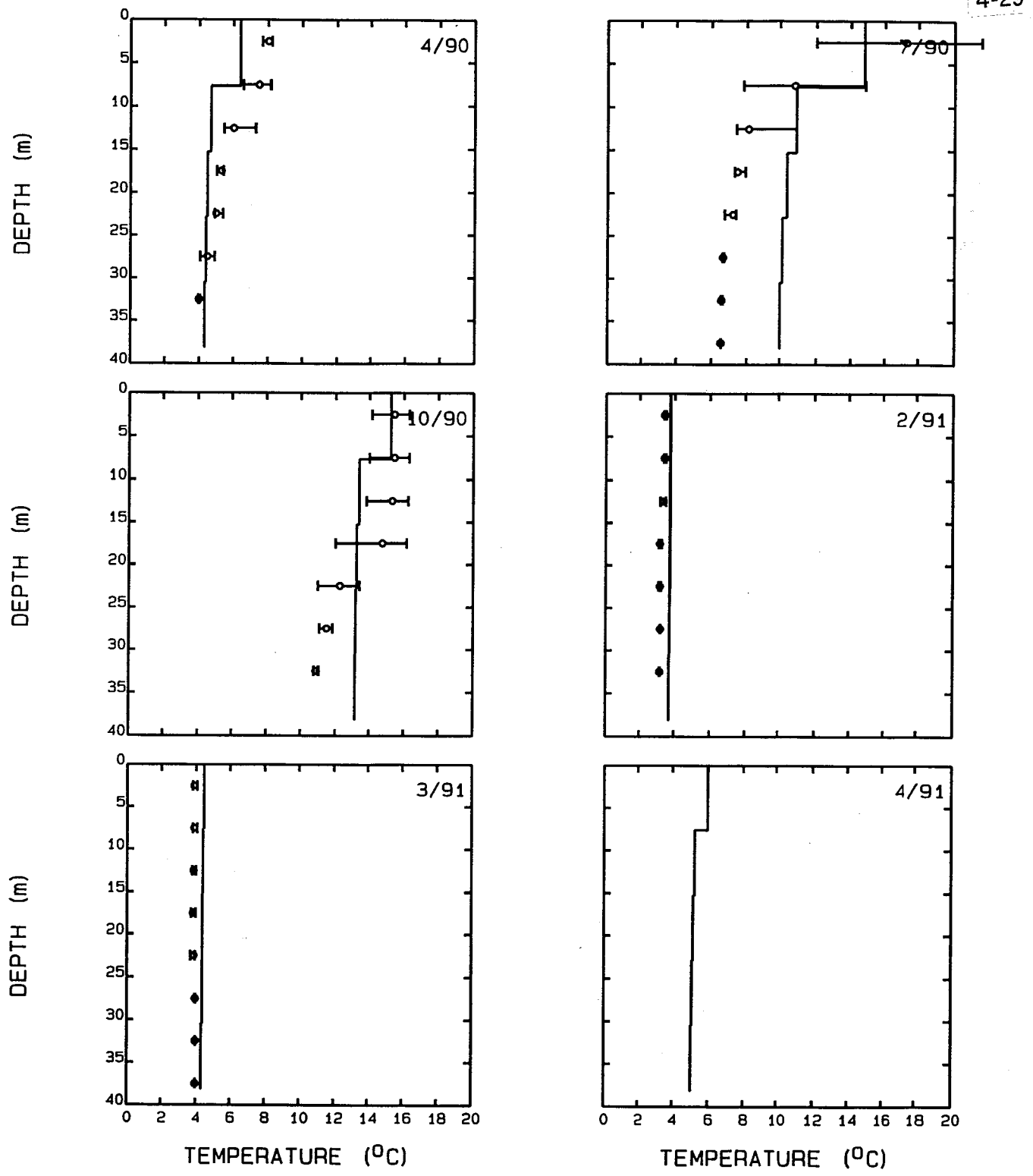

Figure 4-9

1990-1991 Temperature Calibration Results
for Segments 10, 42, 74, 106, 138
in Western Cape Cod Bay

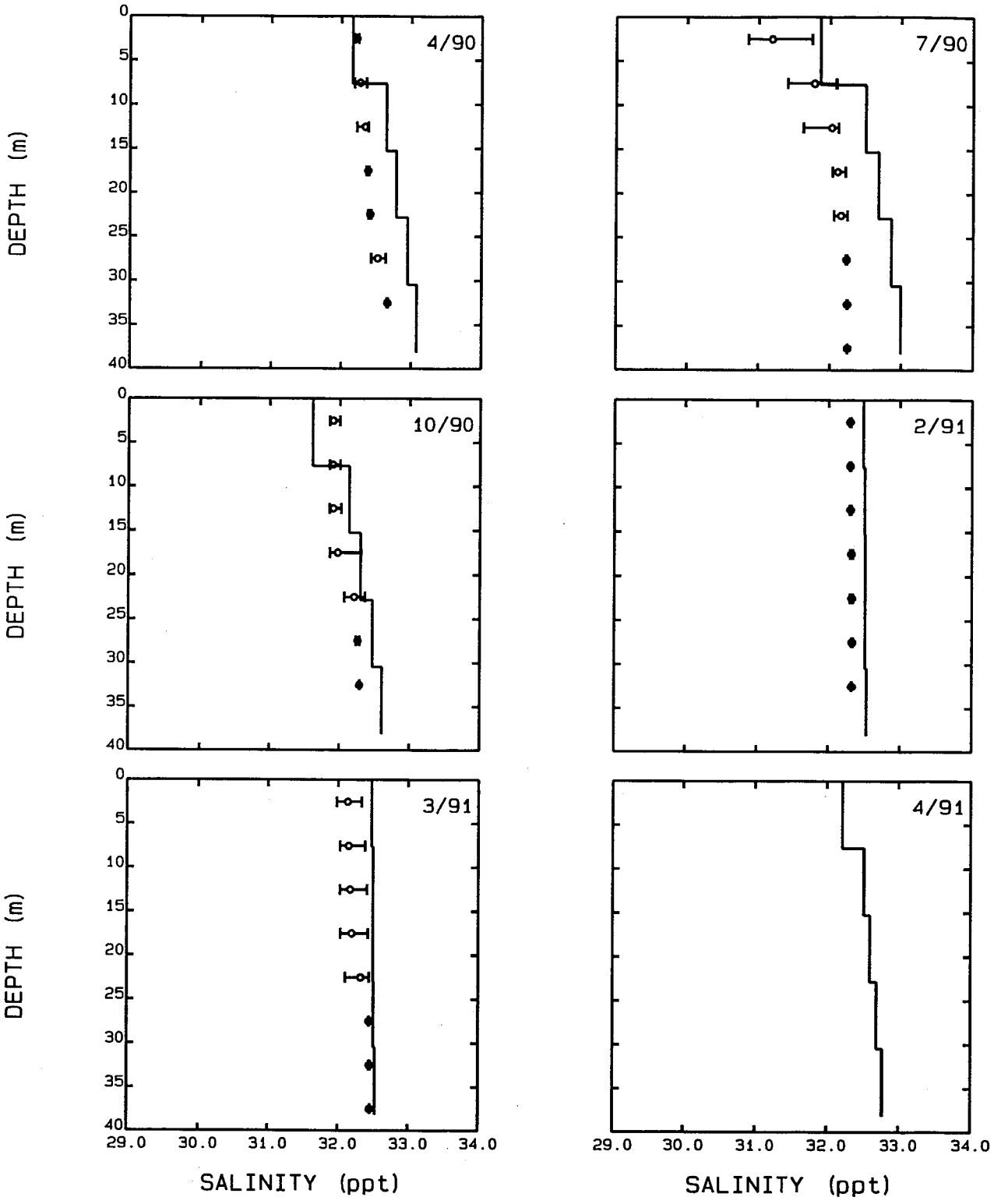

Figure 4-10

1990-1991 Salinity Calibration Results
for Segments 10, 42, 74, 106, 138
in Western Cape Cod Bay

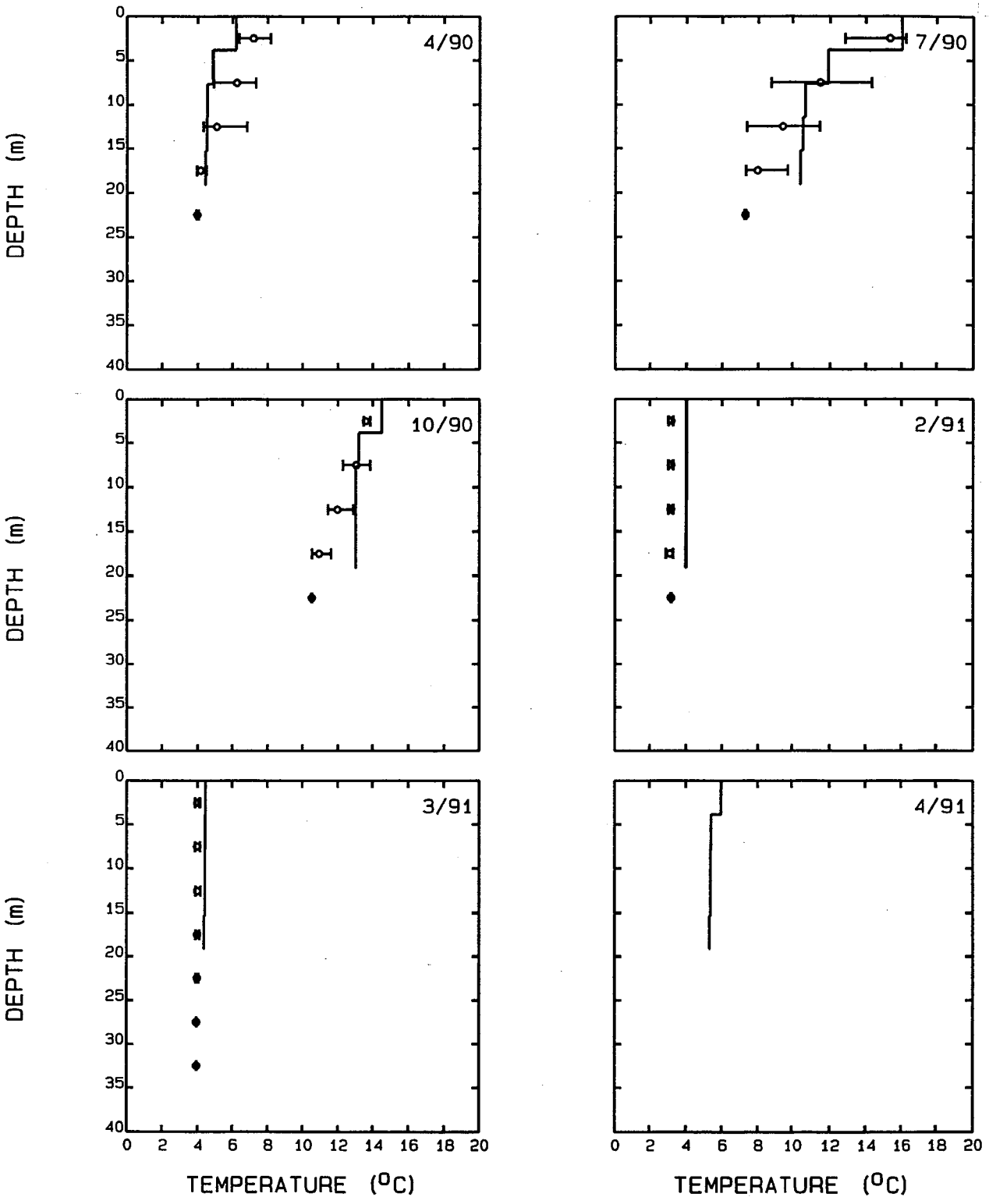

Figure 4-11

1990-1991 Temperature Calibration Results
for Segments 3, 35, 67, 99, 131
off Plymouth Harbor

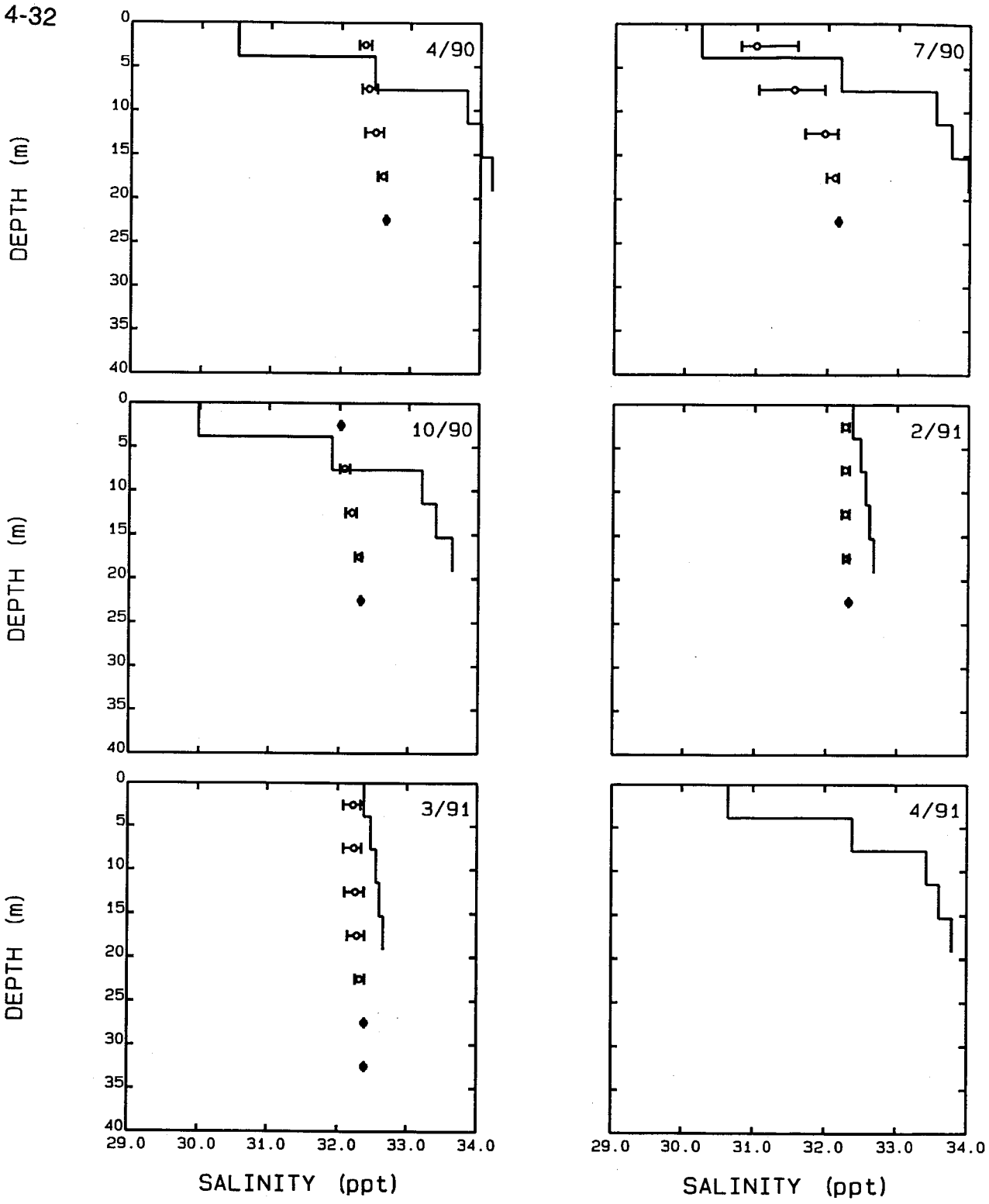

Figure 4-12

1990-1991 Salinity Calibration Results
for Segments 3, 35, 67, 99, 131
off Plymouth Harbor

There are weaknesses in the temperature and salinity calibration. Although the model does well during well mixed periods, during transition and stratified periods the model only represents a fair approximation of the data. This is due to the lack of appropriate hydrodynamics and the vertical profile resolution from only five vertical layers. The lack of data during parts of the year also makes it difficult to verify that the model is correctly reproducing what occurs during these periods. The choice of the final vertical dispersion coefficients and boundary conditions was a compromise between a good model fit of the temperature data versus a good model fit of the salinity data.

4.5.1.2 Phytoplankton, Nutrients and Dissolved Oxygen Calibration

Figures 4-13 through 4-18 present comparison between model computations and observed data for key water quality variables for six model segments in Massachusetts and Cape Cod Bays. These figures are intended to demonstrate the ability of the model to reproduce the observed annual cycle of phytoplankton biomass, dissolved oxygen and nutrients within the Bays system. Each figure presents a comparison of model computation versus observed data for chl-a, (an indicator of phytoplankton biomass), particulate organic carbon (POC), dissolved oxygen (DO), dissolved inorganic nitrogen (DIN) (the sum of ammonia and nitrite + nitrate), dissolved inorganic phosphorous (DIP), dissolved inorganic silica (Diss Si), salinity (SAL), temperature (TEMP), and total extinction coefficient (k_e). The figures present results for both surface and bottom layer segments versus surface and bottom layer data. The model computation for the surface layer is represented by a solid line, while the bottom layer computation is represented by a dashed line. The surface layer observed data are presented as upward pointing triangles, while the bottom observed data are shown as downward pointing triangles. The data are presented as the segment mean and range of the data.

The first water quality model comparison results are presented in Figure 4-13 for segments 15 (surface) and 143 (bottom). These segments are just outside of Boston Harbor proper, and are one group of water segments that receive metropolitan Boston's wastewater effluent. These model segments also have good data coverage over the

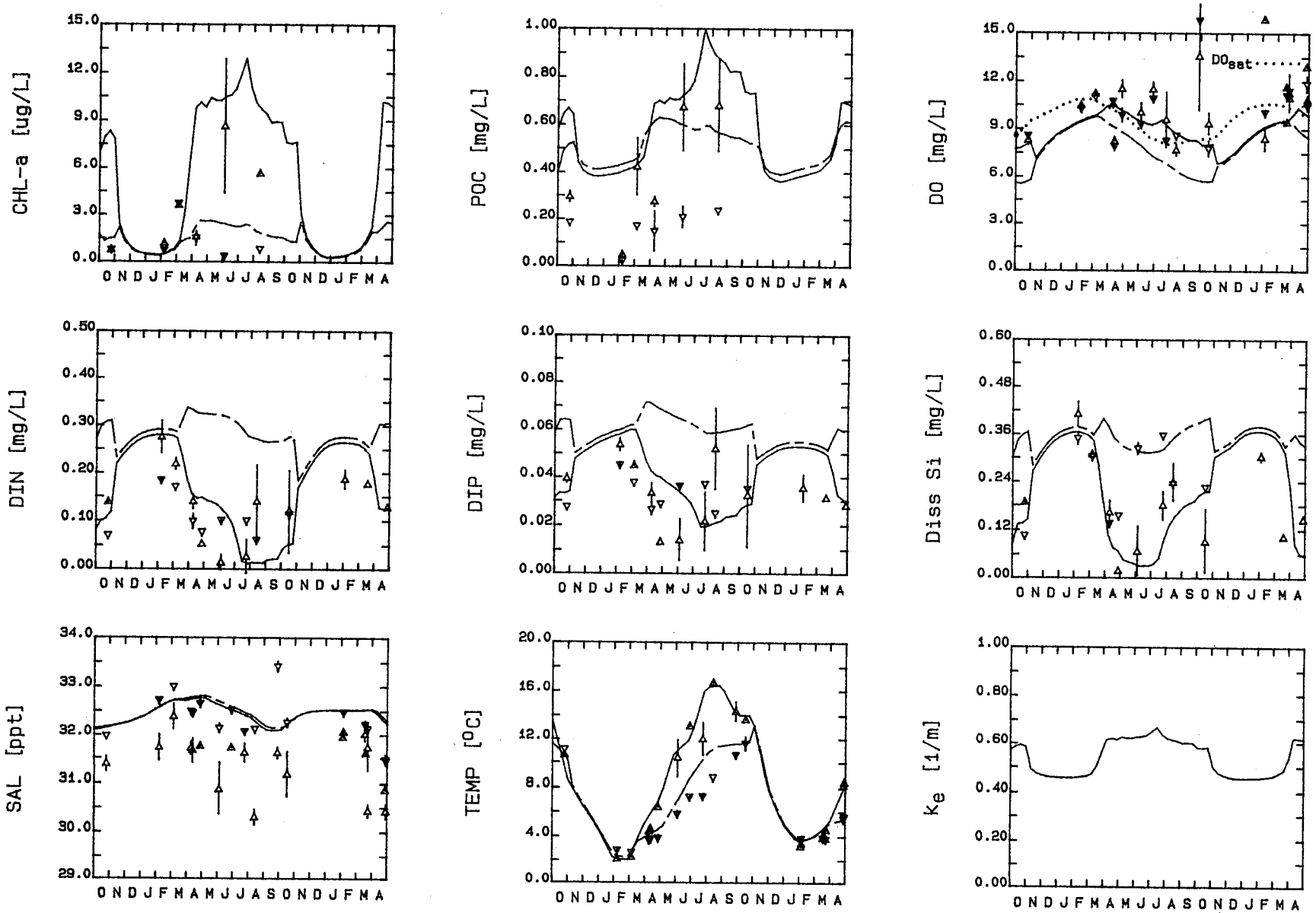

FIGURE 4-13

1989-1991 Calibration Results for Segments 15/143

calibration period. As can be seen the model reproduces the observed temperature, both in terms of its seasonal cycle and seasonal stratification. The salinity, however, is not reproduced as well. This may be due to the lack of freshwater inputs to the model, emanating from Boston Harbor. As has been noted earlier, the hydrodynamic model was run in the absence of freshwater inputs from the various rivers, such as the Charles and Neponset. The freshwater flows from the Deer Island and Nut Island facilities were included, however. Since the hydrodynamic model did not include these freshwater inputs there is less freshwater to dilute salinity concentrations in the area of Boston Harbor.

As can be seen the model approximately reproduces the annual cycle observed in phytoplankton biomass, as indicated by chl-a. The model and the data indicate the highest concentrations occur during the late spring and summer months. This seasonal cycle also appears in the measurement of POC, with the highest concentrations being observed during the summer period. The model, however, does not show as strong an annual cycle, appearing to over-estimate the POC during the winter period in the surface and over-estimate the bottom concentrations of POC year-round. We believe a major reason for this discrepancy is that a significant portion of the model POC in this region of the model domain is associated with effluent POC from the wastewater treatment facilities and that the residence time of this POC (as well as other pollutants) within this region of Massachusetts Bay is over-estimated by the water quality model. Furthermore, in this model run, sludge is discharged as a constant load, not as a three hour discharge during the beginning of ebb tide. As a consequence of this over-estimation of POC, the dissolved oxygen in the bottom layer of the water column is under-estimated, especially during the summer stratification period. This is due to the oxidation of the excess POC in the bottom layers of the water column.

Two possible reasons for the over-estimation of the residence time is that the transport fields used in the water quality model and provided by the hydrodynamic model do not include the effects of freshwater outflow from the harbor, or that the tidally averaged Eulerian residual current under-estimates the net movement of water and

water-borne material. Signell and Butman (1992) demonstrated the latter hypothesis using a fine-mesh vertically integrated hydrodynamic model of Boston Harbor.

An over-estimate of residence time also would tend to explain the over-estimation of DIN and DIP in these segments. Although the model appears to approximately reproduce the annual cycle of nutrient uptake by phytoplankton in the surface layer of the water column, it can been seen that overall nutrient concentrations are too high, especially in the bottom waters during the summer period. This also is probably due to an under-estimation of the net export from Boston Harbor.

Figure 4-14 presents model versus data comparisons for segments 13/141, located just off Scituate. As can be seen, the annual cycle of surface and bottom water temperature is approximately reproduced by the water quality model. The salinity calibration, however, is not very good. The model fails to reproduce the observed summertime stratification. The model compares favorably to the data for chl-a, reproducing the observed spring-summer peak in chl-a. The model computation of POC compares more favorably to the observed data than did segments 15/143. This reflects the fact that the Boston Harbor load makes up a smaller proportion of the computed POC in segments 13/141 than in segments 15/143.

The improvement in the POC calibration also results in a better calibration to observed dissolved oxygen, as compared to segments 15/143, although the surface dissolved oxygen is under-estimated by the model during much of the calibration period. The reasons for this discrepancy are yet unclear, although an under-estimation of primary productivity is a possible cause.

The model versus data comparisons for the nutrients (DIN, DIP and Si) are encouraging. As can be seen both the data and model computations are lower in this region of the Bay, relative to the Boston Harbor area (segment 13 - Figure 4-14). The model computation indicates that Si becomes the limiting nutrient for algal growth during late April and May, with the observed Si data slightly lagging. As a consequence of the

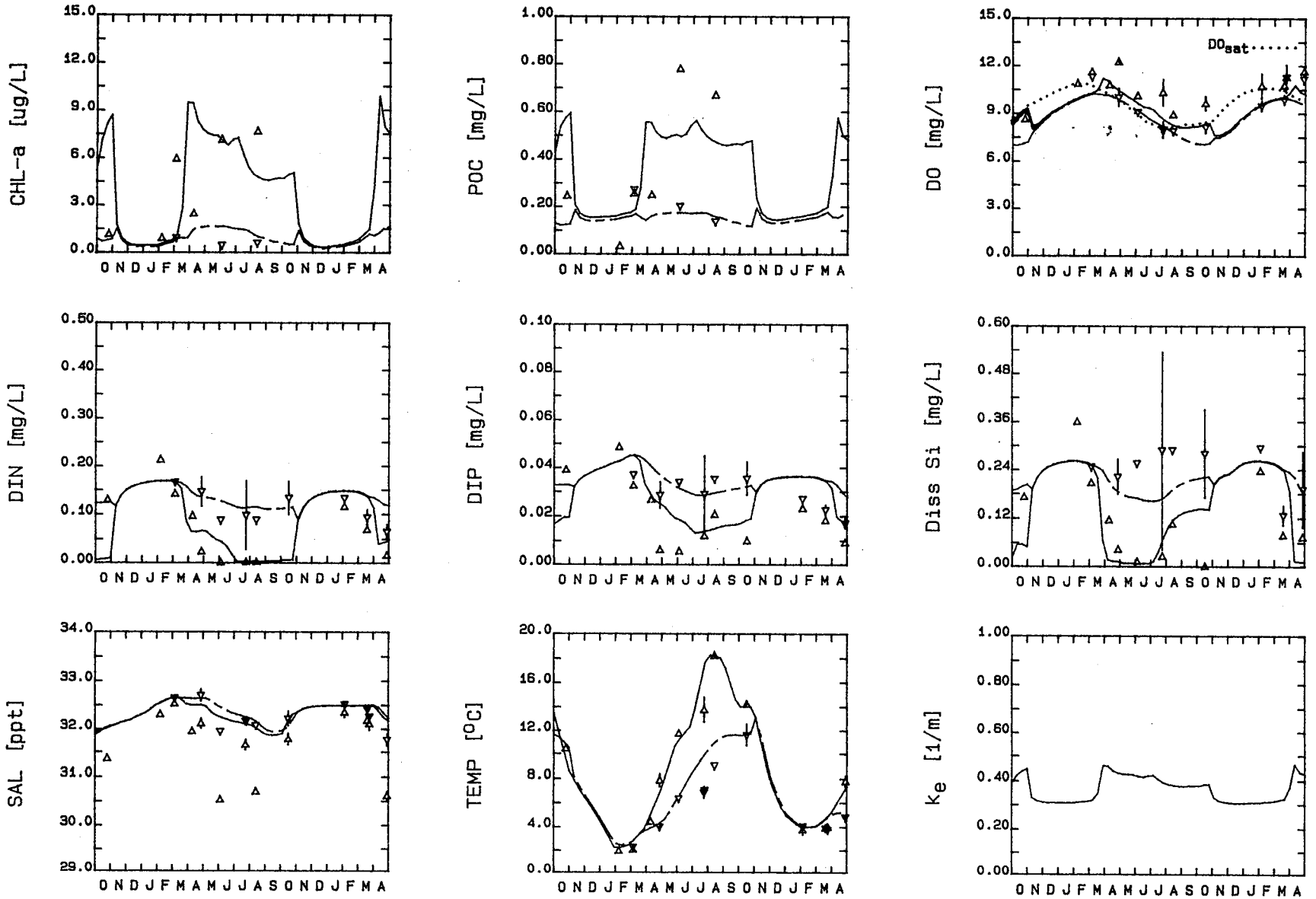

FIGURE 4-14

1989-1991 Calibration Results for Segments 13/141

Si limitation computed by the model, not all of the DIN is utilized until July and August. The data, however, indicate that DIN is virtually depleted a month earlier, in June. The reason for this discrepancy may lie either in the incorrect specification of the silica to carbon stoichiometry for the diatoms, or possibly to too high a growth rate for the winter diatom group or too low a growth rate for the summer assemblage, which would delay the onset of the summer bloom. This will be explored further in the fine-grid version of the water quality model.

A second discrepancy can be noted in the surface nutrient data, which shows a depletion of silica and a reduction in DIP during the fall period, around the month of October. This depletion may be due to the occurrence of a fall diatom bloom which is not computed by the model. Unfortunately no chl-a or POC measurements were available for this period with which to confirm the occurrence of such a bloom.

Figure 4-15 presents model calibration results for segments 19/147, located just northwest of Race Point on the northern tip of Cape Cod. The quantity of data for this area is limited to observations of salinity, temperature, dissolved oxygen and nutrients. However, some comments can be made concerning the model versus data comparisons. In this region of the model, the calibration to salinity was better than for segments 13/141 and 15/143. The model approximately reproduces the observed vertical gradients between surface and bottom water nutrients as indicated by the data. The model does, however, appear to over-estimate surface phosphorus, perhaps indicating that the choice of Redfield stoichiometry may not be appropriate for the summer assemblage. In addition, it can be seen that the model over-estimates the surface Si concentration in October 1990; again perhaps indicative of a late summer/fall diatom bloom.

The next results are presented in Figure 4-16 for segments 22/150. The model computations of salinity and temperature compare favorably to the observed data. The model-data comparison of the annual cycle of primary productivity as indicated by chl-a, POC and dissolved oxygen is encouraging. The model reproduces the spring-summer peaks in chl-a and POC and computes slightly super-saturated conditions for surface dissolved

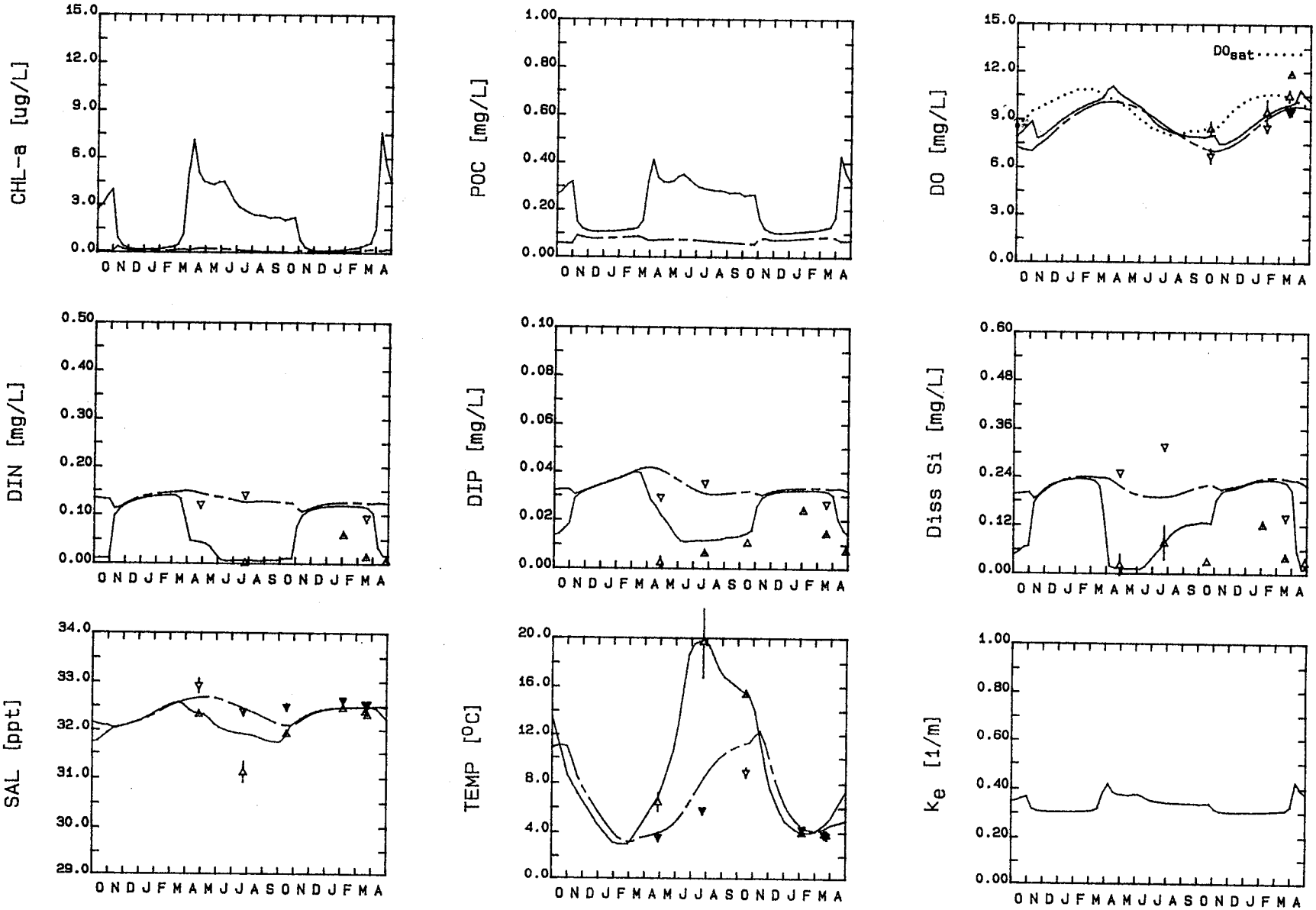

FIGURE 4-15

1989-1991 Calibration Results for Segments 19/147

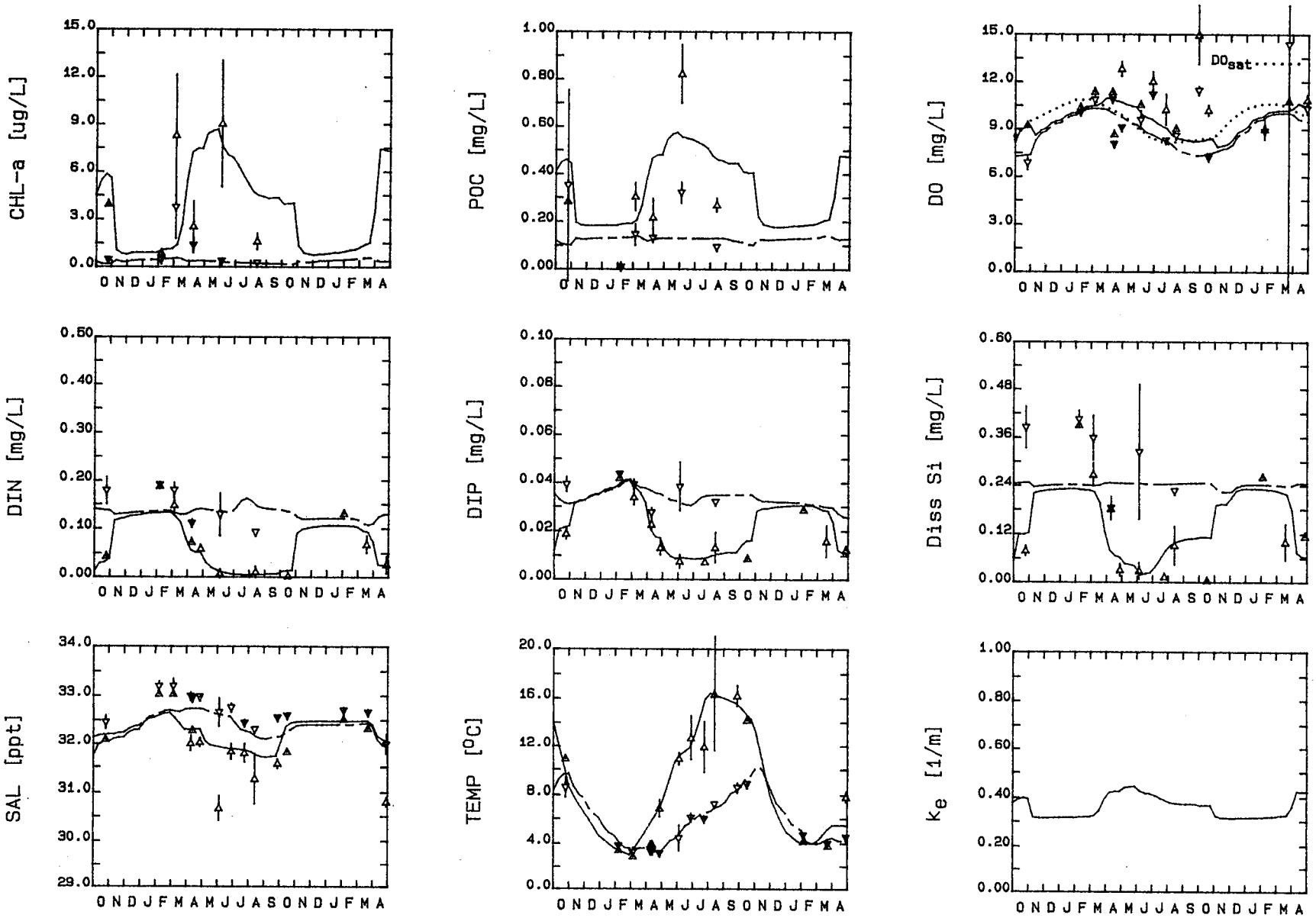

FIGURE 4-16

1989-1991 Calibration Results for Segments 22/150

oxygen, which is also observed in the data. The model also computes the under-saturated dissolved oxygen concentrations observed in the data during the winter months. The model compares well to the observations of DIN, DIP and Si, indicating that nitrogen is the limiting nutrient during the summertime, with silica being the potentially limiting nutrient in the spring. As has been observed in the previous model versus data comparisons, the observed Si is over-estimated by the model in October 1990.

The final two surface/bottom segment pairs presented for comparison are adjacent to the boundary. The first of these segment pairs are segments 28/156 (Figure 4-17). These segments straddle Stellwagen Bank and Stellwagen Basin, a region of rapidly changing bottom bathymetry. As can been seen on this figure, the model performs well in reproducing the annual and vertical gradients observed in the data. The model computes the annual cycle in observed chl-a, POC and dissolved oxygen including the slightly over-saturated conditions observed in the summer and slightly under-saturated conditions observed in the late fall and winter periods. The annual cycle and vertical stratification of the nutrients are also captured by the model, although there appears to be considerable variation in bottom Si that is not reproduced by the model.

The final water column comparison is presented in Figure 4-18 for segments 30/158. These segments are located just south of Cape Ann, on the northern boundary of the model domain. The comparisons for all water quality state-variables are favorable. This might be as expected since segments 30 and 158 (as are segments 28 and 156) are adjacent to the boundary.

A review of Figures 4-13 through 4-18 indicate that, in general, the model captures the principal features of primary productitvity within Massachusetts Bay. The model is approximately able to reproduce the summer maximum in phytoplankton biomass, as indicated by surface chl-a and POC, and the slightly super-saturated concentrations of dissolved oxygen. Coincident with the summer maximum in phytoplankton biomass are the summertime minima in surface nutrients.

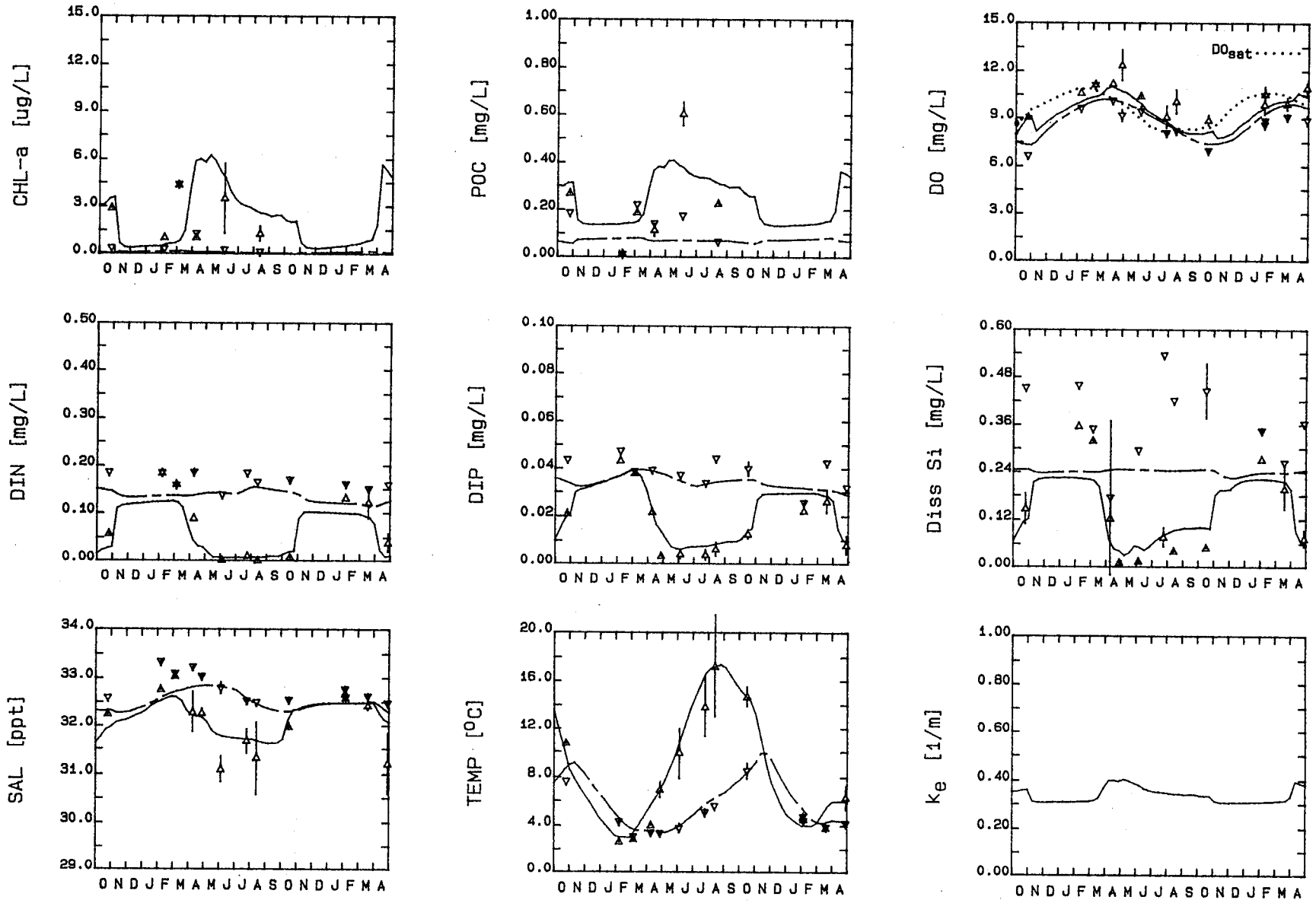

FIGURE 4-17

1989-1991 Calibration Results for Segments 28/156

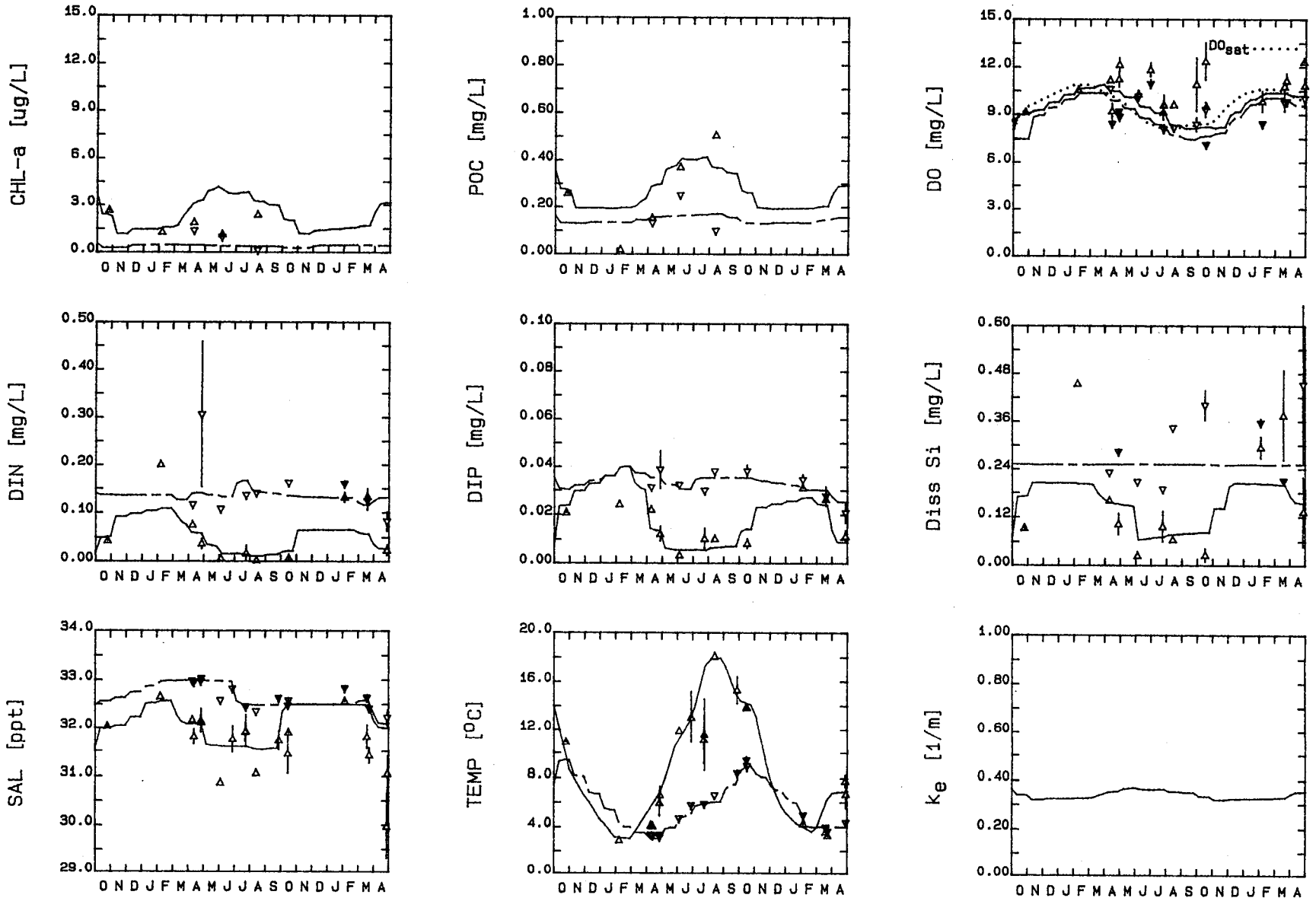

FIGURE 4-18

1989-1991 Calibration Results for Segments 30/158

It is clear from the model versus data comparisons that the water quality model is limited by not having an annual computation of circulation and vertical mixing from the hydrodynamic model. Also apparent is that tidally averaged transport is insufficient to resolve the transport of nutrients discharged in the Boston Harbor area. Therefore, intra-tidal computations will be required in Phase 2 of this study.

4.5.2 Sediment Model Results

A limited data set was available with which to evaluate the performance of the sediment model. These data were collected during September and October 1990 by scientists at the Marine Biological Laboratory in Woods Hole (Giblin et al, 1991). The data set consisted of replicated core measurements (2-4 cores/station) of sediment oxygen demand (SOD) and sediment fluxes of ammonia, nitrate, and phosphate at 8 stations located in Boston Harbor and Massachusetts Bay (Figure 4-19 shows the station locations). Figures 4-20 through 4-24 present a series of comparisons between model estimates and measured fluxes of SOD, ammonium (Jnh4), nitrate (Jno3) and inorganic phosphorus (Jpo4). The model computations are shown as time series of computed fluxes for the calibration period (October 1989 through April 1991) and are represented using solid lines, while the data (September/October 1990) are illustrated using an asterisk, representing the average observed flux of the replicated cores plus the observed range in fluxes.

Also included on each of the figures are other model computations used in diagnosing the model performance. These computations include: the flux rate of particulate organic nitrogen (PON) delivered to the sediment (flxpon); the G1 (labile), G2 (refractory) and G3 (inert) concentrations of PON in the sediment; the rate of nitrogen diagenesis (Jn); the concentrations of ammonia (NH4) and nitrate (NO3) in the overlying water column (solid line), in the aerobic layer of the sediment (dashed line) and in the anaerobic layer of the sediment (dotted line).

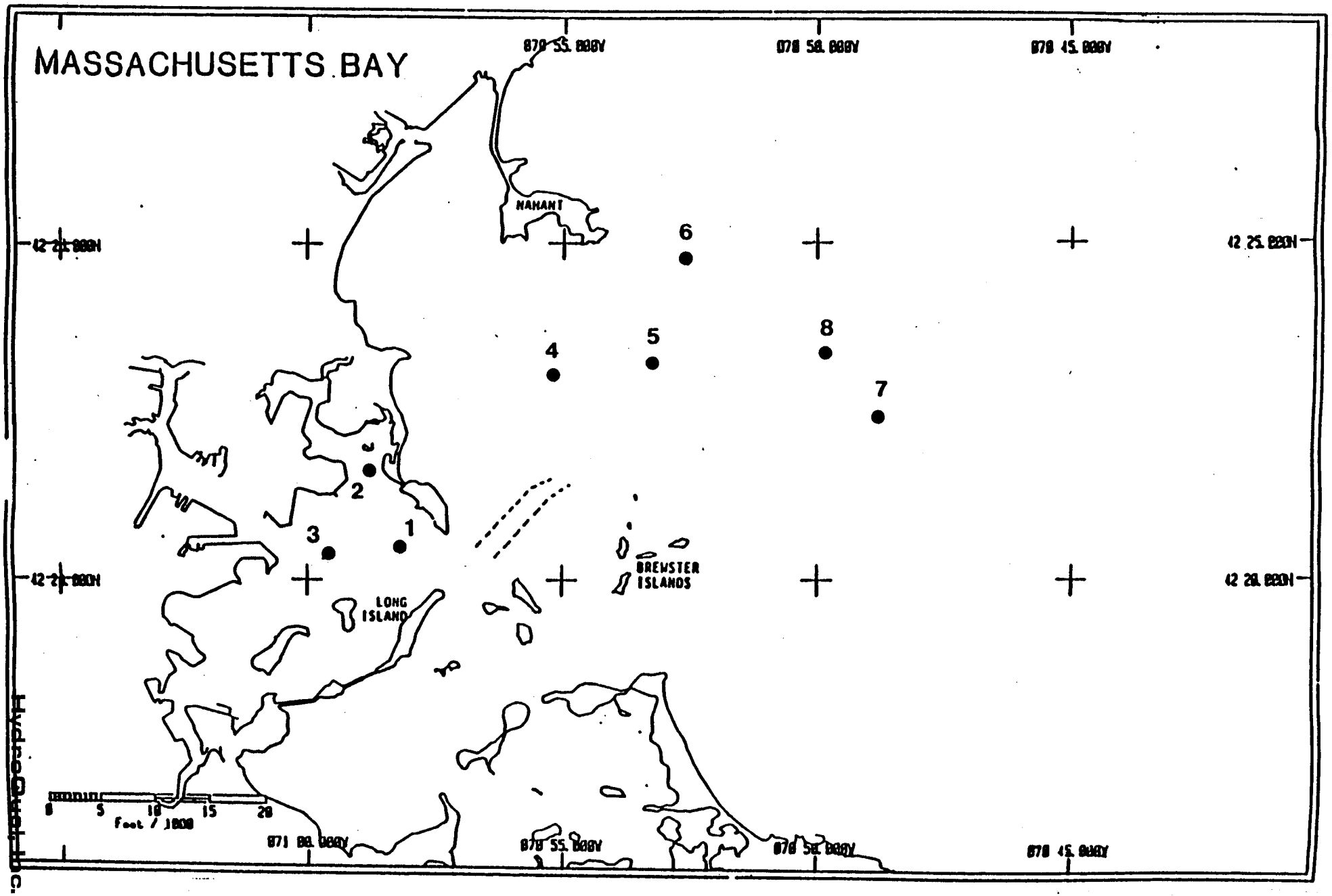

FIGURE 4-19. LOCATION OF 1990 SEDIMENT SAMPLING STATIONS

The first model versus data comparison is presented on Figure 4-20 for the Broad Sound sediment segment 15, which lies underneath water column segment 143 (the bottom layer segment of the segment 15, 143 pair). The data used for comparison purposes are from Stations 4 and 5. As can been seen from the data, the flux measurements for these two stations were markedly different. Station 5 had the higher SOD and ammonia flux measurements, and based on a REMOTS survey (SAIC 1987) this station is thought to be affected by Boston Harbor sewage particulates reaching the area. The model computation lies within the range of the SOD and ammonia flux measurements observed within the model segment area, and in fact are closer to the Station 5 data. As has been pointed out earlier, the water column over sediment segment 15 receives a significant portion of the MWRA pollutant load.

The model computes a positive (from the sediment to the overlying water column) nitrate flux of approximately 5 mg N/m^2-day, versus an observed positive flux of approximately 1 mg N/m^2-day for Station 4 and a negative (from the overlying water column to the sediment) flux of approximately 5 mg N/m^2-day at Station 5. The model is computing a positive inorganic phosphorus flux of approximately 6 mg P/m^2-day versus an observed positive phosphorus flux of about 5 mg P/m^2-day for Station 5 and a negative flux of about 1 mg P/m^2-day observed for Station 4.

Figures 4-21 and 4-22 present calibration results for sediment segments 14 and 23. Segment 14 lies underneath water column segment 142 (of the 14/142 pair) off Nantasket Beach, while segment 23 lies underneath segment 151 (of the 23/151 pair)off Marblehead. Segment 14 contains data from Giblin et al (1991) at Station 7 and segment 23 contains data from Stations 6 and 8. These sediment sampling stations lie within apparent depositional zones located near the proposed outfall site (SAIC 1987, Bothner et al. 1990) and were reported by Giblin et al (1991) to contain good infaunal communities. All three stations are marked by lower measurements of SOD and ammonia flux compared to Station 5. The model also computes lower SOD and ammonia flux relative to segment 15, and compares favorably to the observed data for all flux measurements.

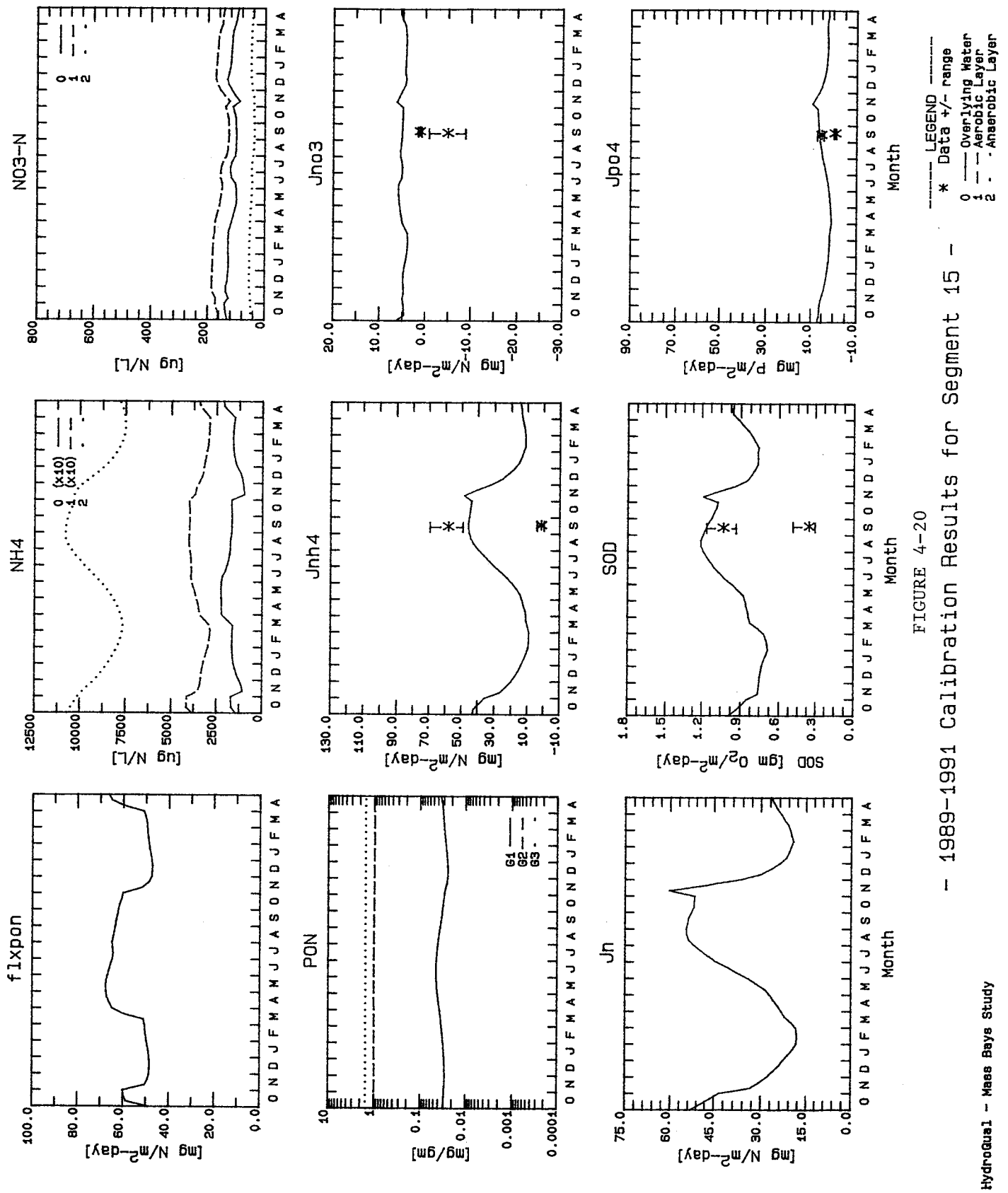

FIGURE 4-20

- 1989-1991 Calibration Results for Segment 15 -

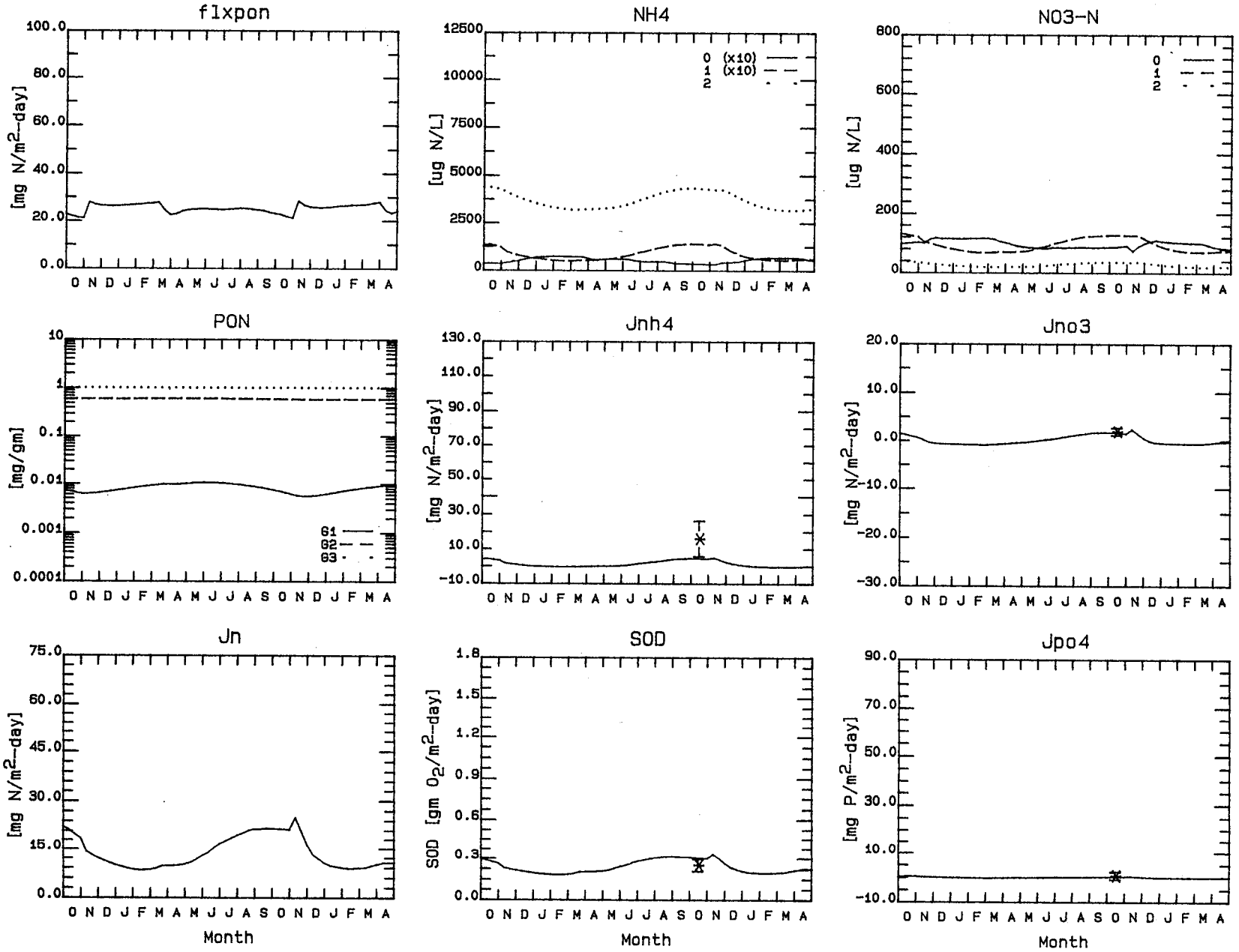

FIGURE 4-21
- 1989-1991 Calibration Results for Segment 14 -

----- LEGEND -----
* Data +/- range
0 —— Overlying Water
1 — — Aerobic Layer
2 · · Anaerobic Layer

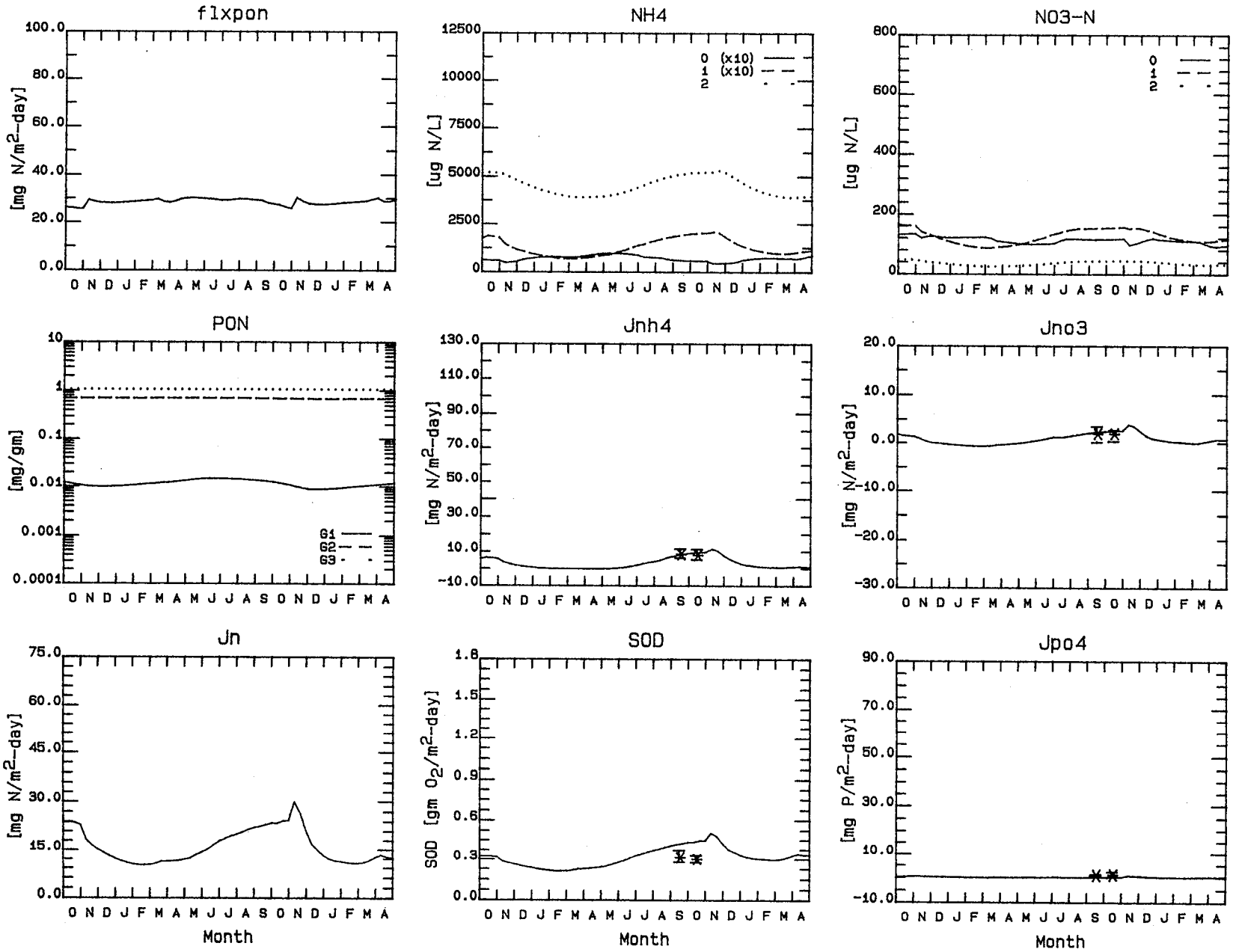

FIGURE 4-22

- 1989-1991 Calibration Results for Segment 23 -

Figure 4-23 presents the model/data comparison for sediment segment 7, which includes most of Boston's Outer Harbor. Data shown are from Station 1, the station closest to the Deer Island sewage outfall. Some infauna were reported in the sediments around this station, as were epibenthic animals (shrimp and crabs). The model comparison to observed ammonia flux for September 1990 is good, with both the model and data indicating a flux of approximately 60 mg N/m^2-day. The model considerably over-estimates the observed SOD, however, computing a value of approximately 1.4 g O_2/m^2-day versus the observed value of about 0.6 g O_2/m^2-day. The reason for this may have to do with the under-estimation of the flushing from Boston Harbor for POC as described in Section 4.5.1.2. The model also over-estimates the fluxes of nitrate and inorganic phosphorus, possibly due to the under-estimation of the flushing time for the harbor area.

The final presentation of sediment model calibration results is shown on Figure 4-24. Results are presented for sediment segment 8, which represents the Dorchester Bay and Boston Inner Harbor. Data from Stations 2 and 3 are plotted against model computations. The model compares favorably to the observed ammonia flux (note the change in the y-axis for ammonia). Both the model and the data show ammonia fluxes on the order of 100-120 mg N/m^2-day. The model over-estimates the observed SOD, computing about 2.7 gm O_2/m^2-day versus 1.2 to 2.0 gm O_2/m^2-day observed in the data (note the change in y-axis for SOD). The model considerably under-estimates the negative flux of nitrate into the sediment (actually computing a slight positive nitrate flux) and markedly under-estimates the positive inorganic phosphorus flux from the sediment. It is unclear why these discrepancies exist, although it should be noted that the phosphorus fluxes are much higher than would be expected for aerobic conditions based on other estuarine systems such as Long Island Sound and Chesapeake Bay.

Although an extensive calibration for the sediment submodel could not be made with the existing data set, the initial results for the sediment flux model are encouraging. The model was, in general, able to approximately reproduce the spatial trends in the observed sediment flux data. In the vicinity of the present outfall, both observed and

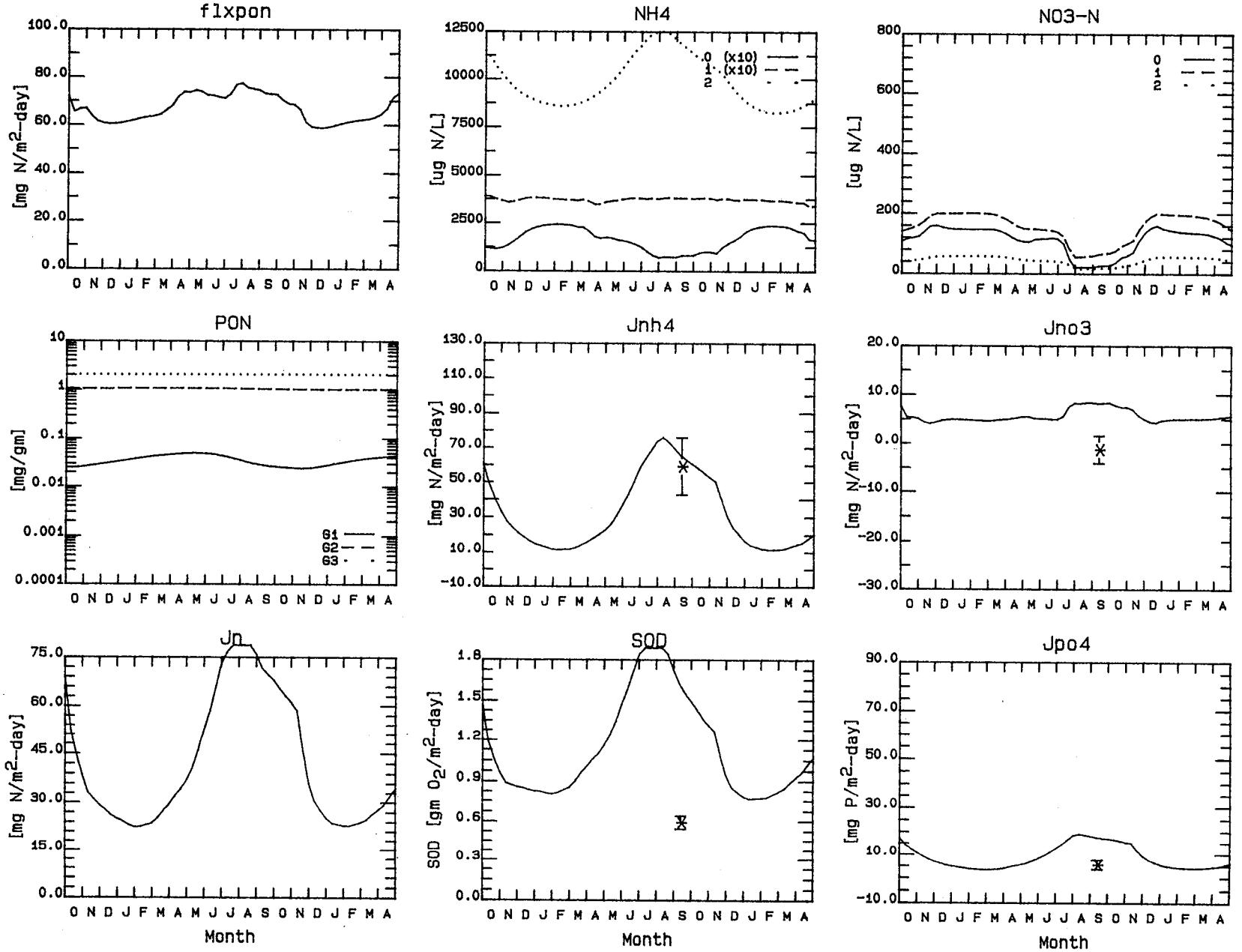

FIGURE 4-23

- 1989-1991 Calibration Results for Segment 7 -

LEGEND
* Data +/- range
0 Overlying Water
1 Aerobic Layer
2 Anaerobic Layer

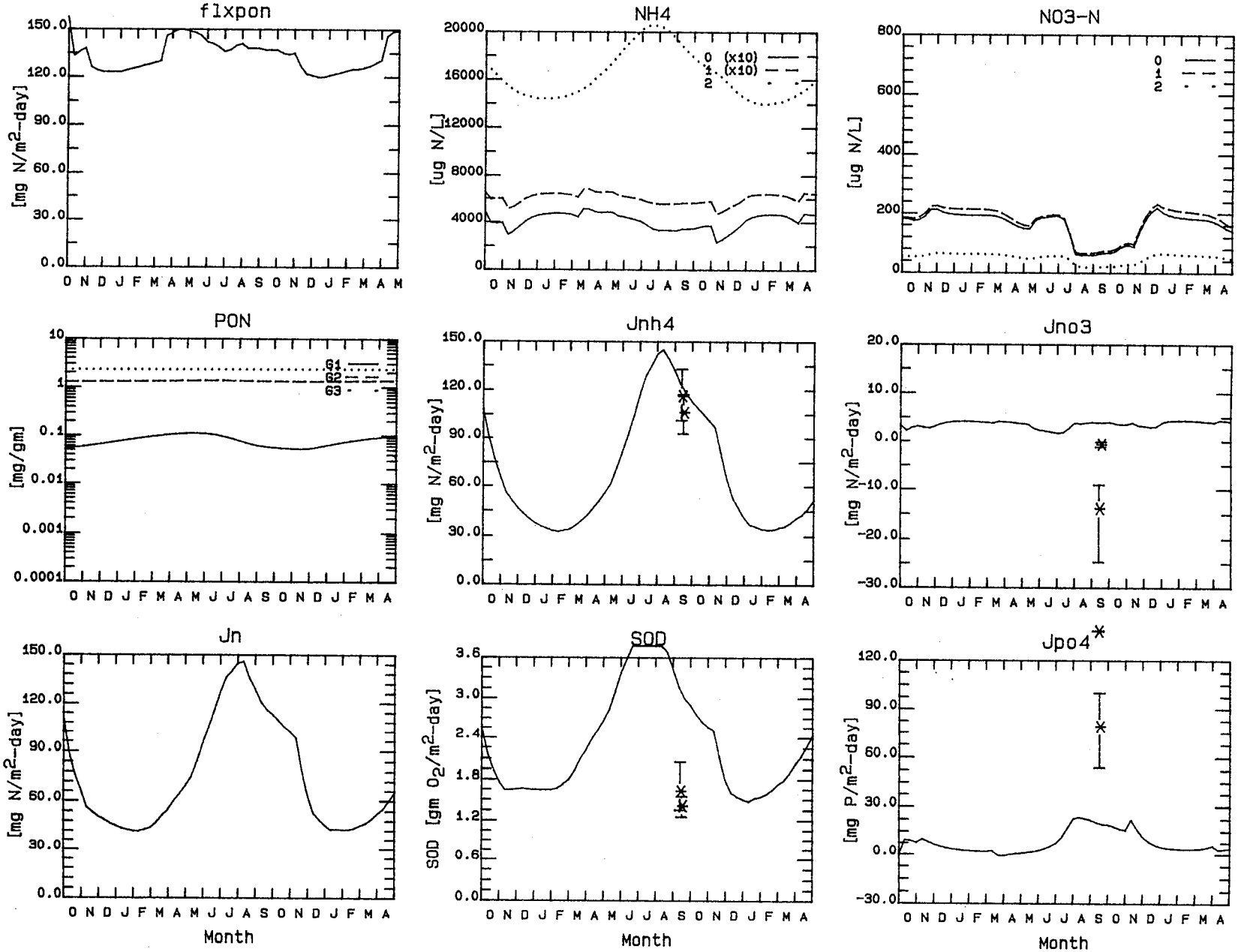

FIGURE 4-24

- 1989-1991 Calibration Results for Segment 8 -

----- LEGEND -----
* Data +/- range

computed fluxes were high relative to areas well removed from the present outfall, which had lower fluxes of SOD and ammonia.

SECTION 5

REFERENCES

Bienfang, P.K., P.J. Harrison and L.M. Quarmby, 1982. Sinking Rate Response to Depletion of Nitrate, Phosphate and Silicate in Four Marine Diatoms, Marine Biology, 67, 295-302.

Bothner, M.H., 1987. Geochemical and Geological Studies of Sediments in Boston Harbor and Massachusetts Bay (abs.) in Program, Science and Policy of Boston Harbor and Massachusetts Bay; Planning for the Twenty-First Century. Annual Boston Harbor/Massachusetts Bay Symposium of the Massachusetts Bay Marine Studies Consortium, November 12 & 13.

Cerco, C.F. and T. Cole, 1992. Application of the 3-D Eutrophication Model CD-QUAL-ICM to Chesapeake Bay, Draft Report to the U.S. EPA Chesapeake Bay Program. Prepared by U.S. Army Corps of Engineers, WES, Vicksburg, Mississippi.

Coupe, R.H. Jr., and W.E. Webb, 1984. Water Quality of the Tidal Potomac River and Estuary: Hydrologic Data Report Supplement; 1979 through 1981 water years, U.S. Geological Survey Open-File Report 84-132.

Culver, M.E. and W.O. Smith, Jr., 1989. Effects of Environmental Variation on Sinking Rates of Marine Phytoplankton, J. Phycol. 25, 262-270.

Duffie, J.A. and W.A. Beckman, 1974. "Solar Radiation Thermal Processes." John Wiley and Sons, New York, New York.

Fitzgerald, M.G., 1980. Anthropogenic Influence of the Sedimentary Regime of an Urban Estuary - Boston Harbor, Woods Hole Oceanographic Institution Report WHOI-80-38, Woods Hole, Massachusetts.

Giblin, A.E., J. Tucker and C. Hopkinson, 1991. Sediment Oxygen Demand and Nitrogen Flux in Massachusetts Bay, Prepared for Massachusetts Water Resources Authority Harbor Studies Group. MWRA Environmental Quality Technical Report 92-1.

Hendry, G.S., 1977. Relationships Between Bacterial Levels and Other Characteristics of Recreational lakes in the District of Muskoka, Interim Microbiology Report, Laboratory Service Branch, Ontario Ministry of the Environment.

HydroQual, Inc., 1991. Water Quality Modeling Analysis of Hypoxia in Long Island Sound, Prepared for Management Committee Long Island Sound Estuary Study and New England Interstate Water Pollution Control Commission.

HydroQual, Inc., 1989. Development and Calibration of a Coupled Hydrodynamic/Water Quality/Sediment Model of Chesapeake Bay, prepared for the U.S. EPA Chesapeake Bay Program, Mahwah, New Jersey.

HydroQual, Inc., 1987. A Steady-State Coupled Hydrodynamic/Water Quality Model of the Eutrophication and Anoxia Process in Chesapeake Bay, Prepared for the U.S. EPA Chesapeake Bay Program, Mahwah, New Jersey.

Hyer, P.V., C.S. Fang, E.P. Ruzeck, and W.J. Hargis, 1971. Hydrography and Hydrodynamics of Virginia Estuaries, Studies of the Distribution of Salinity and Dissolved Oxygen in the Upper York System, Virginia Institute of Marine Science.

Jewell, W.J. and P.L. McCarty, 1971. Aerobic Decomposition of Algae. Environ. Sci. Technol. 1971, 5(10), p. 1023.

Lowe, W.E., 1976. Personal Communication. Canada Centre for Inland Waters, Burlington, Canada.

Menon, A.S., W.A. Gloschenko and N.M. Burns, 1972. Bacteria-Phytoplankton Relationships in Lake Erie, Proc. 15th Conf. Great Lakes Res., 94, Inter. Assoc. Great Lakes Res., 101.

Menzie-Cura & Associates, 1991. Sources and Loadings of Pollutants to Massachusetts Bays Program Task 1 of the Massachusetts Bays Programs. Prepared for the Massachusetts Bay Program, Massachusetts Coastal Zone Management, U.S. EPA. MBP 91-01.

Metcalf and Eddy, 1990. Boston Harbor Project - Deer Island Related Facilities: Trailer Pilot Plant Report. Submitted to MWRA, Program Management Div., Boston, Massachusetts.

Morel, F.M., 1983. Principles of Aquatic Chemistry, John Wiley and Sons, New York, New York.

Riley, G.A., H. Stommel and D.F. Bumpus, 1949. Quantitative Ecology of the Plankton of the Western North Atlantic, Bull. Bingham Oceangr. Coll., 12(3), 1-169.

Science Application International Corp., 1987. REMOTS Survey of Broad Sound, Massachusetts Bay. Report # SAIC-8717511 & 141. Submitted to Stone and Webster, April 1987.

Signell, R.P. and B. Butman, 1992. Model Tidal Exchange and Dispersion in Boston Harbor, Journal of Geophysical Research, Vol. 97, No. C10, pp. 15, 491-15, 606.

Steele, J.M., 1962. Environmental Control of Photosynthesis in the Sea, Limnol. Oceanogr., 7, 137-150.

U.S. EPA, 1988. "Boston Harbor Wastewater Conveyance System" Vols I & II, Draft Supplemental Environmental Impact Statement.

WEF and ASCE, 1991. Design of Municipal Wastewater Treatment Plants Volume I. WEF Manual of Practice No. 8, ASCE Manual and Report on Engineering Practice No. 76.

APPENDIX A

WATER COLUMN KINETICS

APPENDIX A

WATER COLUMN KINETICS

This appendix presents the biological and chemical reaction rate equations used in the water quality model of Massachusetts and Cape Cod Bays. A general description of the overall model framework has been presented in Section 2.0 of this report. The appendix will provide the mathematical realization of the model framework for the variables contained in Table A-1.

Table A-2 presents the phytoplankton net growth equations as influenced by temperature, light and nutrients.

Table A-3 presents the biological and chemical source/sink terms for the various organic carbon state-variables.

Table A-4 presents the biological and chemical source/sink terms for the phosphorus state-variables including the effects of algal uptake, cell lysing and grazing, and hydrolysis and mineralization.

Table A-5 presents the biological and chemical source/sink terms for the nitrogen state-variables including the effects of algal uptake, cell lysing and grazing, hydrolysis and mineralization.

Table A-6 presents the biological and chemical source/sink terms for biogenic and dissolved silica including the effects of algal uptake, cell lysing and grazing and mineralization.

Table A-7 presents the biological and chemical source/sink terms for dissolved oxygen and oxygen equivalents (i.e., hydrogen sulfide released from the sediment under anaerobic conditions). These effects include atmospheric reaeration, algal photosynthesis

and respiration, oxidation of organic carbon, nitrification and oxidation of oxygen equivalents (hydrogen sulfide).

TABLE A-2. PHYTOPLANKTON NET GROWTH EQUATIONS
(continued)

Description	Notation	Rate Constants: Winter Diatoms	Rate Constants: Summer Assemblage	Units
Maximum Specific Growth Rate at T_{opt}	G_{Pmax}	2.00	2.50	day^{-1}
Temperature Coefficient	θ_P	1.068	1.068	-
Temperature Optimum	T_{opt}	12.	18.	^oC
Phytoplankton Self-Shading Attenuation	k_c	0.017	0.017	m^2/mg chl-a
Half-Saturation Constant for Nitrogen	K_{mN}	0.010	0.010	mgN/L
Half-Saturation Constant for Phosphorus	K_{mP}	0.001	0.001	mgP/L
Half-Saturation Constant for Silica	K_{mSi}	0.035	0.015	mgSi/L
Algal Endogenous Respiration	k_{PR}	0.20	0.25	day^{-1}
Temperature Coefficient	θ_{PR}	1.047	1.047	-
Base Algal Settling Rate	v_{sPb}	0.10	0.10	m/day
Nutrient Dependent Algal Settling Rate	v_{sPn}	0.2	0.2	m/day
Temperature Coefficient	θ_{sP}	1.029	1.029	
Loss Due to Zooplankton Grazing	k_{grz}	0.050	0.050	day^{-1}
Temperature Coefficient	θ_{grz}	1.130	1.130	
Carbon/Chlorophyll Ratio	a_{cchl}	40.	65.	mgC/mg chl-a

TABLE A-2. PHYTOPLANKTON NET GROWTH EQUATIONS
(continued)

Endogenous Respiration

$$k_{PR}(T) = k_{PR}(20^oC) \bullet \theta_{PR}^{(T-20)}$$

Algal Settling

$$k_{sP}(T) = \left(\frac{v_{sPb}}{H} + \frac{v_{sPn}}{H} \bullet (1 - G_N(N))\right) \bullet \theta_{sP}^{(T-20)}$$

Zooplankton Grazing

$$k_{grz}(T) = k_{grz}(20^oC) \bullet \theta_{grz}^{(T-20)}$$

Exogenous Variables

Description	Notation	Units
Total Extinction Coefficient	k_e	m^{-1}
Base Extinction Coefficient	k_{ebase}	m^{-1}
Total Daily Surface Solar Radiation	I_o	langleys
Temperature	T	^oC
Segment Depth	H	m
Fraction of Daylight	f	-

TABLE A-2. PHYTOPLANKTON NET GROWTH EQUATIONS

Net Growth Rate

$$S_P = (G_{Pmax} \bullet G_T(T) \bullet G_I(I) \bullet G_N(N) - k_{PR}(T) - k_{sP}(T) - k_{grz}(T)) \bullet P_c$$

Temperature Correction

$$G_{Pmax}(T) = G_{Pmax}(T_{opt}) \bullet \theta_P^{(T-T_{opt})} \qquad T \leq T_{opt}$$

$$G_{Pmax}(T) = G_{Pmax}(T_{opt}) \bullet \theta_P^{(T_{opt}-T)} \qquad T > T_{opt}$$

Light Reduction

$$G_I(I) = \frac{ef}{k_e H} \bullet (e^{-\alpha_1} - e^{-\alpha_0})$$

$$\alpha_1 = \frac{I_o}{I_s} e^{-k_e H} \qquad \alpha_o = \frac{I_o}{I_s}$$

$$k_e = k_{e_{base}} + 1{,}000\ k_c \bullet P_c / a_{cchl}$$

Nutrient Uptake

$$G_N(N) = \text{Min}\left(\frac{DIN}{K_{mN} + DIN}, \frac{DIP}{K_{mP} + DIP}, \frac{Si}{K_{mSi} + Si}\right)$$

DIN = dissolved inorganic nitrogen = $NH_3 + NO_2 + NO_3$
DIP = dissolved inorganic phosphorus
Si = available silica

TABLE A-1. STATE-VARIABLES UTILIZED BY THE KINETIC FRAMEWORK

1. - salinity (S)
2. - temperature (T)
3. - phytoplankton carbon - winter diatoms (P_{c1})
4. - phytoplankton carbon - summer assemblage (P_{c2})
5. - labile particulate organic carbon (LPOC)
6. - refractory particulate organic carbon (RPOC)
7. - labile dissolved organic carbon (LDOC)
8. - refractory dissolved organic carbon (RDOC)
9. - reactive dissolved organic carbon (ReDOC)
10. - algal exudate dissolved organic carbon (ExDOC)
11. - labile particulate organic phosphorus (LPOP)
12. - refractory particulate organic phosphorus (RPOP)
13. - labile dissolved organic phosphorus (LDOP)
14. - refractory dissolved organic phosphorus (RDOP)
15. - dissolved inorganic phosphorus (DIP)
16. - labile particulate organic nitrogen (LPON)
17. - refractory particulate organic nitrogen (RPON)
18. - labile dissolved organic nitrogen (LDON)
19. - refractory dissolved organic nitrogen (RDON)
20. - ammonia nitrogen (NH3)
21. - nitrite + nitrate nitrogen (NO2 + NO3)
22. - biogenic silica (BSi)
23. - available silica (Si)
24. - dissolved oxygen (DO)
25. - dissolved oxygen equivalents (O_2^*)

TABLE A-3. ORGANIC CARBON REACTION EQUATIONS
(Numbering scheme refers to the variable list in Table A-1)

Labile Particulate Organic Carbon (LPOC)

$$S_5 = f_{LPOC} \bullet k_{grz}(T) \bullet P_c - k_{5,7}\theta_{5,7}^{T-20} \bullet LPOC \bullet \frac{P_c}{K_{mP_c} + P_c} - v_{sPOM}(T) \bullet LPOC$$

Refractory Particulate Organic Carbon (RPOC)

$$S_6 = f_{RPOC} \bullet k_{grz}(T) \bullet P_c - k_{6,8}\theta_{6,8}^{T-20} \bullet RPOC \bullet \frac{P_c}{K_{mp_c} + P_c} - v_{sPOM}(T) \bullet RPOC$$

Labile Dissolved Organic Carbon (LDOC)

$$S_7 = f_{LDOC} \bullet k_{grz}(T) \bullet P_c + k_{5,7}\theta_{5,7}^{T-20} \bullet LPOC \bullet \frac{P_c}{k_{mP_c} + P_c}$$

$$- k_{7,0}\theta_{7,0}^{T-20} \bullet LDOC \bullet \frac{P_c}{K_{mP_c} + P_c} \bullet \frac{DO}{K_{DO} + DO}$$

Refractory Dissolved Organic Carbon (RDOC)

$$S_8 = f_{RDOC} \bullet k_{grz}(T) \bullet P_c + k_{6,8}\theta_{6,8}^{T-20} \bullet RPOC \bullet \frac{P_c}{K_{mP_c} + P_c}$$

$$- k_{8,0}\theta_{8,0}^{T-20} \bullet RDOC \bullet \frac{P_c}{K_{mP_c} + P_c} \bullet \frac{DO}{K_{DO} + DO}$$

TABLE A-3. ORGANIC CARBON REACTION EQUATIONS
(Numbering scheme refers to the variable list in Table A-1)
(continued)

Reactive Dissolved Organic Carbon (ReDOC)

$$S_9 = - k_{9,0}\theta_{9,0}^{T-20} \bullet ReDOC \bullet \frac{P_c}{K_{mP_c} + P_c} \bullet \frac{DO}{K_{DO} + DO}$$

Algal Exudate Dissolved Organic Carbon (ExDOC)

$$S_{10} = f_{ExDOC} \bullet G_P \bullet P_c$$

$$- k_{10,0}\theta_{10,0}^{T-20} \bullet ExDOC \bullet \frac{P_c}{K_{mP_c} + P_c} \bullet \frac{DO}{K_{DO} + DO}$$

TABLE A-3. ORGANIC CARBON REACTION EQUATIONS
(Numbering scheme refers to the variable list in Table A-1)
(continued)

Description	Notation	Value	Units
Phytoplankton Biomass	P_c	-	mgC/L
Specific Phytoplankton Growth Rate	G_P		day^{-1}
Half Saturation Constant for Phytoplankton Limitation	K_{mPc}	0.15	mgC/L
Fraction of Grazed Organic Carbon Recycled to:			
the LPOC pool	f_{LPOC}	0.25	
the RPOC pool	f_{RPOC}	0.05	
the LDOC pool	f_{LDOC}	0.65	
the RDOC pool	f_{RDOC}	0.05	
Fraction of Primary Productivity Going to the Algal Exudate DOC pool	f_{ExDOC}	0.10	
Hydrolysis Rate for LPOC	$K_{5,7}$	0.10	day^{-1}
Temperature Coefficient	$\theta_{5,7}$	1.08	
Base Settling Rate of POM (LPOC,RPOC)	v_{sPOM}	0.10	m/day
Hydrolysis Rate for RPOC	$k_{6,8}$	0.01	day^{-1}
Temperature Coefficient	$\theta_{6,8}$	1.12	
Segment depth	H	-	m
Oxidation Rate of LDOC	$k_{7,0}$	0.100	day^{-1}
Temperature Coefficient	$\theta_{8,0}$	1.047	
Oxidation Rate of RDOC	$k_{7,0}$	0.010	day^{-1}
Temperature Coefficient	$\theta_{8,0}$	1.120	
Oxidation Rate of ReDoc	$k_{9,0}$	0.20	day^{-1}
Temperature Coefficient	$\theta_{9,0}$	1.047	
Oxidation Rate of ExDOC	$k_{10,0}$	0.05	day^{-1}
Temperature Coefficient	$\theta_{10,0}$	1.080	
Half Saturation for Oxygen Limitation	K_{DO}	0.30	mgO_2/L
Dissolved Oxygen	DO	-	mgO_2/L

TABLE A-4. PHOSPHORUS REACTION RATES
(Numbering scheme refers to the variable list in Section A-1)

Labile Particulate Organic Phosphorus (LPOP)

$$S_{11} = a_{PC} \bullet f_{LPOP} \bullet (k_{PR}(T) + k_{grz}(T)) \bullet P_c$$

$$- k_{11,13}\theta_{11,13}^{T-20} \bullet LPOP \bullet \frac{P_c}{K_{mP_c} + P_c} - v_{sPOM}(T) \bullet LPOP$$

Refractory Particulate Organic Phosphorus (RPOP)

$$S_{12} = a_{PC} \bullet f_{RPOP} \bullet (k_{PR}(T) + k_{grz}(T)) \bullet P_c - v_{sPOM}(T) \bullet RPOP$$

$$-k_{12,14}\theta_{12,14}^{(T-20)} \bullet RPOP \bullet \frac{P_c}{K_{mP_c} + P_c}$$

Labile Dissolved Organic Phosphorus (LDOP)

$$S_{13} = a_{PC} \bullet f_{LDOP} \bullet (k_{PR}(T) + k_{grz}(T)) \bullet P_c$$

$$+ k_{11,13}\theta_{11,13}^{T-20} \bullet RPOP \bullet \frac{P_c}{K_{mP_c} + P_c}$$

$$- k_{13,15}\theta_{13,15}^{T-20} \bullet LDOP \bullet \frac{P_c}{K_{mP_c} + P_c}$$

TABLE A-4. PHOSPHORUS REACTION RATES
(Numbering scheme refers to the variable list in Section A-1)
(continued)

Refractory Dissolved Organic Phosphorus (RDOP)

$$S_{14} = a_{PC} \bullet f_{RDOP} \bullet (k_{PR}(T) + k_{grz}(T)) \bullet P_c$$

$$+ k_{12,14}\theta_{12,14}^{T-20} \bullet RPOP \bullet \frac{P_c}{K_{mP_c} + P_c}$$

$$- k_{14,15}\theta_{14,15}^{T-20} \bullet RDOP \bullet \frac{P_c}{K_{mP_c} + P_c}$$

Dissolved Inorganic Phosphorus (DIP)

$$S_{15} = a_{PC} \bullet f_{DIP} \bullet (k_{PR}(T) + k_{grz}(T)) \bullet P_c$$

$$+ (k_{13,15}\theta_{13,15}^{T-20} \bullet LDOP + k_{14,15}\theta_{14,15}^{T-20} \bullet RDOP) \bullet \frac{P_c}{K_{mP_c} + P_c}$$

$$- a_{PC} \bullet (1 - f_{ExDOC}) \bullet G_P \bullet P_c$$

TABLE A-4. PHOSPHORUS REACTION RATES
(Numbering scheme refers to the variable list in Section A-1)
(continued)

Description	Notation	Value	Units
Phytoplankton Biomass	P_c	-	mgC/L
Temperature Corrected Algal Respiration Rate	$k_{PR}(T)$		day^{-1}
Temperature Corrected Grazing Rate	$k_{grz}(T)$		day^{-1}
Specific Phytoplankton Growth Rate	G_P		day^{-1}
Phosphorus to Carbon Ratio	a_{PC}	0.025	mgP/mgC
Fraction of Primary Productivity Going to the Algal Exudate DOC pool	f_{ExDOC}	0.1	
Fraction of Respired and Grazed Algal Phosphorus Recycled to			
the LPOP pool	f_{LPOP}	0.30	
the RPOP pool	f_{RPOP}	0.05	
the LDOP pool	f_{LDOP}	0.10	
the RDOP pool	f_{RDOP}	0.05	
the DIP pool	f_{DIP}	0.50	
LPOP Hydrolysis Rate at 20°C	$k_{11,13}$	0.05	day^{-1}
Temperature Coefficient	$\theta_{11,13}$	1.08	
Base Settling Rate of POM (LPOP, RPOP)	v_{sPOM}	0.1	m/day
RPOP Hydrolysis Rate at 20°C	$k_{12,14}$	0.01	day^{-1}
Temperature Coefficient	$\theta_{12,14}$	1.08	
LDOP Mineralization Rate at 20°C	$k_{13,15}$	0.10	day^{-1}
Temperature Coefficient	$\theta_{13,15}$	1.08	
RDOP Mineralization Rate at 20°C	$k_{14,15}$	0.02	day^{-1}
Temperature Coefficient	$\theta_{14,15}$	1.08	

TABLE A-5. NITROGEN REACTION RATES
(Numbering scheme refers to the variable list in Table A-1)

Labile Particulate Organic Nitrogen (LPON)

$$s_{16} = a_{NC} \bullet f_{LPON} \bullet (k_{PR}(T) + k_{grz}(T)) \bullet P_c$$

$$- k_{16,18}\theta_{16,18}^{T-20} \bullet LPON \bullet \frac{P_c}{K_{mP_c} + P_c} - v_{sPOM}(T) \bullet LPON$$

Refractory Particulate Organic Nitrogen (RPON)

$$S_{17} = a_{NC} \bullet f_{RPON} \bullet (k_{PR}(T) + k_{grz}(T)) \bullet P_c$$

$$- k_{17,19}\theta_{17,19}^{T-20} \bullet RPON \bullet \frac{P_c}{K_{mP_c} + P_c} - v_{sPOM}(T) \bullet RPON$$

Labile Dissolved Organic Nitrogen (LDON)

$$S_{18} = a_{NC} \bullet f_{LDON} \bullet (k_{PR}(T) + k_{grz}(T)) \bullet P_c$$

$$+ k_{16,18}\theta_{16,18}^{T-20} \bullet LPON \bullet \frac{P_c}{K_{mP_c} + P_c}$$

$$- k_{18,20}\theta_{18,20}^{T-20} \bullet LDON \bullet \frac{P_c}{K_{mP_c} + P_c}$$

TABLE A-5. NITROGEN REACTION RATES
(Numbering scheme refers to the variable list in Table A-1)
(continued)

Refractory Dissolved Organic Nitrogen (RDON)

$$S_{19} = a_{NC} \bullet f_{RDON} \bullet (k_{PR}(T) + k_{grz}(T)) \bullet P_c$$

$$+ k_{17,19}\theta_{17,19}^{T-20} \bullet RPON \bullet \frac{P_c}{K_{mP_c} + P_c}$$

$$- k_{19,20}\theta_{19,20}^{T-20} \bullet RDON \bullet \frac{P_c}{K_{mP_c} + P_c}$$

Ammonia Nitrogen (NH_3)

$$S_{20} = a_{NC} \bullet f_{NH3} \bullet (k_{PR}(T) + k_{grz}(T)) \bullet P_c$$

$$+ (k_{18,20}\theta_{18,20}^{T-20} \bullet LDON + k_{19,20}\theta_{19,20}^{T-20} \bullet RDON \bullet \frac{P_c}{K_{mP_c} + P_c}$$

$$- a_{NC} \bullet \alpha_{NH_3} \bullet (1 - f_{ExDOC}) \bullet G_P \bullet P_c - k_{20,21}\theta_{20,21}^{T-20} \bullet NH_3 \bullet \frac{DO}{K_{nitr} + DO}$$

Nitrite + Nitrate Nitrogen ($NO_2 + NO_3$)

$$S_{21} = k_{20,21}\theta_{20,21}^{T-20} \bullet NH_3 \bullet \frac{DO}{K_{nitr} + DO} - a_{NC} \bullet (1 - \alpha_{NH_3}) \bullet (1 - f_{ExDOC}) \bullet G_P \bullet P_c$$

$$- k_{21,0}\theta_{21,0}^{T-20} \bullet (NO_2 + NO_3) \bullet \frac{K_{NO_3}}{K_{NO_3} + DO}$$

TABLE A-5. NITROGEN REACTION RATES
(Numbering scheme refers to the variable list in Table A-1)
(continued)

Description	Notation	Value	Units
Phytoplankton Biomass	P_c	-	mgC/L
Temperature Corrected Algal Respiration Rate	$k_{PR}(T)$		day^{-1}
Temperature Corrected Grazing Rate	$k_{grz}(T)$		day^{-1}
Specific Phytoplankton Growth Rate	G_P		day^{-1}
Nitrogen to Carbon Ratio	a_{NC}	0.176	mgN/mgC
Fraction of Respired and Grazed Algal Nitrogen Recycled to			
the LPON pool	f_{LPON}	0.35	
the RPON pool	f_{RPON}	0.05	
the LDON pool	f_{LDON}	0.25	
the RDON pool	f_{RDON}	0.05	
the NH_3 pool	fNH_3	0.30	
LPON Hydrolysis Rate at 20°C	$k_{16,18}$	0.05	day^{-1}
Temperature Coefficient	$\theta_{16,18}$	1.08	
Base Settling Rate of POM (LPON, RPON)	v_{sPOM}	0.1	m/day
RPON Hydrolysis Rate at 20°C	$k_{17,19}$	0.01	day^{-1}
Temperature Coefficient	$\theta_{17,19}$	1.08	
LDON Mineralization Rate at 20°C	$k_{18,20}$	0.085	day^{-1}
Temperature Coefficient	$\theta_{18,20}$	1.08	
RDON Mineralization Rate at 20°C	$k_{19,20}$	0.017	day^{-1}
Temperature Coefficient	$\theta_{19,20}$	1.08	
Nitrification Rate at 20°C	$k_{20,21}$	0.05	day^{-1}
Temperature Coefficient	$\theta_{20,21}$	1.08	
Half Saturation constant for Oxygen Limitation	K_{nitr}	1.5	mgO_2/L
Denitrification Rate at 20°C	$k_{21,0}$	0.05	day^{-1}
Temperature Coefficient	$\theta_{21,0}$	1.045	
Michaelis Constant for Denitrification	K_{NO3}	0.01	mgO_2/L

TABLE A-6. SILICA REACTION EQUATIONS
(Numbering scheme refers to the variable list in Table A-1)

Biogenic Silica (BSi)

$$S_{22} = (k_{PR}(T)+k_{grz}(T))\bullet P_C - k_{22,23}\theta_{22,23}^{T-20}\bullet BSi\bullet\frac{P_C}{K_{mP_c}+P_C} - v_{sPOM}\bullet BSi$$

Available Silica (Si)

$$S_{23} = k_{22,23}\theta_{22,23}^{T-20}\bullet BSi\bullet\frac{P_C}{K_{mP_c}+P_C} - (1-f_{ExDOC})\bullet a_{SC}\bullet G_P\bullet P_C$$

Description	Notation	Value	Units
Phytoplankton Biomass	P_C	-	mgC/L
Temperature Corrected Algal Respiration Rate	$k_{PR}(T)$		day^{-1}
Temperature Corrected Grazing Rate	$k_{grz}(T)$		day^{-1}
Specific Phytoplankton Growth Rate	G_P		day^{-1}
Silica to Carbon Ratio: Winter Summer	a_{SC}	0.36 0.10	mgSi/mgC
Mineralization Rate of Biogenic Silica	$k_{22,23}$	0.08	day^{-1}
Temperature Coefficient	$\theta_{22,23}$	1.08	
Base Settling Rate of POM (BSi)	v_{sPOM}	0.1	m/day

TABLE A-7. DISSOLVED OXYGEN AND O_2^* REACTION RATES
(Numbering scheme refers to the variable list in Table A-1)

Dissolved Oxygen (DO)

$$S_{24} = a_{OC} \bullet \alpha_{NH3} \bullet G_P \bullet P_c + (a_{NO_3C}) \bullet (1-\alpha_{NH_3}) \bullet G_P \bullet P_c$$

$$+ k_a \theta_a^{\,T-20} \bullet (DO_{sat} - DO) - a_{OC} \bullet k_{PR}(T) \bullet P_c$$

$$- 2 \bullet a_{ON} \bullet k_{20,21} \theta_{20,21}^{\,T-20} \bullet NH_3 \bullet \frac{DO}{K_{nitr} + DO}$$

$$- k_{7,0} \theta_{7,0}^{\,T-20} \bullet LDOC + k_{8,0} \theta_{8,0}^{\,T-20} \bullet RDOC + k_{9,0} \theta_{9,0}^{\,T-20} \bullet ReDOC$$

$$+ k_{10,0} \theta_{10,0}^{\,T-20} \bullet ExDOC) \bullet \frac{P_c}{K_{mP_c} + P_c} \bullet \frac{DO}{K_{DO} + DO}$$

$$- k_{O_2^*}^{\,T-20} \bullet O_2^* \bullet \frac{DO}{K_{DO} = DO}$$

Oxygen Equivalents (O_2^*)

$$S_{25} = - k_{O_2^*} \theta_{O_2^*}^{\,T-20} \bullet O_2^* \bullet \frac{DO}{K_{DO} + DO}$$

Rate Constants

Description	Notation	Value	Units
Phytoplankton Biomass	P_c	-	mg C/L
Specific Phytoplankton Growth Rate	G_p		day^{-1}
Oxygen to Carbon Ratio	a_{OC}	32/12	$mgO_2/mg\ C$
Oxygen to Nitrogen Ratio	a_{ON}	32/14	$mgO_2/mg\ N$
Oxygen to Carbon Ratio for Nitrate Uptake	α_{NO3C}	$\frac{48}{14} a_{NC}$	mgO_2/mgC

TABLE A-7. DISSOLVED OXYGEN AND O_2^* REACTION RATES
(Numbering scheme refers to the variable list in Table A-1)
(continued)

Rate Constants

Description	Notation	Value	Units
Ammonia Preference Term for Nitrogen Uptake	α_{NH_3}		-
Nitrogen to Carbon Ratio	a_{NC}	0.176	mg N/mgC
Temperature Corrected Algal Respiration Rate	$k_{PR}(T)$		day^{-1}
Half Saturation Constant for Oxygen Limitation	K_{nitr}	1.5	mg O_2/L
Reaeration Rate at 20°C	k_a	Eq. 2-15a	day^{-1}
Temperature Coefficient	θ_a	1.024	
Oxygen Transfer Coefficient	k_L	0.75-1.8	m^{-1}
Dissolved Oxygen Saturation	DO_{sat}	Eq. 2-16	mgO_2/L
Oxidation Rates and Temperature Coefficients			
for LDOC	$k_{7,0}$ $\theta_{7,0}$	0.100 1.047	day^{-1}
for RDOC	$k_{8,0}$ $\theta_{8,0}$	0.010 1.120	day^{-1}
for ExDOC	$k_{10,0}$ $\theta_{10,0}$	0.05 1.080	day^{-1}
for NH_3	$k_{20,21}$ $\theta_{20,21}$	0.050 1.08	day^{-1}
Oxidation Rate of Oxygen Equivalents	$k_{O_2^*}$	0.30	day^{-1}
Temperature Coefficient	$\theta_{O_2^*}$	1.047	
Half Saturation for Oxygen Limitation	K_{DO}	0.20	mg O_2/L
Dissolved Oxygen	DO		mg O_2/L

APPENDIX B

DOCUMENTATION OF SEDIMENT FLUX MODEL

Table of Contents

half life); more slowly reactive (1 year half life); and very slowly reactive (50 year half life). However, no reactive organic matter is allowed to be removed by burial. The reason is that reactive material will react at some time after its burial and the soluble end products will become available for recycling. Hence all deposited organic material will eventually react. The G classes only control the time scale over which changes in input fluxes will be reflected in changes in diagenesis fluxes.

The kinetic equations for particulate organic carbon, nitrogen, and phosphorus are analogous. Let $G_{POC,i}$ be the concentration of POC in the i^{th} diagenesis class (i=1, 2 or 3). The kinetic equation for diagenesis is:

$$H_2 \frac{dG_{POC,i}}{dt} = -K_{GPOC,i}\theta_{GPOC,i}^{(T-20)} G_{POC,i} H_2 + J_{GPOC,i}(t)$$

where:

$G_{POC,i}$	concentration of particulate organic carbon in reactivity class i in layer 1; [M/L^3]	
$K_{GPOC,i}$	first order reaction rate coefficient: [T^{-1}]	
$\theta_{GPOC,i}$	temperature coefficient	
$J_{GPOC,i}(t)$	POC flux of the i^{th} G class to the sediment from the overlying water. [M/L^2-T]	

The water column sources that contribute to each reactivity class are:

$J_{GPOC,1}$:	Chl_1	Chl_2	$LPOC$
$J_{GPOC,2}$:	$f_{G2}RPOC$		
$J_{GPOC,3}$:	$f_{G3}RPOC$		

where:

f_{G2}	fraction of water column refractory POC that is in reactivity class G2	0.5	-

DOCUMENTATION FOR CHESAPEAKE BAY SEDIMENT FLUX MODEL

I. Model Framework

This report provides the equations and parameter values for the Chesapeake Bay Sediment Model. It includes the final stand alone calibration results.

The sediment receives the fluxes of particulate organic carbon, POC, particulate organic nitrogen, PON, and particulate organic phosphorus, POP, and particulate silica, PSi, from the overlying water. This is collectively referred to as particulate organic matter, POM. Mineralization, which is termed diagenesis, produces soluble end-products. These can react in the aerobic and anaerobic layers of the sediment. The difference between the resulting aerobic layer dissolved concentration and the overlying water concentration determine the flux to or from the sediment. The magnitude of the flux is determined by the surface mass transfer coefficient. The situation is diagrammed in Fig. 1.

II. Diagenesis

The water column model state variables that settle are: the two chlorophyll groups, Chl_1 and Chl_2, particulate silica, Psi, and labile and refractory particulate organic carbon, POC, particulate organic nitrogen, PON, and particulate organic phosphorus, POP. The fluxes of these state variables make up the incoming sources of particulate organic matter to the sediment. Carbon, nitrogen and phosphorus are treated analogously. However, these is no organic particulate detrital silica system. All biogenic silica is assumed to be inorganic. Hence, the biogenic silica flux is a direct source to the silica mass balance equations.

The multi-class G model is used to model the diagenesis of POM. Each class represents a portion of the organic material that reacts at a specific rate. The reaction rates for each class are approximately an order of magnitude smaller than the previous class. For this application three G classes are chosen. The three class represent three scales of reactivity: quickly reactive (20 day

are expressed in terms of the total concentration of the chemical. The distribution between particulate and dissolved fractions is modeled using a linear partitioning model. The mass balance equations of the model can be expressed in a general form which is quite convenient for numerical solution. The layer 1 and 2 equations are:

$$H_1 \frac{dC_{T1}}{dt} = K_{L01}(f_{d1}C_{T1} - C_{d0}) + w_{12}(f_{p2}C_{T2} - f_{p1}C_{T1}) + K_{L12}(f_{d2}C_{T2} - f_{d1}C_{T1}) - K_1 H_1 C_{T1} + J_{T1}$$

$$H_2 \frac{dC_{T2}}{dt} = -w_{12}(f_{p2}C_{T2} - f_{p1}C_{T1}) - K_{L12}(f_{d2}C_{T2} - f_{d1}C_{T1}) - K_2 H_2 C_{T2} - w_2 C_{T2} + J_{T2}$$

where:

C_{T1}	total concentration in layer 1	[M/L^3]
C_{T2}	total concentration in layer 2	[M/L^3]
J_{T1}	total source into layer 1	[M/L^2-T]
J_{T2}	total source into layer 2	[M/L^2-T]
H_1	depth of layer 1	[L]
H_2	depth of layer 2	[L]
K_{L01}	aqueous mass transfer coefficient between layer 1 and the overlying water	[L/T]
K_{L12}	aqueous mass transfer coefficient between layer 1 and layer 2	[L/T]
w_{12}	particle mixing velocity between layer 1 and layer 2	[L/T]
w_2	sedimentation velocity out of layer 2	[L/T]

f_{G3}	fraction of water column refractory POC that is in reactivity class G3	0.5	-

The kinetic coefficients are:

$K_{GPOC,1}$	reaction rate constant for $G_{POC,1}$	3.50E-02	day^{-1}
$\theta_{GPOC,1}$	temperature coefficient for $G_{POC,1}$	1.100	-
$K_{GPOC,2}$	reaction rate constant for $G_{POC,2}$	1.80E-03	day^{-1}
$\theta_{GPOC,2}$	temperature coefficient for $G_{POC,2}$	1.150	-
$K_{GPOC,3}$	reaction rate constant for $G_{POC,3}$	4.00E-05	day^{-1}
$\theta_{GPOC,3}$	temperature coefficient for $G_{POC,3}$	1.170	-

These reaction rates and temperature coefficients are taken from values reported in the literature.

Carbon diagenesis flux, J_C, is computed from the rates of mineralization of the three G classes:

$$J_C = \sum_{i=1}^{3} K_{GPOC,i}\theta_{GPOC,i}^{(T-20)} G_{POC,i} H_2$$

Nitrogen and phosphorus are completely analogous.

$$J_N = \sum_{i=1}^{3} K_{GPON,i}\theta_{GPON,i}^{(T-20)} G_{PON,i} H_2$$

$$J_P = \sum_{i=1}^{3} K_{GPOP,i}\theta_{GPOP,i}^{(T-20)} G_{POP,i} H_2$$

The reaction rates and temperature coefficients are identical to those listed above for carbon.

III. The General Sediment Model Equations

The sediment model is constructed from a mass balance equation in the aerobic layer, denoted as layer 1, and the anaerobic layer, layer 2. Fig. 2 presents the notation. The equations

f_{p2}	particulate fraction in layer 2	[unitless].

$$f_{p2} = 1 - f_{d2}$$

where:

m_1	solids concentration in layer 1	[M/L^3]
m_2	solids concentration in layer 2	[M/L^3]
π_1	partition coefficient in layer 1	[L^3/M]
π_2	partition coefficient in layer 2	[L^3/M].

A. Surface Mass Transfer Coefficient and Reaction Velocities

The surface mass transfer coefficient, K_{LO1}, quantifies the mixing between layer 1 and the overlying water. The critical observation is that it can be related to the sediment oxygen demand, SOD. The SOD is the mass flux of dissolved oxygen into the sediment. Thus, it can be calculated from the mass transfer equation:

$$D_1 \frac{d[O_2]}{dz}\Big|_{z=0} \approx D_1 \frac{[O_2(0)]-[O_2(H_1)]}{H_1} = \frac{D_1}{H_1}[O_2(0)]$$

where a straight line approximation to the derivative is used. The second equality follows from $[O_2(H_1)] = 0$ since H_1 is the depth of zero oxygen concentration. Therefore, the surface mass transfer coefficient can be expressed as:

$$K_{LO1} = \frac{D_1}{H_1} = \frac{SOD}{[O_2(0)]} \equiv s$$

which is the ratio of SOD and overlying water oxygen concentration. For notational simplicity this ratio is termed s.

K_1	first order decay rate coefficient removal processes in layer 1	[T^{-1}]
K_2	first order decay rate coefficient removal processes in layer 2	[T^{-1}]

The dissolved and particulate concentrations and fractions are:

C_{d1} dissolved concentration in layer 1 [M/L^3]

$$C_{d1} = f_{d1} C_{T1}$$

f_{d1} dissolved fraction in layer 1 [unitless]

$$f_{d1} = \frac{1}{1 + m_1 \pi_1}$$

C_{p1} particulate concentration in layer 1 [M/L^3]

$$C_{p1} = f_{p1} C_{T1}$$

f_{p1} particulate fraction in layer 1 [unitless]

$$f_{p1} = 1 - f_{d1}$$

C_{d2} dissolved concentration in layer 2 [M/L^3]

$$C_{d2} = f_{d2} C_{T2}$$

f_{d2} dissolved fraction in layer 2 [unitless]

$$f_{d2} = \frac{1}{1 + m_2 \pi_2}$$

C_{p2} particulate concentration in layer 2 [M/L^3]

$$C_{p2} = f_{p2} C_{T2}$$

B. Particulate Phase Mixing

The rate of mixing of sediment particles by macrobenthos (bioturbation) has been quantified by estimating the apparent particle diffusion coefficient. The variation has been found to be proportional to the biomass of the benthos. In order to make the model self consistent - that is to use only internally computed variables in the parameterizations - it seems reasonable to assume that benthic biomass is proportional to the labile carbon in the sediment which is calculated by the model as $G_{POC,1}$.

A series of experiments have examined the relationship between particle mixing due to benthic organisms and the overlying water oxygen concentration. There is a general dependency of mixing rate on DO, with the lower rates occurring at the lower DO concentrations. This dependency is modeled using a Michaelis Menton expression. The particle mixing mass transfer coefficient that results is:

$$w_{12}^{*} = \frac{D_p \theta_{Dp}^{(T-20)}}{H_2} \frac{G_{POC,1}}{G_{POC,R}} \frac{[O_2(0)]}{K_{M,Dp} + [O_2(0)]}$$

with units [L/T]. The superscript * is used to denote this formulation from the final expression for w_{12} that is developed below. The parameter values are:

D_p	Diffusion coefficient for particle mixing	1.2E-04	m^2/d
θ_{Dp}	Temperature coefficient for D_p	1.117	-
$G_{POC,R}$	Reference concentration for $G_{POC,1}$.	1.0E+05	mg/m^3
$K_{M,Dp}$	Particle mixing half saturation constant for oxygen	4.0	mg/L

C. Benthic Stress

In addition to the reduction in particle mixing velocity due to the instantaneous oxygen concentration, it has been found necessary to include a more lasting effect. In particular if anoxia

The reaction rate in the aerobic layer is formulated as a conventional first order reaction with reaction rate constant K_1. The term in the layer 1 equation is $K_1 H_1$. The depth of the aerobic zone follows from the definition of the surface mass transfer coefficient: $s = D_1 / H_1$. Hence $K_1 H_1 = K_1 D_1 / s$. The reaction velocity, which has units [L/T], is defined as:

$$\kappa_1 = \sqrt{D_1 K_1}$$

The square root is used to conform to the parameter group that appears in the spatially continuous form of the model. With these definitions the reaction rate - aerobic layer depth product becomes:

$$K_1 H_1 = \frac{\kappa_1^2}{s}$$

The reaction velocity in layer 2 is defined for convenience of nomenclature only.

$$\kappa_2 = K_2 H_2$$

It has units of [L/T]. However it is not equivalent to the aerobic layer reaction velocities which include diffusion coefficient as well as a reaction rate constant.

With these definitions the layer 1 and 2 equations become:

$$H_1 \frac{dC_{T1}}{dt} = s(f_{d1} C_{T1} - C_{d0}) + w_{12}(f_{p2} C_{T2} - f_{p1} C_{T1})$$

$$+ K_{L12}(f_{d2} C_{T2} - f_{d1} C_{T1}) - \frac{\kappa_1^2}{s} C_{T1} + J_{T1}$$

$$H_2 \frac{dC_{T2}}{dt} = -w_{12}(f_{p2} C_{T2} - f_{p1} C_{T1}) - K_{L12}(f_{d2} C_{T2} - f_{d1} C_{T1})$$

$$- \kappa_2 C_{T2} - w_2 C_{T2} + J_{T2}$$

D. Dissolved Phase Mixing

Dissolved phase mixing between layers 1 and 2 is via passive molecular diffusion which is enhanced by the mixing activities of the benthic organisms (bio-irrigation). This is modeled by increasing the diffusion coefficient by a factor of 10 over the molecular diffusion coefficient.

$$K_{L12} = \frac{D_d \theta_{Dd}^{(T-20)}}{H_2}$$

D_d	Pore water diffusion coefficient	1.0E-3	m^2/d
θ_{Dd}	Temperature coefficient for D_d	1.08	-

E. Solids Burial

The deposition of solids to the sediment causes an increase in the depth of the sediment relative to a fixed datum. If the sediment surface is regarded as the point of reference, then the increase in the depth of sediment is a loss of mass due to burial from the active sediment layer. For the Chesapeake Bay model, the sedimentation velocities are spatially variable. For the stand alone calibration, an average value is selected.

w_2	Sedimentation velocity for the stand alone calibration.	6.85E-06 (0.25)	m/d (cm/yr)

F. Geometry and Solids Concentrations

Since these parameters are associated with other fitted parameters, the sediment solids concentrations are chosen to be representative values.

m_1	Aerobic layer solids concentration	0.5	kg/L
m_2	Anaerobic layer solids concentration	0.5	kg/L

The active layer depth is chosen to represent the depth of organism mixing. Particles buried below this depth can longer be recycled to the aerobic layer. They are permanently buried.

occurs the benthic fauna population is reduced or eliminated. This is modeled using a first order differential equation that accumulates stress, S, when overlying water dissolved oxygen is below the particle mixing half saturation constant for oxygen, $K_{M,Dp}$. Thus:

$$\frac{dS}{dt} = -K_S S + \frac{K_{M,Dp}}{K_{M,Dp} + [O_2(0)]}$$

where:

S	Accumulated benthic stress	[T].
K_S	First order decay coefficient for accumulated stress	[T^{-1}]

The behavior of this formulation can be understood by evaluating the limiting steady state stresses at the two oxygen extremes:

$$[O_2(0)] \to 0 \qquad K_S S \to 1 \qquad (1 - K_S S) \to 0$$

$$[O_2(0)] \to \infty \qquad K_S S \to 0 \qquad (1 - K_S S) \to 1$$

Note that as $[O_2(0)]$ approaches zero at the onset of anoxia, the term $(1 - K_S S)$ also approaches zero. This suggests that $(1 - K_S S)$ is the proper variable to quantify the degree of benthic stress. The expression is unitless and requires no additional parameter - for example a half saturation constant for benthic stress. The final formulation for the particle mixing velocity which includes the benthic stress is:

$$w_{12} = w_{12}^{*} \min_{each\,year} \{(1 - K_S S)\}$$

where w_{12}^{*} is defined above. The stress is continued at its minimum value through the end of the year, in order to conform to the observation that once the benthos has been suppressed by low oxygen, it does not recover until the next year.

J_{T1}	Aerobic layer ammonia source	0.0	mg N/m^2-d
$J_{T2} = J_N$	Nitrogen diagenesis. Computed from equation is section III		mg N/m^2-d

B. Nitrate

Nitrate is produced by nitrification in the aerobic layer. The nitrate source in the aerobic layer is the ammonia produced by diagenesis decremented by the ammonia that escapes to the overlying water. Thus:

$$J_{T1} = J_N - J[NH_4]$$

Nitrate is removed by denitrification in both the aerobic and anaerobic layers.

$$\kappa_1^2 = \kappa_{NO3,1}^2 \theta_{NO3}^{(T-20)}$$

$$\kappa_2 = \kappa_{NO3,2} \theta_{NO3}^{(T-20)}$$

The carbon required by denitrification is supplied by carbon diagenesis. No other reactions occur. The parameters are:

$\kappa_{NO3,1}$	Reaction velocity for denitrification in the aerobic layer	0.10	m/d
$\kappa_{NO3,2}$	Reaction velocity for denitrification in the anaerobic layer	0.25	m/d
θ_{NO3}	Temperature coefficient for denitrification	1.08	-
J_{T2}	Anaerobic layer source of nitrate	0.0	mg N/m^2-d

C. Sulfide

Sulfide is produced by carbon diagenesis, decremented by the organic carbon consumed by denitrification.

H_2	Depth of the anaerobic layer	0.1	m

IV. Parameter Values for Individual Solutes

The parameters that vary with the solute being considered are the reaction velocities, the partition coefficients, and the source terms. The specific form for these parameters are given below for each of the modeled solutes.

A. Ammonia

Ammonia is nitrified in the aerobic layer. A Michaelis Menton expression is used for the ammonia concentration dependency of the nitrification rate and for the oxygen dependency. The temperature dependence is applied to κ^2 since this is proportional to the first order reaction rate constant. Thus:

$$\kappa_1^2 = \kappa_{NH4,1}^2 \theta_{NH4}^{(T-20)} \left(\frac{K_{M,NH4}}{K_{M,NH4} + [NH_4(1)]} \right) \left(\frac{[O_2(0)]}{K_{M,NH4,O2} + [O_2(0)]} \right)$$

Partitioning is included although it has a negligible effect on the computation. No anaerobic layer reactions occur. The parameters values are:

$\kappa_{NH4,1}$	Reaction velocity for nitrification	0.1313	m/d
θ_{NH4}	Temperature coefficient for nitrification	1.08	-
$K_{M,NH4}$	Nitrification half saturation constant for ammonia	1500.	mg N/m^3
$K_{M,NH4,O2}$	Nitrification half saturation constant for oxygen	3.68.	mg O_2/L
$\pi_{NH4,1}$	Aerobic layer partition coefficient	1.0	L/kg
$\pi_{NH4,2}$	Anaerobic layer partition coefficient	1.0	L/kg
κ_2	Aerobic layer reaction velocity	0.0	m/d

D. Oxygen

Oxygen is consumed by the oxidation reactions in the aerobic layer. Carbonaceous sediment oxygen demand (CSOD) - so named because it originates with carbon diagenesis - is computed from the rate of oxygen utilization during sulfide oxidation. No stoichiometric coefficient is needed because the sulfide concentrations are computed in oxygen equivalents. The nitrogenous sediment oxygen demand (NSOD) is the consumption of oxygen due to nitrification with the indicated stoichiometry. No other oxygen consuming reactions are considered.

$$CSOD = \frac{(\kappa_{s,dl}^2 f_{dl} + \kappa_{s,pl}^2 f_{pl})\theta_{HS}^{(T-20)}}{s} \frac{[O_2(0)]}{K_{M,HS,O2}} [\Sigma H_2S(1)]$$

$$NSOD = \alpha_{O2,NH4} \left(\frac{K_{M,NH4}}{K_{M,NH4} + [NH_4(1)]} \right) \left(\frac{[O_2(0)]}{K_{M,NH4,O2} + [O_2(0)]} \right) \frac{\kappa_{NH4,1}^2}{s} [NH_4(1)]$$

where:

$[\Sigma H_2S(1)]$	Total aerobic layer sulfide concentration		$g\ O_2^*/m^3$
$\alpha_{O2,NH4}$	oxygen consumed by nitrification	4.5714	$g\ O_2/g\ N$

E. Phosphate

Phosphate is conservative in both layers, with partitioning controlling the fraction that is dissolved and particulate. Phosphorus flux is strongly affected by the overlying water oxygen concentration, $[O_2(0)]$. The mechanism usually suggested is that the phosphorus which is transferred to the aerobic layer is sorbed to freshly precipitated iron oxyhydroxides which prevents it from diffusing into the overlying water. At low oxygen concentrations, the iron oxyhydroxides are reduced and dissolved, the sorption barrier is removed, and the phosphorus flux escapes unimpeded. A simple way to implement this mechanism is to make the aerobic layer partition coefficient larger than in the anaerobic layer during oxic conditions and to remove this additional

$$J_{T2} = J_C - \alpha_{O2,NO3}\left(\frac{\kappa^2_{NO3,1}}{s}[NO_3(1)] + \kappa_{NO3,2}[NO_3(2)]\right)$$

where:

$\alpha_{O2,NO3}$	diagenesis (in O_2 equivalents) consumed by denitrification	2.8571	g O_2*/g N

Dissolved and particulate sulfide are oxidized in the aerobic layer. The reaction rate is linear in oxygen concentration, consistent with reported formulations for these reactions. The constant $K_{M,HS,O2}$ scales the overlying water oxygen concentration.

$$\kappa_1^2 = (\kappa^2_{s,d1} f_{d1} + \kappa^2_{s,p1} f_{p1})\theta_{HS}^{(T-20)} \frac{[O_2(0)]}{K_{M,HS,O2}}$$

Partitioning between dissolved and particulate sulfide represents the formation of iron sulfide, FeS(s). No other reactions occur. The parameters are:

$\kappa_{d,1}$	Reaction velocity for dissolved sulfide oxidation in the aerobic layer	0.20	m/d
$\kappa_{p,1}$	Reaction velocity for particulate sulfide oxidation in the aerobic layer	0.40	m/d
θ_{HS}	Temperature coefficient for sulfide oxidation	1.08	-
$K_{M,HS,O2}$	Sulfide oxidation normalization constant for oxygen	4.0.	mg O_2/L
$\pi_{HS,1}$	Partition coefficient for sulfide in the aerobic layer	100	L/kg
$\pi_{HS,2}$	Partition coefficient for sulfide in the anaerobic layer	100	L/kg
κ_2	Anaerobic layer reaction velocity	0.0	m/d
J_{T1}	Aerobic layer sulfide source	0.0	g O_2*/m^2-d

$$S_{Si} = k_{Si}\theta_{Si}^{(T-20)}\frac{P_{Si}}{P_{Si}+K_{M,PSi}}([Si]_{sat}-[Si]_{d2})$$

where k_{Si} is the specific reaction rate for silica dissolution; P_{Si} is the concentration of particulate biogenic silica; $[Si]_{sat}$ is the saturation concentration of silica in the interstitial water that is in equilibrium with biogenic silica, and $[Si]_{d2}$ is the dissolved silica concentration in layer 2.

The mass balance equation for biogenic particulate silica is:

$$H_2\frac{dP_{Si}}{dt} = -S_{Si}H_2 - w_2P_{Si} + J_{PSi}$$

The mass balance equation for mineralized silica can be formulated using the general mass balance equation as follows. The two terms in S_{Si} correspond to the source term: J_{T2}, and the layer two reaction velocity, κ_2, respectively.

$$J_{T2} = k_{Si}\theta_{Si}^{(T-20)}\frac{P_{Si}}{K_{M,PSi}+P_{Si}}[Si]_{sat}H_2$$

$$\kappa_2 = k_{Si}\theta_{Si}^{(T-20)}\frac{P_{Si}}{K_{M,PSi}+P_{Si}}[Si]_{d2}H_2$$

Partitioning controls the extent to which dissolved silica sorbs to solids. The same formulation as applied to phosphorus is included because it has been reported that silica can sorb to iron oxide.

$$\pi_1 = \pi_{Si,2}(\Delta\pi_{Fe,Si}) \qquad O_2(0) > O_{2,crit}$$

$$\pi_{Si,2}(\Delta\pi_{Fe,Si})^{([O_2(0)]/[O_2(0)]_{crit})} \qquad [O_2(0)] \le [O_2(0)]_{crit}$$

No other reaction is included. The parameter values are:

κ_1	Aerobic layer reaction velocity	0.0	m/d

sorption as $[O_2(0)]$ approaches zero. Hence if $[O_2(0)] > [O_2(0)]_{crit}$ sorption in the aerobic layer is enhanced by an amount $\Delta\pi_{Fe,PO4}$. However if oxygen falls below a critical concentration, $[O_2(0)] < [O_2(0)]_{crit}$, then:

$$\pi_1 = \pi_2(\Delta\pi_{Fe,PO4})^{([O_2(0)]/[O_2(0)]_{crit})} \qquad [O_2(0)] \le [O_2(0)]_{crit}$$

which smoothly reduces the aerobic layer partition coefficient to that in the anaerobic layer as $[O_2(0)]$ goes to zero. No other reactions affect the phosphorus concentrations. The parameter values are:

κ_1	Aerobic layer reaction velocity	0.0	m/d
κ_2	Anaerobic layer reaction velocity	0.0	m/d
J_{T1}	Aerobic layer phosphorus source	0.0	mg P/m^2-d
$J_{T2} = J_P$	Phosphorus diagenesis. Computed from the equation in section III		mg P/m^2-d
$\Delta\pi_{Fe,PO4}$	Incremental partition coefficient for phosphate in the aerobic layer	3.0	L/kg
$\pi_{PO4,2}$	Partition coefficient for phosphate in the anaerobic layer	2.0E+04	L/kg
$[O_2(0)]_{crit}$	Overlying water oxygen concentration at which aerobic layer incremental partitioning starts to decrease	2.0	mg/L

F. Silica

The mechanism for the production of silica in sediments is different than the diagenetic formulation used for carbon, nitrogen, and phosphorus. The kinetics of dissolution have been found to be represented by a reversible reaction. A recent set of experimental data indicate that the dissolution rate is more properly formulated as a Michaelis Menton expression in particulate silica. Hence the kinetic source is:

$$H_2\frac{C_{T2}^{t+\Delta t}-C_{T2}^{t}}{\Delta t}=-w_{12}(f_{p2}C_{T2}^{t+\Delta t}-f_{p1}C_{T1}^{t+\Delta t})-Kl_{12}(f_{d2}C_{T2}^{t+\Delta t}-f_{d1}C_{T1}^{t+\Delta t})$$
$$-\kappa_2 C_{T2}^{t+\Delta t}-w_s C_{T2}^{t+\Delta t}+J_{T2}^{t+\Delta t}$$

which can be put into a form that is similar to the steady state equations:

$$0=-w_{12}(f_{p2}C_{T2}^{t+\Delta t}-f_{p1}C_{T1}^{t+\Delta t})-Kl_{12}(f_{d2}C_{T2}^{t+\Delta t}-f_{d1}C_{T1}^{t+\Delta t})$$
$$-\kappa_2 C_{T2}^{t+\Delta t}-w_s C_{T2}^{t+\Delta t}-\frac{H_2 C_{T2}^{t+\Delta t}}{\Delta t}+J_{T2}^{t+\Delta t}+\frac{H_2 C_{T2}^{t}}{\Delta t}$$

The terms corresponding to the derivatives: $H_2 C_{T2}^{t+\Delta t}/\Delta t$ and $H_2 C_{T2}^{t}/\Delta t$, simply add to the layer two removal rate and the forcing function respectively. Hence the solution algorithm for these equations is the same as the steady state model. $C_{T1}^{t+\Delta t}$ and $C_{T2}^{t+\Delta t}$ are the two unknowns in the two equations which are solved at every time step.

For the sake of symmetry the diagenesis equations are also solved in implicit form:

$$H_2\frac{G_{POC,i}^{(t+\Delta t)}-G_{POC,i}^{(t)}}{\Delta t}=-K_{G,i}\theta_{G,i}^{(T-20)}G_{POC,i}^{(t+\Delta t)}H_2+J_{GPOC,i}^{\left(t+\frac{\Delta t}{2}\right)}$$

so that:

$$G_{POC,i}^{(t+\Delta t)}=\left[G_{POC,i}^{(t)}+\frac{\Delta t}{H_2}J_{GPOC,i}^{\left(t+\frac{\Delta t}{2}\right)}\right]\left[1+\Delta t K_{G,i}\theta_{G,i}^{(T-20)}\right]^{-1}$$

Similarly the particulate biogenic silica equation becomes:

$$P_{Si}^{(t+\Delta t)}=\left[P_{Si}^{(t)}+\frac{\Delta t}{H_2}J_{PSi}^{\left(t+\frac{\Delta t}{2}\right)}\right]\left[1+\frac{w_2\Delta t}{H_2}+k_{Si}\theta_{Si}^{(T-20)}\Delta t\frac{[Si]_{sat}-[Si]_{d2}^{(t)}}{P_{Si}^{(t)}+K_{M,PSi}}\right]^{-1}$$

k_{Si}	Biogenic silica dissolution rate constant	0.20	d^{-1}
θ_{Si}	Temperature coefficient for silica oxidation	1.08	-
$[Si]_{sat}$	Saturation concentration for pore water silica	26500	mg Si/m^3
$K_{M,PSi}$	Particulate biogenic silica half saturation constant for dissolution	5.0E+07	mg/m^3
J_{T1}	Aerobic layer silica source	0.0	mg Si/m^2-d
$\Delta\pi_{oxicFe,Si,1}$	Incremental partition coefficient for silica in the aerobic layer	1	L/kg
$\pi_{Si,2}$	Partition coefficient for silica in the anaerobic layer	100	L/kg
J_{PSi}	Flux of biogenic silica from the overlying water to the sediment		mg Si/m^2-d

V. The Finite Difference Equations

The most convenient method of solution is to use an implicit integration scheme. This is due to the similarity of the equations that result to the steady state equations for which a simple solution algorithm is available. Given the concentrations at t, the finite difference equations are solved for the unknown concentrations at $t+\Delta t$. Since layer 1 is quite thin, $H_1 \sim 1$ mm = 10^{-3} m, and the surface mass transfer coefficient is of order $s \sim$ 0.1 m/day, the residence time in the layer is: $H_1/s \sim 10^{-2}$ days. Hence it can be assumed to be at steady state without any loss of accuracy. The layer 1 equation is:

$$0 = H_1 \frac{dC_{T1}^{(t+\Delta t)}}{dt} = s(f_{d1}C_{T1}^{(t+\Delta t)} - C_{d0}^{(t+\Delta t)}) + w_{12}(f_{p2}C_{T2}^{(t+\Delta t)} - f_{p1}C_{T1}^{(t+\Delta t)})$$

$$+ K_{L12}(f_{d2}C_{T2}^{(t+\Delta t)} - f_{d1}C_{T1}^{(t+\Delta t)}) - \frac{\kappa_1^2}{s}C_{T1}^{(t+\Delta t)} + J_{T1}$$

The layer 2 mass balance finite difference equation which is implicit in time is:

Lower Chesapeake Bay

D. Burdige. Old Dominion Univ.

Hunting Creek

C. Cerco. Corp of Engineers, Vicksburg, Miss.

Pore Water Data

O. Bricker. USGS

The sediment flux data analyzed below are from four stations in the main stem of Chesapeake Bay, two stations in the Potomac estuary, and two stations in the Patuxent estuary. The locations are shown in Fig. 3. The data spans the four year period from 1985 to 1988. The next sections describe the method used to calibrate the time variable sediment model.

B. Estimates of Particulate Organic Matter Depositional Fluxes

The diagenesis fluxes are produced by the diagenesis of POM as specified by the three G model. The forcing function for this model are: $J_{GPOC,i}(t)$, the sources of the three G classes of POC that settle to the sediment. In order to calibrate the time variable model, it is necessary to specify these fluxes for each station over the four years of to be calibrated.

The method employed to estimate these depositional fluxes is basically an approximate inverse calculation. The calibration is based on the ammonia flux since it is least subject to complex transformations so that the relationship between ammonia flux and ammonia diagenesis is elementary. First the ammonia diagenesis flux, J_N, is estimated from a regression analysis. Then an approximate estimate is made of the depositional fluxes to the sediment that required to produce this diagenesis flux. Finally adjustments are made to the depositional fluxes to better reproduce the diagenesis fluxes.

1. Ammonia Diagenesis

The steady state equation for ammonia flux used in the regression analysis to estimate J_N:

A. Solution Technique

The solution of the layer 1 and layer 2 mass balance equations require and iterative technique since the surface mass transfer coefficient, $s = SOD/[O_2](0)$, is a function of the SOD which, in turn, is a function of the ammonia and sulfide mass balance equations. A simple back substitution method can be used to solve the equations at each time step. The procedure is:

(1). Guess an SOD

(2). Solve Layer 1 and 2 equations for ammonia, nitrate, and sulfide.

(3). Compute SOD = NSOD + CSOD.

(4). Refine the estimate of SOD. A root finding method is used to make the new estimate.

(5). Go to (2) if no convergence.

(6). Compute the phosphorus and silica fluxes

This method has been found to be quite reliable.

VI. Data Analysis

A. Data Set

The construction of this model would not have been possible without the efforts of the scientists that developed the methods for reliably measuring sediment fluxes and applied these techniques in a systematic investigation of the Chesapeake Bay. Their efforts are specifically acknowledged and appreciated.

Upper Chesapeake Bay

W. Boynton, J. Cornwell, J. Garber, W.M. Kemp, P. Sampou. Univ. of Maryland

Since there appears to be no unambiguous way of specifying the intra-annual variation, the depositional flux is assumed to be constant within the year but varies from year to year as indexed by j.

The total depositional flux, J_{POC} is apportioned to the three G classes as follows:

$$J_{GPOC,1} = f_{G1} J_{POC}$$

$$J_{GPOC,2} = f_{G2} J_{POC}$$

$$J_{GPOC,3} = f_{G3} J_{POC}$$

where:

J_C	total carbon diagenesis		g O_2*/m^2-d
f_{G1}	fraction of total carbon diagenesis that is in reactivity class G1	0.5	-
f_{G2}	fraction of total carbon diagenesis that is in reactivity class G2	0.25	-
f_{G3}	fraction of total carbon diagenesis that is in reactivity class G3	0.25	-

This specifies the source to the diagenesis equations. Their solution produces the temporal variation of $G_{POC,i}(t)$. The carbon diagenesis flux that is the sum of the carbon produced by the diagenesis reaction of each G class:

$$J_C(t) = \sum_{i=1}^{3} K_{G,i} \theta_{G,i}^{(T-20)} G_{POC,i}(t) H_2$$

Nitrogen, and phosphorus diagenesis, and the silica biogenic source are computed using the stoichiometric ratios observed at the station R-64 sediment trap. They are quite close to Redfield, and additionally provide a carbon to silica ratio. Thus:

$$J[NH_4](i,t_j) = J_N(i,j)\theta_N^{(T_{i,j}-20)} \frac{s_{i,j}^2}{s_{i,j}^2 + \kappa_{NH4,1}^2 \theta_{NH4}^{(T_{i,j}-20)}}$$

$$-[NH_4(0)]_{i,j}\left(\frac{1}{s_{i,j}} + \frac{s_{i,j}}{\kappa_{NH4,1}^2 \theta_{NH4}^{(T_{i,j}-20)}}\right)^{-1}$$

where the subscripts i,j indicate that the temperature, $T_{i,j}$, the surface mass transfer coefficient, $s_{i,j}$, and overlying water ammonia concentrations, $[NH_4(0)]_{i,j}$, are at station i and time tj. The parameters are: κ_{NH4}, θ_{NH4}, and θ_N, and $J_N(i,j)$, i = 1, 8 corresponding to the eight SONE stations, and j = 1, 4 corresponding to 1985 through 1988.

Unfortunately this nonlinear regression problem proved to be infeasible. Instead an initial nonlinear regression was performed for which the dependency of J_N on year j, was suppressed so that the unknowns are $J_N(i)$, κ_{NH4}, θ_{NH4}, and θ_N. This provided estimates for the latter three parameters. Using these estimates in the regression equation yields a linear regression problem for the 32 unknowns: $J_N(i,j)$, i = 1, 8; j = 1, 4, which is a straightforward problem.

The above analysis produces estimates of nitrogen diagenesis, $J_N(i,j)$. The carbon diagenesis flux, $J_C(i,j)$ can be estimated from the nitrogen diagenesis flux, $J_N(i,j)$, using Redfield stoichiometry:

$$J_C(i,j) = \alpha_{C,N} J_N(i,j)$$

2. Depositional fluxes.

In order to calibrate the sediment we require the POC, PON, POP, and PSi depositional fluxes to the sediment. Consider, first, the total POC input flux, $J_{POC}(t)$. This differs from the carbon diagenesis flux, $J_C(i,j)$, because (1) the intra-annual time variation of $J_{POC}(t)$ is difficult to estimate solely from the sediment fluxes; and (2) the time lags introduced by the reaction kinetics of the three G model.

the these initial conditions should reflect the past history of the depositional fluxes and overlying water conditions. However, this would require estimates for the previous years. Since this is impractical owing to lack of data for these years it is necessary to adopt some other strategy to obtain initial conditions.

Two possibilities are available. The first is to assign these initial conditions using some calibration procedure. This can be quite arbitrary and subject to a large uncertainty. The alternate is to equilibrate the model to the first year inputs and overlying water data. That is, the model equations are solved using any set of initial conditions. In order to speed up the convergence, the steady state solution for the annual average conditions are used. This insures that the diagenesis equations are near steady state. The model is then integrated for one year. The final concentrations at the end of the first year are used as the initial conditions and the equations are again solved for the first year. This procedure is repeated until the final conditions at the end of the year are equal, within a tolerance, to the initial conditions. At this point the model is at periodic steady state. It is as if the conditions for 1985 had repeatedly occurred until the sediment had equilibrated to these inputs.

The utility of this method is that the initial conditions result from a well specified requirement: that of periodic steady state, rather than a less well specified criterion. When changes are made in the kinetic parameters to improve the calibration, the initial conditions are recalculated with the new model coefficients. This removes the initial conditions from the parameters that require calibration. They are always set at the concentrations that produce a periodic steady state for 1985.

$$J_N(t) = J_C(t)/\alpha_{C,N}$$

$$J_P(t) = J_C(t)/\alpha_{C,P}$$

$$J_{Si}(t) = J_C(t)/\alpha_{C,Si}$$

where:

$\alpha_{C,N}$	carbon to nitrogen ratio (Redfield = 5.68)	6.42	g C/g N
$\alpha_{C,P}$	carbon to phosphorus ratio (Redfield = 41.0)	52.9	g C/g P
$\alpha_{Si,P}$	carbon to silica ratio	1.02	g C/g Si

These are the forcing functions for the ammonia, nitrate, oxygen, phosphorus, and silica flux models.

C. Overlying Water Concentrations

In order to calibrate the sediment model it is necessary to specify the overlying water concentrations and temperature as a function of time at each station for the four years. This is done using a four term Fourier series fit to the data for each year:

$$C_{d0}(t) = a_0 + \sum_{i=1}^{4}\left\{a_i \sin\left(\frac{2\pi t}{T}\right) + b_i \cos\left(\frac{2\pi t}{T}\right)\right\}$$

Fig. 4 presents an example of the data and the Fourier series fit.

D. Sediment Initial Conditions

The carbon diagenesis and the sediment flux model equations require initial conditions, the concentrations at t = 0: $G_{POC,i}(0)$, $P_{Si}(0)$, and the total concentrations for ammonia, nitrate, sulfide, phosphorus, and silica: $C_{T1}(0)$, and $C_{T2}(0)$ to start the computations. Strictly speaking

The right hand panel is a comparison of the probability distributions of the data and model values. The plot is constructed as follows. The values of the model and data fluxes are the same as in the point wise comparison. The difference is that the model values are ordered from lowest to highest. The data are also ordered from lowest to highest. Then the ordered model values and data are plotted against each other. For example, the lowest model flux is plotted against the lowest observed flux. Then the next in order are plotted against each other, and so on until the largest values are plotted. The main stem data are analyzed separately from the tributaries. The modeled fluxes are slightly larger, in general, from the observed fluxes. However, the range of values are well represented. This comparison indicates that, considered as whole without regard to station or time, the distribution of the main stem and tributary ammonia fluxes are reproduced by the model. Since this is quite a weak form of calibration it is reassuring that this comparison is reasonable.

Fig. 11 examines the observed and modeled distribution of fluxes as a function of the surface mass transfer coefficient $s = SOD/[O_2(0)]$. The model results conform more closely to the expected relationship than the observations. However, the general pattern is the same.

Fig. 12 presents the observed and modeled fluxes versus overlying water dissolved oxygen concentration. For this comparison the distributions appear to be reasonably similar.

VII. Calibration

The calibration plots that follow are from the stand alone calibration procedure that is described above. Fig. 3 locates the sediment sampling stations. The sign convention followed is that positive fluxes are from the sediment to the overlying water. For dissolved oxygen, however, the convention is reversed. Positive oxygen fluxes corresponding to sediment oxygen demand (SOD) are from the overlying water to the sediment. This is to conform to the standard practise in DO modeling.

A. Ammonia

The ammonia diagenesis for the 8 stations are shown, together with that computed from the multi G diagnoses model in Fig. 5-6. Fig. 5 are the Chesapeake Bay main stem stations. Fig. 6 presents the Patuxent stations (upper panels) and the Potomac stations (lower panels). In some cases the estimate from the regression model has been adjusted to better fit these data.

The corresponding ammonia flux data are compared to the model computation in Fig. 7-8. The data are from 1985 to 1988. The mean of the triplicated measurement is shown, together with the range of the measurements, denoted by the vertical line. If no line is shown, the range is smaller than the symbol used for the mean.

The sediment data for nitrogen is compared in Fig. 9. The particulate organic nitrogen (PON) and pore water ammonia concentrations for the main stem of Chesapeake bay are compared to the computations for the four main bay stations. The model computations for the four years are superimposed for each of the stations. The pore water data are from the Bricker data set from the 1970s.

Fig. 10 compares the measured and modeled fluxes in two ways. The left hand panel is a point wise comparison. The plot is an alternate presentation of the data and computation in Fig. 7-8. Note the considerable scatter. This appears to be mostly a matter of mismatches in timing between the data and the model.

C. Oxygen

The time series of observed and computed oxygen fluxes are shown in Fig. 17-18. Note that the fluxes at Still Pond in the main bay, and all but Ragged Point in the tributaries have a seasonal distribution not unlike the ammonia fluxes. However, the fluxes for the stations that experience anoxia are quite different. The lack of a strong seasonal cycle is apparent. The model produces this behavior by inhibiting the particle mixing with the benthic stress formulation. This is the reason that benthic stress is incorporated in the model. Figs 19-20 display the particle mixing velocity and the effect benthic stress has on its magnitude and seasonal distribution. There is a different pattern of oxygen fluxes from the stations which are aerobic throughout the year and those which experience hypoxia or anoxia.

Fig. 21-22 display the time series of sulfide fluxes. Only two observations are available for main stem stations. The model computes fluxes that are comparable. The sulfide fluxes occur when the overlying water DO is sufficiently low to limit the oxidation of sulfide in the aerobic layer. The result is that sulfide is transferred to the overlying water by surface mass transfer.

Fig. 23 compares the sediment data for carbon and sulfide to the model computations. The particulate organic carbon concentrations are in reasonable agreement for all but the uppermost station. This probably reflects a slightly larger G3 component in the Susquehanna river input, relative to algal POC. This is not unlikely since a larger fraction of the POC in the river input is from soil derived carbon, which is already weathered so that a larger fraction would be in the refractory classes.

The comparison of the sulfide data highlights the fact that the sulfur cycle in the model is not complete. The model computations are substantially in excess of the observations for acid volatile sulfide, which is a measure of the iron monosulfide, FeS, in the sediment. The model considers the formation of FeS which is reactive and can be oxidized. However, iron monosulfide can react with

B. Nitrate

The observed and computed time series of nitrate fluxes are shown in Fig. 13-14. Still Pond, the station nearest the head of the bay, exhibits a strong seasonal distribution of nitrate fluxes to the sediment. This is due to the large overlying water nitrate concentrations at this station. The other main bay stations are characterized by almost zero nitrate fluxes throughout the year. The Potomac river stations, Fig. 14, are more dynamic. The upstream station is predicted to have substantial fluxes to the sediment, due to a high overlying water concentration. The Ragged Point station is predicted to have the largest positive fluxes from the sediment to the overlying water. The time series of observations seem to reflect this behavior.

The point wise comparison, Fig. 15, again displays considerable scatter, whereas the quantile comparison is quite satisfactory.

The relationship between nitrate flux and overlying water nitrate concentration is examined in Fig. 16. For the observations for which $[O_2(0)]$ is less than two, both the modeled as observed fluxes are essentially zero. This is due to the reduced internal nitrate source from reduced ammonia nitrification at low DO concentrations. The tendency for large overlying water nitrate concentrations to be associated with negative fluxes is apparent in the modeled fluxes and less strongly but still evident in the observed fluxes.

D. Phosphorus

The time series of phosphorus fluxes are shown in Fig. 26-27. The dramatic effect of hypoxic and anoxic conditions is apparent. Phosphorus fluxes are small for the aerobic periods. However, anoxia produces dramatic increases, approaching 50 to 100 mg P/m^2-d. This is nearly one-half of the ammonia fluxes at that time. Since the ratio of ammonia to phosphorus production by diagenesis is approximately 8 to 1, the excess phosphorus is being released from the phosphorus stored in the sediment during the aerobic periods. The momentary and sharp peaks in the tributary stations are due to short periods of anoxia.

The comparison to sediment properties is shown in Fig. 28. The particulate organic phosphorus comparison is quite satisfactory as is the pore water phosphorus. The computed particulate inorganic phosphorus is much lower than observations for the stations that experience anoxia. These data are oxalic acid extractable phosphorus. This procedure may extract more than just the sorbed phosphorus that is being modeled. It may be that the sorbed phosphorus is being transformed to more stable forms, such as $Fe_3(PO_4)_2$, which is also being extracted. The situation is comparable to the sulfur cycle discussed above.

Fig. 29 presents the point wise and quantile comparisons. The scales are for an arcsech transformation of the data:

$$J[PO_4]^* = \ln\left(\frac{J[PO_4]}{\beta} + \sqrt{\left(\frac{J[PO_4]}{\beta}\right)^2 + 1}\right)$$

where $\beta = 1$. This transformation is linear for values less than β and logarithmic for larger values. It also preserves the signs of the variables. The scales are constructed by applying the transformation to 0, 1, 2, ... , 10, 20, ... etc., and plotting the results as tick marks. This transformation allows the simultaneous examination of positive and negative fluxes with widely varying values.

elemental sulfur to form iron pyrite, FeS_2, which is much less reactive. This reaction would lower the concentration of FeS computed by the model and bring it into closer agreement with the observations.

Fig. 24 presents the point wise and quantile comparison. The results are similar to the ammonia and nitrate fluxes. The individual comparison is quite scattered, whereas the quantile distributions are comparable.

Fig. 25 presents the relationship between oxygen and ammonia flux. The model exhibits a stronger relationship than suggested by the aerobic data. However, both the model and the observations indicate that low oxygen concentration favors a lowered SOD and an increased ammonia flux.

E. Silica

The time series of silica fluxes are shown in Fig. 33-34. The seasonal cycle, which is present at all the stations, arises from the temperature dependency of the dissolution reaction. The flux of particulate silica is constant in this calibration so that only the temperature variation can provide the seasonal variability. The sediment data is presented in Fig. 35. The longitudinal distribution of biogenic particulate silica from a survey in the fall of 1988 is compared to the model calculation at the same time. The observed silica is somewhat less than the model computations. Perhaps the carbon to silica stoichiometry is less than the station R 64 sediment trap results which are assumed to apply to all the stations. Pore water silica is well reproduced by the model.

The point wise and quantile comparisons, Fig. 36, are much like the previous results: a substantial amount of scatter for the point wise comparison, and essentially the same probability distribution as indicated from the quantile plots. The silica to ammonia flux relationship is shown in Fig. 37. The patterns are similar. The relationship to surface mass transfer coefficient is shown in Fig. 38. The increasing trend is captured. However, the larger observed fluxes at low DO are not well represented by the model. A similar observation can be made from the plot of silica to overlying water DO, Fig. 39. Perhaps an enhanced aerobic layer sorption is required.

The bulk of the fluxes are reasonably well reproduced. The largest fluxes occur for the low DO cases. However, there are a number of fluxes where the signs are incorrectly predicted. A number of cases occur where the model predicts a negative flux and the observation is positive. This appears to occur just after turnover when the overlying water oxygen increases. The model recreates the aerobic layer immediately, with its high partition coefficient. The resulting low aerobic layer phosphorus concentration causes a flux to the sediment. A more realistic formulation would model the iron cycle as well as phosphorus and sulfide. Then the formation of iron oxide would take place more slowly, and the aerobic layer partition coefficient would increase more slowly. Remarkably the quantile comparison is quite good, indicating that the global model variability is consistent with the variations of the observations.

Fig. 30 presents the relationship of phosphorus flux to ammonia flux. The model reproduces the general features of the relationship: a generally increasing relationship with the highest fluxes associated with the periods of low DO. Fig. 31 presents the relationship to surface mass transfer. The difficulty with the negative fluxes can be seen more clearly. Fig. 32 presents the relationship of phosphorus flux to overlying water DO. The general trend is well reproduced by the model.

at Buena Vista in the spring of 1986 and 1987 suggest a large diagenesis flux. However, the ammonia and phosphorus fluxes suggest a smaller flux. Similarly, high oxygen and silica fluxes at St. Leonard for 1985 and 1986 are not reflected in the ammonia flux. Since the diagenesis is estimated from the ammonia flux, the other fluxes are underestimated. These discrepancies cannot be reconciled within a framework that is restricted to constant stoichiometric ratios for the particulate organic matter that settles into the sediment.

By contrast, for Maryland Point, Fig. 46, and Ragged Point, Fig. 47, on the Potomac estuary, the magnitude of the fluxes are in reasonable agreement with the large diagenesis flux suggested by the ammonia fluxes. These stations support the constant stoichiometry of diagenesis.

G. Conclusions

The stand alone calibration of the sediment flux model highlights both the strengths and weaknesses of the model. The key insight is that the surface mass transfer coefficient can be obtained from the $SOD/[O_2(0)]$ ratio. This greatly simplifies the data analysis and the formulation. The relationships between the concentrations of solutes in the solid phase, pore water, and the sediment fluxes are rationalized within the framework of a mass balance analysis. The seasonal patterns are reproduced with reasonable fidelity for the oxic stations. The influence of anoxia on phosphorus and oxygen fluxes - enhancing the former and suppressing the latter - is captured as well. The phosphorus flux model employs a parameterization of the aerobic layer phosphorus partitioning that depends on the overlying water DO. The suppression of the oxygen flux that persists after the anoxic period relies on the formulation of benthic stress. Although these formulations are empirical, they appear to produce a reasonable simulations.

The model is not able to reproduce the point wise distribution of the fluxes. Plots of observed versus modeled fluxes display a significant scatter. This appears to be related to a lack of precise timing between computed and observed fluxes. A visual inspection of the time series plots

F. Station Composite Plots

The sediment flux time series for ammonia, oxygen, phosphorus, and silica are grouped by stations in Fig. 40-47. Since each of the fluxes are driven by the same diagenesis flux, suitability modified by the stoichiometric ratios, the relationships between the various fluxes are determined by the overlying water concentrations and their interactions with the kinetics that determine the fluxes.

For Still Pond, Fig. 40, the fluxes have a seasonal variation which are all in phase and are not disturbed since no overlying water hypoxia occurs. By contrast, the relationship among the fluxes at station R-78 is quite different, Fig. 41. The ammonia and silica fluxes show a seasonal variation related to temperature. However the oxygen and phosphorus fluxes are quite different. The oxygen flux is almost constant throughout the year. The phosphorus flux increases dramatically during the periods of anoxia.

The comparisons for station R-64, Fig. 42, also illustrates the effects of overlying water hypoxia. The very large phosphorus fluxes relative to the ammonia flux are the result of the storage of phosphorus during aerobic periods and its release during anoxia. However, the model cannot reconcile the high ammonia, phosphorus and silica fluxes, and the lack of variation in the oxygen flux during the first part of the year. The relationship between nitrogen, silica, phosphorus, and carbon diagenesis requires that the model predicts a substantial oxygen flux as the sulfide that is produced is oxidized during the first half of the year. The onset of anoxia and the persistence of benthic stress suppresses the oxygen flux for the latter half of the year.

The relationships at Point No Point, Fig. 43, are between the fully oxic and the anoxic stations. The higher silica flux suggests that the carbon to silica stoichiometry should be smaller - more silica per unit carbon settled to the sediment for this station.

The fluxes at Buena Vista, Fig. 44, and St. Leonard, Fig. 45, on the Patuxent estuary illustrate an inconsistency which the model cannot reconcile. The large fluxes of oxygen and silica

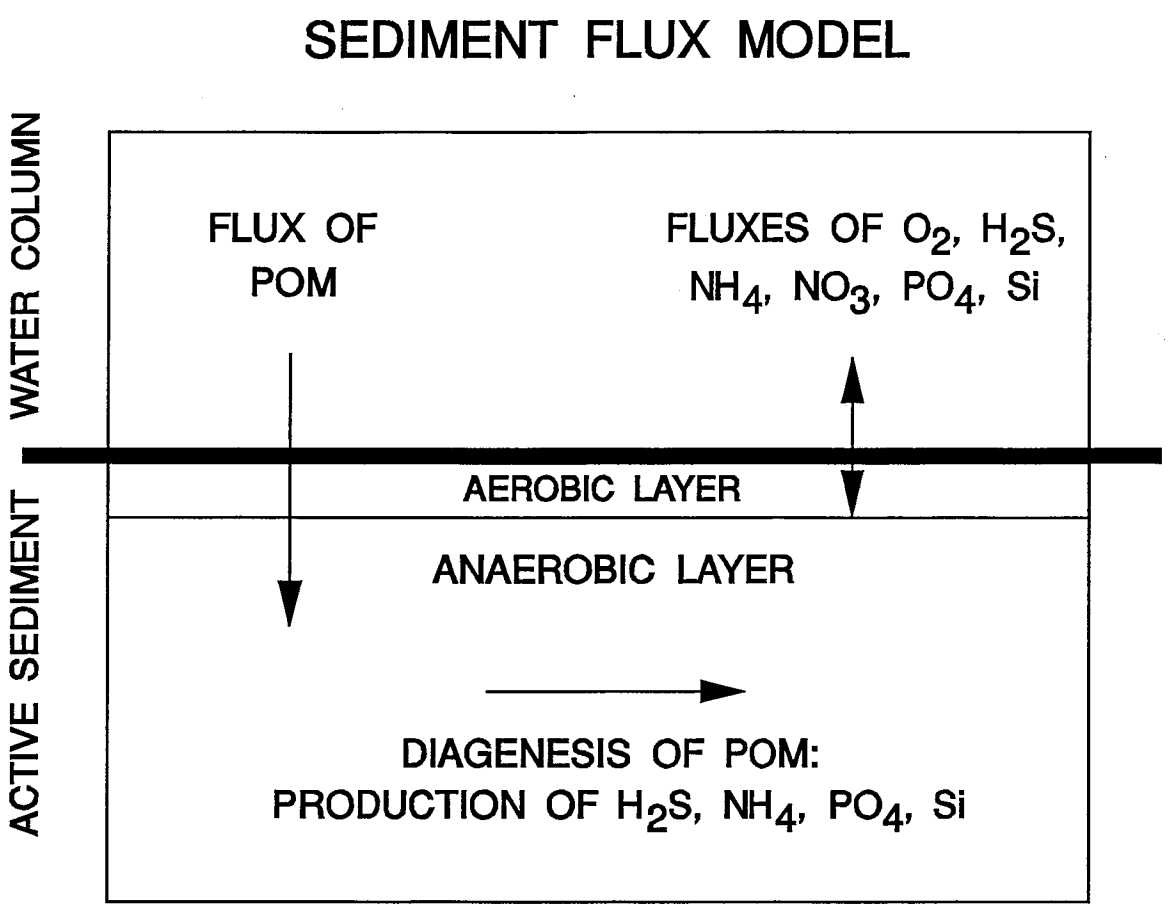
SEDIMENT FLUX MODEL
WATER COLUMN
ACTIVE SEDIMENT
FLUX OF POM
FLUXES OF O_2, H_2S, NH_4, NO_3, PO_4, Si
AEROBIC LAYER
ANAEROBIC LAYER
DIAGENESIS OF POM:
PRODUCTION OF H_2S, NH_4, PO_4, Si

FIGURE 1

supports this observation. By contrast, the quantile plots demonstrate that the model reproduces the overall distribution of fluxes in the main stem and the tributaries if station location and timing is not considered.

The overall impression of the calibration is that the fine scale variations cannot be captured, but that the overall quantitative relationships between the fluxes, together with the solid and pore water concentrations, are successfully rationalized. The seasonal behavior and the relative variations are reproduced. Of course, the final judgement of the utility of the flux model is its performance as part of the coupled Chesapeake Bay model. Interim comparisons indicate that the modeled fluxes are in reasonable agreement with the measurements. In particular, the extensive measurements made in 1988 can be used to examine the model performance over more pronounced spatial gradients.

SEDIMENT FLUX MODEL

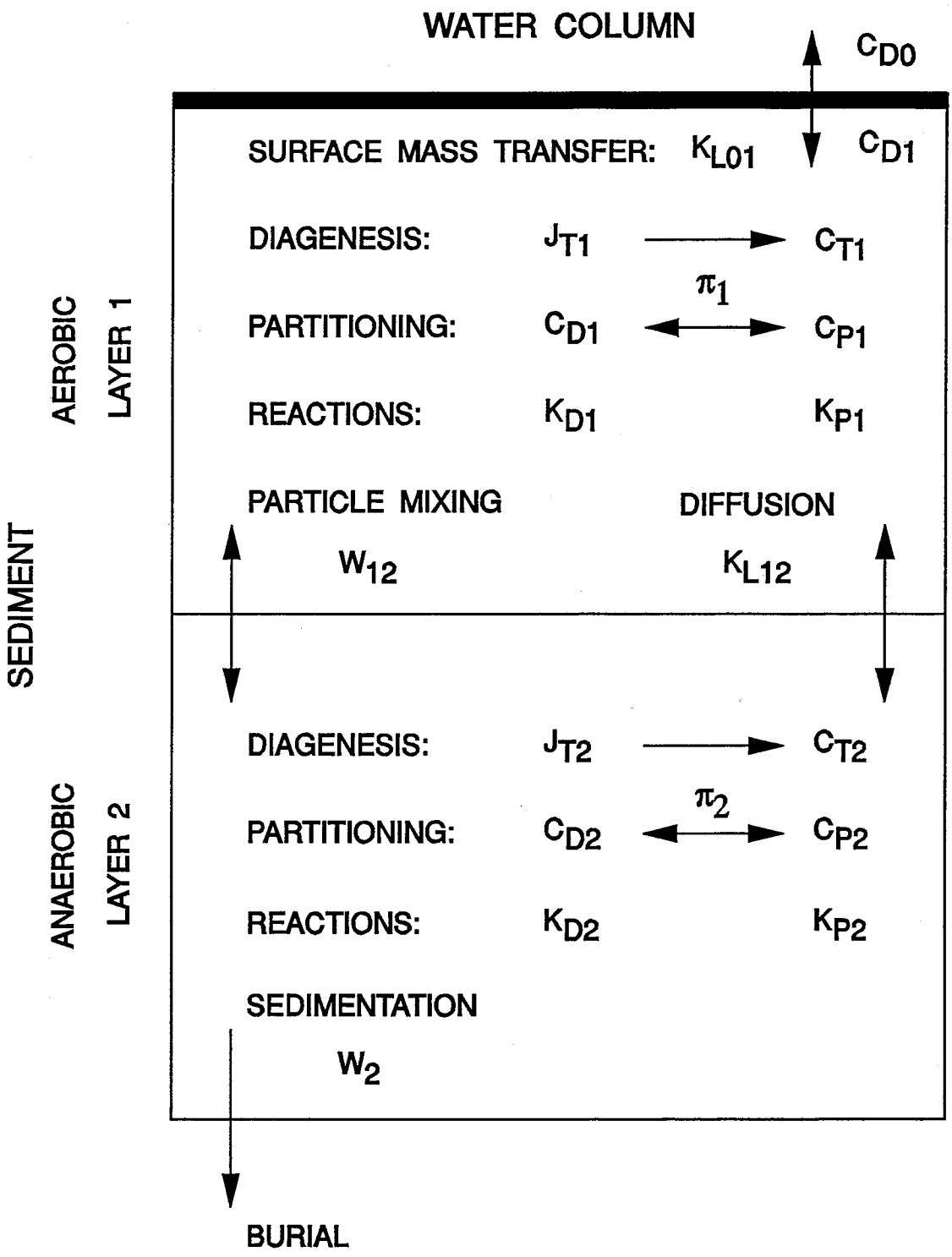

FIGURE 2

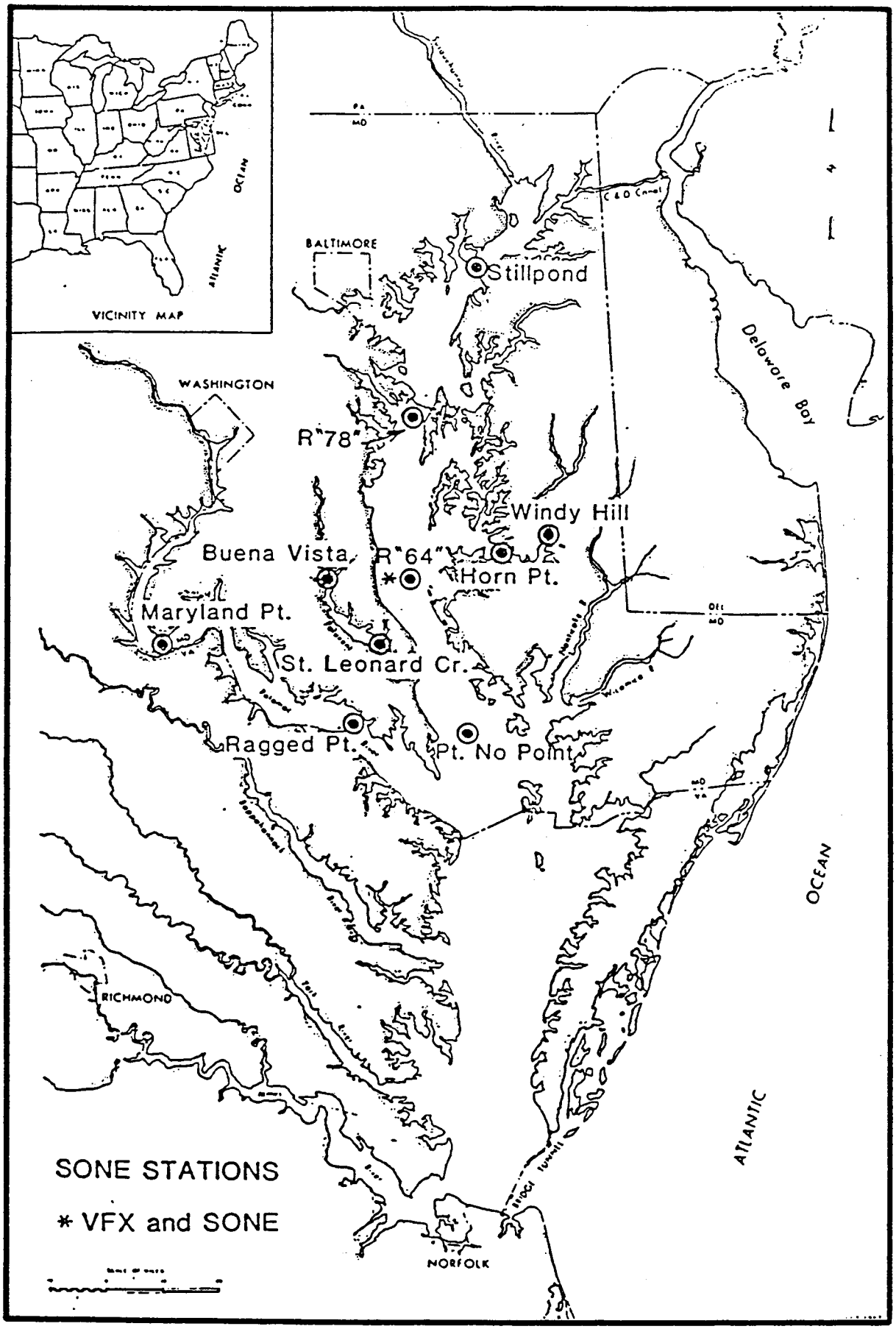
VICINITY MAP
BALTIMORE
Stillpond
WASHINGTON
R"78"
Delaware Bay
Windy Hill
Buena Vista
R"64"
Horn Pt.
Maryland Pt.
St. Leonard Cr.
Ragged Pt.
Pt. No Point
OCEAN
RICHMOND
ATLANTIC
SONE STATIONS
* VFX and SONE
NORFOLK

FIGURE 3

OVERLYING WATER CONCENTRATIONS - OXYGEN

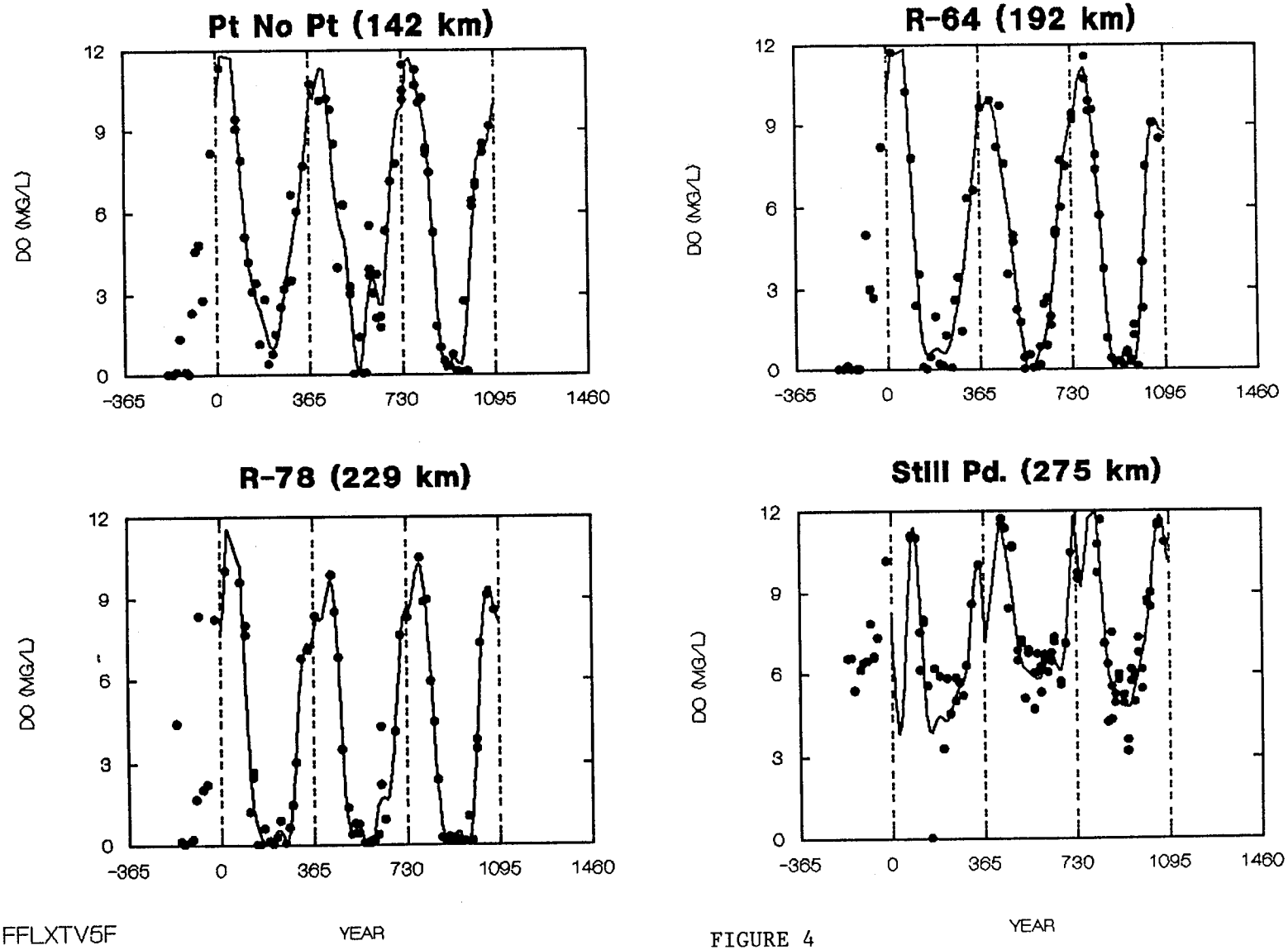

FFLXTV5F

FIGURE 4

HydroQual, Inc.

AMMONIA DIAGENESIS

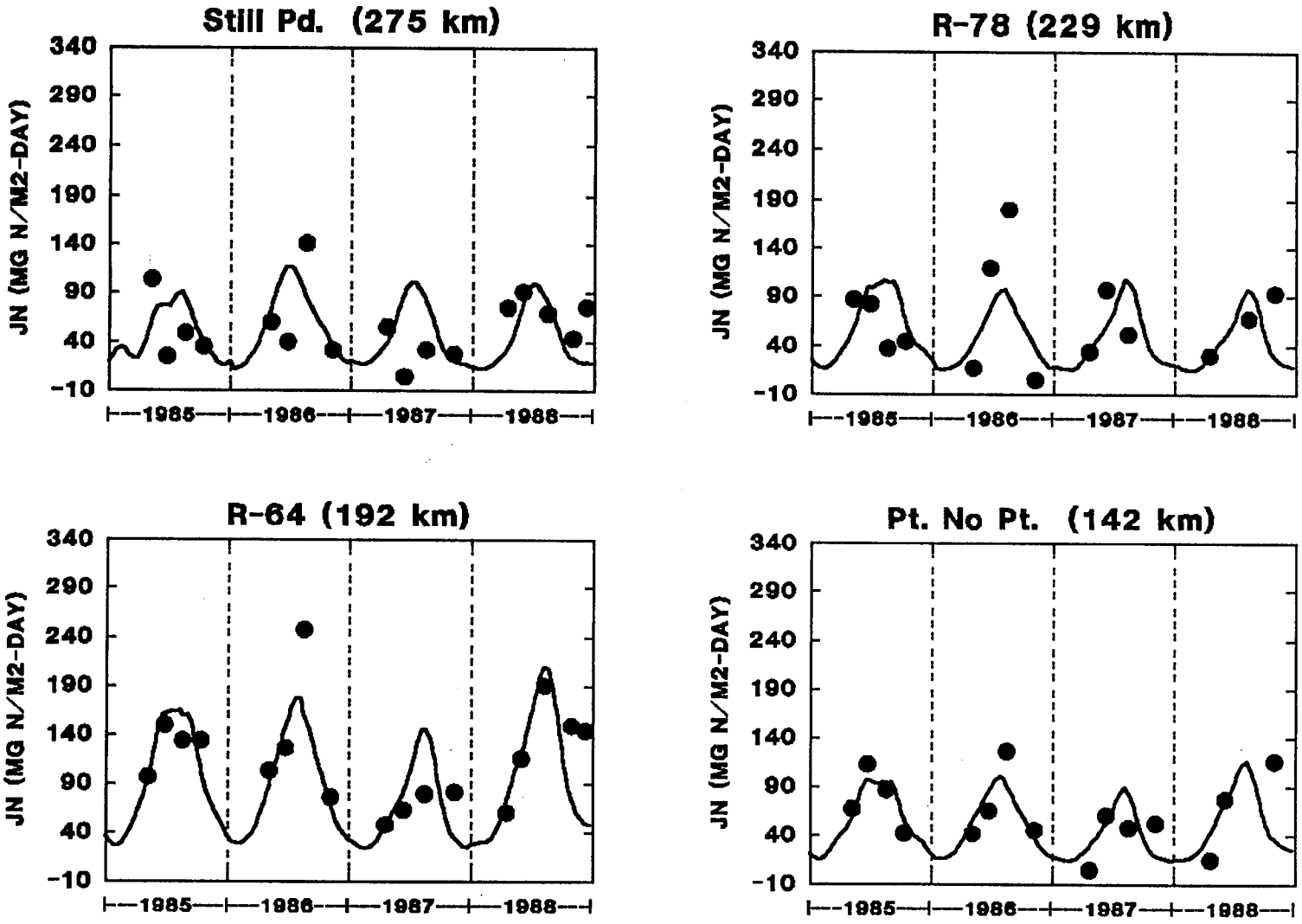

run066 - plotjn1

FIGURE 5

AMMONIA DIAGENESIS

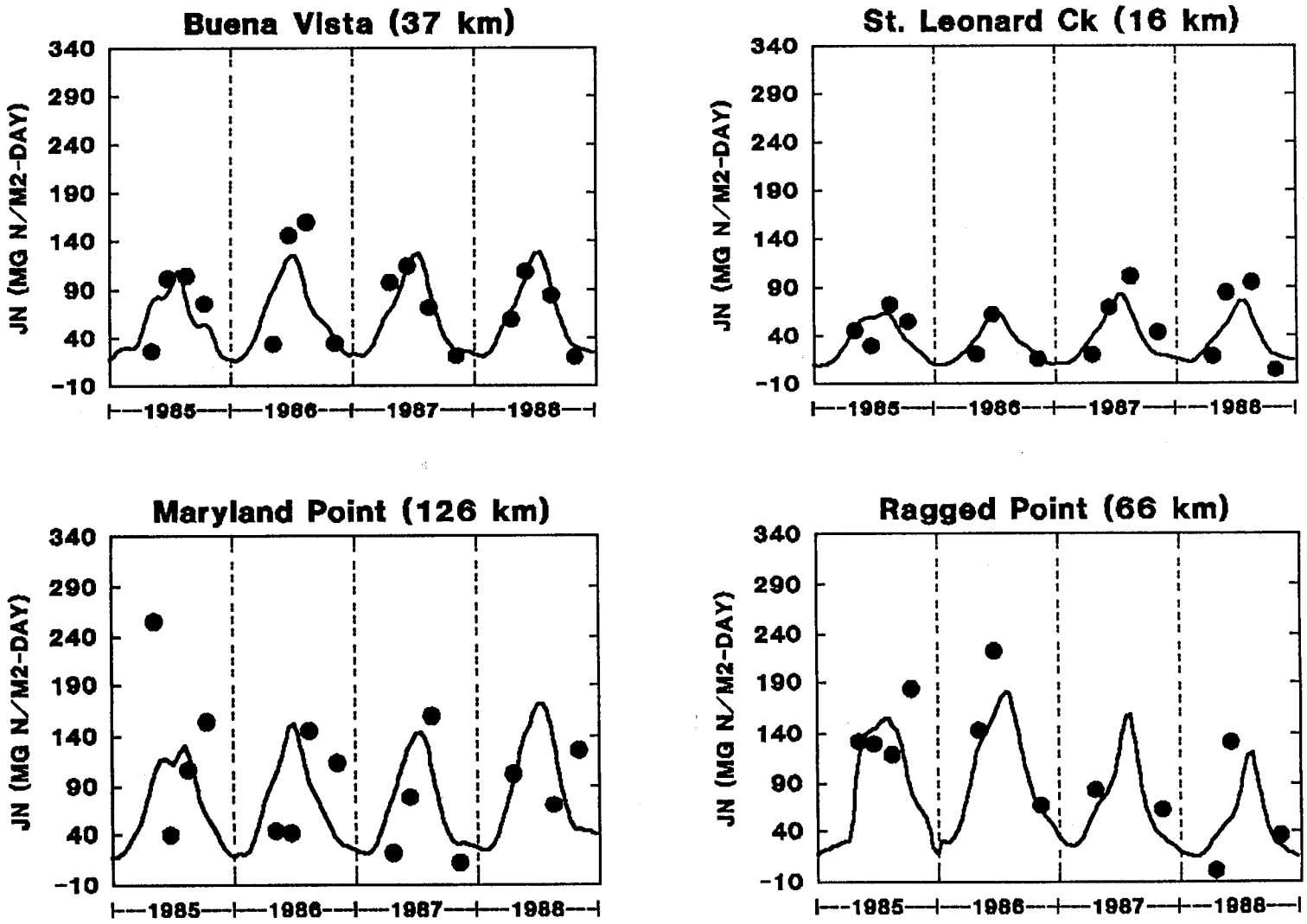

HydroQual, Inc.

run066 - plotjn2

FIGURE 6

AMMONIA FLUX

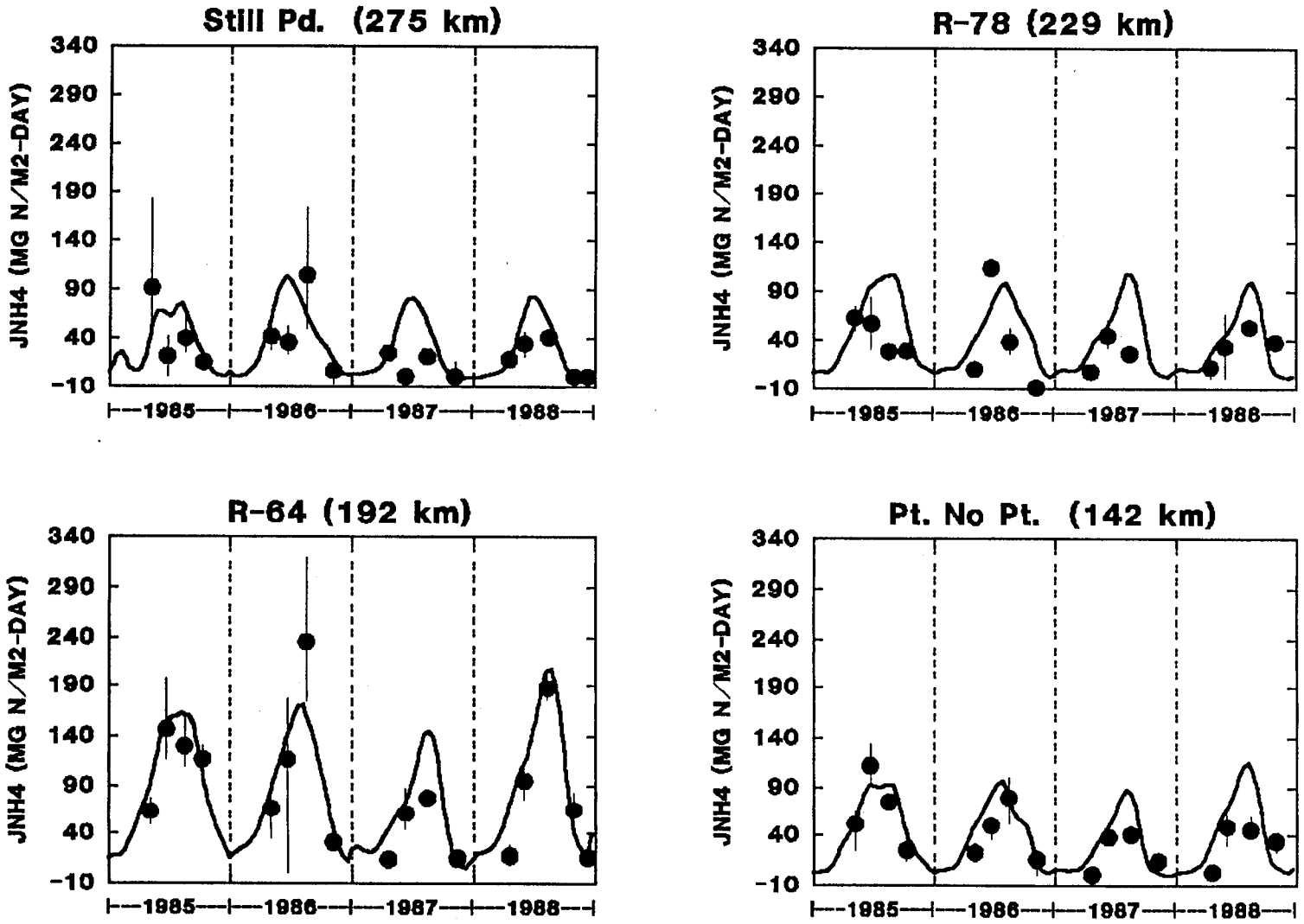

run066 - plotnh41

FIGURE 7

AMMONIA FLUX

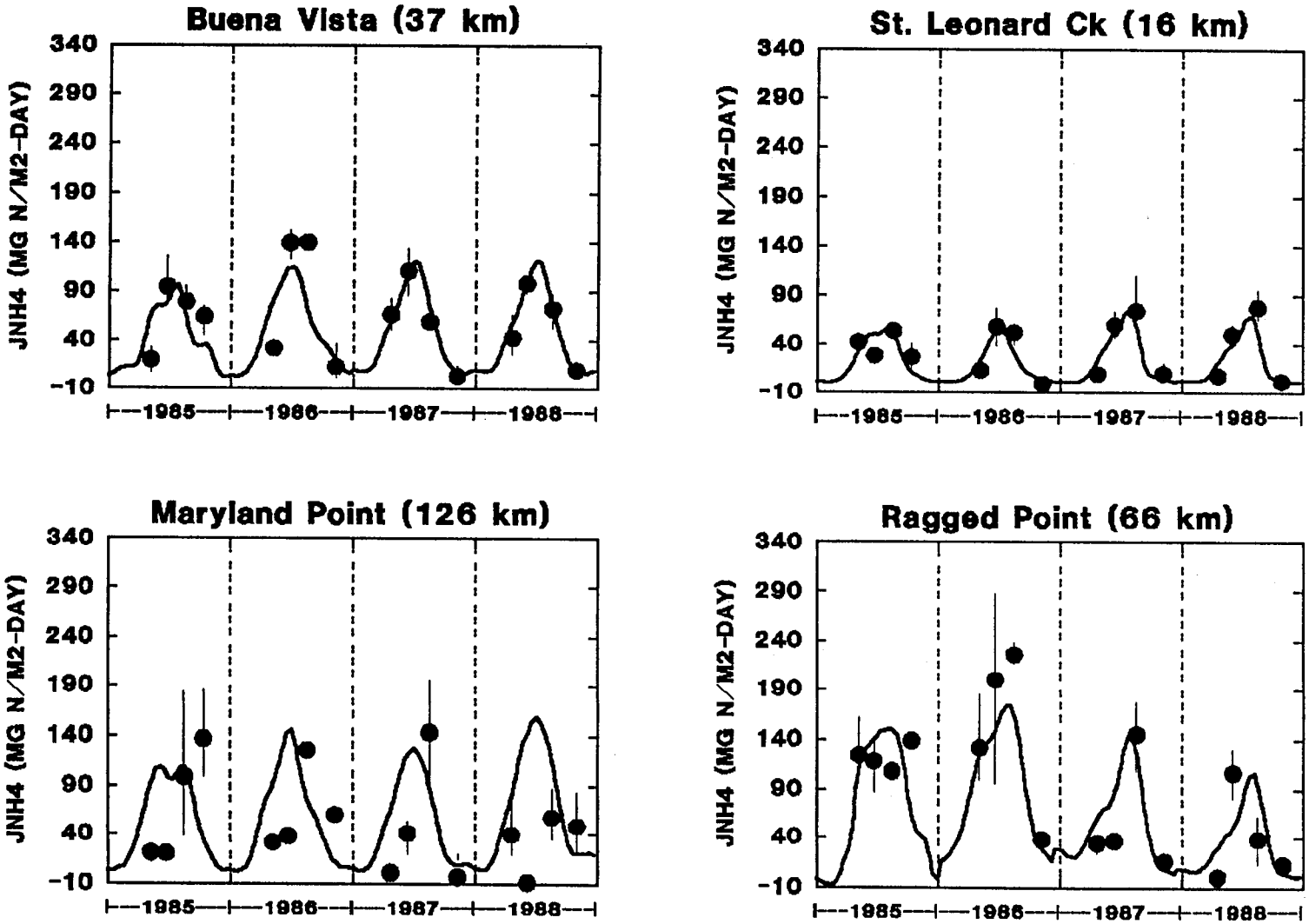

HydroQual, Inc.

run066 - plotnh42

FIGURE 8

CHESAPEAKE BAY

SEDIMENT MODEL COMPARISON - NITROGEN

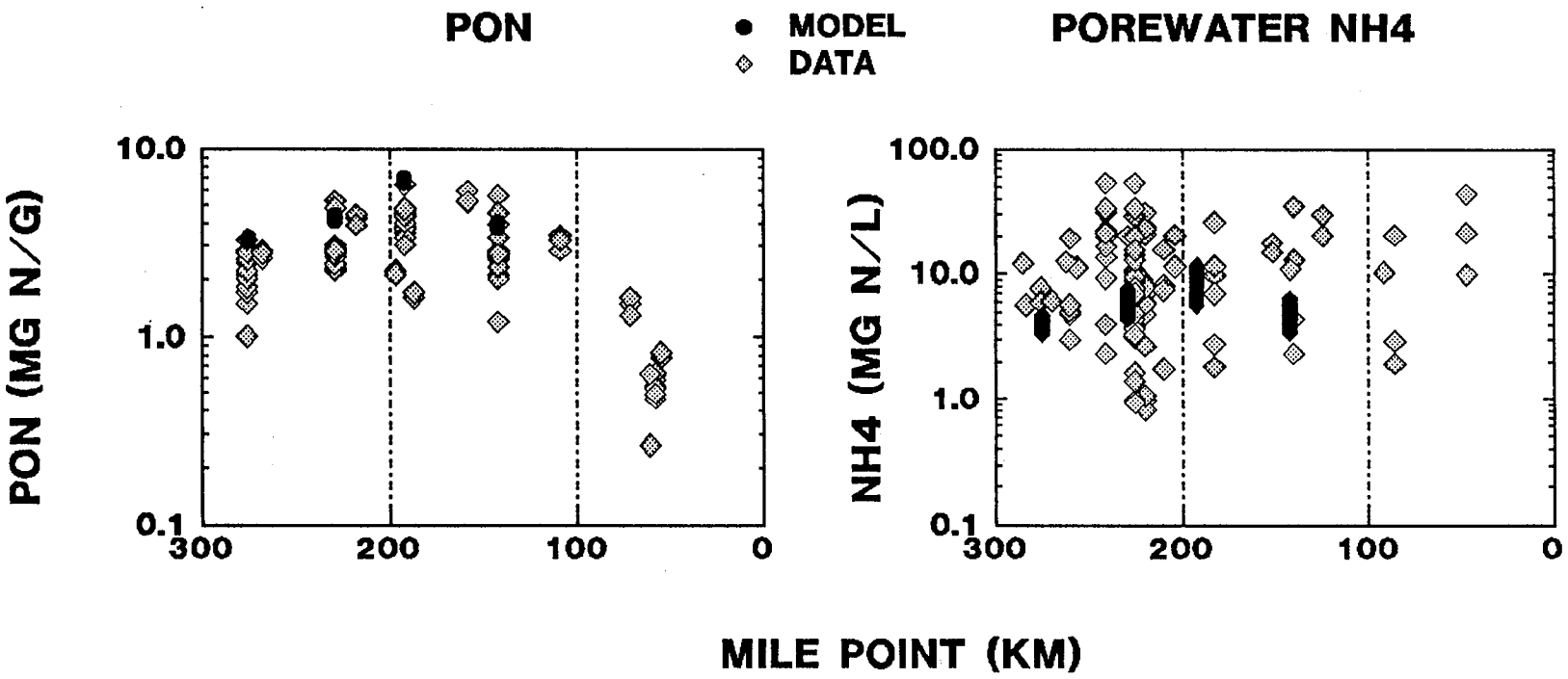

run066 - plotlwn

FIGURE 9

CHESAPEAKE BAY

SEDIMENT MODEL COMPARISON - AMMONIA

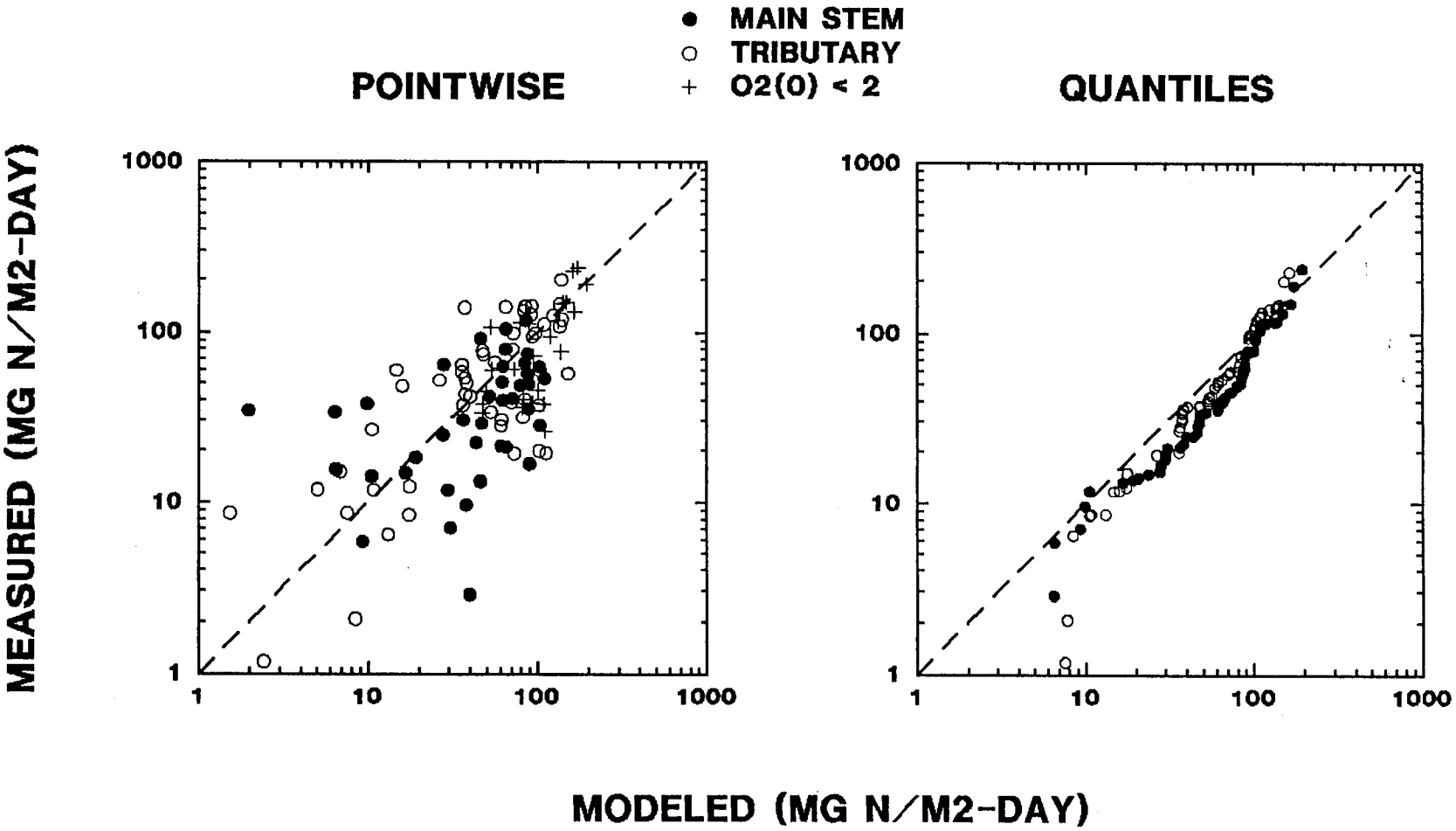

HydroQual, Inc.

run066 - plotmma

FIGURE 10

CHESAPEAKE BAY

SEDIMENT MODEL COMPARISON - AMMONIA vs SOD/O2(0)

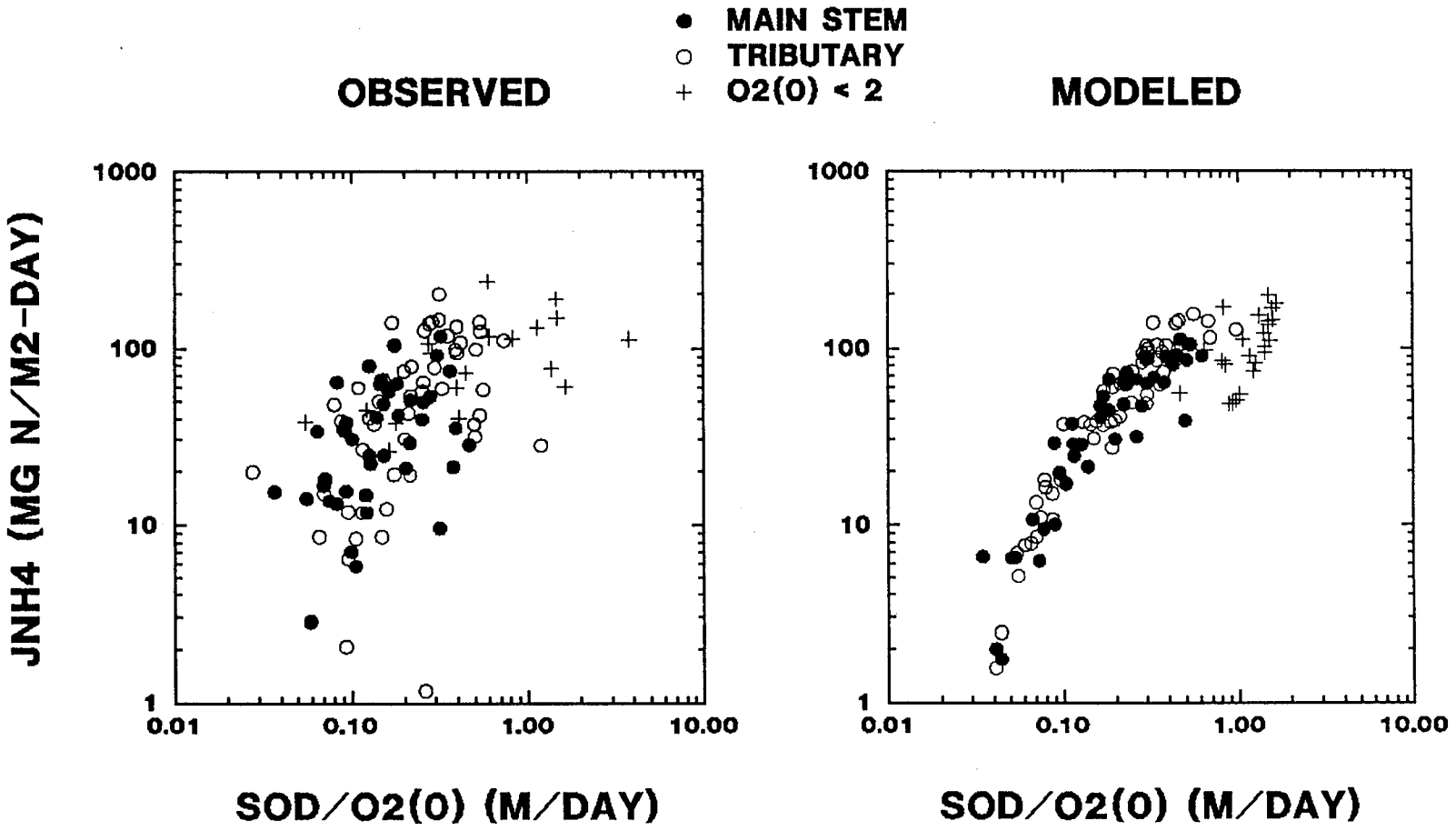

run066 - plotso1

FIGURE 11

CHESAPEAKE BAY

SEDIMENT MODEL COMPARISON - AMMONIA vs O2(0)

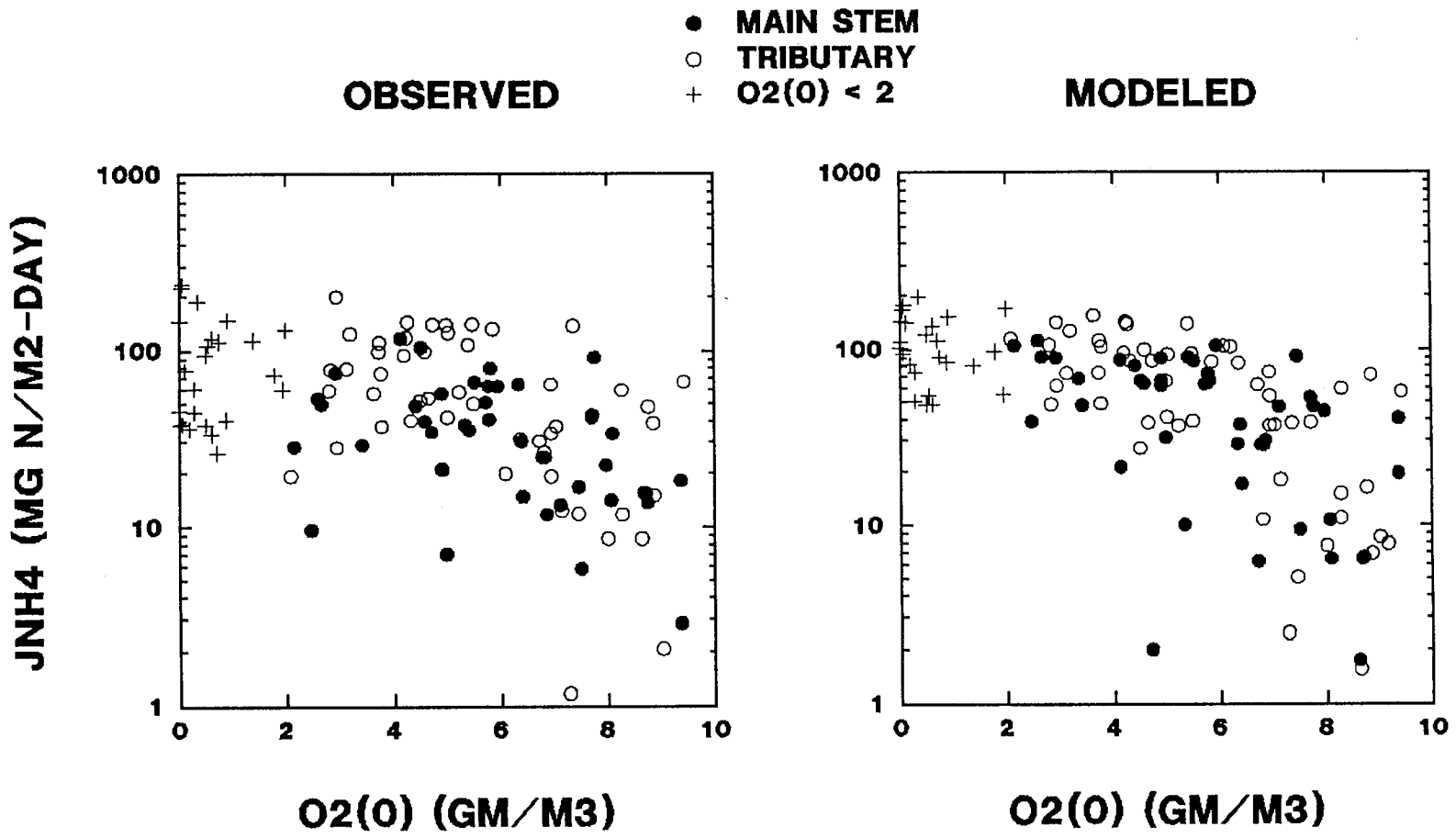

HydroQual, Inc.

run066 - plotno1

FIGURE 12

NITRATE FLUX

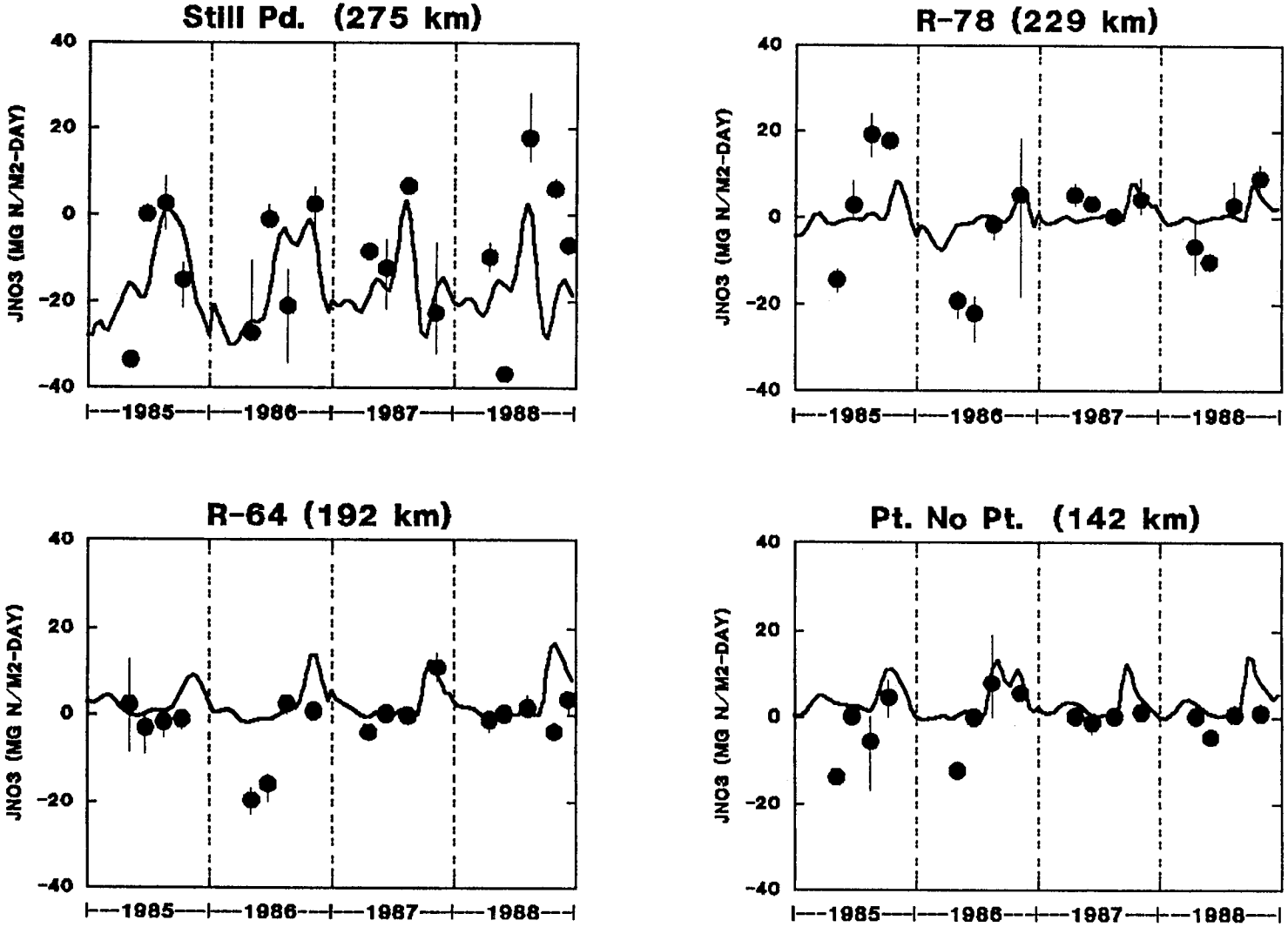

run066 - plotno31

FIGURE 13

NITRATE FLUX

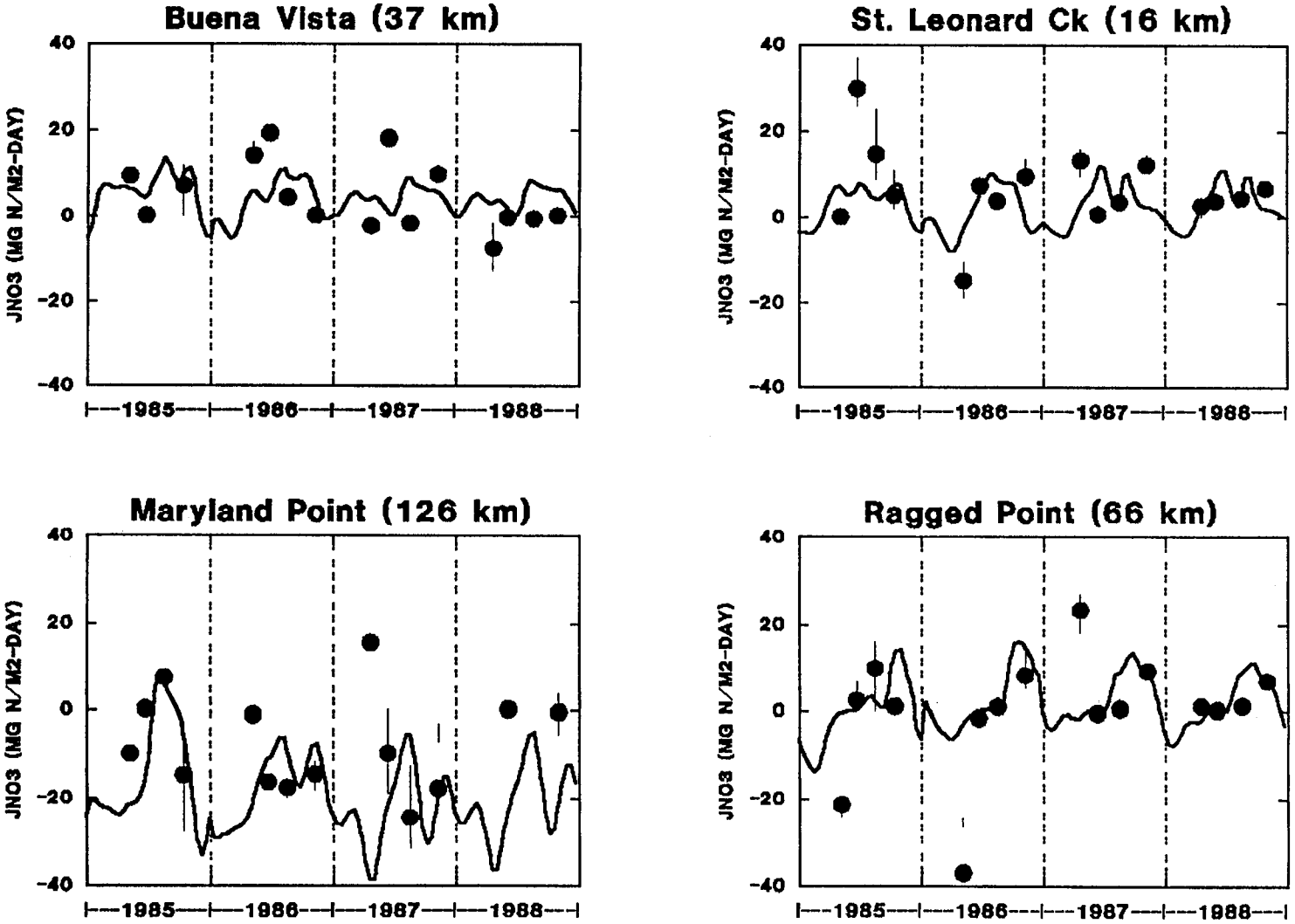

HydroQual, Inc.

run066 - plotno32

FIGURE 14

CHESAPEAKE BAY

SEDIMENT MODEL COMPARISON - NITRATE

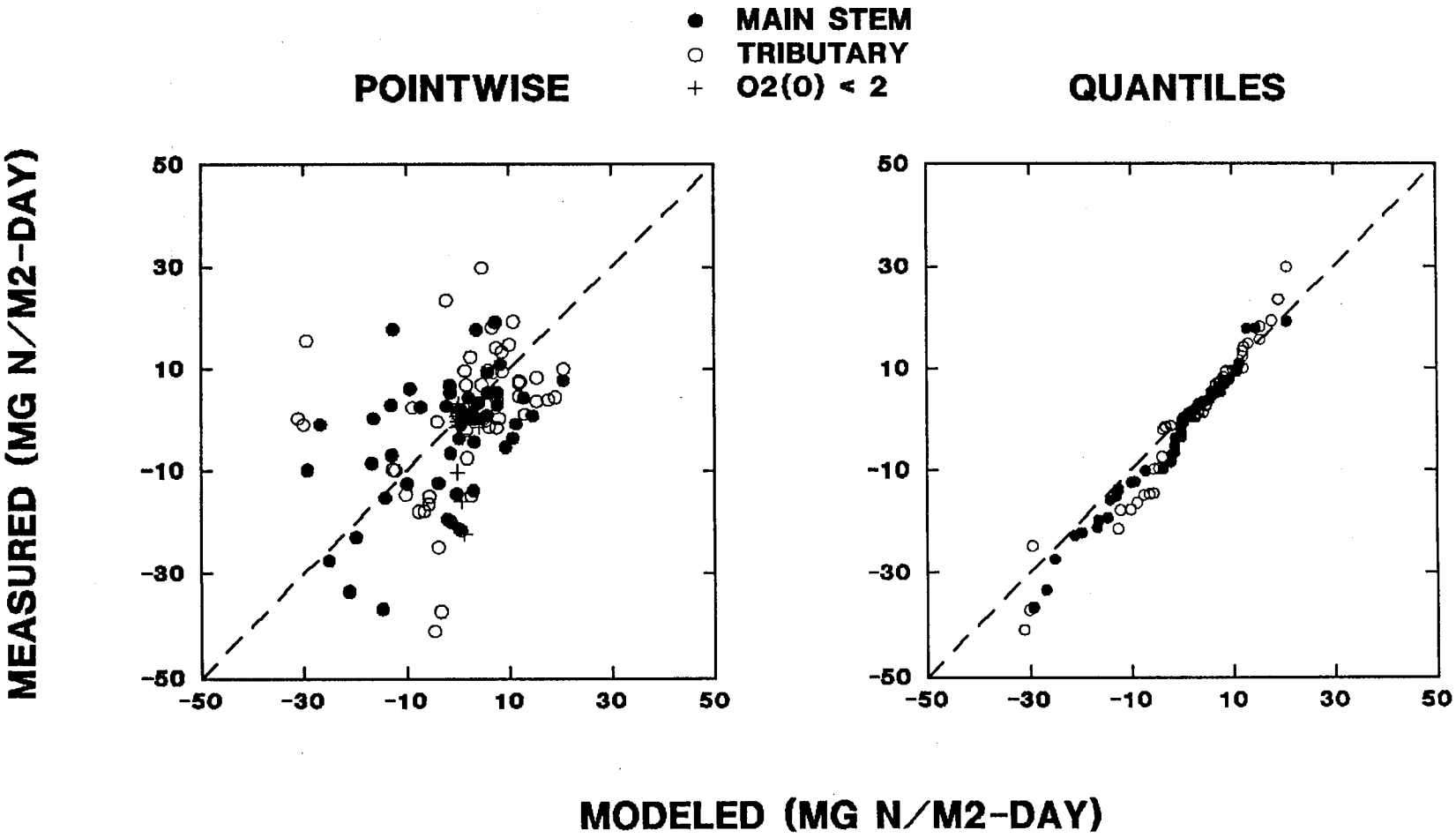

run066 - plotmmno

FIGURE 15

CHESAPEAKE BAY

SEDIMENT MODEL COMPARISON - NITRATE FLUX vs NO3(0)

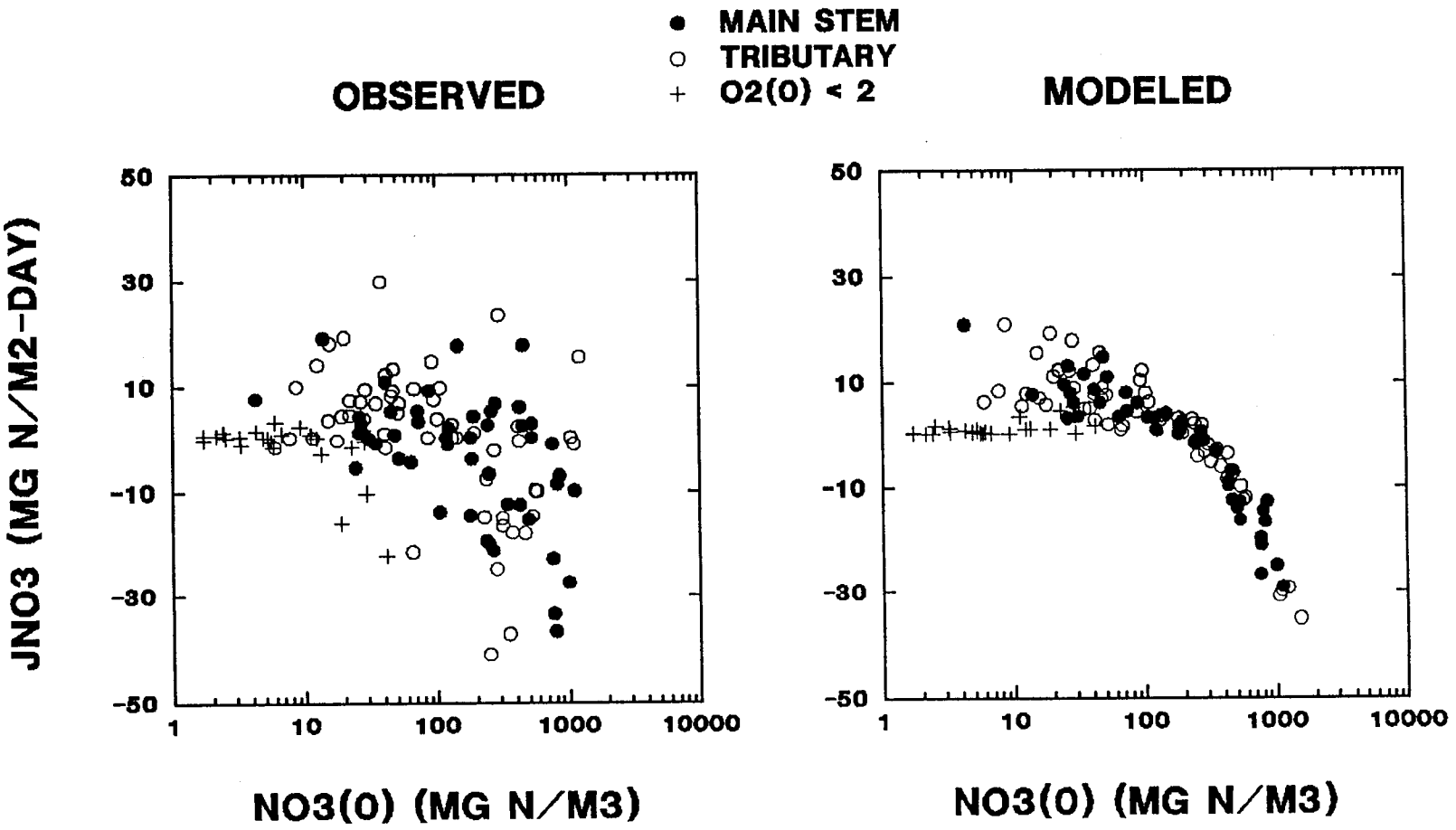

HydroQual, Inc.

run066 - plotnn1

FIGURE 16

OXYGEN FLUX

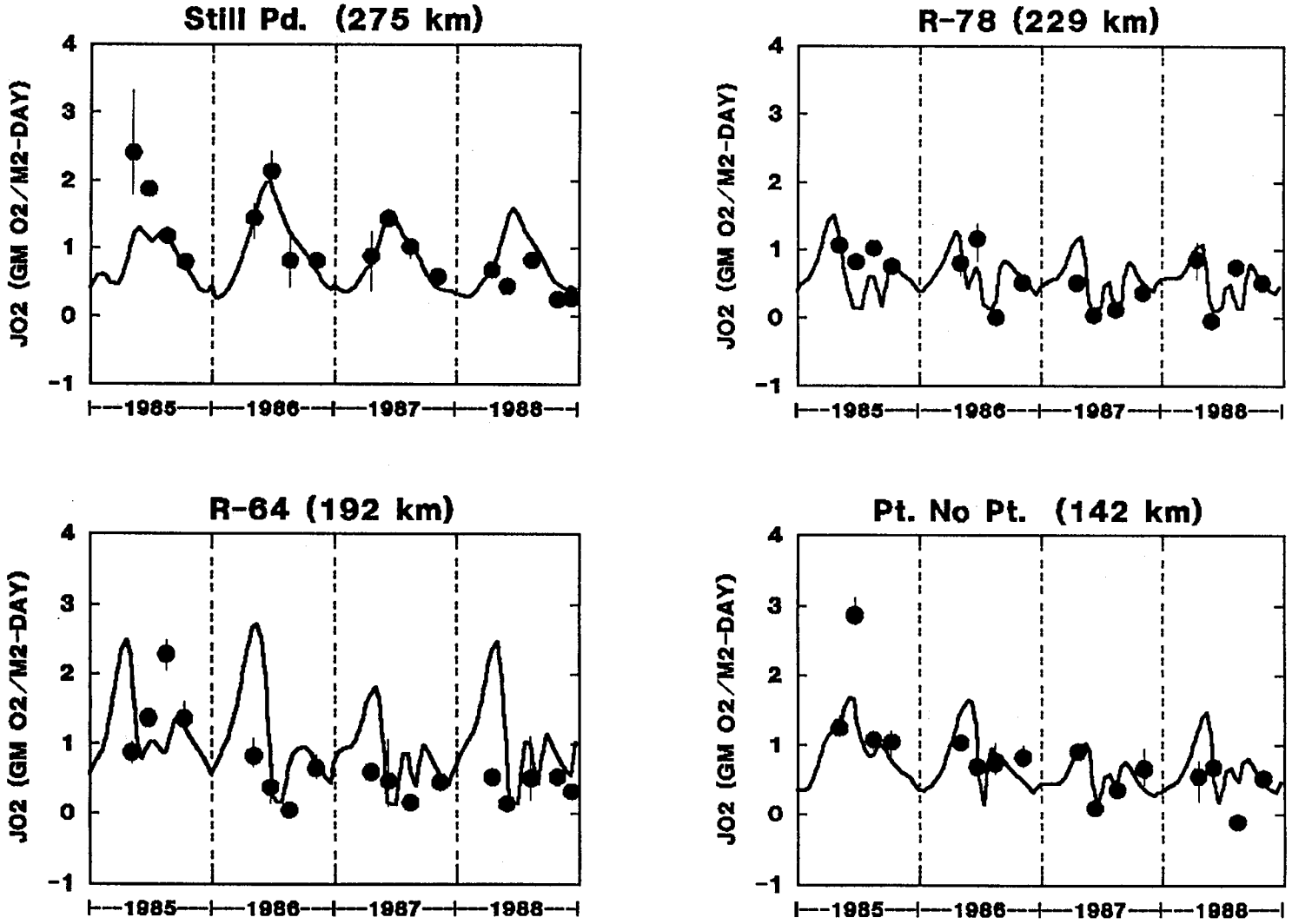

run066 - plotsod1

FIGURE 17

OXYGEN FLUX

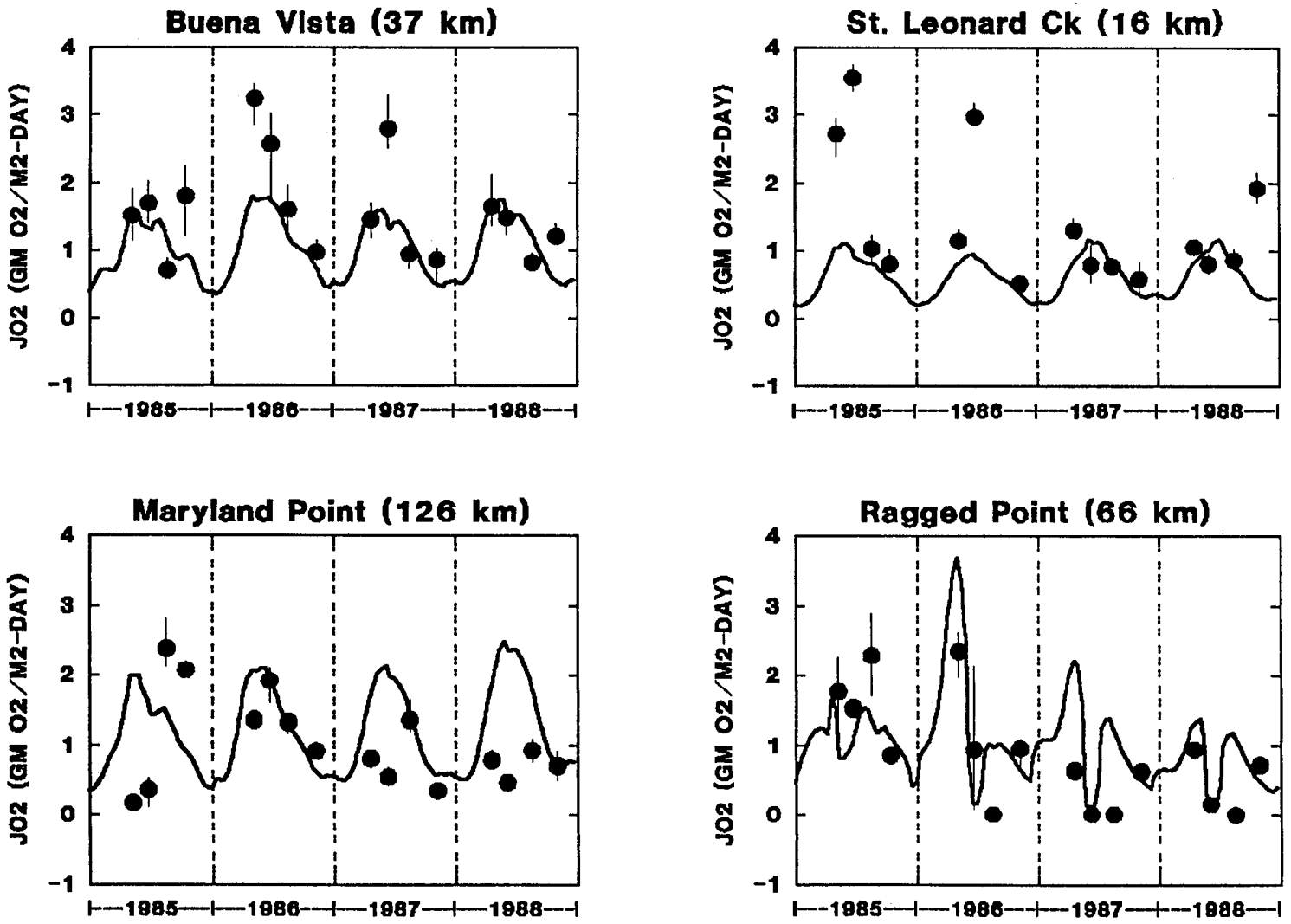

HydroQual, Inc.

run066 - plotsod2

FIGURE 18

BENTHIC PARTICLE MIXING

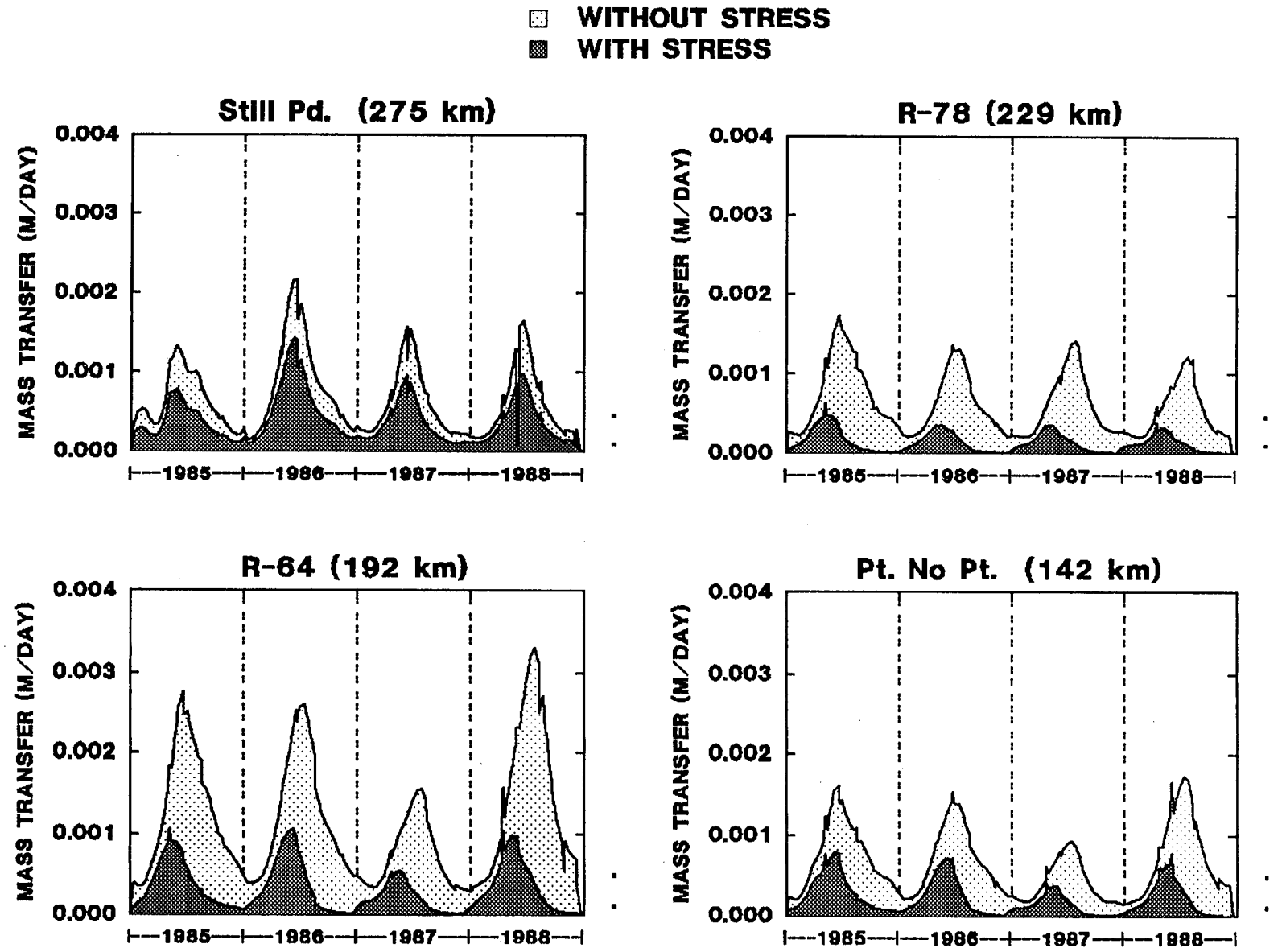

run066 - plotmlx1

FIGURE 19

BENTHIC PARTICLE MIXING

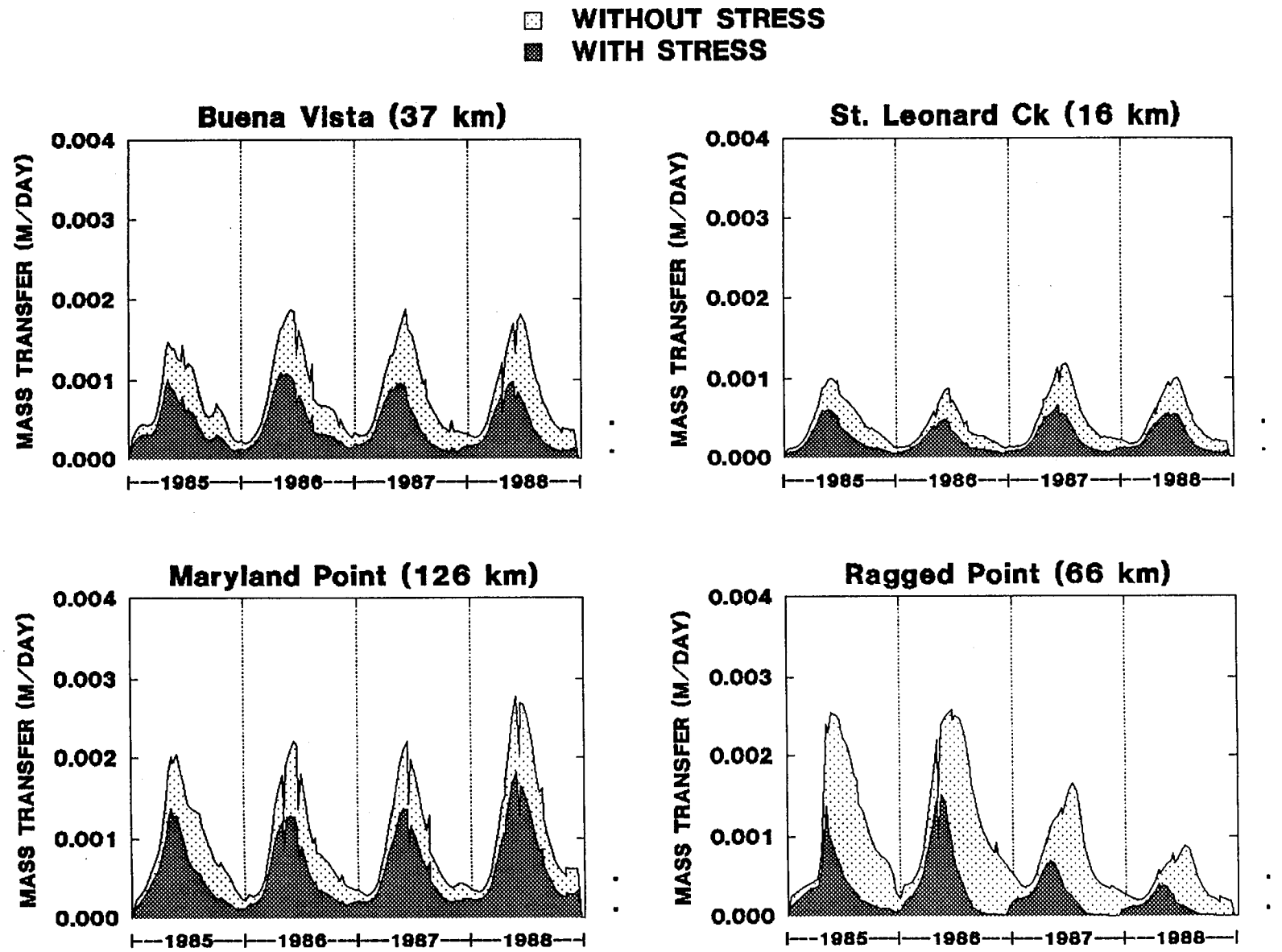

run066 - plotmix2

FIGURE 20

SULFIDE FLUX

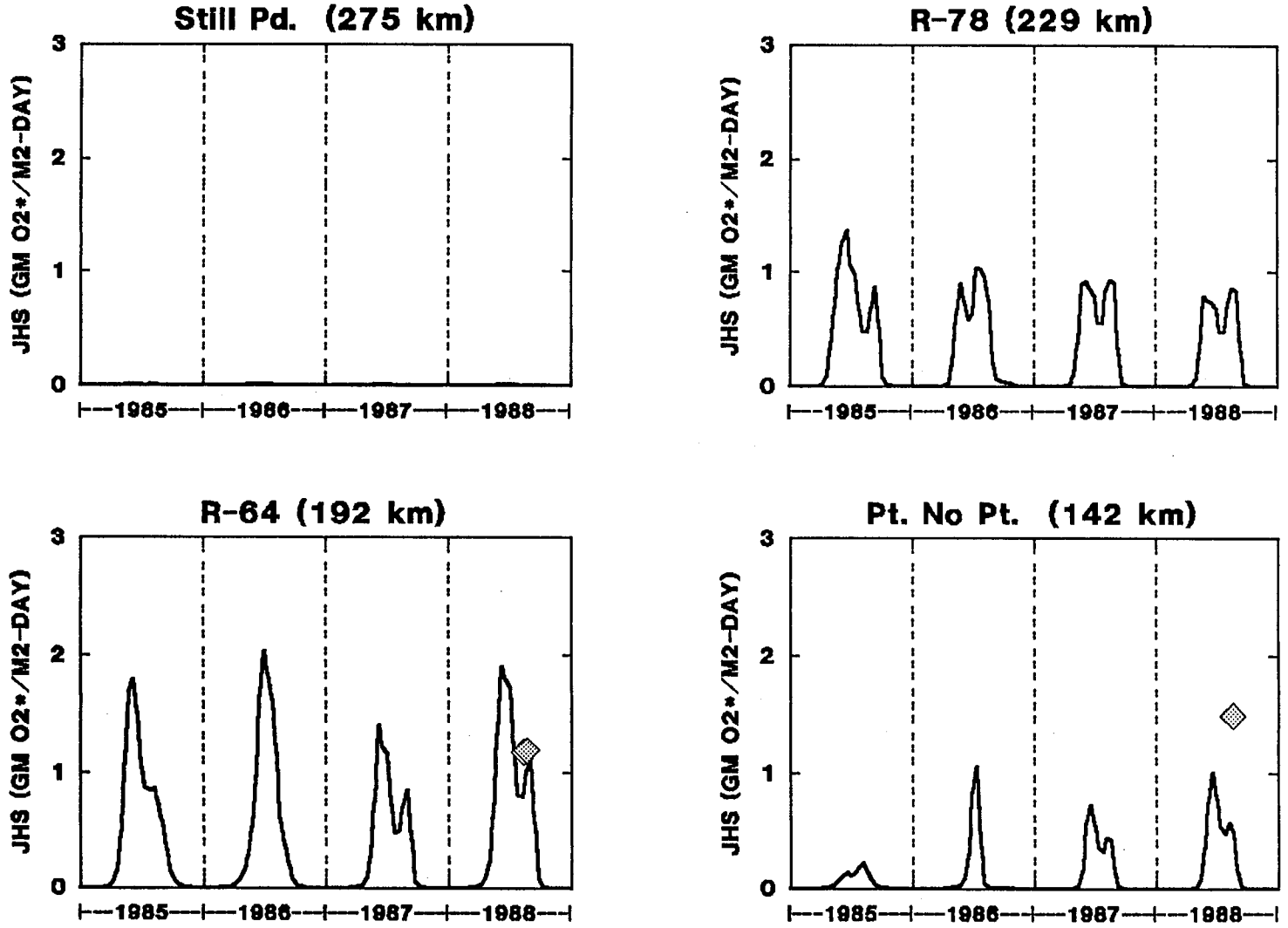

run066 - ploths1

FIGURE 21

SULFIDE FLUX

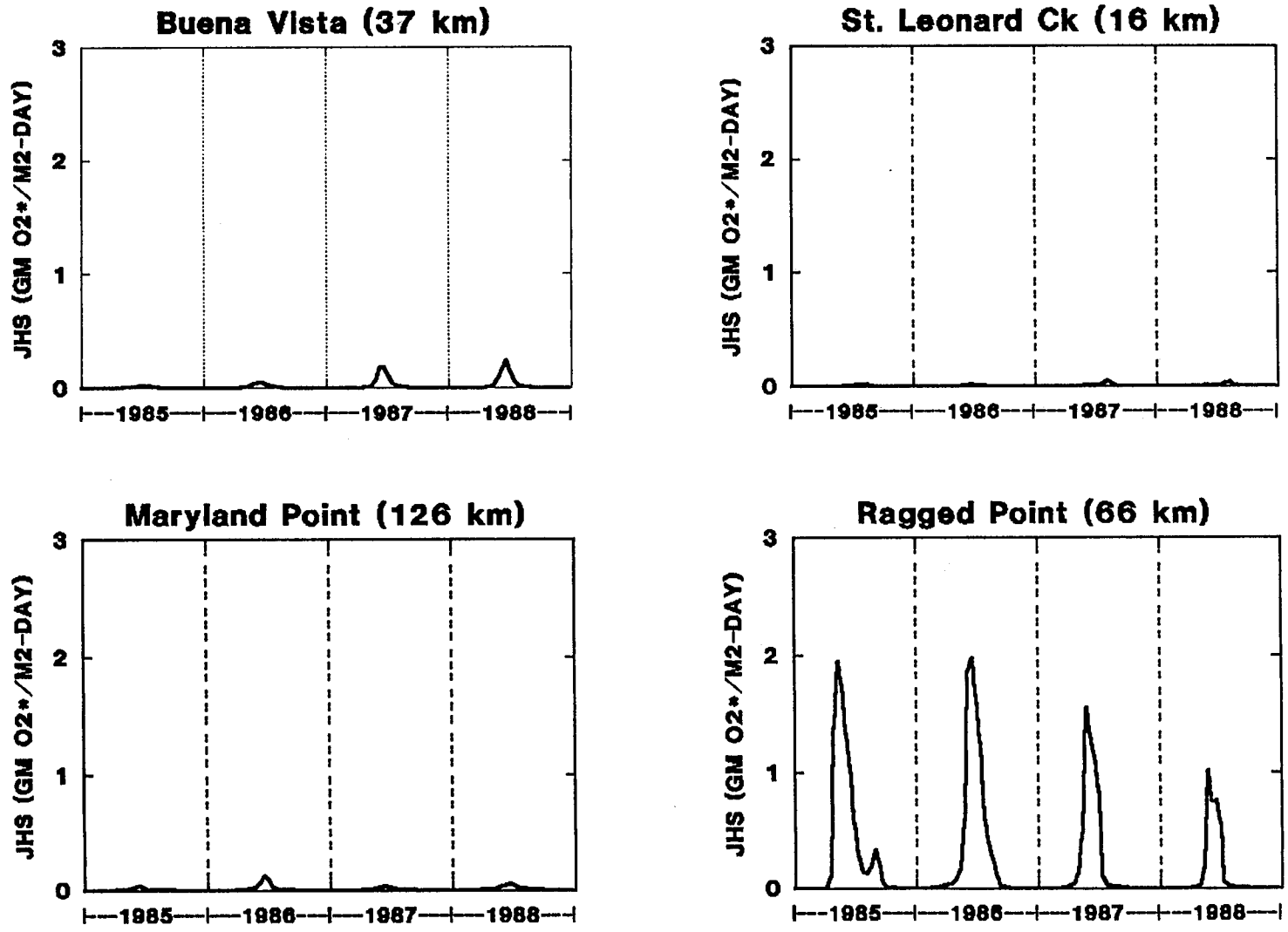

HydroQual, Inc.

run066 - ploths2

FIGURE 22

CHESAPEAKE BAY

SEDIMENT MODEL COMPARISON - C,S

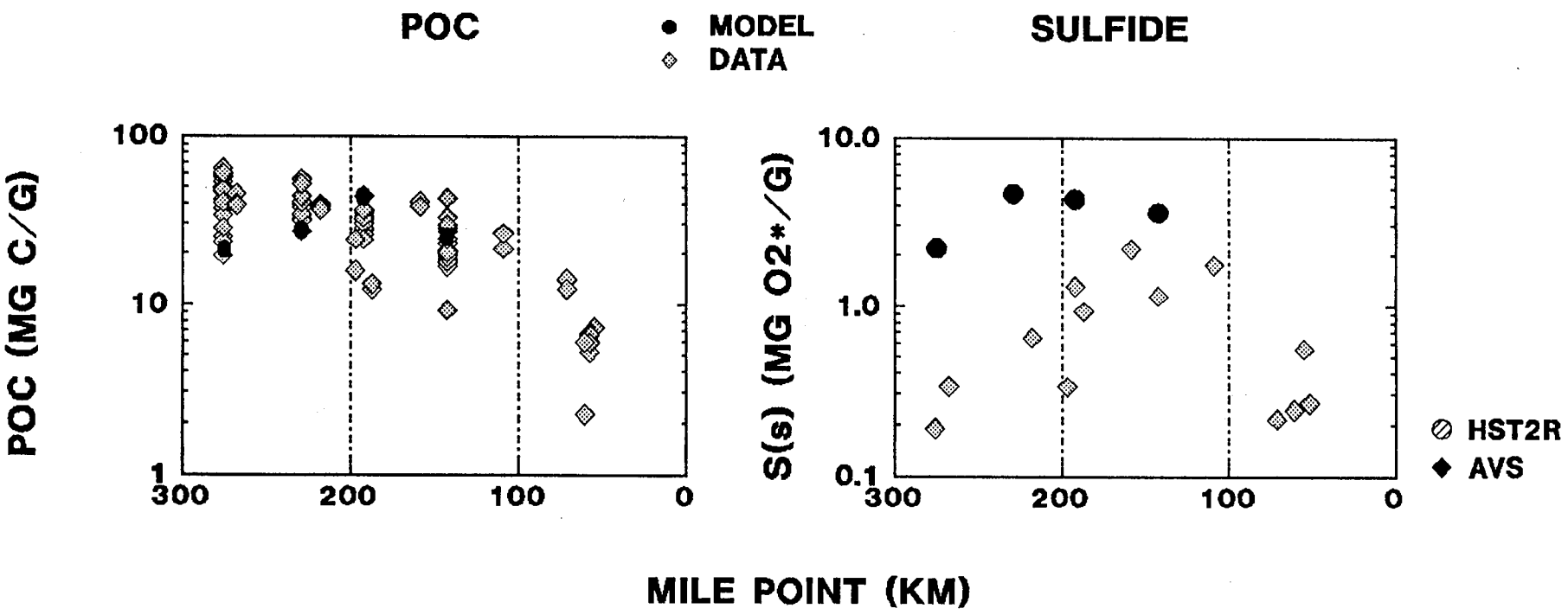

run066 - plotlwc

FIGURE 23

CHESAPEAKE BAY

SEDIMENT MODEL COMPARISON - SOD

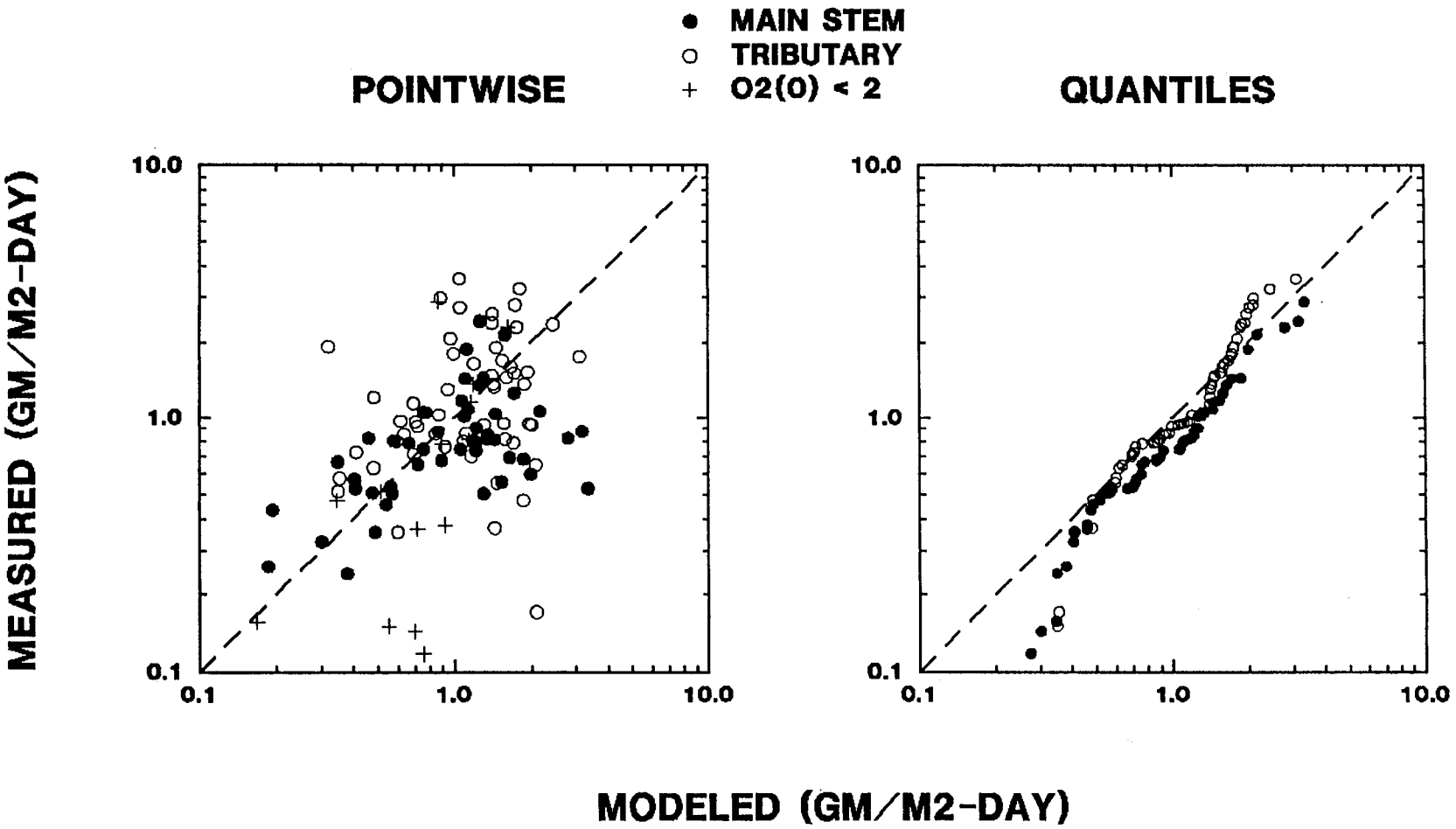

HydroQual, Inc.

run066 - plotmms

FIGURE 24

CHESAPEAKE BAY

SEDIMENT MODEL COMPARISON - SOD vs AMMONIA

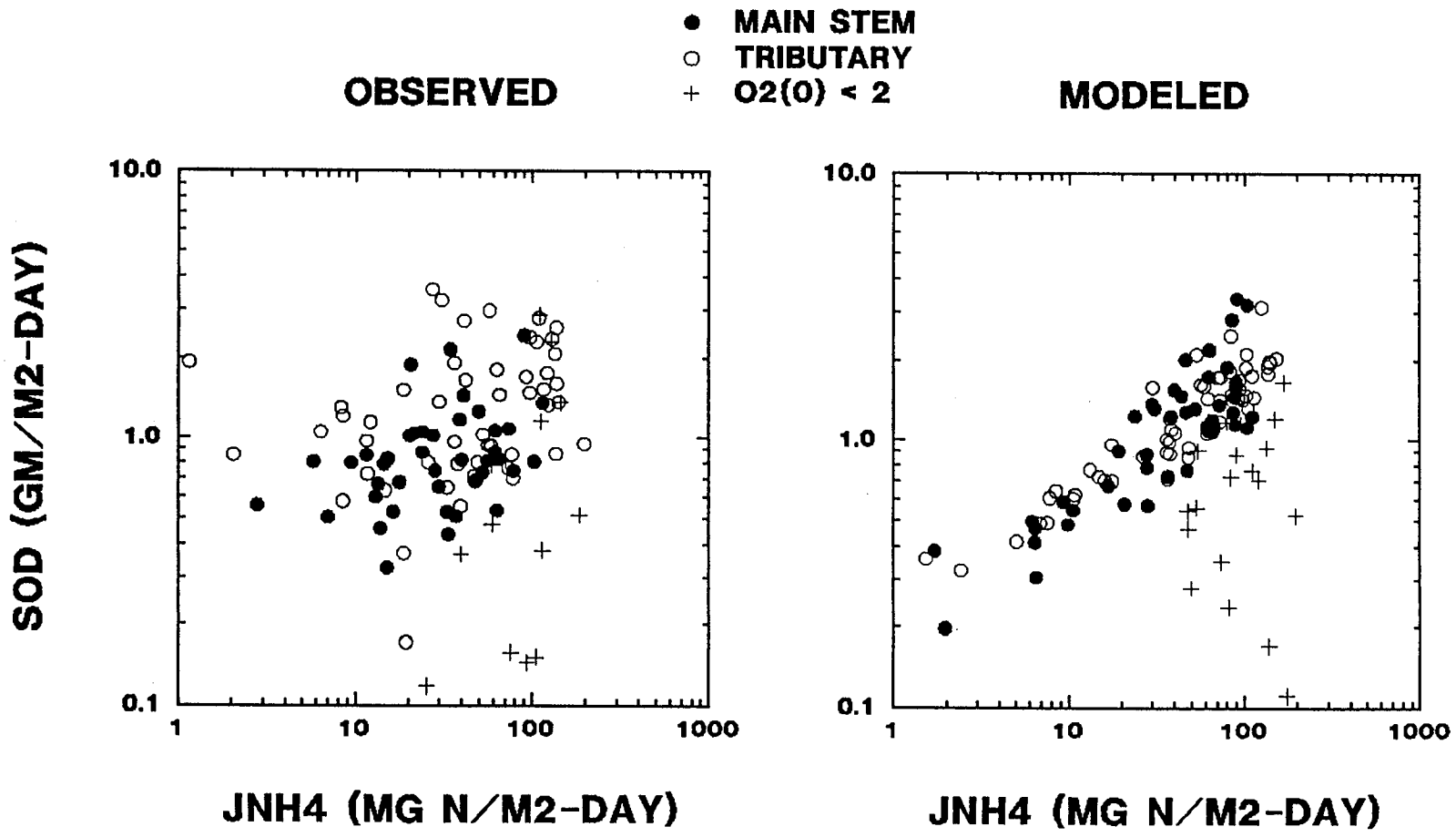

run066 - plotns1

FIGURE 25

PHOSPHORUS FLUX

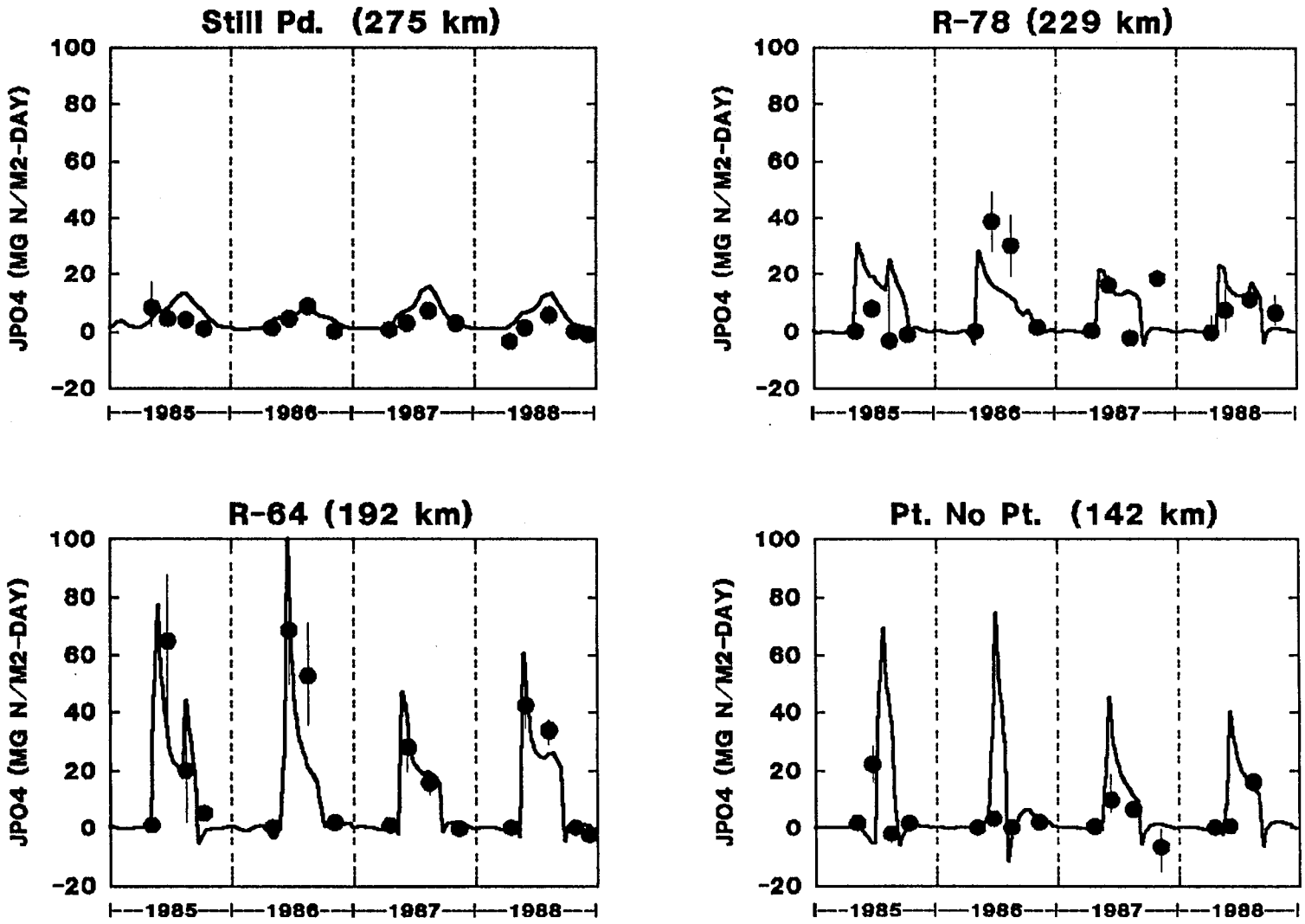

FIGURE 26

PHOSPHORUS FLUX

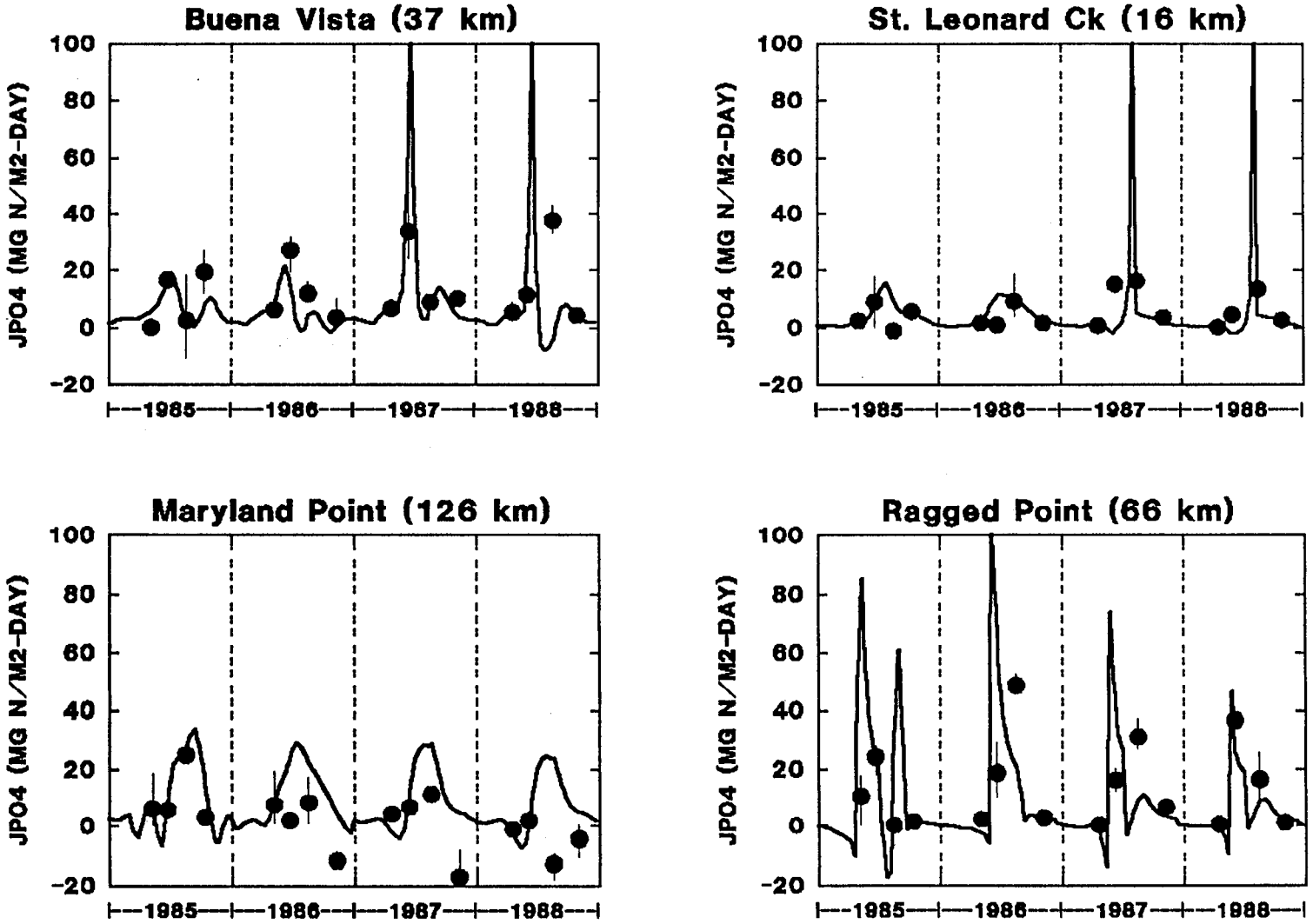

run066 - plotpo42

FIGURE 27

SEDIMENT MODEL COMPARISON - PHOSPHORUS

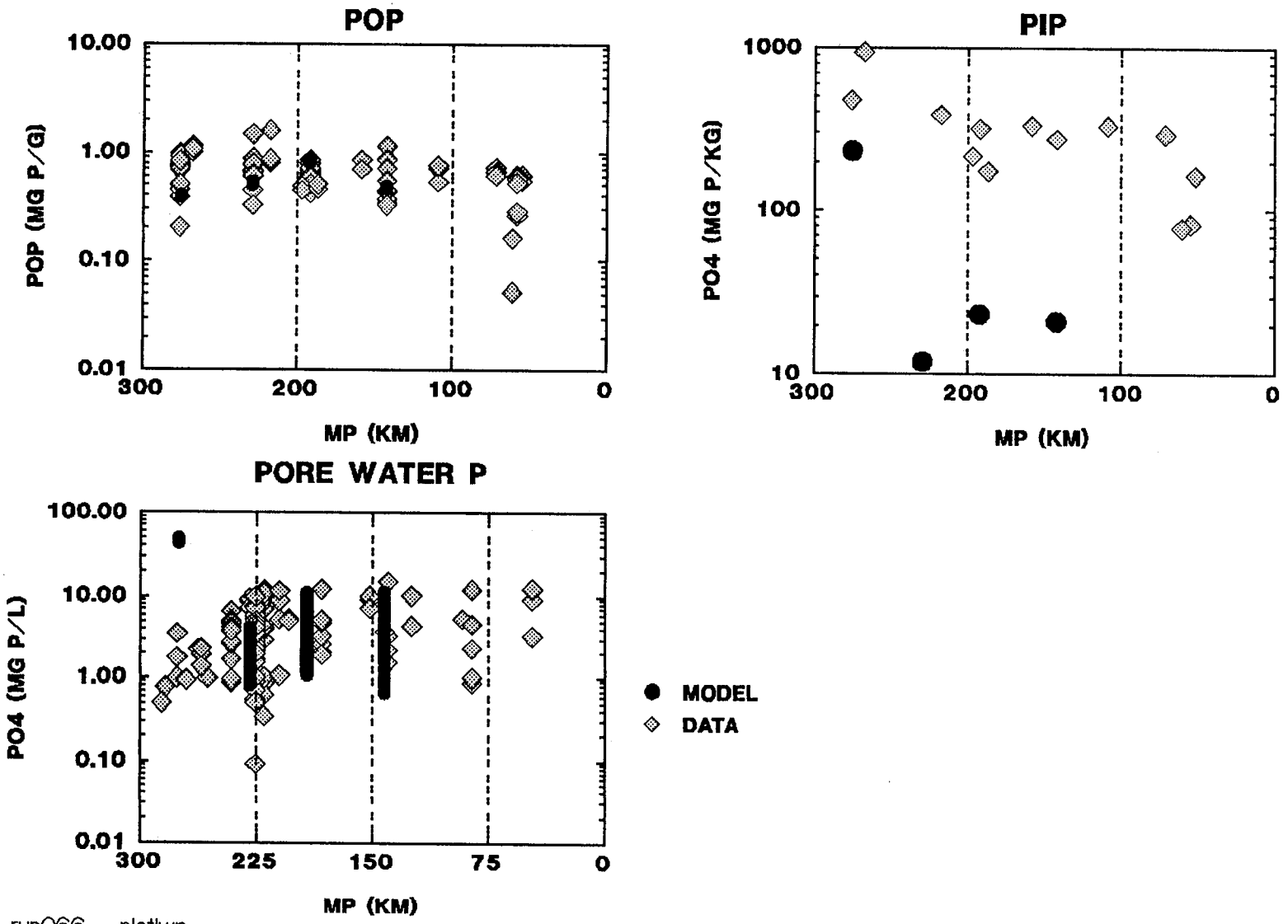

HydroQual, Inc.

run066 - plotlwp

FIGURE 28

CHESAPEAKE BAY

SEDIMENT MODEL COMPARISON - PHOSPHATE

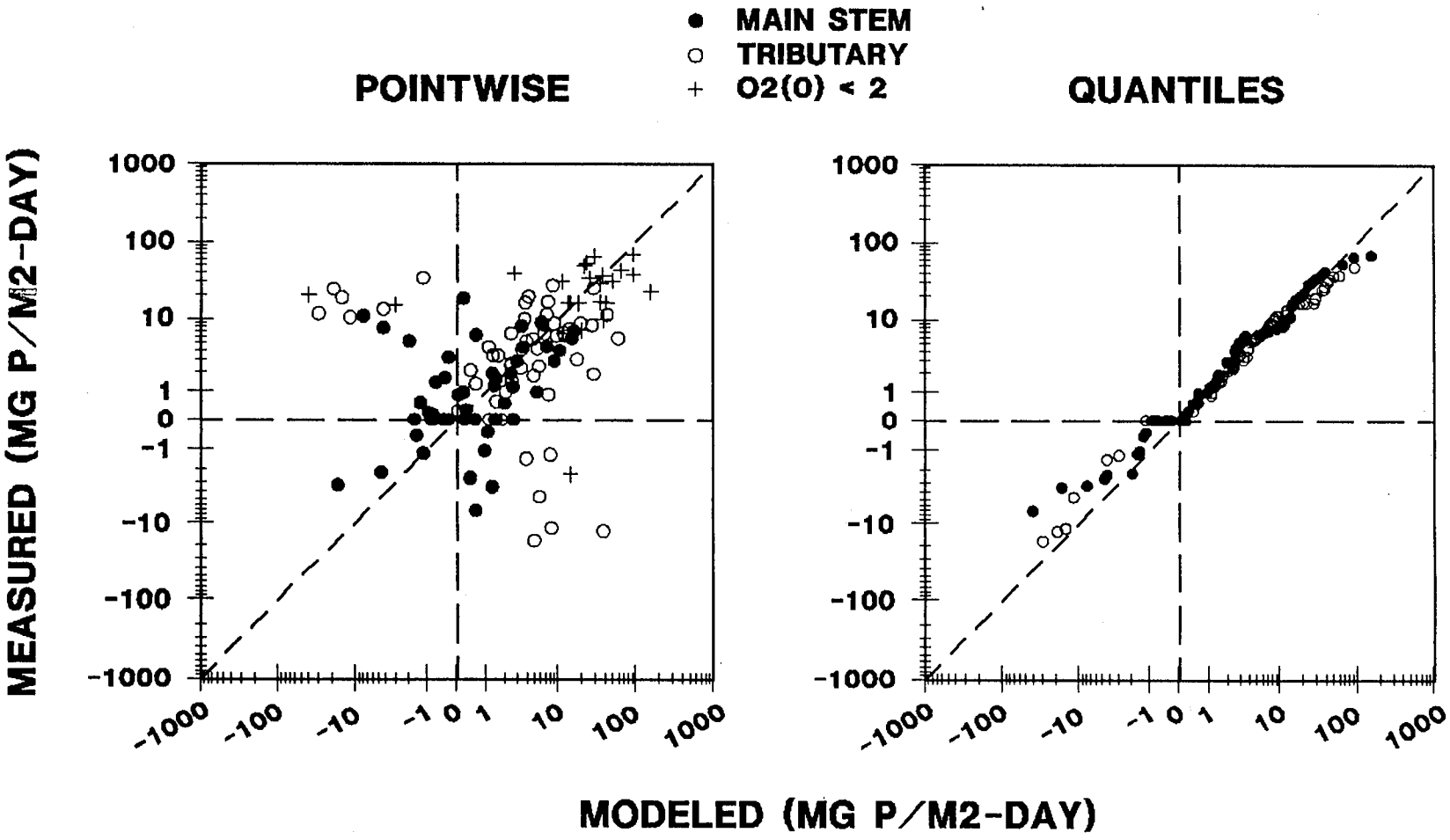

run066 - plotmmp

FIGURE 29

CHESAPEAKE BAY

SEDIMENT MODEL COMPARISON - PHOSPHATE vs AMMONIA

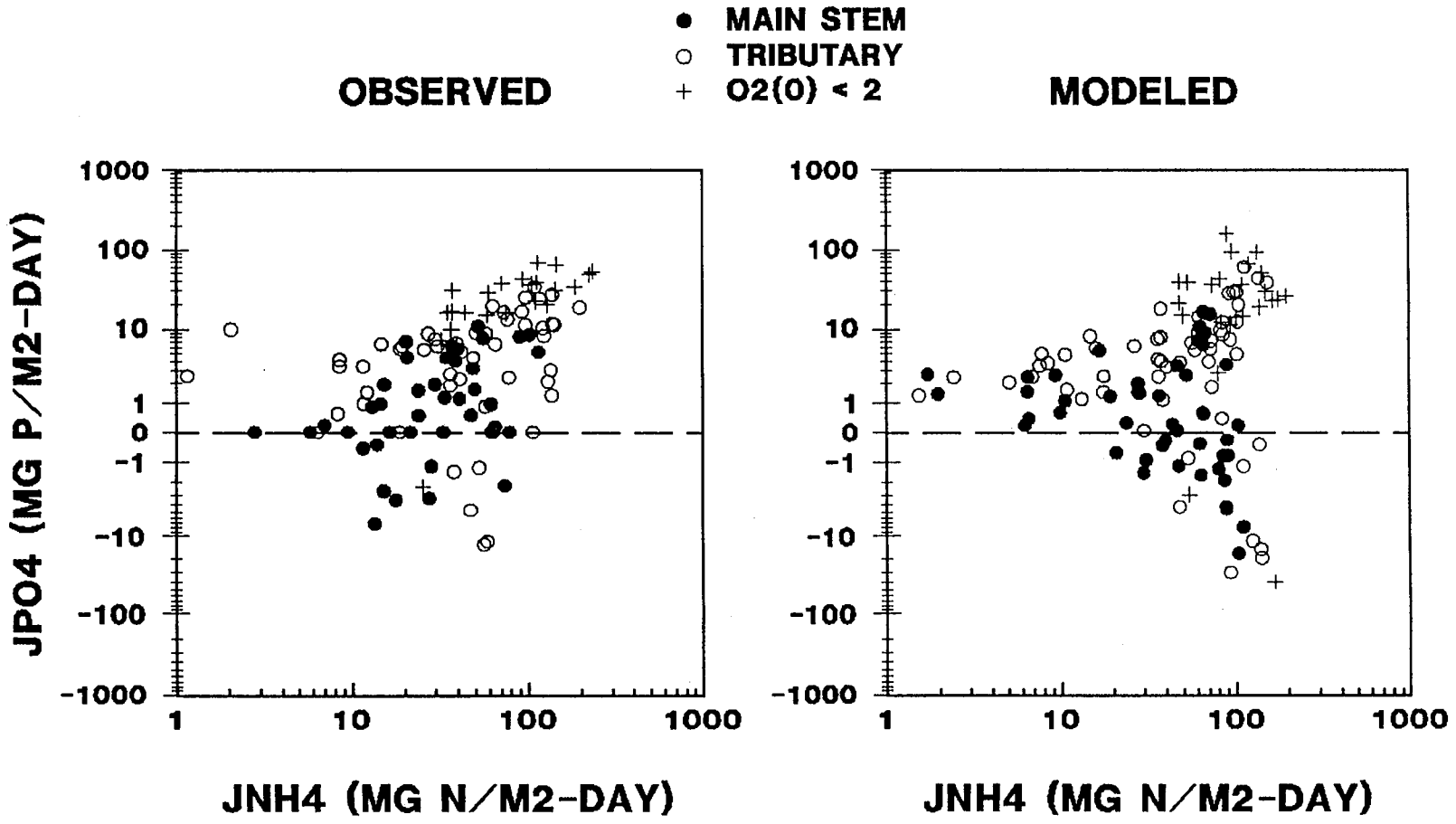

HydroQual, Inc.

run066 - plotnp1

FIGURE 30

CHESAPEAKE BAY

SEDIMENT MODEL COMPARISON - PHOSPHATE vs SOD/O2(0)

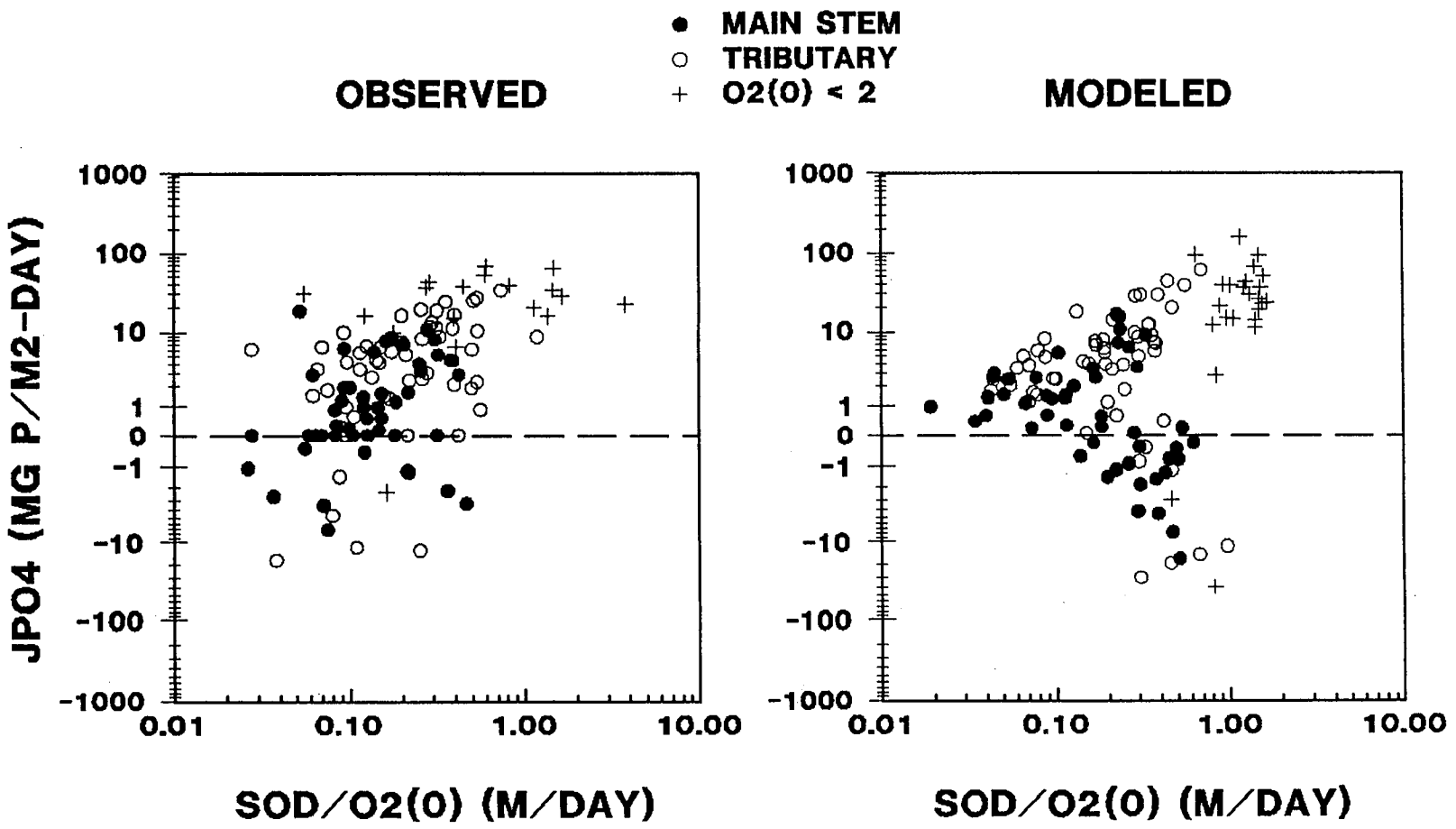

run066 - plotso2a

FIGURE 31

CHESAPEAKE BAY

SEDIMENT MODEL COMPARISON - PHOSPHATE vs O2(0)

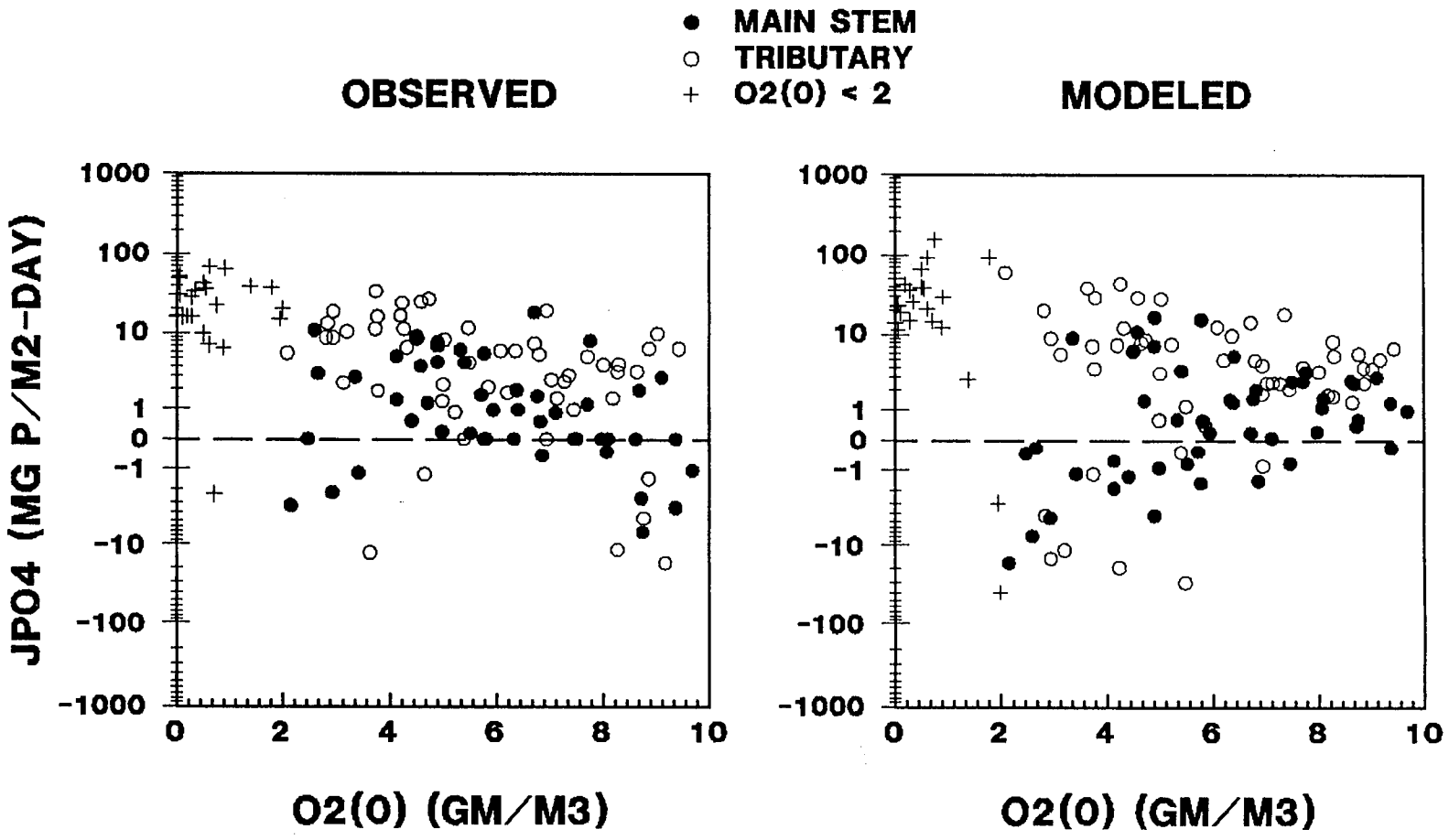

HydroQual, Inc.

run066 - plotpo2

FIGURE 32

SILICA FLUX

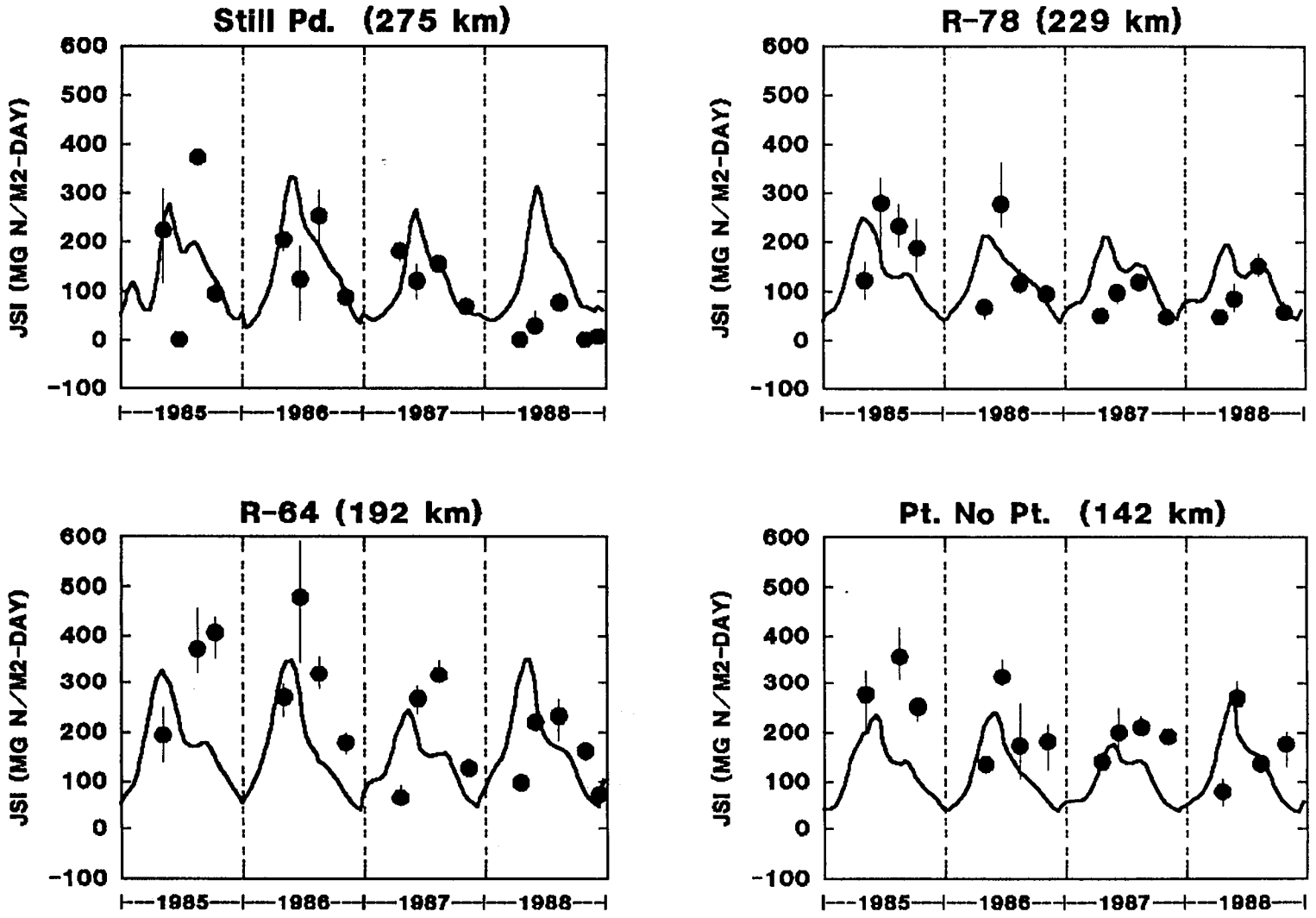

run066 - plotsl1

FIGURE 33

SILICA FLUX

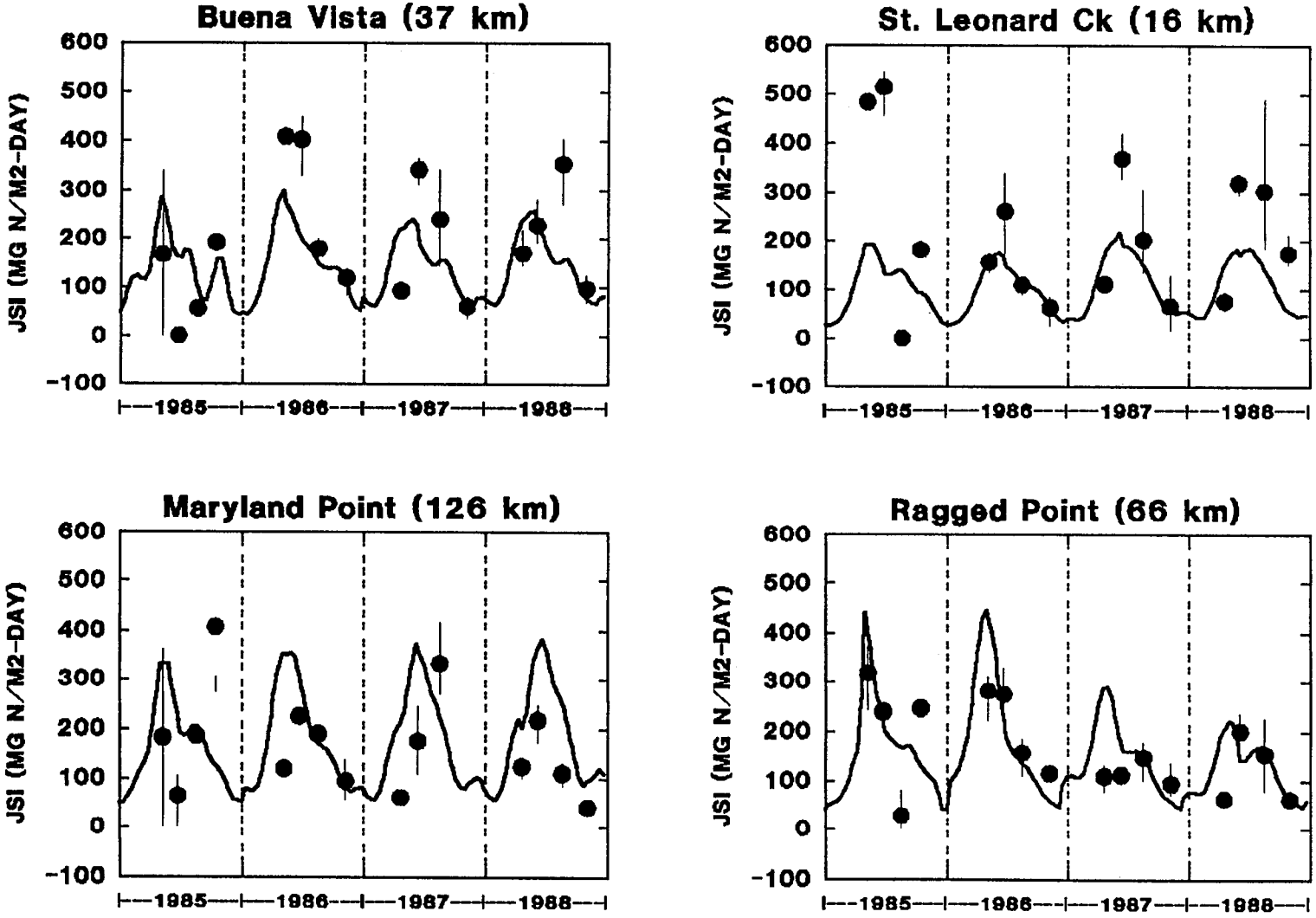

HydroQual, Inc.

run066 - plotsl2

FIGURE 34

CHESAPEAKE BAY

SEDIMENT MODEL COMPARISON - SILICA

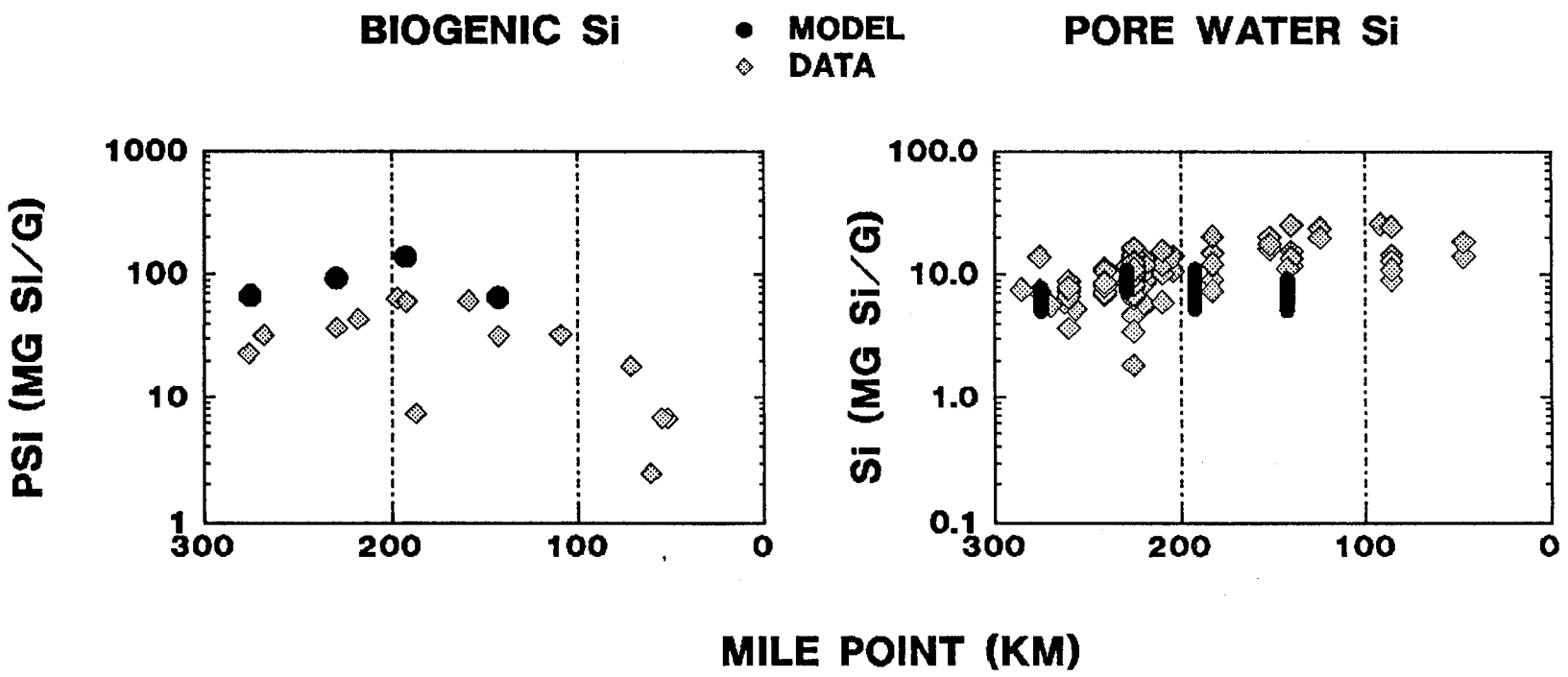

run066 - plotiwsi

FIGURE 35

CHESAPEAKE BAY

SEDIMENT MODEL COMPARISON - SILICA

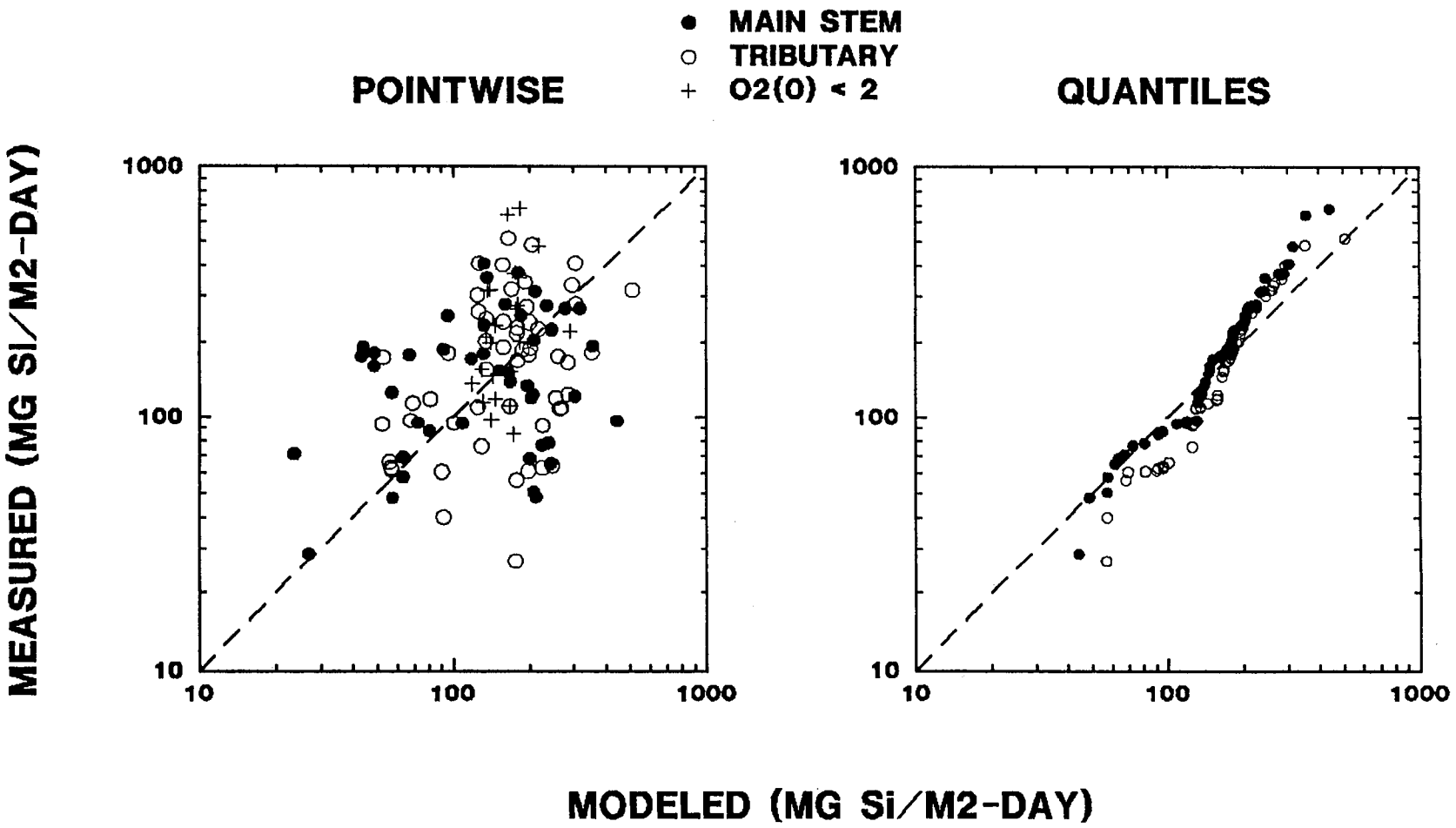

HydroQual, Inc.

run066 - plotmmsl

FIGURE 36

CHESAPEAKE BAY

SEDIMENT MODEL COMPARISON - SILICA vs AMMONIA

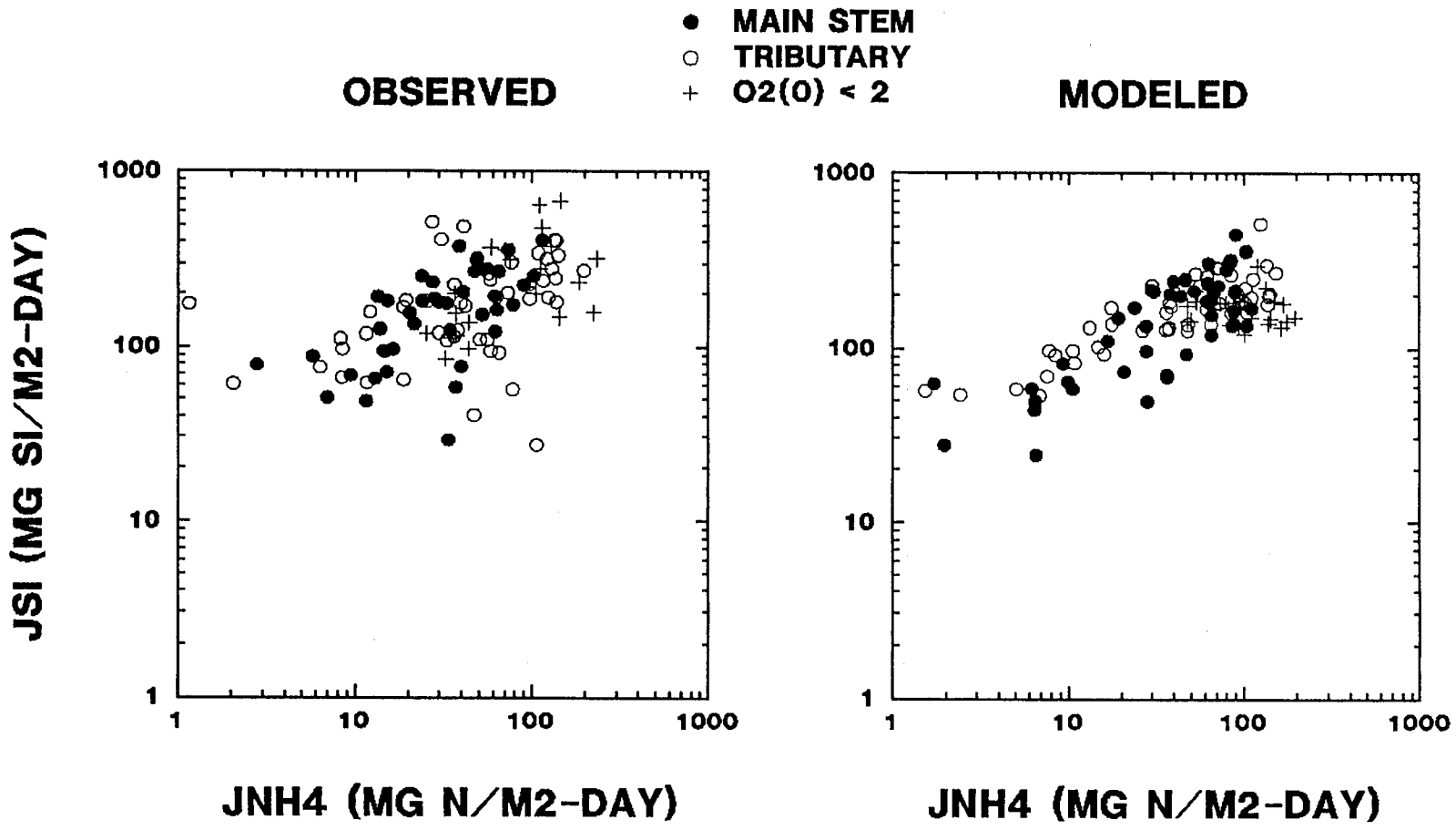

run066 - plotnsl1

FIGURE 37

CHESAPEAKE BAY

SEDIMENT MODEL COMPARISON - SILICA vs SOD/O2(0)

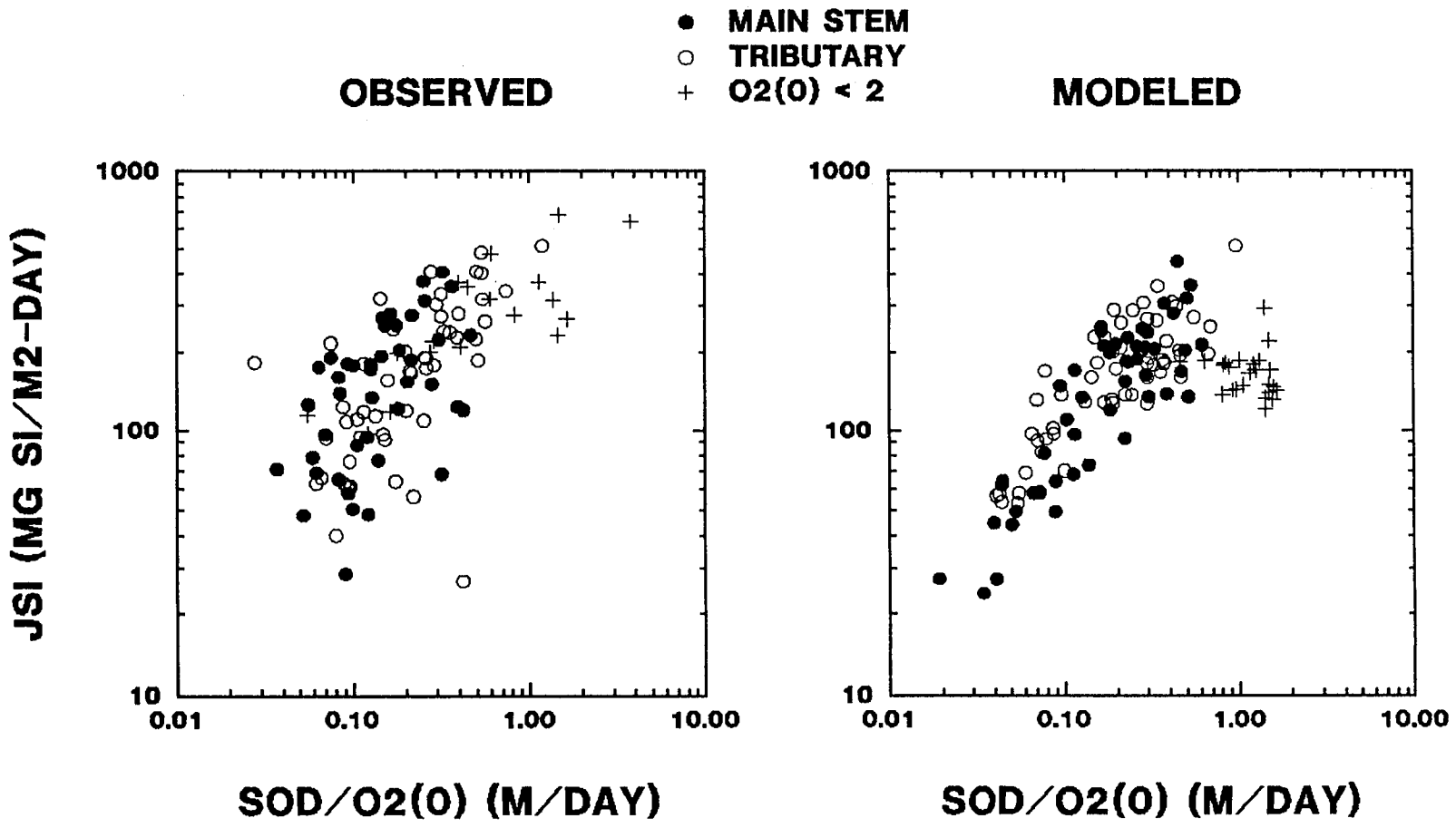

HydroQual, Inc.

run066 - plotso3

FIGURE 38

CHESAPEAKE BAY

SEDIMENT MODEL COMPARISON - SILICA vs O2(0)

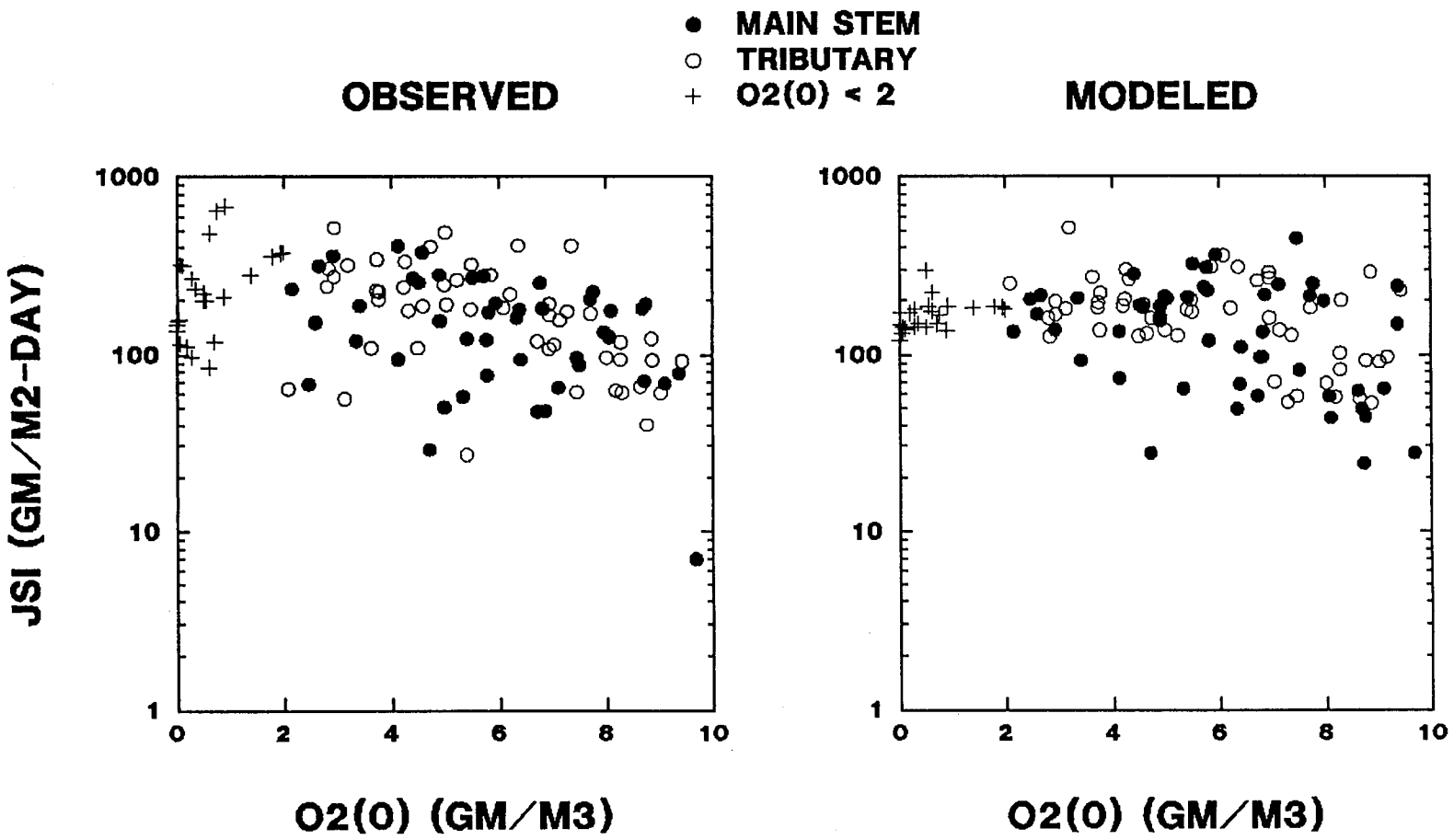

run066 - plotslo1

FIGURE 39

CHESAPEAKE BAY - STILL POND

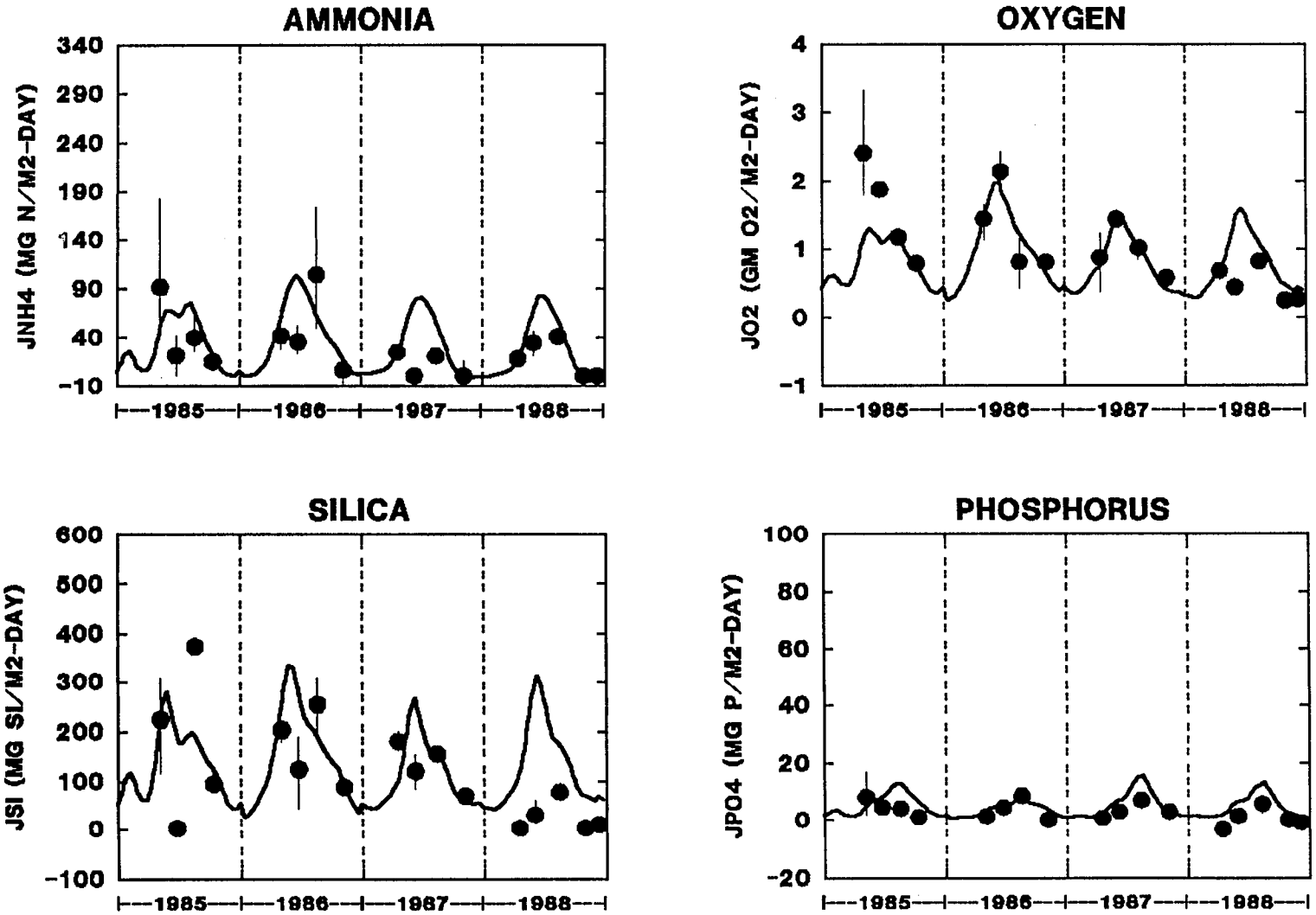

HydroQual, Inc.

run066 - plotpond

FIGURE 40

CHESAPEAKE BAY - STATION R-78

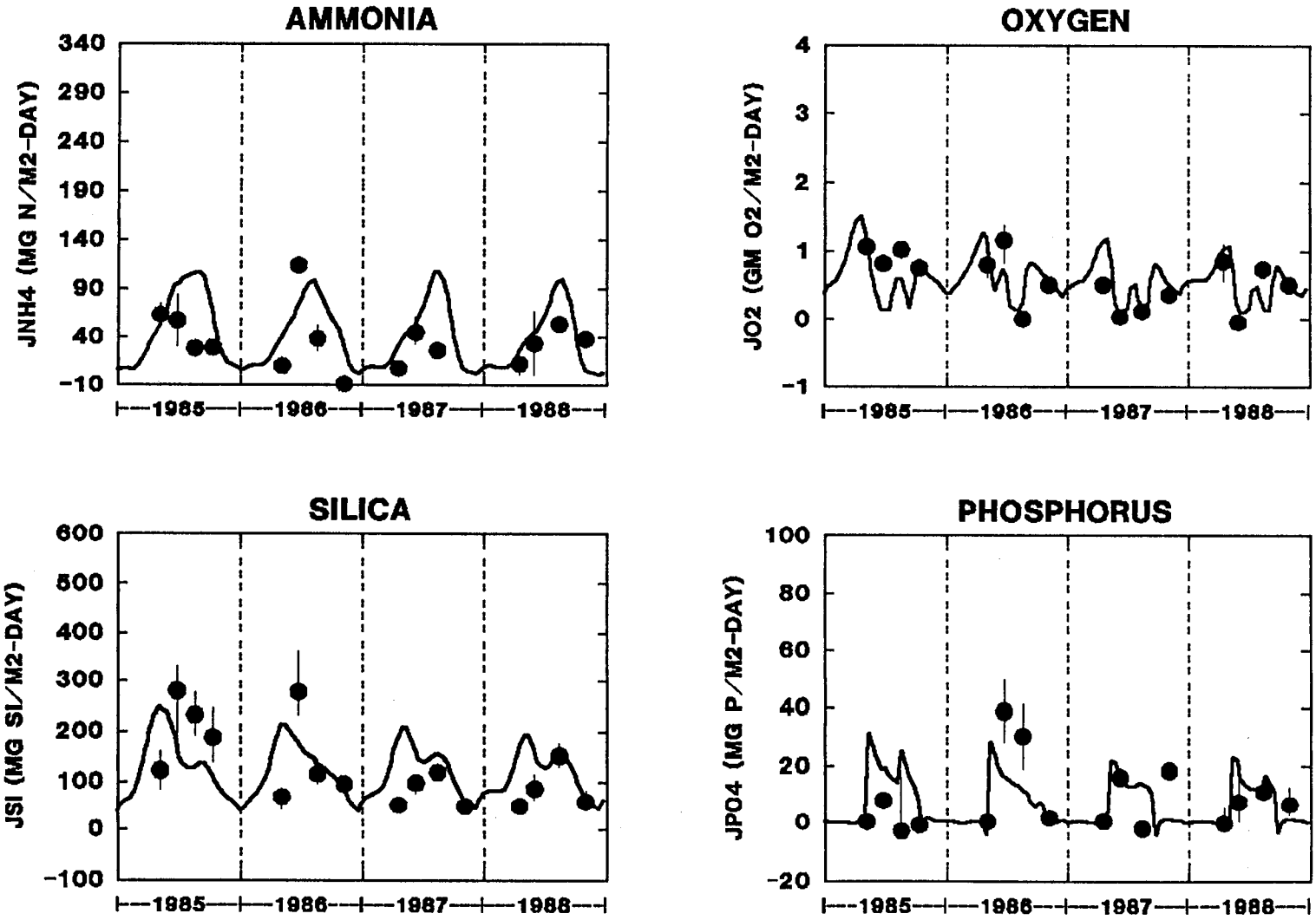

run066 - plotr78

FIGURE 41

CHESAPEAKE BAY - STATION R-64

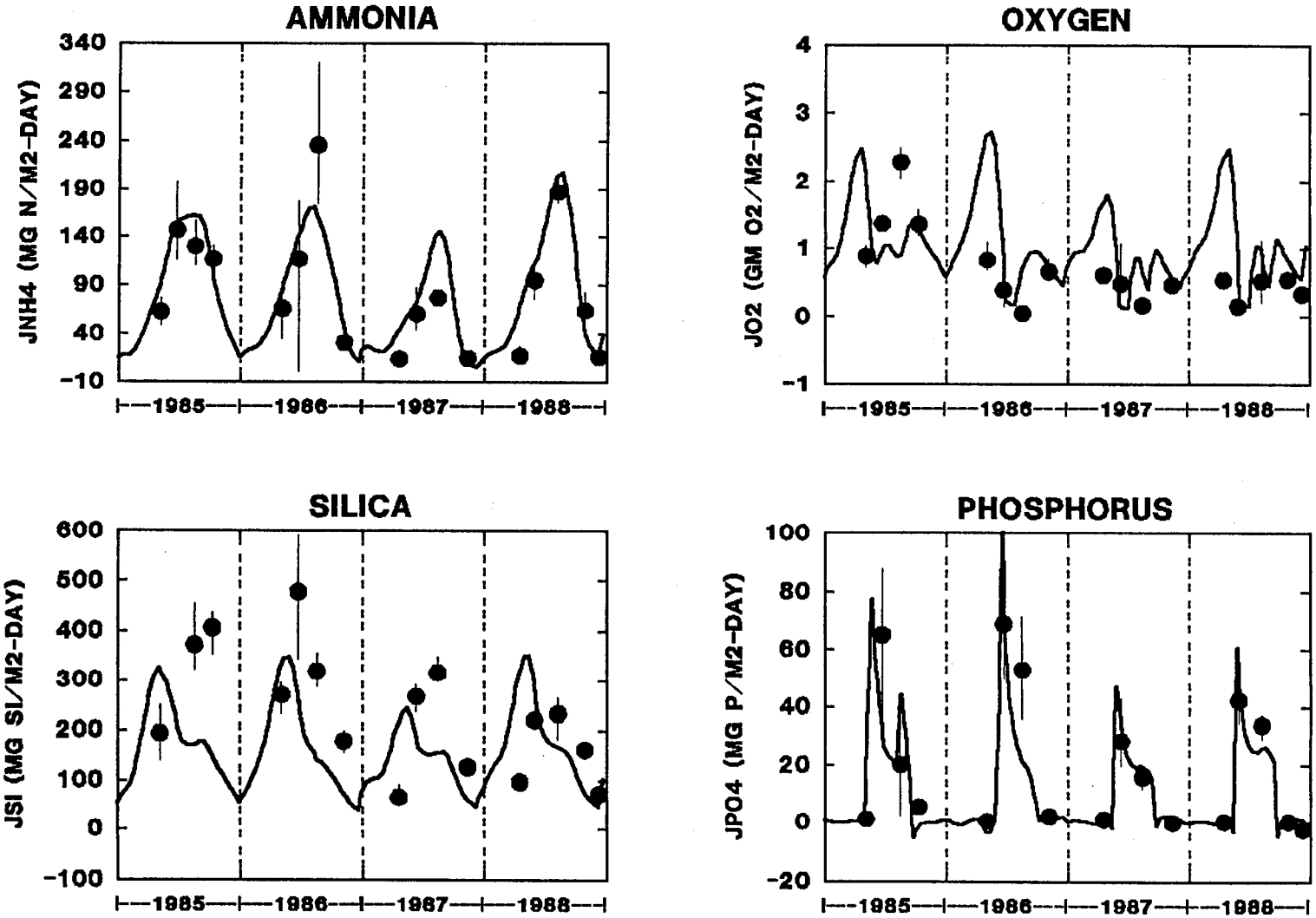

HydroQual, Inc.

run066 - plotr64

FIGURE 42

CHESAPEAKE BAY - POINT NO POINT

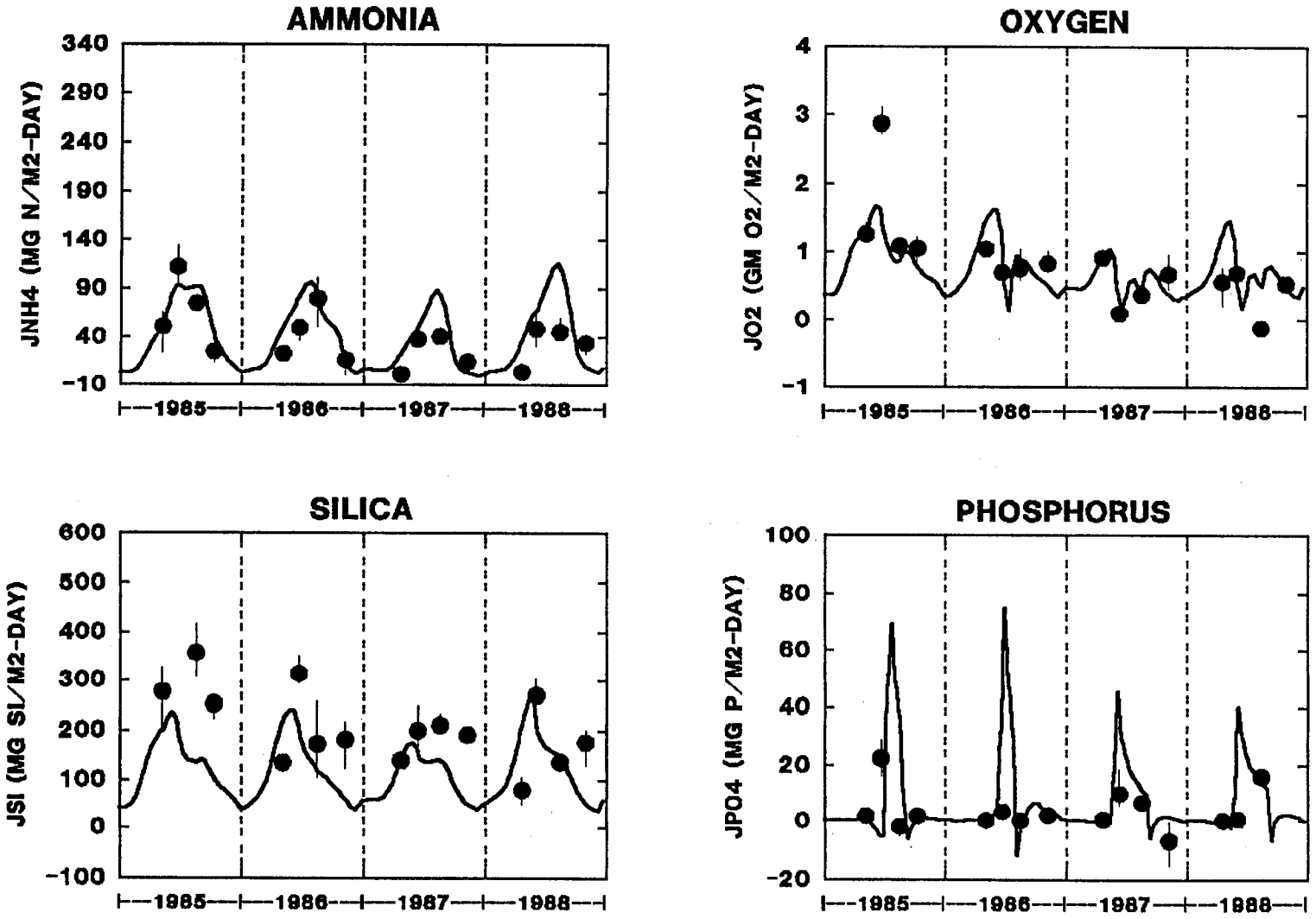

run066 - plotpt

FIGURE 43

CHESAPEAKE BAY - BUENA VISTA

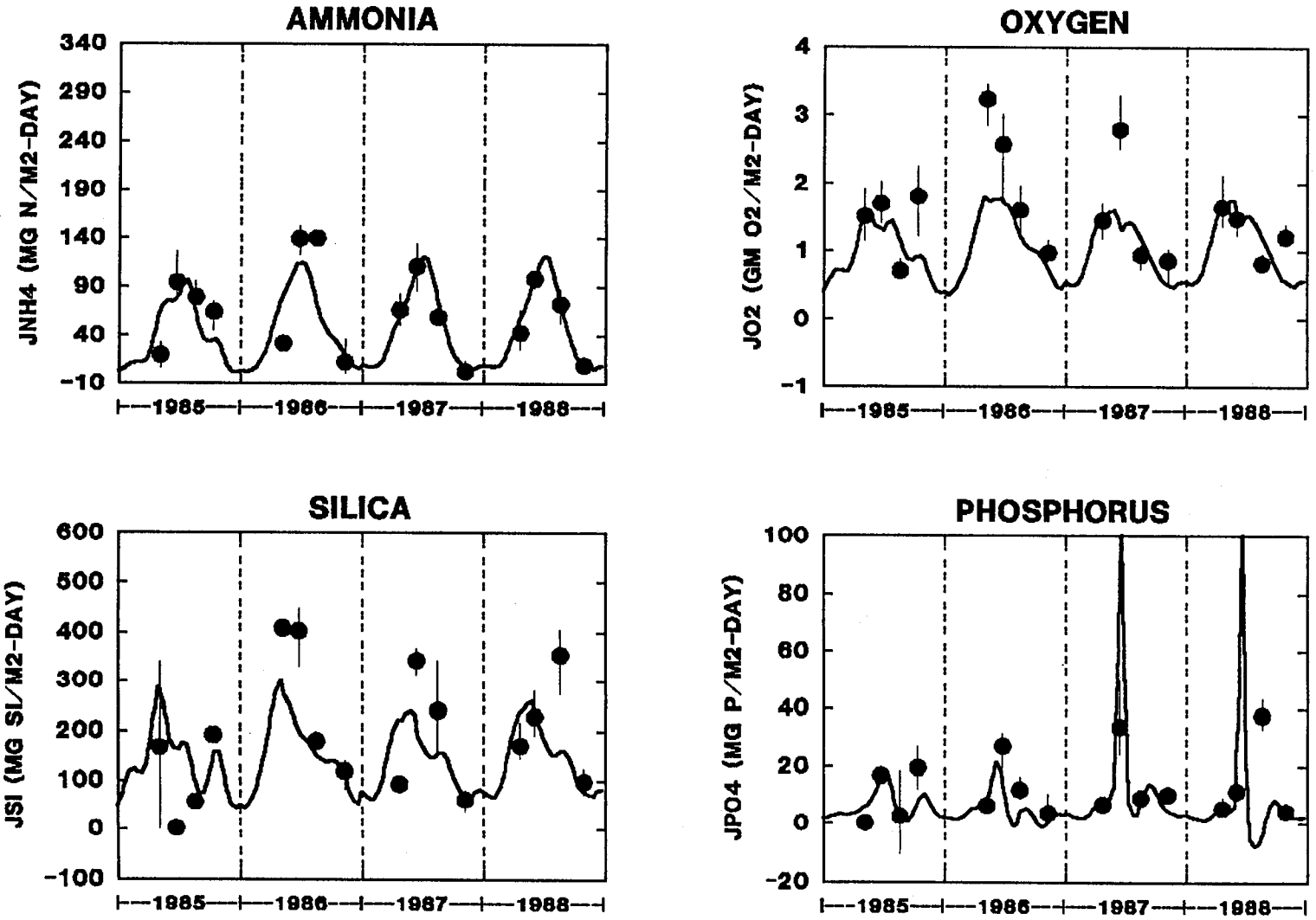

HydroQual, Inc.

run066 - plotbuen

FIGURE 44

CHESAPEAKE BAY - ST. LEO

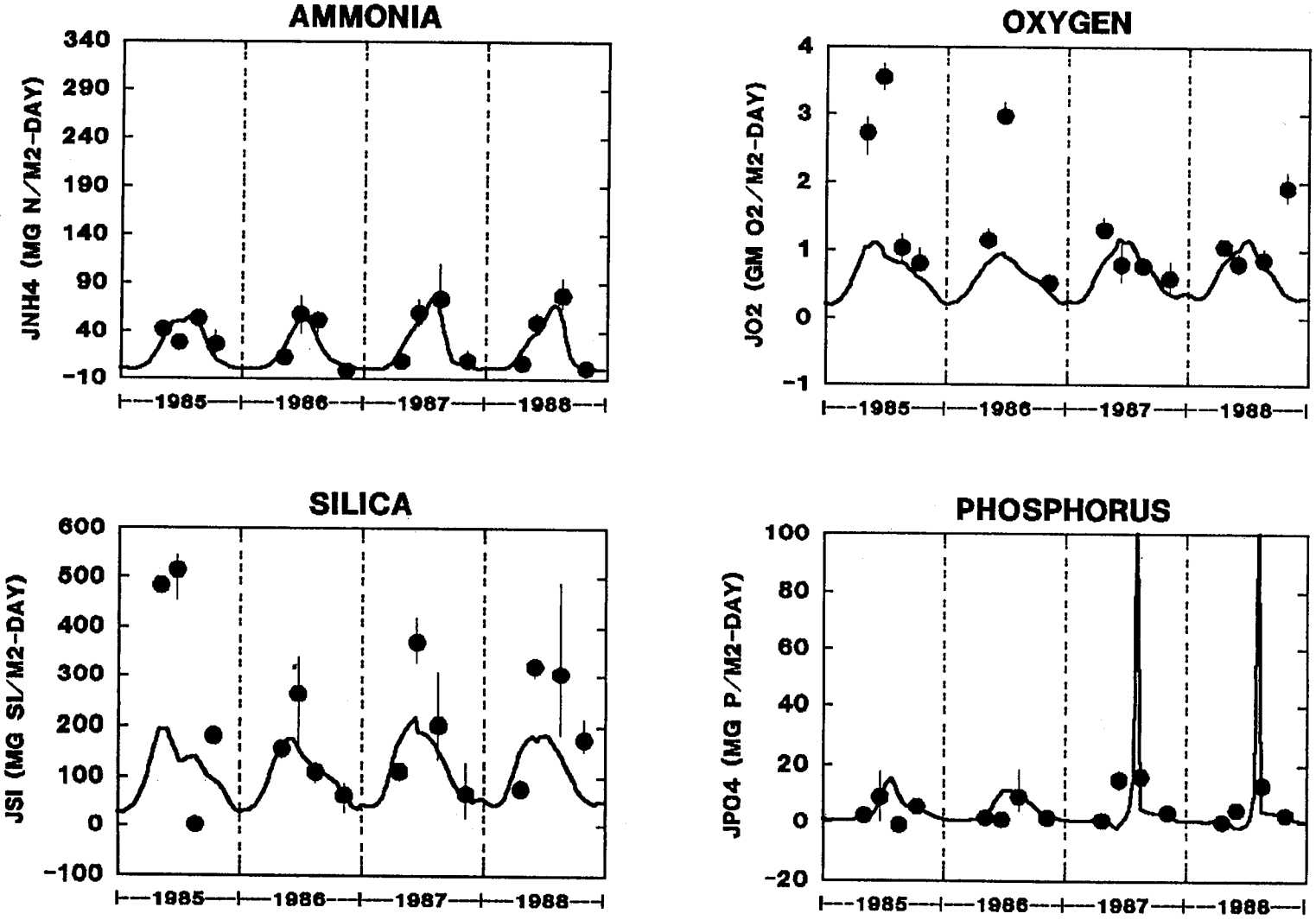

run066 - plotleo

FIGURE 45

CHESAPEAKE BAY - MARYLAND POINT

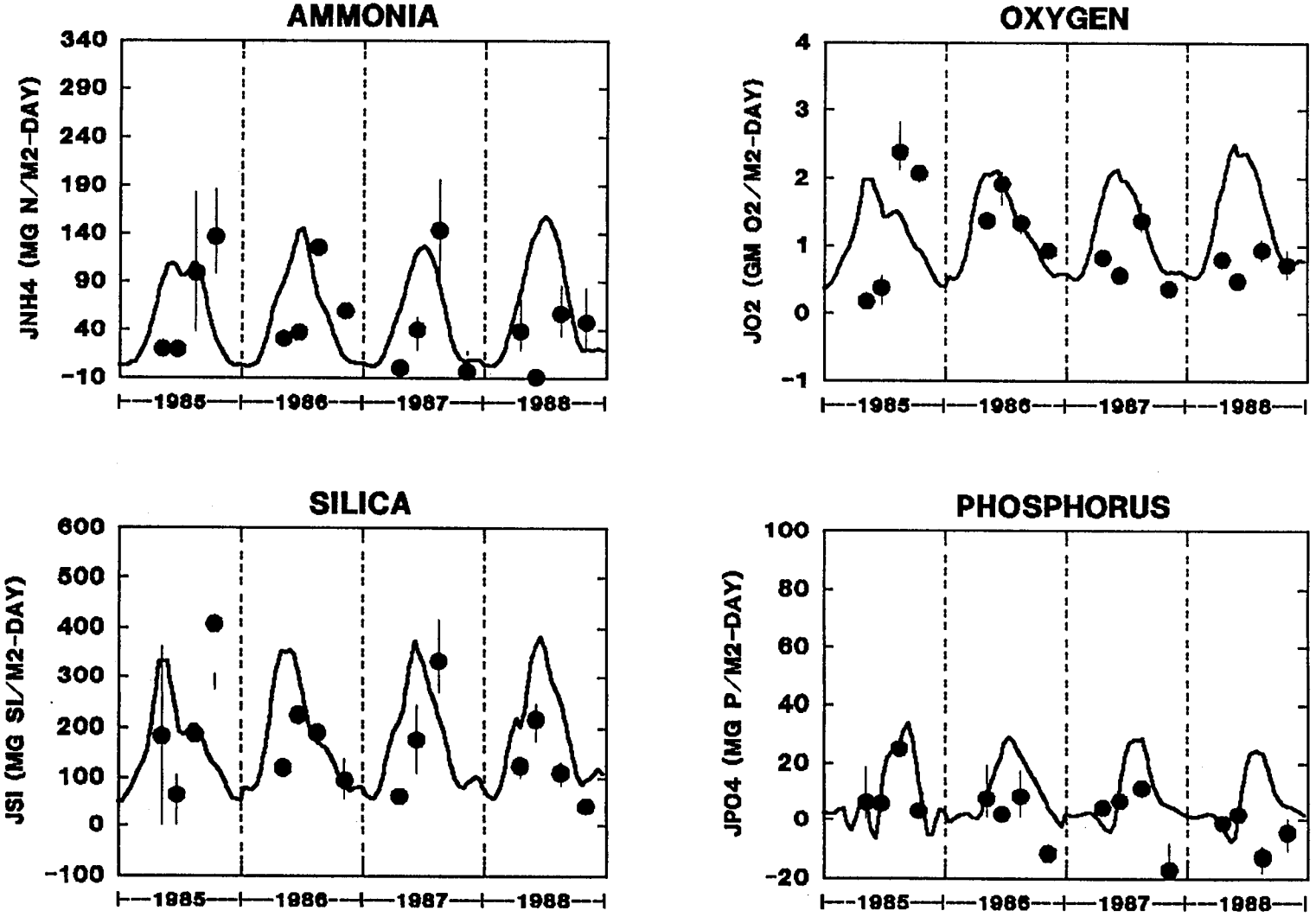

HydroQual, Inc.

run066 - plotmary

FIGURE 46

CHESAPEAKE BAY - RAGGED POINT

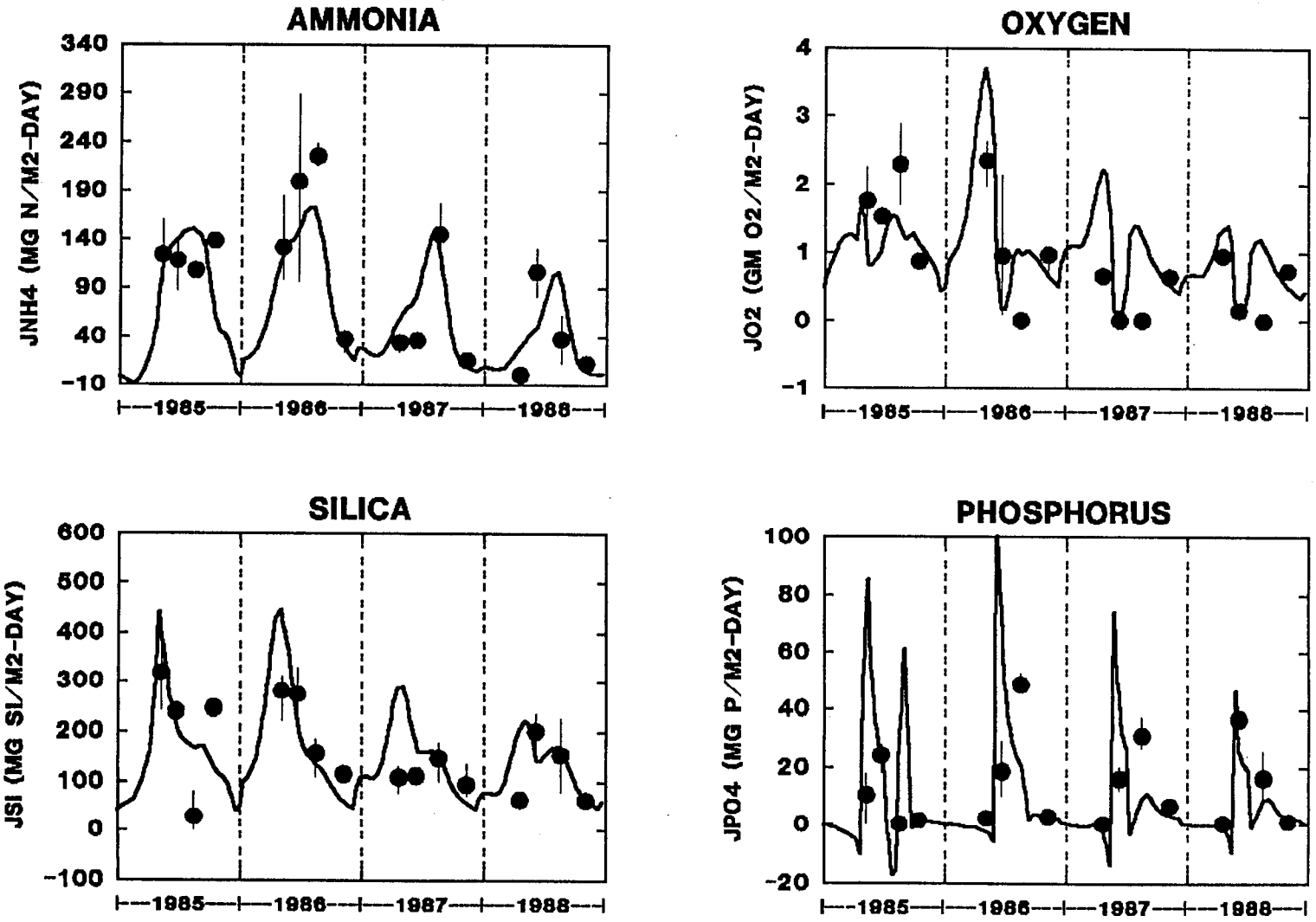

run066 - plotrag

FIGURE 47

The Massachusetts Water Resources Authority
Charlestown Navy Yard
100 First Avenue
Charlestown, MA 02129
(617) 242-6000